2008-01-01

Expert System Design Guide for Lower Classification Roads over High PI Clays

Yaqi Wanyan
University of Texas at El Paso, wanyanyaqi@miners.utep.edu

EXPERT SYSTEM DESIGN GUIDE FOR LOWER CLASSIFICATION ROADS OVER HIGH PI CLAYS

YAQI WANYAN

Department of Civil Engineering

APPROVED:

Soheil Nazarian, Ph.D., Chair

Carlos M. Chang, Ph.D.

Vivek Tandon, Ph.D.

Jack Chessa, Ph.D.

Anand J. Puppala, Ph.D.

Patricia D. Witherspoon, Ph.D.
Dean of the Graduate School

DEDICATION

To my family:

Father: Hua Wanyan

Mother: Cailian Tian

Husband: Gengzong Qiu

Son: Ryan Qiu

Many thanks for your love, support and patience.

EXPERT SYSTEM DESIGN GUIDE FOR LOWER CLASSIFICATION ROADS OVER HIGH PI CLAYS

BY

YAQI WANYAN, M.S., EIT

DISSERTATION

Presented to the Faculty of the Graduate School of

The University of Texas at El Paso

in Partial Fulfillment

of the Requirements

for the Degree of

DOCTOR OF PHILOSOPHY

Department of Civil Engineering

THE UNIVERSITY OF TEXAS AT EL PASO

December, 2008

ACKNOWLEDGEMENTS

I am indebted to my advisor, Dr. Soheil Nazarian for his invaluable guidance, patience and kindness throughout my graduate studies. I also wish to express my thanks to him for providing me an enthusiastic interest in the subject of study. His guidance and support made this work a memorable experience. Special thanks go to Dr. Anand J. Puppala. In our meetings, he provided ideas and constructive criticism that significantly added to the research. Appreciation is also extended to my other committee members, Dr. Vivek Tandon, Dr. Jack Chessa and Dr. Carlos M. Chang for their helpful advice and comments. The encouragement, and help with finite element analysis modeling offered by Dr. Cesar Carrasco and Mr. Cesar Tirado during the research are greatly appreciated.

I am grateful to all professors, staff and colleague students of the Department of Civil engineering for their helps and supports. I would like to thank the Texas Department of Transportation (TxDOT) for providing me an opportunity to work in the high PI clay project. Great thanks to the Center for Transportation Infrastructure Systems (CTIS) for providing financial support through out my graduate studies and for making it so easy to delve into the research sources. I greatly acknowledge Mr. Imad Abdallah, Mr. Anup Sabnis, Mr. Portillo, Enrique, Mr. Thammanoon Manosuthkij and Miss Pacheco, Lourdes for their helps provided to complete this research.

I would like to express my love and gratitude to my parents, Mr. Hua Wanyan and Mrs. Cailian Tian for their endeavor to provide me with the opportunity to gain this tremendous education and the necessary tools to succeed in life. Thank you to my husband, Gengzong Qiu for his love, understanding and encouragement, and my son Ryan, for having sacrificed his affectionate attention during my study.

ABSTRACT

This research was focused on low-volume roads over expansive clayey soils in Texas. In spite of the redundant pavement designs recommended and widely used in Texas for roads in high PI clay areas, these pavements often fail prematurely. This failure occurs primarily because of the highly variable properties of the clayey subgrade throughout the year due to moisture fluctuations. The problematic nature of high PI clays, despite the fact that volumetric changes such as heaving are sometime considered in the design, is of concern since they contribute to roughness and longitudinal shrinkage cracking of the road, and as such the loss of the functional serviceability of the roads. Therefore, it is imperative to improve the design and laboratory procedures to address expansive subsoil conditions and then design pavements accordingly to extend the life expectancy of these roads. The intent of this research project was to cultivate the vital features of strategies for improving low-volume flexible pavement design and thus improving the overall low-volume road performance. These include:

1) Identify the shortcomings of current design and construction practices associated with the less than desirable performance of pavements in low-volume roads constructed on high PI clays;
2) Identify the most significant soil parameters directly related to the performance of these types of roads;
3) Propose practical laboratory test methods and analyzing models to address the problem of premature failure of low-volume roads on high PI expansive subgrade;
4) Qualify and quantify current remediation procedures, climatic effects and road condition assessment (both successful and unsuccessful) used to mitigate the shrink-swell problems;

5) Develop a user-friendly expert system design tool to guide the designers through the process for more realistic designs and rehabilitations.

The focus of this research is on how to improve design procedures of low-volume roads over expansive clayey subgrades. A computer guide to assist pavement engineers to design lower classification roads over high PI clays using the expert system approach has been developed. The guide combines numerical and engineering analyses with heuristic information about the site to recommend best design and construction practices. Numerical analysis is performed to predict longitudinal cracking distress, which reported by a district survey throughout Texas to be one of the most prevailing distresses. Other common distresses are studied. Traditional and new remediation methods are proposed to address the problem of pre-mature failure of low-volume roads on high-PI clays. Finally cost and benefit analysis are added to the design guide framework to compare cost-effectiveness of recommended strategies and to accomplish the objectives of this project.

TABLE OF CONTENTS

LIST OF FIGURES

LIST OF TABLES

CHAPTER ONE - INTRODUCTION

1.1. BACKGROUND

Rural, farm-to-market access roads, roads connecting communities, and roads for logging or mining are significant parts of any transportation system. These roads are commonly referred as low-volume, or lower classification roads which have an average daily traffic (ADT) of less than 400 vehicles per day, and usually have design speeds less than 50 mph (80 kph) (AASHTO, 2002).

Roads that are constructed on soft and problematic soils are the source of frequent maintenance problems. Clayey soils that exhibit volume change due to seasonal moisture fluctuation are known as expansive soils. Examples of expansive clays include high plasticity index (PI) clays, over-consolidated clays rich with montmorillonite minerals, and shales. For roads built on expansive subgrades, moisture content is one of the most significant factors that affect the subgrade behavior, and thus, the pavement performance. Expansive soils shrink when dry and swell when wet. In the rainy seasons, the clay exhibits exceptionally low strength and tends to expand. The low strength of subgrade contributes to the structural damage to the road. The narrow width of the low-volume roads as well as the poor surrounding drainage conditions accelerates the intrusion of water. In summer months, the soil dries out with time. Such loss of moisture results in significant increase in the strength and modulus of the clay which has a positive impact on the life of the pavement. However, the increase in stiffness results in the increase in the brittleness of the clay. The loss of moisture also contributes to the shrinkage of the clay. This tendency to shrink along with the increase in the brittleness will cause desiccation cracks that will propagate to the surface of the road. These cracks, sometimes an inch or more

wide, act as conduit for water to penetrate more rapidly in the subgrade, causing a vicious circle of continuous damage to pavement.

Besides the strength and stiffness changes throughout the year, total or differential volume movements caused by swell or shrinkage strains of expansive soils can exert enough pressure to damage the pavements and cause maintenance problems. Differential movements induce large changes in moments and shear forces in the structures, which lead to failure in both rigid and flexible pavements since these forces are not accounted for in the rigid pavement design practice and flexible pavement materials are weak in flexural strength. Damages sustained by the pavements include distortion and cracking of pavements in all directions as well as heave related bumps and roughness which cause ride discomfort. Maintenance and repair requirements can be extensive, often exceeding the capitol costs.

This project focused on how to improve design procedures of low-volume roads build over expansive clayey soils. In spite of the redundant pavement designs recommended and widely used in Texas for roads in high PI clay areas, these pavements often fail prematurely. A significant amount of work is required to maintain and rehabilitate these roads. The problemetic nature of high PI clays, despite the fact that volumetric changes such as heaving are sometime considered in the design, is of concern since they contribute to roughness and longitudinal shrinkage cracking of the road, and as such the loss of the functional serviceability of the roads. Therefore it is imperative to improve the design and laboratory procedures to address expansive subsoil conditions and then design pavements accordingly to extend the life expectancy of these roads. A new design guide to assist pavement engineers with low classification roads over high PI clays is the focus of this study.

1.2. OBJECTIVES

Current practices used in Texas often recommend a thick and costly pavement structure and an over-design road to compromise the impacts of expansive subgrade. But these pavements often fail prematurely. A more realistic design approach should be developed and established for these low volume roads to allow more miles of rehabilitation with the same amount of funding with less distress problems in the future. The intent of this research is to cultivate the vital features of positive strategies for improving low-volume flexible pavement design and to improve the overall low-volume road performance. These include:

1) Identify the shortcomings of current design and construction practices associated with the less than desirable performance of pavements in low-volume roads constructed on high PI clays;
2) Identify the most significant soil parameters directly related to the performance of these types of roads;
3) Propose practical laboratory test methods and structural models to address the problem of premature failure of low-volume roads on high PI expansive subgrade;
4) Qualify and quantify current remediation procedures, climatic effects and road condition assessment (both successful and unsuccessful) used to mitigate the shrink-swell problems;
5) Develop a user-friendly computer design program to guide the designers through the process for more realistic designs and remediation strategies.

1.3. SCOPE OF STUDY

The overall objective of this research is to establish a new design program that would hopefully provide the following information to pavement engineers:

1) Identify most relevant soil properties and corresponding test procedures to characterize and address highly expansive subgrade problems;
2) Propose quantitative predictive models to assess flexible pavement failures on expansive subgrade, specifically for low-volume roads longitudinal cracking;
3) Create an interactive design program to guide users through design procedures and provide realistic layer thicknesses for low volume roads;
4) Provide feasible design alternatives and remediation strategies to minimize cost without compromise performance.

Although this research is focused on Texas, this new low-volume flexible road design program may be helpful to other states with similar problems by generalizing and adopting new design criteria and field data.

1.4. ORGANIZATION OF DISSERTATION

Chapter Two contains a thorough literature review of recent studies addressing following six main topics: commonly used laboratory tests and models to characterize expansive subgrade properties; promising remediation strategies; currently used design procedures and their limitations for flexible pavements; expert system approach to reach feasible decision-making solutions and different cost analysis methods.

Chapter Three describes the overall research approach. The results of district survey conducted at the beginning of this research were analyzed. The most prevailing low-volume road distresses and their causes are identified. The survey also collected commonly used stabilizer and whether geosynthetics have been successfully used in Texas districts. The conceptual design and methodologies are also presented.

Chapter Four addresses developmental details of four evaluation models used in the design guide software, which deal with four major distress problems, namely, fatigue cracking and rutting, subgrade shear failure, excessive roughness and longitudinal cracking. The causes of longitudinal cracking and finite element models to estimate such cracks are presented in full detail including use of laboratory test data to develop prediction relationships; finite element modeling; parametric study and validation of the results. Programming considerations are also addressed.

Chapter Five provides information on six remediation strategies out of many possible solutions and groups them into two categories: either to improve subgrade strength and stiffness or to minimize moisture variation induced swell/shrink problems. Some remediation strategies are deemed to be suitable for both purpose, such as stabilization, geosynthetics and undercut-backfill. Programming algorisms are depicted and useful information discussed.

Chapter Six presents the cost and benefit analyses. Assumptions and procedures to perform cost assessment are discussed. "Before and after" analyses used to compare the costs/benefits of the alternatives; and output results are presented based on cost-effectiveness comparison of the alternatives.

Chapter Seven illustrates the use of the developed **Ex**pert **S**ystem for **P**avement **R**emediation **S**trategies (ExSPRS) program with case studies of five TxDOT district baseline study sites, namely, Fort Worth, San Antonio, Paris, Houston and Atlanta..

Finally, conclusions and recommendations for future research are given in Chapter Eight.

CHAPTER TWO - LITERATURE REVIEW

Low-volume roads over highly expansive subsoils are under-performing despite being overly-designed and constructed. To address this problem, a comprehensive literature review was conducted to answer the following six questions:

1) Which laboratory tests and models can we use to characterize the expansive soil problems? What are their limitations?
2) How will road conditions and climatic effects influence the performance of the low-volume roads?
3) What are the available remediation strategies?
4) Which flexible pavement design software packages are currently in use and what are their limitations?
5) What is an expert system? How will an expert system help solving our problem?
6) What is cost analysis? What is life cycle cost analysis (LCCA)? What are the differences? How to evaluate different design alternatives?

2.1. LABORATORY TESTS AND MODELS TO CHARACTERIZE EXPANSIVE SOILS

Roads build on expansive soil fails prematurely primarily because of the highly variable properties of expansive clays due to moisture fluctuations throughout the year. Failures occur as a result of variations in strength and stiffness or subgrade volumetric change or both. It is important to characterize these variations and predict their effects on pavement performance.

2.1.1. Tests to Characterize Strength and Stiffness Variations

Subgrade materials are typically characterized by (1) stiffness, which is their resistance to deformation under load, and/or (2) strength, which is their bearing capacity. Stiffness of pavement layers defines their efficiency to distribute load-induced stresses within the pavement system. Many studies have demonstrated that for fine-grained soils, moisture content appears as the dominant variable with regard to strength and stiffness. Strength and stiffness properties of subgrade soils are often determined by conducting appropriate strength and stiffness tests at compacted moisture levels. Ways to characterize strength and stiffness properties include laboratory testing, field testing and using empirically-derived models. A comprehensive understanding of strength and stiffness variations relies significantly on soil properties such as soil classifications, moisture content, dry densities, specific gravities as well as pavement layer thicknesses and subgrade profiles.

2.1.1.1. LABORATORY TESTING

Most strength and stiffness measurements are performed in the laboratory. These include the triaxial test with static or cyclic loading, the resilient modulus test and nondestructive free-free resonant column test.

2.1.1.1.1. Static Triaxial Test

The triaxial compression test is the most widely used technique to determine the shear strength of soils. The test is called "triaxial" because the three principal stresses are assumed to be known and are controlled. A cylindrical soil specimen is enclosed and tested in a apparatus as shown in Figure 2.1. The pressure in the cell is raised to the desired value, and the sample is then brought to failure by applying an additional vertical stress.

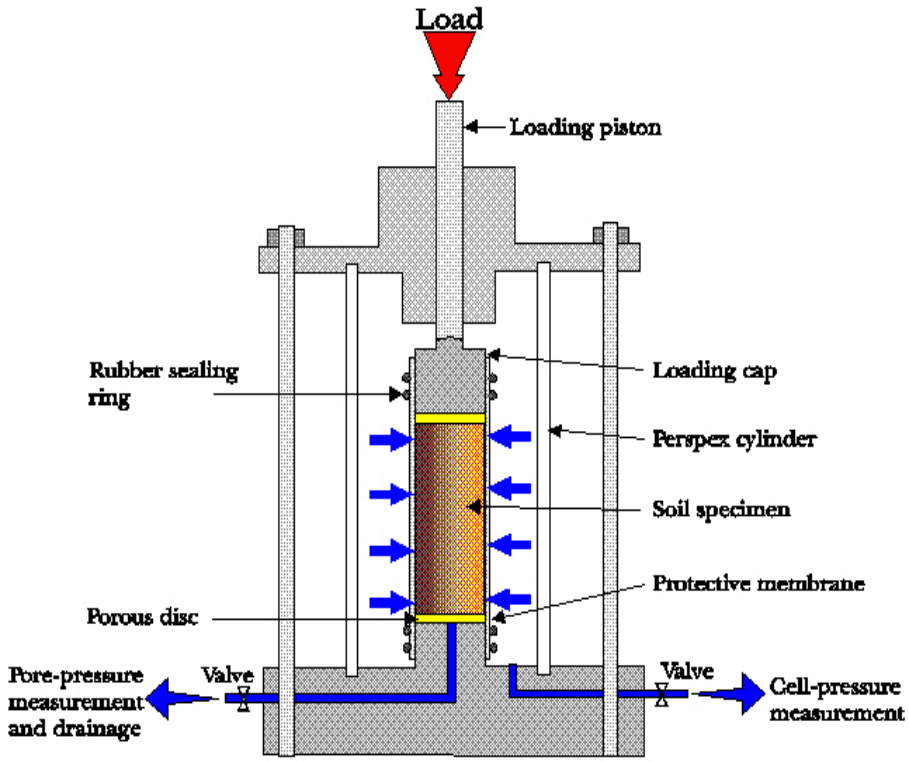

Figure 2.1—Triaxial Test Apparatus

To obtain the shear strength parameters of the soil, a number of specimens (normally at least three) are tested at different cell pressures (typically 0, 5, 10, and 15 psi). For each test, the deviatory stress at failure is determined and used to plot a Mohr circle. The tangential envelope to touch these circles then defines the shear strength parameters.

Figure 2.2 shows typical results from triaxial tests. The triaxial strength parameters obtained from these tests such as cohesion and angle of internal friction and the classification of materials can be utilized to predict pavement performance in many pavement design and modeling programs. As shown in Figure 2.3, the stress-strain curves (especially post-failure) obtained during these tests can be good indicators of the brittleness of the material.

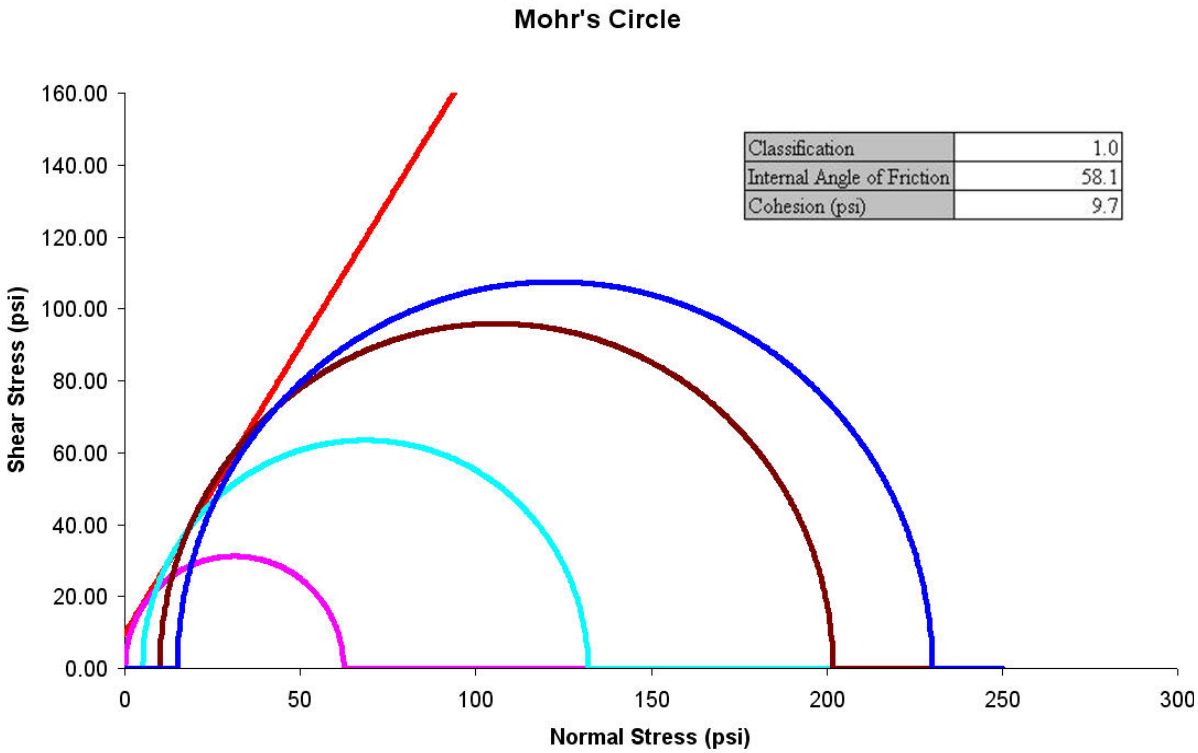

Figure 2.2—Typical Results of Triaxial Test

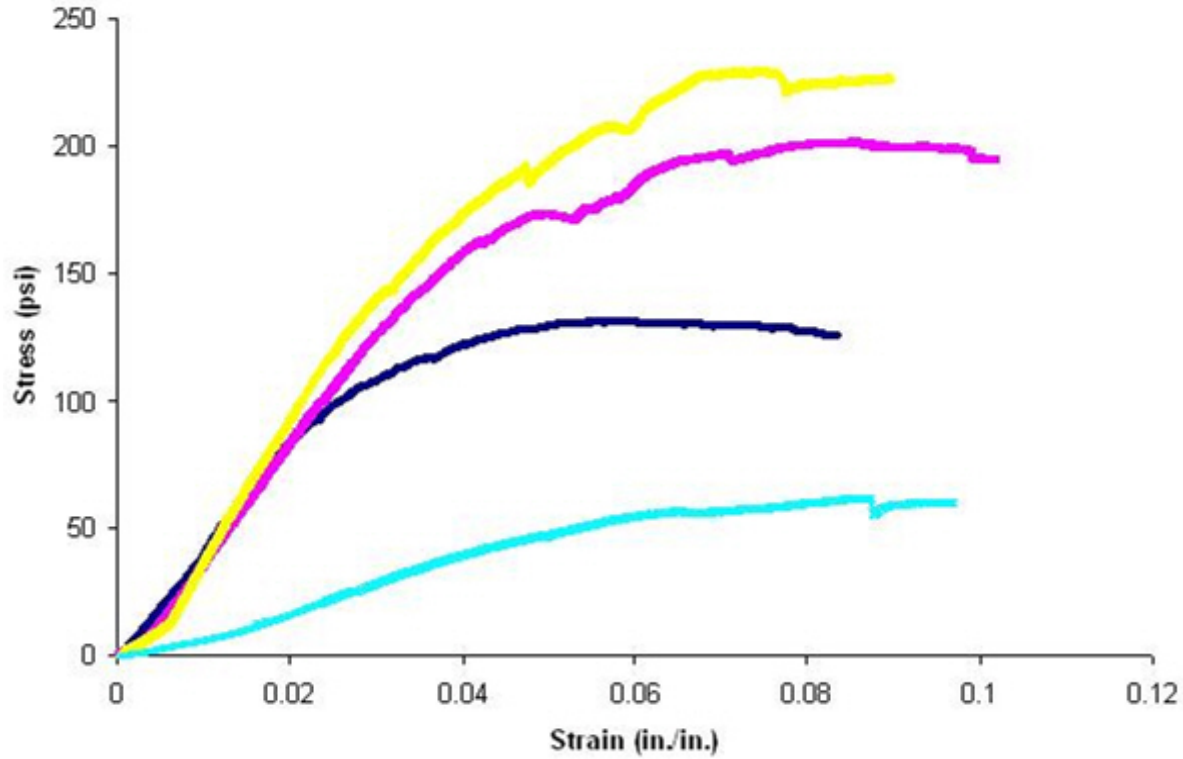

Figure 2.3—Typical Stress-Strain Curve of Triaxial Test

2.1.1.1.2. Cyclic Triaxial Test

Cyclic Triaxial test is widely used to investigate changes in strength and stiffness under cyclic loading conditions. The cyclic triaxial test apparatus applies cyclic or dynamic loading to the soil specimen. This form of loading can simulate traffic loading conditions. The test system controls three parameters, axial stress, confining pressure and back pressure. The cylindrical specimen is prepared and tested to study pore water pressure, deformation response and effect of repeated loading conditions.

Cyclic loading on saturated undrained clays induces a decrease in effective stress as well as a rearrangement of the soil particle structure, which may lead to degradation in strength and stiffness. This phenomenon of high PI subgrade having low strength during rainy season contributes to the structural damage of the road. Miller *et al.* (2000) reported that for highly plastic clay, the cyclic shear strength was sensitive to the initial degree of saturation. The cyclic strength may decrease by approximately 80% as the initial degree of saturation is increased from 90 to 100%. Shahu and Yudhbir (1999) proposed cyclic triaxial tests on samples prepared at optimum moisture content and at saturated condition to better evaluate the strength and stiffness variations of subgrade materials. In their study, significant degradation of the subgrade soil under saturated condition was observed.

2.1.1.1.3. Resilient Modulus Test

The resilient modulus (M_R) test is a stiffness test. It measures the soil response under repeat loading which provides the primary means to determine the variation in modulus of subgrade with a range of variable conditions, such as moisture, density, and stress conditions in a pavement subjected to moving wheel loads. Under repeated loads, the modulus becomes nearly

constant after a number of loading cycles and the response can be assumed to be approximately elastic. This steady value of modulus is defined as the resilient modulus and is assumed to occur after about 200 cycles of loading. (AASHTO, 1993). Most modern pavement design methods are based on the resilient modulus of the supporting subgrade soils. Typically, the resilient modulus is determined in the laboratory in accordance with AASHTO T307 under conditions of maximum dry density and optimum water content (Drumm and Madgett, 1997). In the test a repeated axial cyclic stress of fixed magnitude, load duration and cyclic duration is applied to a cylindrical test specimen. While the specimen is subjected to this dynamic cyclic stress, it is also subjected to a static confining stress provided by a triaxial pressure chamber. The total resilient (recoverable) axial deformation response of the specimen is measured and used to calculate the resilient modulus using the following equation:

$$M_R = \frac{\sigma_1 - \sigma_3}{\varepsilon_r} = \frac{\sigma_d}{\varepsilon_r} \tag{2.1}$$

where σ_1 = major principal stress (axial stress); σ_3 = minor principal stress (confining stress); σ_d = deviatoric stress (applied load divided by sample cross section area); ε_r = recoverable (or elastic) axial strain, which can be obtained by $\Delta L/L$, in which L represents the gauge length over which the sample deformation is measured; and ΔL is change in sample length due to applied load.

Figure 2.4 shows a simplified version with only 6 load repetitions, where normally there are 1000 specimen conditioning repetitions followed by several hundred load repetitions during the test at different deviator stresses and confining pressures.

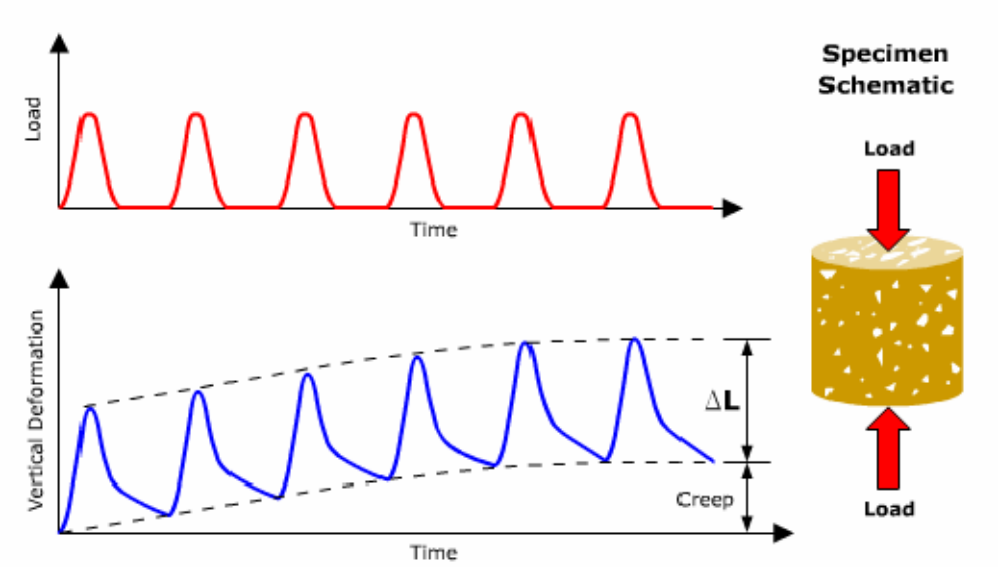

Figure 2.4—Simplified Resilient Modulus Test Illustration

2.1.1.1.4. Free-Free Resonant Column Test

The free-free resonant column test is suitable for measuring the seismic modulus in the laboratory. When a cylindrical specimen is subjected to an impulse load at one end, seismic energy over a large range of frequencies will propagate within the specimen. Depending on the dimensions and the stiffness of the specimen, energy associated with one or more frequencies is trapped and resonate as they propagate within the specimen. The goal of this test is to determine these resonant frequencies. Since the dimensions of the specimen are known and if one can determine the resonant frequencies; then, one can readily determine the modulus of the specimen using principles of wave propagation in a solid rod.

The free-free resonant column (FFRC) device is a reasonably low cost device that has been successfully utilized by some TxDOT personnel. Due to the nondestructive nature of this test, one specimen can be tested repeatedly to obtain the variation in modulus with moisture (Yuan and Nazarian, 2002). Also, the same specimen can be used to measure the change in length and diameter of the specimen during saturation and drying. Test results have shown that

the modulus from the FFRC device is reasonably well-correlated to the modulus from the resilient modulus tests and the angle of internal friction from the triaxial tests (Nazarian and Yuan, 2003). The schematic of the device is shown in Figure 2.5. Typical results of FFRC are shown in Figure 2.6. As the specimen is dried the modulus significantly increases and the moisture content decreases. However, as soon as the water is introduced, the modulus significantly decreases and the moisture content increases.

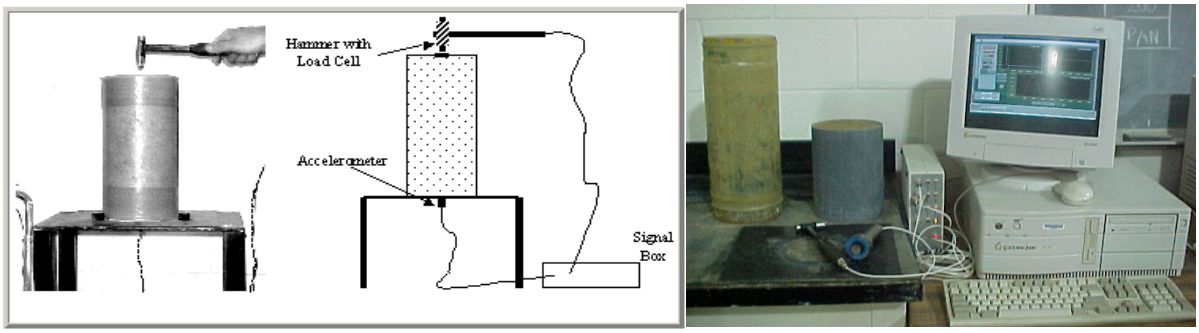

Figure 2.5—Free-Free Resonant Column System
(from Nazarian and Yuan, 2003)

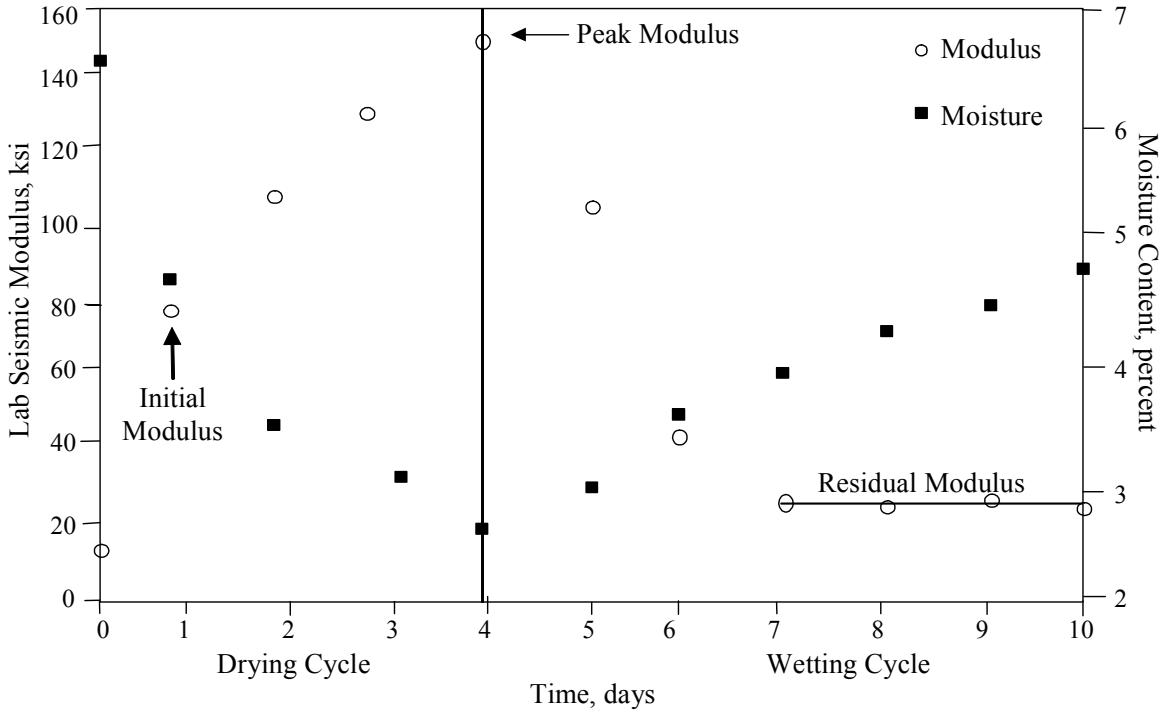

Figure 2.6—Typical Variation of Modulus with Time
(from Nazarian and Yuan, 2003)

A number of moisture patterns have to be studied to determine the most appropriate test protocol. However this method has the potential for providing the relevant information for the design at a minimal cost.

2.1.1.2. FIELD TESTING

2.1.1.2.1. Standard Penetration Test (SPT)

The results of penetration type soil tests represent the response of soil to an imposed deformation. One of the most widely used in-situ test is the Standard Penetration test (SPT). The testing method was standardized in 1958 as ASTM D1586. It is performed inside exploratory boring using inexpensive and readily available equipment, and thus adds little cost to its performance. The SPT test involves drilling a 2.5 in. to 8 in. diameter exploratory boring, then, a standard cylindrical sampler is driven into the bottom of the borehole. Using a rope or an automatic tripping mechanism, the hammer is raised a distance of 30 in. and is allowed to fall. This process is repeated until the sampler has penetrated a distance of 18 in. The total blows required from a hammer, over the interval of 6 in. to 18 in. are summed to obtain the N-value, in blows per foot. Figure 2.7 depicts the test procedure. The N-value is used as a basis for foundation design and as the primary index of liquefaction resistance.

2.1.1.2.2. Dynamic Cone Penetration (DCP) Test

The Dynamic Cone Penetration (DCP) test is a low-cost, easy-to-use test that characterizes subgrade soils. It involves a 17.6-lb hammer that is raised to a height of 23 in. and then dropped, driving the cone into the soil or other material being tested. A ruler is used to measure the increments of penetration the rod sinks into the soil after several blows. DCP measurements are recorded as a Dynamic Penetration Index (DPI), where DPI is equal to the depth divided by number of blows for cone-tipped rod to reach that depth. A graph of depth

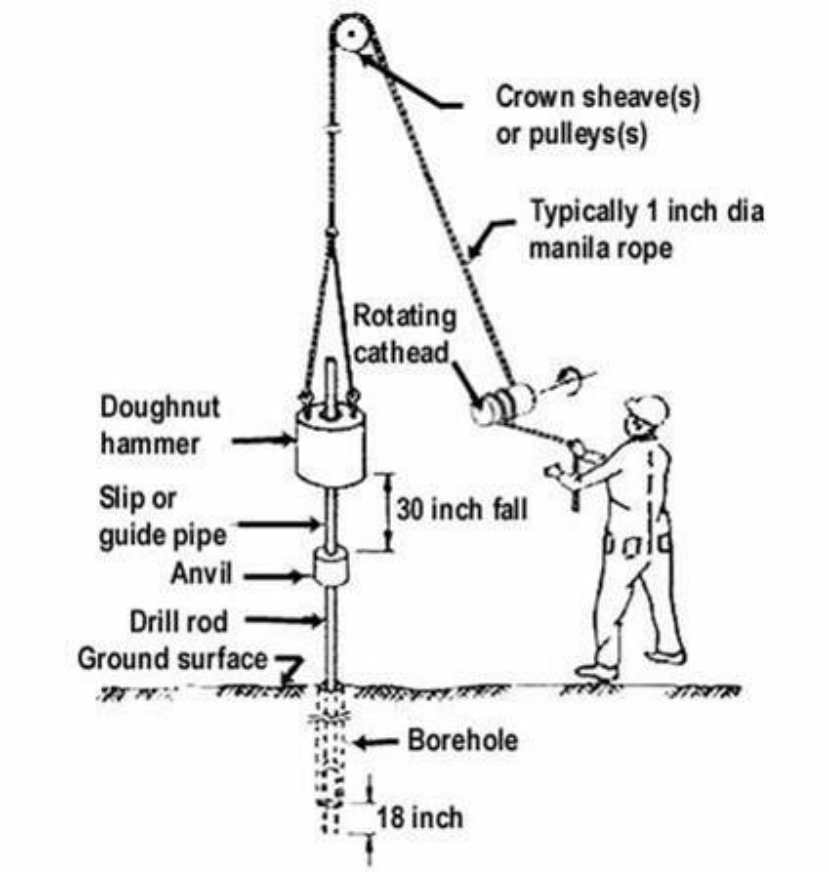

Figure 2.7—Illustration of Standard Penetration Test

versus California Bearing Ratio (CBR) value is then plotted, where the CBR value is a correlation developed between DPI and soil strength.

The SPT and DCP both have good applicability in estimating various soil properties, like moduli, strength, and liquefaction resistance. However, DCP test is becoming increasingly popular for in-situ investigations (Jefferies and Davies, 1993).

2.1.1.2.3. Plate Bearing Test

The Plate Bearing Test method is used to determine the deformation modulus of foundations, subbase and subgrade of road and airport pavements. It is also used to determine the in-situ bearing capacity of the soil, designing for static loads on spread footings, and for

repetitive plate loading tests of soils and flexible pavements. The test setup and loading procedure are as follows: An area of the soil is stripped to the proposed elevation of the subgrade surface. The stripped area should be at least twice the diameter of the plates to eliminate surcharge or confining effects. The bearing plate is seated on the soil area under test. A 24-in. or 18-in. diameter plates are then centered on a 30-in.-diameter plate, and the hydraulic jack is centered on an 18-in.-diameter plate. The plate bearing test apparatus are shown in Figure 2.8. The load reaction device must be long enough so that its supports are at least 8 ft from the bearing plate. Three dial micrometers are used to measure deformation of the soil under load. The loading system and bearing plate are then seated by applying a load of 700 lb when the thickness of the pavement is less than 15 in., or a load of 1400 lb when the design thickness of the pavement is 15 in. or more. The results are evaluated graphically by plotting a load-deformation curve. Correction is needed if the load-deformation relation plots as a straight line not passing through the origin.

Figure 2.8—Plate Bearing Test Apparatus

2.1.1.2.4. Falling Weight Deflectometer (FWD)

The Falling Weight Deflectometer (FWD) is a nondestructive deflection based device that operates on the principle of applying an impulse load to a pavement and then recording the

surface deflections at predetermined intervals. It is capable of applying dynamic loads to the pavement surface. The duration and magnitude of the force applied is representative of the load pulse induced by a single heavy moving wheel load or of that of an aircraft moving at moderate speeds. The response of the pavement system is measured in terms of vertical deformation, or deflection, over a given area. Figure 2.9 illustrate the mechanism of a typical FWD and a FWD in operation.

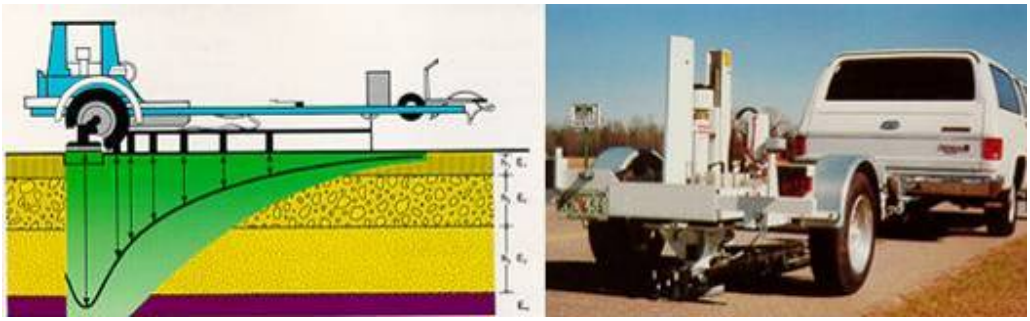

Figure 2.9—FWD Device Applying Dynamic Loads to Pavement Surface

Data from FWD is reduced to find a theoretical deflection bowl that matches that of the measured deflection bowl. Data generated from FWD, combined with layer thickness, can be used to obtain the "in-situ" moduli of a pavement structure. This information can be then used in a structural analysis to determine the bearing capacity, estimate expected life, and calculate overlay requirements over a desired design life. FWD tests are also used to observe the pavement response during different seasons. Daleiden *et al.* (1994) modified AASHTO Guide (1986) equations for predicting in situ backcalculated subgrade moduli from deflection test for different type of soils. They reported thicknesses of the pavement layers, in situ moisture contents, dry densities and specific gravity as significant variables in the prediction.

2.1.1.2.5. Seismic Pavement Analyzer (SPA) and Portable Seismic Pavement Analyzer (PSPA)

The Seismic Pavement Analyzer (SPA) combines several wave propagation techniques in a single unit and can rapidly perform nondestructive tests to determine the condition of

pavement. The modulus of each layer of pavements is a major parameter estimated with the SPA. The SPA and its portable version, the Portable Seismic Pavement Analyzer (PSPA), have been successfully used to detect the variation in properties of different layers of the pavement. (Nazarian *et al.*, 1993).

The Seismic Pavement Analyzer (SPA) uses high- and low-frequency pneumatic hammers to introduce interrogating waves into the pavement (one of each). It has three geophones to sense the responses of the pavement to the waves and five accelerometers to collect data. The data collection process consists of the generation of surface waves from the two sources and measuring the motion of the surface with the sensors. The signals are analyzed using Fourier and spectral analysis methods to obtain a representative dispersion curve.

The Portable Seismic Pavement analyzer (PSPA) can be thought of as a smaller version of the SPA. It consists of two transducers (accelerometers in this case) and a source packaged into a hand-portable system. The source package is also equipped with a transducer for consistency in triggering and for some advanced analysis of the signals (Celaya and Nazarian, 2006). Figure 2.10 shows photographs of the SPA and PSPA sensor units. The operating principle of the PSPA is based on generating and detecting stress waves in a medium. The Ultrasonic Surface Wave (USW) interpretation method (Nazarian *et al.*, 1993) is used to determine the modulus of the material.

2.1.1.3. EMPIRICAL ESTIMATIONS

Due to the variety of soil types involved, their inherent seasonal variation of strength characteristics, and the influence of water availability on soil suction, it is difficult to decide

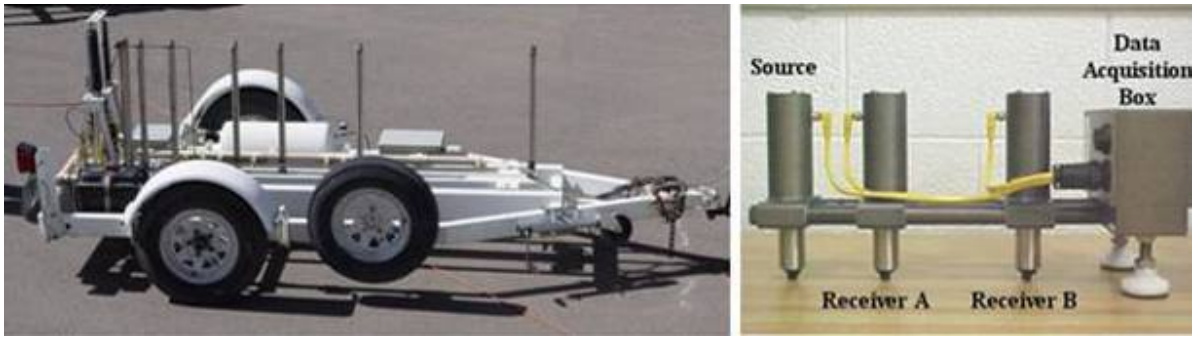

Figure 2.10—Photograph of SPA (left) and PSPA Sensors (right)

load-bearing values for clay subgrades. Table 2.1 summarizes some of the empirical relationships to estimate subgrade resilient modulus.

Although the CBR of subgrade soils is a measure of shear strength, which is not necessarily correlated with a measure of stiffness or modulus such as M_R, several CBR-based relationships were identified in the literature review. Emery (1988) pointed out that the modulus of lower quality subgrades could be expressed as a probabilistic function of CBR and moisture since neither could be explicitly defined. The uncertainty associated with modulus could be expressed as a joint probability density function of the individual probabilities.

2.1.1.4. STRENGTH AND STIFFNESS TESTS LIMITATIONS

Rowe and Barden (1964) pointed out that in triaxial tests, test errors occur due to end restriction, sample barreling and strain non-uniformity. Use of the repeated load triaxial test to obtain data on the resilient characteristics of base and subgrade materials implies that two of the stresses are equal because of axial symmetry. A well-established relationship to relate resilient modulus to stress level has the following formula (See Table 2.1, bulk stress model):

$$M_R = a\theta^b \tag{2.2}$$

where θ = bulk stress, given by $\sigma_{ar}+2\sigma_c = 3\sigma_c+\sigma_d$; or $\sigma_1+\sigma_2+\sigma_3$; σ_{ar} = peak axial stress; σ_c = constant confining stress and a, b = model constants.

Table 2.1—Subgrade Resilient Modulus Models

Model Name	Reference	Equation	Note
Bulk Stress Model		$M_R = a\theta^b$	
Power Model		$M_R = A\sigma_d^B$	
Arithmetic Model		$M_R = a + b\sigma_d$	
Bilinear Model	Thompson and Robnett (1979)	$M_R = M_{Ri} + k_1 \cdot (\sigma_d - \sigma_{di}), where \quad \sigma_d \le \sigma_{di}$ $M_R = M_{Ri} + k_2 \cdot (\sigma_d - \sigma_{di}), where \quad \sigma_d \le \sigma_{di}$	
Semi-Log Model	Fredlund *et al*. (1977)	$\log M_R = a + b\sigma_d$	
Hyperbolic Model	Drumm *et al*. (1990)	$M_R = \frac{a' + b'\sigma_d}{\sigma_d}$	Accounts for stress softening behavior
Brown and Loach Models	Loach (1987)	$M_R = A \times \left[\frac{P_0'}{\sigma_d}\right]^B$ $M_R = C \times \left[\frac{P_0'}{\sigma_d}\right]^D$	Takes into account the effect of mean normal stress.
Universal Model	Uzan (1985)	$M_R = k_1\theta^{k2}{\sigma_d}^{k3}$	All pavement layers
Triaxial Stress State Model	Puppala and Mohammad (1997)	$\frac{M_R}{\sigma_{atm}} = k_1 \times \left(\frac{\sigma_3}{\sigma_{atm}}\right)^{k2}\left(\frac{\sigma_d}{\sigma_{atm}}\right)^{k3}$	σ_{atm} is atmospheric pressure in psi.
AASHTO (1986)		$M_R = 1500CBR$	Fine-grained soils
Alabama	Newcomb and Birgission (1999)	$M_R = 10^{(0.851 \times \log CBR + 2.971)}$	
Transportation and Road Research Laboratory	Powell *et al*. (1984)	$M_R = 2555CBR^{0.64}$	Used by new guide (NCHRP, 2004) for Level 2 input.
U.S. Army Corps of Engineers		$M_R = 5409CBR^{0.71}$	
South African Council on Scientific and Industrial Research		$M_R = 3000CBR^{0.65}$	
Unconfined Compressive Strength 1	Thompson and Robnett (1979)	M_R (at σ_d of 6 psi) $= 0.86 + 0.317\ q_u$	$R^2 = 0.468$ $SEE = 2.61ksi$
Unconfined Compressive Strength 2	Thompson and Robnett (1979)	M_R (at σ_d of 6 psi) $= -1.287 + 0.219\ q_u$	$R^2 = 0.914$ $SEE = 1.32ksi$

Brown and Pappin (1981) pointed out the limitations of above equation. First, confusion arises over the factor a because it is not dimensionless. Second, there is no distinction between total stress and effective stress. Although this has no effect on dry materials, it is of fundamental

importance when pore water is present. Equation 2.2 is likely to lead to inaccurate results because it has been established from data that used a very limited range of stress paths. Brown and Pappin (1981) suggested whenever possible, characteristics of soil and granular material should be expressed in terms of effective stresses. For fine-grained soils, more research is required for a better understanding of the resilient properties.

The deviatoric stress models generally ignore the effect of confining pressure. According to Puppala and Mohammad (1997), this kind of modeling is adequate for cohesive soils found at shallower depths, but is necessary to include the confining stress in the deviatoric stress model for greater depths and at higher traffic loads. The triaxial stress state model is a function of confining and deviatoric stresses applied in a repeated load triaxial test and therefore provides results in triaxial stress environments. A limitation of this model is that it is not valid for test results obtained at unconfined conditions. According to Fredlund *et al.* (1977), confining pressure has no significant effect on the resilient response for soils compacted wet of optimum.

2.1.2. Tests to Characterize Swelling and Shrinkage Variations

Swell and shrinkage characteristics of subsoils will enable engineers and practitioners to select appropriate measures to mitigate pavement distress caused by expansive soils. Expansive soils are mainly characterized based on swell characterization tests. Use of shrinkage tests is limited in practice. However, it is equally important to understand both swelling and shrinkage variations to address related pavement distress issues.

2.1.2.1. SWELL CHARACTERIZATION TESTS

In conventional engineering practice, majority of laboratory swell tests are conducted in oedometer type apparatus with low seating pressures. Descriptions of three direct swell property measurements are provided in the following paragraphs.

2.1.2.1.1. Free Swell Test

The free swell test measures the amount of swell potentials of a soil sample in an oedometer. This test can be conducted to measure swell potentials in vertical direction only or three-dimensionally. Figure 2.11 illustrates the schematic of free swell test set up. Compacted soil specimens prepared at three different compaction moisture contents – dry, optimum and saturated conditions are placed between two porous stones at the top and bottom, covered by a rubber membrane, fully inundated with water at both ends and monitored for the vertical and diametric swell movement until there was no further significant swell occurs over a twelve-hour period. For vertical free swell test, a linear variable displacement transformer (LVDT) is placed on top of the soil specimen to monitor and record free vertical swell movements. The three-dimensional free swell test setup is the same except a LVDT and a dial gauge are used to monitor both vertical and diametric swell movements. All tests should be conducted at room temperature and three identical soil specimens should be used for each variable condition.

The swell pressure test measures the amount of overburden pressures necessary for preventing the expansion of soils. The swell pressure of expansive soils is commonly determined by restraining the soil specimen from undergoing any volume change under fully soaked conditions. Several types of swell pressure tests are reported in the literature including: (1) conventional consolidation test procedure which yields an upper bond value; (2) method of equilibrium void ratio at different consolidation pressures, which gives the least swell pressure;

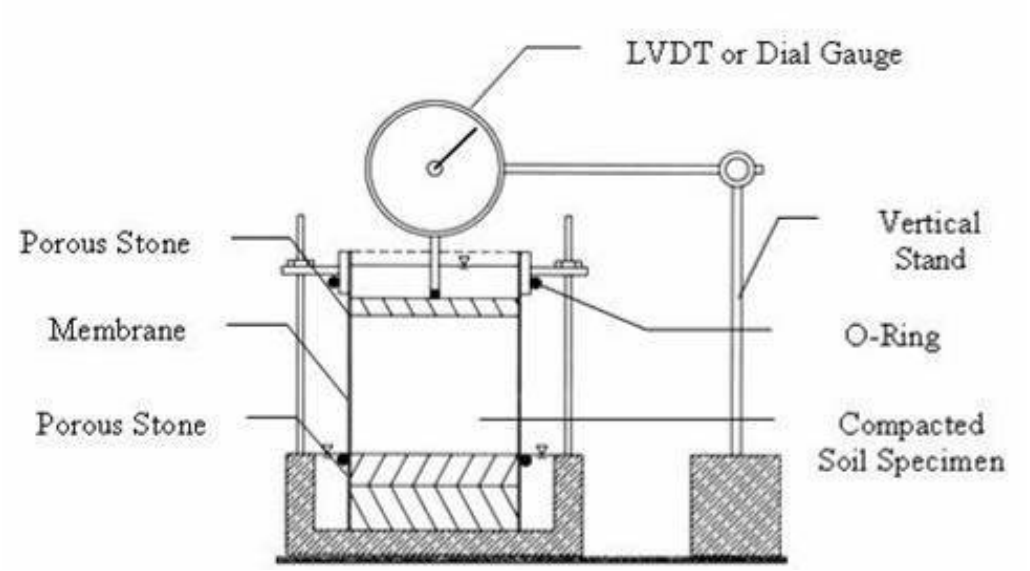

Figure 2.11—Schematic Free Swell Test Setup (Vertical or 3-D)

and, (3) constant volume method, which yields an intermediate value. Further details on these test methods are available in Ohri (2003). Among them, constant volume test is the most frequently used one.

2.1.2.1.2. Swell Pressure Tests

The same oedometer test setup as for free swell test is used to conduct the swell pressure test. The soil specimen placed in the test setup exhibits swell behavior within an hour after full submersion. The free swell recorded will be zeroed by adding loads to the consolidation frame. When the sample does not undergo any swell movement for more than two days, the test is discontinued. Figure 2.12 depicts a swell pressure test apparatus. Water is supplied from the bottom while the specimen is confined. The final total load applied along with the surcharge load is used to determine swell pressures. Ramamurthy (1971) suggested the use of low height cylindrical specimen and a rubber membrane to overcome laboratory test errors caused by side friction and non-uniform distribution of moisture over the soil specimen during saturation.

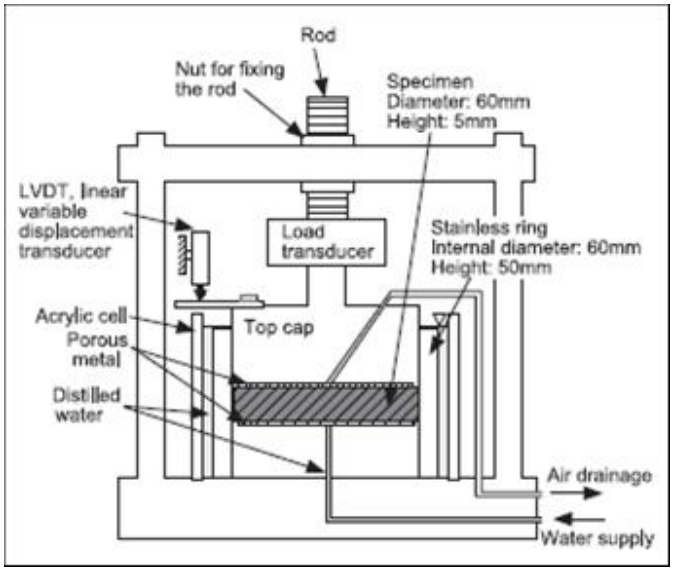

Figure 2.12—Swell Pressure Test Apparatus

2.1.2.1.3. Suction Measurement Tests Using Filter Paper Method

Suction measurements have been recently used to characterize the heave potentials of expansive soils. Soil suction is a macroscopic property which indicates the degree of affinity of the soil towards water. The suction changes associated with the movement of water in the liquid and vapor phases are called matric suction and osmotic suction, respectively. The total suction is equal to the sum of matric and osmotic suction. The filter paper suction test method evaluates the total and matric suction of the soil specimen in the laboratory (Tsai and Petry, 1995). A soil specimen is first cut into two halves and smoothened for establishing a close contact with the filter paper for matric suction measurements. A single filter paper (Schleicher & Schuell No. 589-WH type) is used along with two larger diameter protective filter papers to collect the moisture from the test specimen (Figure 2.13). The moisture contents of the filter papers are calculated to measure both total and matric suctions. Detailed procedural steps are presented in Bulut *et al.*, (2001).

Figure 2.13—Filter Paper Suction Measurement

2.1.2.2. SHRINKAGE CHARACTERIZATION TESTS

2.1.2.2.1. Coefficient of Linear Extensibility (COLE) Test

The COLE test is a shrinkage test used routinely by the U.S. Soil Conservation Service and National Soil Survey Laboratory, for characterizing expansive clays. The COLE test determines the linear strain of an undisturbed, unconfined sample on drying from 5 psi suction to oven dry suction. The procedure involves coating undisturbed soil samples with a flexible plastic resin. The resin is impermeable to liquid water, but permeable to water vapor. Natural clods of soil are brought to a soil suction of 5 psi in a pressure vessel. They are weighed in air and water to obtain their volumes. The samples are then oven dried and another volume measurement is performed in the same manner. The value of COLE is given by:

$$COLE = \Delta L / \Delta L_D = \left(\gamma_{dB} / \gamma_{dM} \right)^{0.33} - 1 \tag{2.3}$$

where $\Delta L/\Delta L_D$ = linear strain relative to dry dimensions; γ_{dB} = dry density of oven dry sample and $\gamma_{\delta M}$ = dry density of sample at 5 psi suction.

2.1.2.2.2. Linear Shrinkage Bar Test

The linear shrinkage bar test gives an indication of the plasticity index of the soil, since the shrinkage ratio of the soil when dried in its plastic state is related to its plasticity index. Linear shrinkage bar test can be used to complement the volumetric shrinkage properties and develop correlations between linear and volumetric shrinkage strains. To perform the test, a wooden or metal box without a top and with a square cross section is filled with soil sample and let dry for seven days or oven dry at 230°F (110°C). The shrinkage ratio can be measured by pushing the dried sample to one end of the box and calculate the length of the gap as a percentage of the length of the box. Shrinkage ratio is calculated using:

$$R_{shrink} = \frac{(L_w - L_d) \times 100}{L_w} \tag{2.4}$$

where R_{shrink} = shrinkage ratio, L_w = length of wet bar, and L_d = length of dry bar.

2.1.2.2.3. Volumetric Shrinkage Strain Test

The linear shrinkage strain test uses small amounts of soils and the rigid wall boxes restrain warping movements in soils observed under field conditions. Puppala *et al.* (2004b) developed 3-D volumetric shrinkage strain test method to overcome these limitations. Soil is first crushed in a pulverizer and then oven-dried for 24 hours. The dried soil is then passed through Sieve No. 40, and the fine fraction of soil is collected and used for soil specimen preparation. The fine soil fraction is mixed with water at target moisture contents. For each moisture condition, soil is compacted in a volumetric shrinkage mold (5.0 in. height and 2.3 in. diameter) and the surface is flattened with a straight edge. For liquid limit state, since the clay is in slurry form, it is poured into the cylindrical molds. The mold with either compacted soil specimen or soil slurry is air-dried for 12 hours and then transferred to an oven (set at 160 °F) for 24 hours. After 24 hours, the average height and diameter of the specimen are measured using

vernier calipers to determine the volumetric shrinkage strains. To determine the volumetric shrinkage strain, the digital images of surface and area pictures of cylindrical soil specimen before and after the shrinkage test are captured by digital camera and analyzed. The parameters extracted are used in Equation 2.5 to determine volumetric shrinkage strains.

$$V.S. = \frac{V_i - V_f}{V_i} = 1 - \frac{V_f}{V_i} = 1 - \left[\frac{A_{sf}}{A_{si}} \times \frac{A_{cf}}{A_{ci}} \times \frac{P_{ci}}{P_{cf}} \right] = 1 - (R_s \times R_c \times R_p) \quad (2.5)$$

where V_i, V_f = initial and final volume of the cylindrical specimen respectively; A_{si}, A_{sf} = initial and final surface area of specimen after shrinkage in pixels; A_{ci}, A_{cf} = initial and final circular area of specimen after shrinkage in pixels; P_{ci}, P_{cf} = perimeter of the initial and final circular area after shrinkage in pixels; R_s = ratio of surface area of the soil specimen = $\frac{A_{sf}}{A_{si}}$; R_c = ratio of circular cross-section area of soil specimen = $\frac{A_{cf}}{A_{ci}}$ and R_p = ratio of the circular perimeter of the soil specimen, which is given by $\frac{P_{ci}}{P_{cf}}$.

Puppala *et al.*, (2004b) concluded that the new method provided higher strains compared to the manual test since irregular and hairline cracks were taken into account.

2.1.2.3. SWELL AND SHRINKAGE TESTS LIMITATIONS

Limitations of swelling and shrinkage tests are mostly test setup related. The swell data obtained from oedometer tests correspond to fully restrained cases and volume change occurs in the vertical direction only. In reality, however, lateral swelling can be significant. Al-Shamrani and Al-Mhaidib (1999) compared field and laboratory data from oedometer tests and found out that about one third of the volume change is reflected as a surface heave, the remainder being lateral change. They also reported that samples used in the oedometer tests are thin, and hence

are exposed to an ideal wetting condition. As a result, for a given soil specimen, the swell percentage and swell pressure obtained from oedometer tests, which are completely saturated, are always greater than the actual values in the field.

Shrinkage strain test and Atterberg limit tests use small amounts of soils, measure linear strains in rigid wall boxes that restrain warping movements in soils, and do not address or simulate compaction moisture levels in the field. Shrinkage behavior in soils, in particular warping type of shrinkage near pavement edges, will induce pressures when their volume changes are restrained by the overlying infrastructure. Such shrinkage-induced pressures are not accounted for in the current design of pavements due to difficulties in measuring them. Also, the accuracy of these tests largely depends on the skills of the operator.

Research show that swell and shrinkage strain measurements and correlations developed for certain conditions are not appropriate for other conditions. Rao and Smart (1980) evaluated four different correlations using ten different soils and showed that none of the correlations considered were able to match the laboratory measurements Similar experiences were reported by Snethen *et al.*, (1977) by testing 20 highly expansive soils based on 17 correlations published in the literature.

2.2. OVERVIEW OF ROAD CONDITIONS AND CLIMATIC EFFECTS

Traffic loading, environmental conditions, subgrade soil, construction and maintenance quality are among the factors that influence pavement performance. Environmental conditions can have a particularly significant impact on the performance of a low-volume road due to its narrow width, inadequate stabilization, poor drainage conditions etc. For expansive subgrades,

moisture content is one of the most significant factors that will affect the subgrade behavior and thus the pavement performance.

A number of studies have been carried out to analyze pavements subjected to different environmental conditions. Rauhut *et al.* (1999) documented the site conditions and design/ construction features of flexible pavements that lead to good performance and those lead to poor performance. Data from the LTPP test sections were used along with findings from previous and ongoing analyses of LTPP data. Separate criteria were developed based on a group of experts' opinions for performance in roughness (IRI), rutting, transverse cracking, and fatigue cracking. In many cases, definitive conclusions about the effects of different pavement characteristics on the occurrence of these four distress types could not be drawn due to their interactive relationships. Table 2.2 summarizes the main finding of the effects of variables on pavement distresses. The "D" entries indicate a decrease in distress with an increase in the variable, and the "I" entries indicate an increase in distress. The question marks "?" indicate that the effects are uncertain or variable.

The Thornthwaite moisture index (Im), which is derived from the moisture balance procedure between rainfall and evapo-transpiration (Thornthwaite 1948), is a widely used approach to characterize climatic effects. Positive values of Im indicate a humid climate with a water surplus where as negative values indicate an arid climate with a water deficit. A moisture index of zero indicates that the annual precipitation is just enough to satisfy the demand of water under prevailing climatic conditions.

Table 2.2—Effects of Variables on Pavement Performance (after Rauhut *et al.*, 1999)

Characteristic	Distress Type			
	Rutting	Fatigue Cracking	Transverse Cracking	Roughness
AC Thickness	D	D	D	D
Base Thickness	D	?	?	?
Air Voids in AC	*	*	*	*
Asphalt Viscosity	I	I	D	I
Base Compaction	?	?	?	I
Structural Number	D	D	?	D
Expected ESALs	I	I	I	I
Annual No. of Days with Temp.> 32^{o}C	I	D	D	?
Freeze Index	?	?	I	I
Annual No. of Freeze-Thaw Cycles	?	?	I	I
Annual Precipitation	I	I	I	?
Subgrade < No. 200 (75μm)	?	?	?	I
Annual Days with Freezing Temp.	D	?	I	?
Age	?	?	I	?

* Only initial air voids are controllable but the data available are for air voids after consolidation by traffic.

2.3. REMEDIATION STRATEGIES FOR EXPANSIVE SOILS

Ideally the subgrade should be strong enough to prevent excessive rutting and shoving and sufficiently stiff to minimize resilient deflection. However, for fine-grained silt and clay soils, poor strength, high volumetric instability, and freeze/thaw durability problems are predominant. For expansive soil the volumetric change may be more severe and thus become a bigger challenge. The expansion action may result in intolerable differential heaving of pavements. Commonly used remediation methods can be categorized into two groups: (1) to improve strength and (2) to minimize moisture variation. In order to improve soft subgrade bearing capacity and strength, thick layers of granular material may be used on top of the problematic subgrade. In other instances, stabilization and geosynthetic reinforcement can be used. On the other hand, to minimize moisture variations and fluctuations, following are the commonly used strategies summarized by Raymond and Ismail (2003):

- Treat the expansive soil with lime or other additives to reduce expansion in the presence of moisture;
- Replace the expansive material with a non-expansive material to a depth below which the seasonal moisture content will remain nearly constant;
- Provide an overlaying structural section of sufficient thickness to counteract the expansion pressure by surcharge;
- Stabilize the moisture content by minimize the access of water through surface and subsurface drainage and use waterproof membrane such as rubberized asphalt membrane, geosynthetics. Put moisture barrier and/or remove nearby vegetations.
- Relocate the project to a more favorable soil condition.

The following sections will discuss different remediation methods. For the scope of this research, relocation is not an option and will not be considered further.

2.3.1. Admixture Stabilization

Admixture stabilization refers to mixing and blending a liquid, slurry, or powder with soil to improve soil strength and stiffness properties. One of the most commonly used method of reducing the shrinking or swelling is stabilization with calcium based stabilizer.

Lime stabilization is a widely used means of chemically transforming unstable soils into structurally-sound construction foundations. Lime stabilization creates a number of important engineering properties in soils, including improved strength; improved resistance to fracture, fatigue, and permanent deformation; improved resilient properties; reduced swelling; and resistance to the damaging effects of moisture. The most substantial improvements in these properties are seen in moderately to highly plastic soils, such as fat clays (Little, 2000). Little

(1999) claimed that lime stabilization often induces a ten fold stiffness increase over that of the untreated soil or aggregate. Croft (1967) found that the addition of lime significantly reduces the swelling potential, liquid limit, plasticity index and maximum dry density of the soil, and increases its optimum water content, shrinkage limit and strength.

Cement has been found to be effective in stabilizing a wide variety of soils, including granular materials, silts, and clays; byproducts such as slag and fly ash; and waste materials such as pulverized bituminous pavements and crushed concrete. These materials are used in pavement base, subbase, and subgrade construction (Little, 2000). It is generally more effective and economical to use it with granular soils due to the ease of pulverization and mixing and the smaller quantities of cement required. Fine-grained soils of low to medium plasticity can also be stabilized, but not as effectively as coarse-grained soils. If the PI exceeds about 30, cement becomes difficult to mix with the soil. In these cases, lime can be added first to reduce the PI and improve workability before adding the cement (Hicks, 2002). Addition of cement to clay soil reduces the liquid limit, plasticity index and swelling potential and increases the shrinkage limit and shear strength (Nelson and Miller, 1992).

Fly ash is defined in Cement and Concrete Terminology (ACI Committee 116) as "the finely divided residue resulting from the combustion of ground or powdered coal, which is transported from the firebox through the boiler by flue gases." Fly ash is a by-product of coal-fired electric generating plants. Two main types of fly ash are being used: non self-cementing Class F and lime-fly ash self-cementing Class C. Stabilization of soils and pavement bases with coal fly ash is an increasingly popular option for design engineers. Fly ash decreases swell potential of expansive soils (Ferguson 1993, White *et al.*, 2005a, b). Soils can be treated with self-cementing fly ash to modify engineering properties as well as produce rapid strength gain in

unstable soils. Tests results show that fly ash increases the compacted dry density and reduces the optimum moisture content (White *et al.*, 2005a). Fly ash can also dry wet soils effectively and provide an initial rapid strength gain, which is useful during construction in wet, unstable ground conditions. Çoçka (2001) found that plasticity index and swell potential decrease with increasing fly ash contents. The fly ash addition rates greater than 20% are comparable to lime addition rates of 8% for reducing plasticity and ultimately swell potential in the example soil. Fly ash increases the CBR of fine-grained soils, and in the case of 20% fly ash addition, the CBR can be increased up to 75%. However, Ferguson (1993) noted that the decrease in plasticity and swell potential was generally less than that of lime because fly ash did not provide as many calcium ions that modify the surface charge of clay particles.

Lime and lime fly ash stabilized materials cure much slower, in general, than portland cement stabilized layers. As with strength properties, resilient properties of lime-soil mixtures are very sensitive to level of compaction and molding moisture content. Lime-stabilization may substantially increase shear and tensile strengths. This strength increase provides a stiffer layer with improved load distributing capabilities. However, as the stiffness of the layer increases through the development of cohesion within the stabilized layer, the layer becomes more susceptible to load-induced tensile stresses that can lead to fatigue failure unless proper design steps are taken to reduce the potential of load induced damage. This is generally accomplished by ensuring that the layer thicknesses are such as to insure the development of acceptable flexural stresses within the stabilized layer. Typically the design parameter is the flexural tensile stress ratio. Thompson (1966) determined that the indirect tensile strength of lime-soil mixtures is approximately 0.13 times the unconfined compressive strength. Chou (1987) stated that the

flexural tensile strength of lime-soil mixtures is approximately 0.25 times the unconfined compressive strength.

For sulfate rich soils, a phenomenon called sulfate-induced heave can happen that can severely reduce the long-term strength and durability of stabilized soil. Sulfate concentration can be determined in accordance to Tex-145-E. If the sulfate levels are above 3000 ppm, further recommendations and guidelines can be found in the 'Guidelines for Treatment of Sulfate-Rich Soils and Bases in Pavement Structures Soils' by TxDOT. Puppala *et al.* (2004a, 2003) studied the effectiveness of sulfate resistant stabilizers such as cement Types I/II, V, lime mixed with fibers and Class F fly ash in providing better treatment of sulfate rich soils. Test results indicate sulfate-resistant cement provided the most effective treatment. The combined lime and fibers stabilization method provided the next best effective treatment. The Class F fly ash treatment provided low-to-moderate strength improvements that could be attributed to the low amounts of calcium present in this type of fly ash. On the other hand, the fly ash stabilization method was more cost-effective than the other methods. Kota *et al.* (1996) provide some suggestions to minimize the damage caused by sulfates and calcium-based stabilizers such as double application of lime, use low calcium stabilizers (e.g. cement and fly ash), use non-calcium stabilizers, geosynthetic soil reinforcement, stabilization of the top with non-sulfate select fill, pretreatment with barium compounds, asphalt stabilization of the sulfate bearing soils and compacting to lower densities.

Organic contents in the soil are another consideration when selecting stabilization additives. Organic soil is a soil that would be classified as a clay or silt except that its liquid limit after oven drying (dry sample preparation) is less than 75% of its liquid limit before oven drying (wet sample preparation). Organic content can be determined in accordance to ASTM D-2974. If

the organics content exceeds 1%, additional additive will need to be added to counter the cationic exchange capacity of the organic material.

Use of aqueous solution has been investigated as an alternate stabilization method by some researchers. Pengelly and Addison (2001) used potassium and ammonium as cations and mixed them in a solution of water to modify clays beneath an existing building structure. Clays treated with potassium and ammonium consistently reduced swelling at lower moisture contents. Additionally, swell caused by the introduction of an aqueous solution containing potassium and ammonium was consistently lower than that caused by water alone. Mowafy *et al.* (1985) also suggested that injection of salt solutions could be a possible remediation method to overcome swelling problem, if the soil permeability is sufficiently high.

Although chemical stabilization has proven successful in increasing the strength of the natural expansive soils by twenty to fifty times, and is widely used throughout Texas, situations arise where above mentioned approaches cannot be used. For example, chemical stabilization cannot be used when the temperature is below 40^{o}F and in cases there are not enough time for curing before traffic is routed back (Hopkins *et al.*, 2005)

2.3.2. Moisture Control

For most swell and shrinkage related pavement problems, the source comes from fluctuations in moisture content. It is obvious that the most effective remediation method is to control and minimize seasonal moisture variations.

Moisture barriers have been used in many cases with the intention to control soil movements generated from expansive subgrades. Horizontal moisture barriers are designed to stop rainwater from penetrating into the subgrade soils. By reducing moisture variance, soil

swelling should be reduced and pavement smoothness should be better maintained. However, based on a study by Browning (1999), horizontal moisture barriers did not produce a smoother ride than the unprotected pavement in the roughness tests nor reduce the moisture variance. Jayatilaka *et al.* (1993) suggested that sites in wet and semi-arid climates, with cracked clay soils and shallow root zones, will show the greatest benefit from using vertical moisture barriers. The role of a vertical moisture barrier is to stop the seasonal lateral migration of moisture to and from the subgrade beneath the pavement, thus preventing the subgrade from expanding during wet periods and shrinking during dry periods (Picornell and Lytton, 1986). The main drawback of vertical moisture barrier is the high expense and complicated construction. Using vertical moisture barriers has usually only been reserved for major highways. Evans and McManus (1999) reviewed current vertical moisture barrier construction methods in the United States and developed a new economical barrier construction method for low-volume roads that consist of a spray seal surface over low-quality base and subgrade in Australia. The cost of this new barrier is about $3.10 per linear foot. Further details of this new barrier can be found in the technical memorandum.

One of the most important aspects of a successful road design is drainage. Rollings and Christie (2002) noticed that the lack of adequate surface drainage is one of the critical factors leading to problems with both collapsible and expansive subgrade soils. Some obvious drainage problem signs should be monitored such as water ponding in the drainage ditches, soft spots in the ditch, or the presence of plants and weeds that grow best in saturated or submerged environments. The new Mechanistic-Empirical (M-E) Design Guide (AASHTO, 2002) recommended improving surface drainage by lowering the ground water level, intercepting the lateral flow of subsurface water beneath the pavement structure, and removing the water that

infiltrates the pavement's surface. To be more specific, special solutions should be considered when feasible. For instance, where climate is suitable, it may be possible to place a permeable layer over a swelling soil and limit or prevent drainage from it. Moisture buildup in this layer maintains the soil in a stable, saturated condition. Drainage ditches, sloped sections, water bars, cross-drains and inlet-outlet protections are recommended so that water does not accumulate in the median.

Vegetation transpiration may significantly decrease the moisture content of active soils and cause shrinking and deformation. Researchers reported that climatic extremes played a major role in causing and exacerbating damage to pavements and lightly-loaded structures, and that large vegetation often interacts with climatic extremes to heighten the problem (Ravina, 1984 and Snethen, 2001). Researchers believe that types and locations of trees should be considered in landscaping decisions, particularly involving soil having LL > 40 and PI > 25. Base upon the relative average rank analysis, the most influential trees are in the order of Poplar, Elm, oak, and Ash. Experience and observations show that these types of trees should be planted at 1.6 to 3.3 ft (0.5 to 1.0 m) beyond the anticipated mature drip line or the anticipated mature height of the tree from pavements or pavements or building foundations (Snethen, 2001). Chen and Tian (1985) suggested using a lime trench between the structure and the tree to create a moisture transfer barrier. The depth of the trench should be 6.5 ft (2 m) and the lime fillings should be 4 to 8 in. (10 to 20 cm). The first "proximity rule" of distance to height of tree ratio (D:H) greater than one are widely used to avoid soil shrinkage settlement and damage to structures (Ward, 1953; Biddle, 1983 and 2001; Tucker and Poor, 1974) In New Zealand, Wesseldine (1982) indicated a threshold value of D:H of 0.75 for single trees to cause damage and 1.0 to 1.5 for groups of these trees.

2.3.3. Geosynthetics

2.3.3.1. OVERVIEW

The adoption of geosynthetic for pavement aims to improve long-term bearing capacity and performance of the road. There are eight types of geosynthetics: geotextiles, geogrids, geonets, geomembranes, geosynthetic clay liners, geopipe, geofoam, and geocomposties (Koerner, 2005). Geotextiles and geogrids are the most popular types of geosynthetics used in the road construction industry. Geotextiles are textiles consist of synthetic fibers rather than natural ones. These synthetic fibers have woven, non-woven, or knitted textile fabric. Geogrids are plastics formed into a very open, grid-like configuration. Geofoams are lightweight foam blocks that can be stacked and provide lightweight fill in numerous applications. Geocomposites consist of a combination of geotextiles, geogrids, and/or other geosynthetics in a factory-fabricated unit.

Geogrids have higher tensile strengths than geotextiles. Geogrids should be used on weak subgrades with CBR values less than 3 (Tutumluer *et al.*, 2005). According to the SpectraPave2™ analysis results, the use of geogrids can effectively reduce the aggregate base thickness requirements when compared to the unreinforced section results. Geogrids with higher tensile strength and high aperture stability moduli were found to give overall higher geosynthetic stiffness and hence work better than geotextiles (Giroud and Han, 2004a, b). Stiff biaxial geogrids were first used for the reinforcement of pavement in 1982 at Canvey Island, near London, England to control reflective cracking and use of geogrids and geotextiles is becoming more common nowadays (Austin and Gilchrist, 1996).

The four major functions of geosynthetics used for pavements are: reinforcement, separation, filtration and drainage. Adding a geosynthetic layer can increase bearing capacity of

a pavement structure by forcing the potential bearing capacity surface to develop along alternate, higher shear strength surfaces. The geosynthetic reinforcement can absorb additional shear stresses which would otherwise be applied to the problematic subgrade. If rutting occurs, geosynthetic reinforcement is distorted and thus tensioned. Due to its stiffness, the curved geosynthetic exerts an upward force supporting the wheel load and thus the lateral restraint and/or membrane tension effects may also contribute to load carrying capacity (Hufenus *et al.*, 2006).

Geosynthetics have been used successfully for many pavement projects. Their benefits include: extend service life, reinforce and inhibit reflection of cracks, facilitate compaction, improve bearing capacity, reduce necessary fill thickness, diminish deformations, delay rut formation, prevent water penetration to subgrade and reduce subgrade moisture susceptibility (Gurung, 2003; Hufenus *et al.,* 2006; Steward *et al.*, 1977).

2.3.3.2. DESIGN APPROACHES

The inclusion of geosynthetics in flexible pavement design is difficult since number of uncertainties arise when geosynthetics is applied under distress. The absence of an accepted design technique explains why this topic is still being researched despite the use of geosynthetics in pavement design and construction over many years ago. Following sections summarized methods and procedures identified in the literature search. These approaches shed some light on (1) Where to place geosynthetics layer; (2) How to decide required thickness of aggregate; and (3) How to select appropriate geosynthetic type and appropriate strength to prevent pavement failure, or rutting, under traffic stresses.

2.3.3.2.1. Location to Place Geosynthetics

The four main applications for geosynthetics in roads are overlay stress absorption, overlay reinforcement, base reinforcement, subgrade separation and stabilization. Based on their main targeted function, geosynthetics can be placed below or within the overlay, within base layer, near base-subgrade interface, or within subgrade layers. In this research, the main focus will be improvement of soft and expansive subgrade soils. For low-volume roads, typically there will be an asphalt surface layer over an aggregate base layer. The combined surface and base layers act together to support and distribute traffic loading to the subgrade. However, weak clayey subgrades are often water sensitive and, when wet, may soften and deflect. Tensile stresses will develop at the bottom of the granular layer, which will cause deep rutting and eventually, pavement cracking (Hopkins and Sharpe, 1985; Hopkins and Beckham, 2000). To lessen, or prevent, rutting of the aggregate layer during construction, or cracking due to base deflection after construction, geosynthetics may be placed at, or near, the bottom of the granular base, or on top of the finished subgrade (Figure 2.14). Use of geosynthetic reinforcement in such situation is gaining favor (Hufenus *et al.*, 2006; Hopkins *et al.*, 2005)

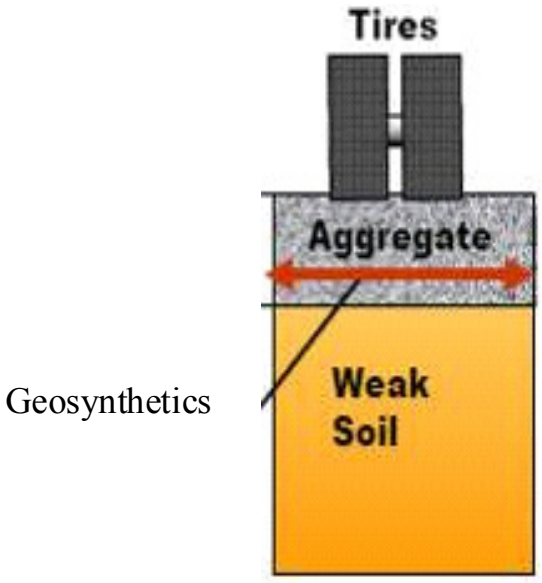

Figure 2.14—Improving Pavement by Using Geosynthetics (from Hopkins *et al.*, 2005)

2.3.3.2.2. Calculation of Required Aggregate Thickness

A structural evaluation and design procedure was recently proposed for thin asphalt roads in the Netherlands by van Gurp and van Leest (2002). This design methodology takes into account cracking and deformation aspects of the base course. Required thickness of the base course can be calculated from:

$$h_d = \frac{125.7\log(N_{constr}) + 496.52\log(P) - 294.14RD_{constr} - 2412.42}{f_{undr}^{0.63}} \quad (2.6)$$

where h_d = desired total base thickness in construction stage (m); N_{constr} = number of axle loads in construction stage; P = average axle load in construction stage (N); D_{constr} = allowable rut depth at surface in construction stage (m); f_{constr} = undrained shear strength of subgrade (Pa) = (20 or 30)*CBR. A factor of 20 is used to estimate CBR, when the ground water level is high, and a factor of 30 is used when the ground water table is deeper than 0.5 m below the bottom of the base course.

The FHWA design method (Holtz *et al.*, 1998) uses bearing capacity factor (N_c) to obtain required aggregate thickness from design charts. This design guideline, in general, is limited to a subgrade unconfined compressive strength of less than 13 psi (90-kPa, approximately a CBR of 3). For certain amount of rutting that occur under various traffic conditions, both with and without geosynthetics, the stress level acting on the subgrade can be expressed in terms of the bearing capacity factor. Table 2.3 summarizes typical bearing capacity factors used by FHWA method based on the tolerable rut depth and the number of axle passes.

Table 2.3—Typical Bearing Capacity Factors Used by FHWA Design Method

Condition	Ruts (mm)	Traffic (ESALs)	Bearing Capacity Factor, N_c
Without Geotextile	< 50	> 1000	2.8
	> 100	< 100	3.3
With Geotextile	< 50	> 1000	5.0
	> 100	< 100	6.0

The FHWA design method is independent of geosynthetic product material properties. The following design procedure is recommended to obtain required aggregate thickness:

Step 1. Determine soil subgrade strength using CBR, vane shear test or any other appropriate test. The undrained shear strength of the soil, *c*, in kPa can be obtained by: *c=30*CBR*; or can be measured directly from vane shear test.

Step 2. Determine subgrade strength at several locations and at different times of the year to obtain a good average value. Assess need for geotextiles.

Step 3. Determine the maximum wheel loading anticipated for the roadway during the design period.

Step 4. Estimate the maximum amount of traffic anticipated for each design vehicle class.

Step 5. Establish the amount of tolerable rutting during the design life of the roadway. For example, 50 to 75 mm of rutting is generally acceptable during construction.

Step 6. Obtain bearing capacity factor from Table 2.3.

Step 7. Determine and select required aggregate thickness from the USFS design charts (Figure 2.15, 2.16 and 2.17) for each maximum loading. Enter the curve with appropriate N_c (from step 6) multiplied by c (from step 1.) to evaluate required stress level (cN_c). The required aggregate thickness can then be determined from the design charts. Select design thickness to the next higher 25 mm.

Step 8. Check geotextile drainage and filtration requirements. (Table 2.4)

Step 9. Determine geotextile survivability requirements. The stresses applied to the subgrade and the geotextile during construction may be much greater than those applied in service by traffic. Therefore, selection of the geotextile in roadway applications is usually governed by the anticipated construction stresses. The concept of geotextile survivability meaning the geotextile must survive the construction operations if it is to perform its intended function. Table 2.4 listed default geotextile property requirements in stabilization applications.

Step 10. Specify geotextile properties that meet or exceed survivability criteria.

Step 11. Specify construction recommendations.

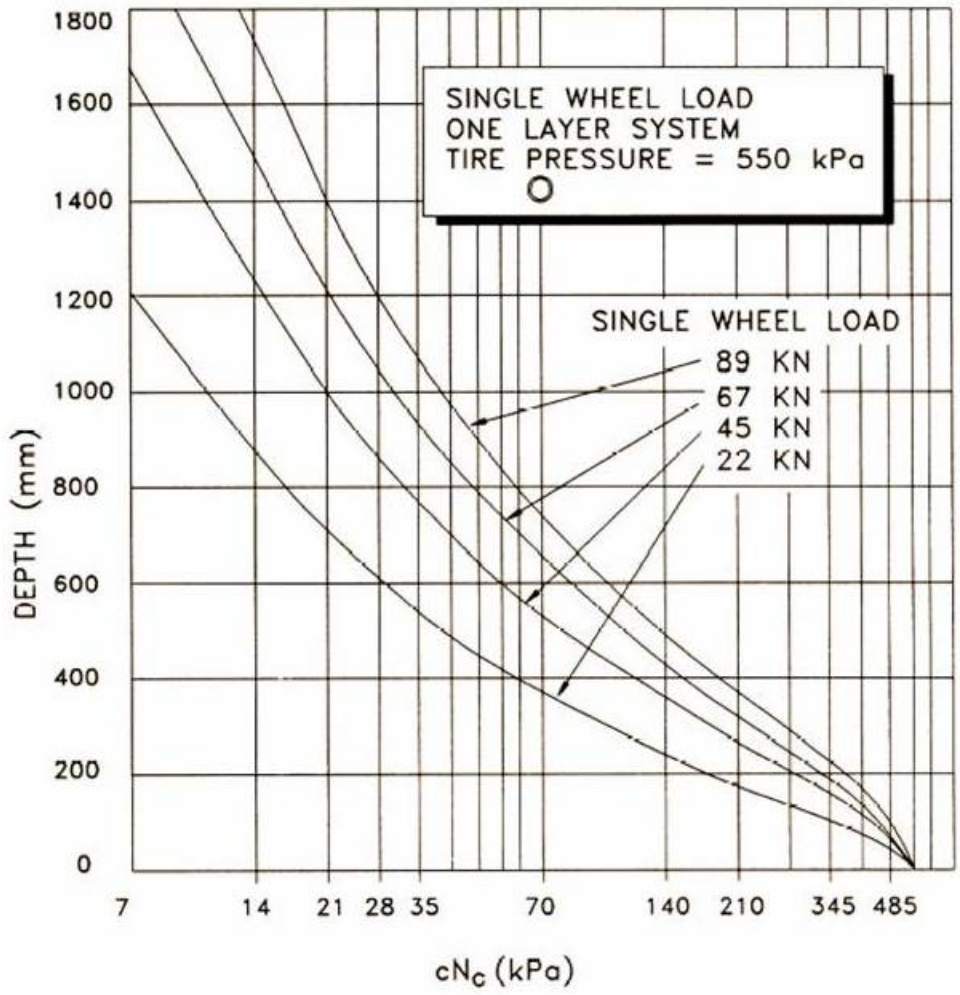

Figure 2.15—US Forest Service Thickness Design Curve for Single Wheel Load (from Steward *et al.*, 1977)

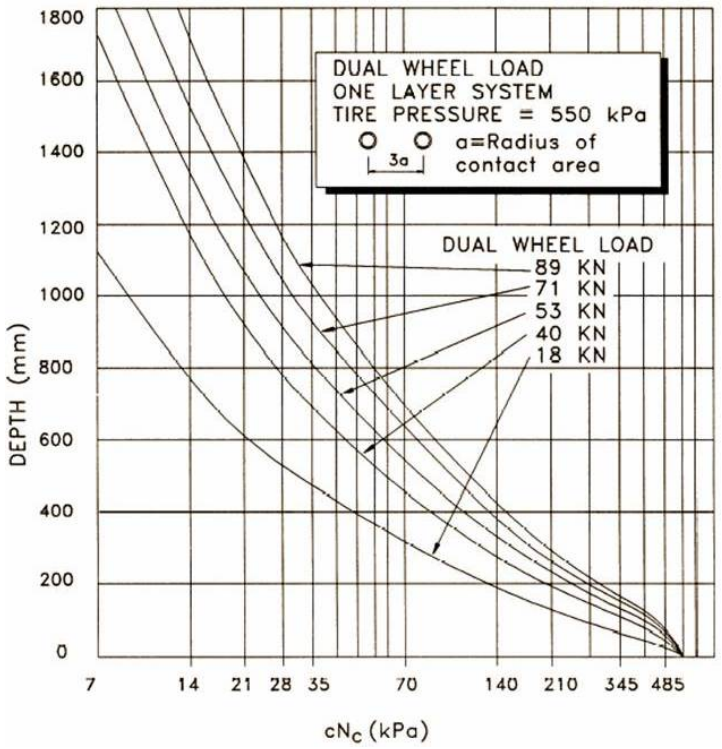

Figure 2.16—US Forest Service Thickness Design Curve for Dual Wheel Load (from Steward *et al.*, 1977)

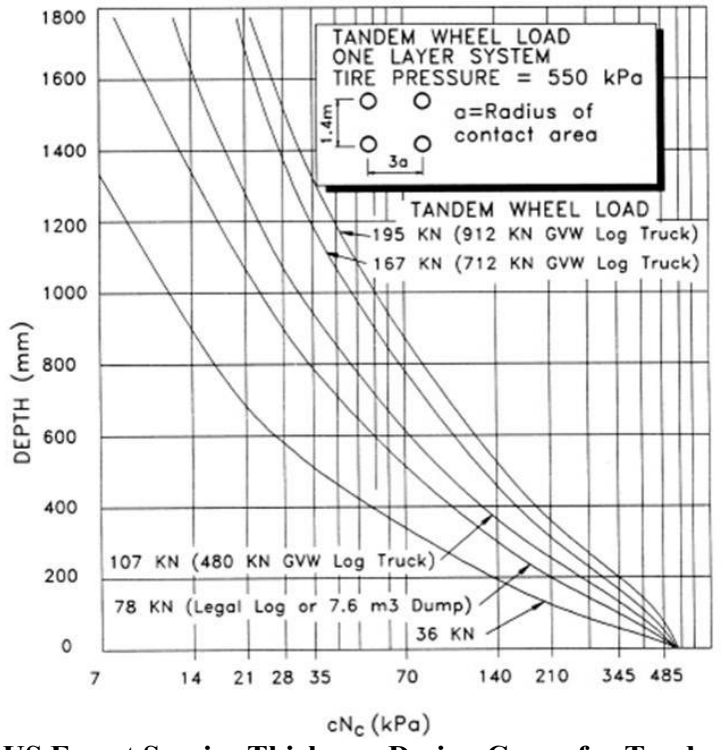

Figure 2.17—US Forest Service Thickness Design Curve for Tandem Wheel Load (from Steward *et al.*, 1977)

Table 2.4—Geotextile Property Requirements in Stabilization Applications (after AASHTO, 1997)

Property	ASTM Test Method	Units	Requirement	
Survivability			Geotextile Class 1 (Note 1)	
			Elongation	
			< 50%	> 50%
Grab Strength	D4632	N	1400	900
Sewn Seam Strength (Note 2)	D4632	N	1200	810
Tear Strength	D4533	N	500	350
Puncture Strength	D4833	N	500	350
Burst Strength	D3786	kPa	3500	1700
Ultraviolet Stability (Retained Strength)	D4355	%	50% after 500 hr of exposure	
Drainage and Filtration (Note 3)				
Apparent Opening Size	D4751	mm	< 0.6 for $P200 < 50\%$; < 0.3 for $P200 \geq 50\%$	
Permittivity	D4491	Sec^{-1}	0.5 for $P200 < 15\%$; 0.2 for $15\% \leq P200 \leq 50\%$: 0.1 for $P200 > 50\%$	

Other relationships to calculate required aggregate thickness include Giroud-Han method (1981, 2004a, b), effective factor method (Koerner, 2005), structural number method (modified AASHTO method by Carroll *et al.*, 1987) and U.S. Army Corps of Engineers Method (developed by Steward *et al.*, 1977). Detailed information about these methods is summarized elsewhere (Wanyan, *et al.,* 2006)

2.3.3.2.3. Selection of Appropriate Geosynthetics

In most of the available design methods, it is assumed that each geosynthetic type produces approximately the same reduction/benefit in subgrade stress. Therefore, the most important criteria used in the selection of the appropriate geosynthetics are the fabric construction, drainage properties, long-term survivability and cost considerations. Table 2.5 gives an example of suggested appropriate geotextile for different survivability levels. Data are

summarized by Cicoff and Sprague (1991) based on their test results of using lightweight geotextiles as permanent road stabilization.

Table 2.5—Geotextile Specifications for construction Survivability in Low-Cost Low-Volume Roads (from Cicoff and Sprague, 1991)

Survivability Level	Subgrade Conditions	Base course Thickness*	Geotextile Mass/Area
Low	Dry, firm, flat	> 6" compacted	4 oz/sy
Moderate	Water sensitive, flat	> 3"-4" compacted	6 oz/sy
High	Water sensitive, grade>2%	> 3"-4" compacted	8 oz/sy

* For base course lifts less than 3", required survivability should be increased one level (i.e. low to moderate).

2.3.3.3. BENEFIT OF USING GEOSYNTHETICS

The benefits of using geosynthetics in flexible pavement system were presented by many researchers. However, there is still a lack of understanding about the behavior of the composite system. A quantified structural contribution by using geosynthetics is yet to be developed and incorporated into pavement design methodology.

Use of geosynthetics inclusions in both wet and dry conditions increased tensile strength of the subsoil (Gurung, 2003; Abd El Halim *et al.*, 1983). The placement of a geotextile beneath an aggregate section increases the permissible stress on a subgrade by a factor of 1.64 to 2.0. (Steward *et al.*, 1977; Giroud and Noiray, 1981) Similar result is reported by Montanelli, *et al.* (1999) with an increased 1.5 to 2 structural layer coefficient of geogrid reinforced flexible pavement. The authors of the RACE design software (www.geotextile.com) therefore recommended using an average design improvement factor of 1.8. Kwon, *et al.* (2008) proved the technical response benefit of using geogrids in pavement base course reinforcement based on a full-scale test study. Much lower subgrade vertical deformations and base course vertical and horizontal deformations were measured in the geogrid reinforced section when compared to the deformations recorded for the unreinforced control section. Cicoff and Sprague (1991) concluded

that geosynthetics may or may not enhance initial pavement performance, but will likely enhance future pavement performance. However, the benefit data could not be utilized for section to section comparisons, measured values of stress, strain and deflection are highly case specific.

2.3.4. Other Remediation Methods

2.3.4.1. Deep Dynamic Compaction

Almost all compacted soils have a tendency to expand and produce uplift pressures of considerable intensity when given access to water. An increase in initial moisture content will reduce the magnitude of swell and swell pressure (Mowafy *et al.*, 1985). In order to reduce swell and swell pressure, compaction should occur at higher moisture content. Deep dynamic compaction is used to maximum unit weight and density of soils. This solution may be temporary due to water infiltration. Deep dynamic compaction treatment was considered as one of the most economical in-situ soil improvement methods available which is approximately $1 to $1.20 sq ft of surface area (Rollins and Christie, 2002).

2.3.4.2. Undercut and Backfill

The Highway Subgrade Stability Manual for Illinois DOT suggested undercut and backfill to be used as a remedial procedure for soft subgrade. The procedure is to cover the soft subgrade with a thick layer of granular material or to remove a portion of the soft material to a predetermined depth and replace it with granular material. The undercut and backfill method is a simple procedure that does not require any specialized equipment, it can be used for large scale treatments and when the backfill material is readily available, this method is relatively inexpensive (Thompson, 1982).

Ahlvin (1962) used Equation 2.7, developed by the Corps of Engineers, to approximate the required depth of granular backfill material:

$$t = F\left[P\left(\frac{1}{8.1CBR} - \frac{1}{p\pi}\right)\right]^{1/2} \tag{2.7}$$

where t = thickness of material layer required (in); P = single or equivalent single wheel load (lb); CBR = California bearing ratio of underlying subgrade soil; p = tire contact pressure (psi); $F=0.23logC+0.15$; and C = number of load repetitions.

2.3.4.3. Decreasing Clay Content by Soil Mixing/Dilution

Mowafy *et al.* (1985) suggested a reduction of swelling potential can be achieved by decreasing the clay content of the problematic soil. For a given initial water content and normal pressure, there is a "critical" clay content at which the amount of swell is zero. Below the critical value the soil will shrink and above that the soil is susceptible to swelling. To accomplish the controlled clay content, the swell-susceptible clay soils could be mixed with coarse fractions of granular materials in the field.

Hudyma and Burcin Avar (2006) also suggested the use of soil mixing to mitigate expansive soils is a promising yet not very well documented modification technique. By mixing two different expansive soils from southern Nevada with different percentage of fine-grained silica sands the plasticity index were decreased by up to 75%, which changed the expansive soils into low-PI non-expansive soils. A simple predictive equation was developed to estimate the PI of the mixture (Equation 2.8).

$$PI_{mixture} = PI_{\exp.soil}V_{\exp.soil} + PI_{sand}V_{sand} \tag{2.8}$$

In their study, Hudyma and Burcin Avar used swell index (or swell pressure in kN/m^2) to quantify the swell potential change. Equation 2.9 shows the generic empirical predictive equation:

$$SwellIndex_{mixture} = SwellIndex_{\exp.soil} - 5\left(\frac{\%Sand}{10}\right)^{2.0} \quad (2.9)$$

Using of mixing or dilution technique to mitigate the effects of expansive soils is only feasible when it can be justified by economics. The process of diluting expansive soils with non-expansive fill would be less time consuming and cheaper compared to undercut and backfill when quantities of non-expansive fills are limited.

2.3.4.4. WATERBOUND MACADAM BASE

Waterbound macadam is widely used in South Africa in 40s and 50s. The single-sized coarse aggregate is placed and compacted separately on a prepared subbase before the voids are filled with fines, and the material is then compacted and slushed (Horak, 1983). Due to the high cost and labor-intensive construction, usage of this type of construction declined. However, roads with waterbound Macadam bases have shown excellent performance and in wet regions of South Africa, this kind of bases could withstand destructive influence of water and heavy traffic better than other granular base and also can provide efficient drainage as a drainage layer. Waterbound Macadam base can provide high shear force resistance due to the coarse granular interlock (Horak and Triebel, 1986). Thompson (1979) pointed out the following two conditions must be satisfied for a success use of this remediation method. First, the granular layer must be thick enough to develop acceptable pressure distribution over the problematic subgrade and second, the backfill material—coarse aggregate must be able to limit rutting under the applied wheel loads to acceptable levels.

2.4. CURRENT PAVEMENT DESIGN SOFTWARE AND LIMITATIONS

Typical low-volume road consists of a thin asphalt top layer, a flexible base layer and sometimes a treated subbase/subgrade over compacted subgrade. Currently in Texas, there is no specific design programs specially targeted for low-volume roads. General purpose flexible pavement design methods are used instead.

The Flexible Pavement System (FPS) software (Scullion and Michalak, 1998) is primarily used for designing pavements in Texas. The current version, called FPS19, uses the backcalculated layer moduli from the Falling Weight Deflectometer (FWD) along with the measurements and the expected number of 18-kip equivalent single axle loads (ESALs) to determine the design thicknesses for the specified pavement materials. Other design input parameters required for the FPS19 are the traffic volume, environmental region, detour type, serviceability levels, reliability, and new material properties. FPS19 can be used for both high-volume and low-volume flexible pavements. It doesn't incorporate special procedures for different types of subgrade. Subgrade properties used include subgrade modulus and swelling potential. As for the high-PI clay subgrades, the FPS program counteracts probable heaving problems with thicker layers, which provide bigger vertical surcharge. For low volume roads, the structural adequacy of the design to protect subgrade shear failure can be further verified using the Modified Texas Triaxial design method. For low-volume roads build over highly expansive subgrade, this program tends to yield pavement structures with unreasonably thick layers.

The Texas Triaxial design method is used to determine the required minimal pavement cover depth (total thickness above subgrade) to ensure against subgrade shear failure due to heavy wheel loads. This method is fully described under the Test Procedure Tex-117-E. Based on the type of the material, different classification methods are used. After materials are

classified, the thickness design can be performed based on the classification, the current and forecasted traffic, and design wheel load. The required design depth can be reduced whenever stabilized layers are used in the pavement structure. From experience, this method results in relative more conservative designs compared to FPS on low-volume roads.

Fernando *et al.* (2001) developed an alternative method for the Triaxial design check (MTRX). MTRX incorporates the layer moduli backcalculated from FWD deflections and strength properties determined from Texas Triaxial tests. Layered elastic theory is used to predict stresses under applied wheel loads, with the option of characterizing pavement materials as linear or nonlinear (stress-dependent). Mohr-Coulomb failure criterion is used to check potential for pavement damage for the specified materials and wheel loads. These features provide a greater flexibility in analyzing different materials and allow engineers to use the same moduli specified in FPS19 for the Texas Triaxial design check. In addition, engineers can directly consider the effects of varying moisture conditions on subgrade strength/stiffness. So far, the indication is that the MTRX method yields required minimal base thickness to prevent subgrade shear failure, which is also relatively more conservative then FPS19 result, but less redundant compared to Texas Triaxial method. MTRX is currently being validated and modified to yield more realistic results.

To summarize, currently in Texas, flexible pavement design programs used are not specially targeted for lower classification roads, and provide no extra considerations for problematic high PI subgrades. Thus, low-volume roads tend to be overly-designed structural wise (strength/stiffness) but not adequately considered performance wise, especially for those problems caused by subgrade volumetric change.

2.5. EXPERT SYSTEM

Expert systems were developed by artificial intelligence researchers during the late 1970s. The early applications were originally termed "expert systems" because they were intended to approach problem solving and analysis in a similar manner, and with similar results, as that of human experts. An expert system is a knowledge-based system whose performance is intended to rival that of human experts while being highly domain specific. It can be used to record and distribute scarce expert knowledge, to apply the expert knowledge to remote locations, to ensure the quality of problem solving, and to train experts out of ordinary people.

2.5.1. Overview

Figure 2.18 illustrates the typical building blocks of an expert system which include: inference engine, knowledge base, explanation subsystem, and a user interface subsystem. The user supplies facts or other information to the expert system and obtains expertise in response by accessing the knowledge base through the system's user interface via the inference engine. Internally, the expert system consists of three main components. The knowledge base contains the knowledge with which the inference engine draws conclusions. These conclusions are the expert system's responses to the user's queries for expertise. The explanation block is one of the most attractive attributes of an expert system. Since the system remembers its logical chain of reasoning, a user may ask for an explanation of a recommendation and the system will display the factors it considered in providing a particular recommendation. This attribute enhances user confidence in the recommendation and acceptance of the expert system.

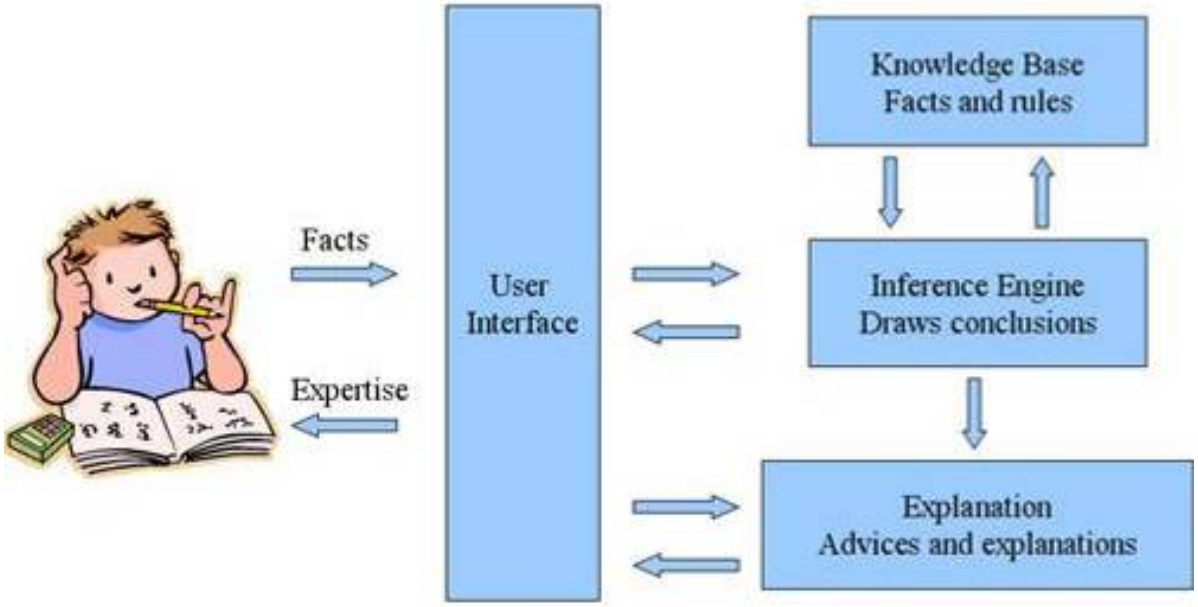

Figure 2.18—Typical Expert System Components

2.5.2. Development Requirement

Turban (1990) pointed out an expert system may be suitable for the following types of problems that are cognitive, well understood and defined with narrow domain, with data available, intended for training purpose, aiming to improve performance or quality related issues and not too complicated or time consuming. He also summarized the methodology of building an expert system into the following steps:

1) Problem identification and justification
2) Appropriateness, requirement fulfillment and availability of knowledge & experts
3) Conceptual design, planning and feasibility study
4) Software and hardware selection
5) Knowledge acquisition (system design and construction)
6) Knowledge representation
7) Testing (case study identification, field testing)
8) Implementation

9) Maintenance and update

10) Evaluation

Steps 5 through 7 loops in a cycle called “Prototyping”. An important characteristic of the development of an expert system is that they can be quickly prototyped and expanded. All the steps are standard, regardless of the nature of the system built; nevertheless, the content on each step varies accordingly to it.

2.5.3. Software Selection

Different types of expert systems are widely used in different areas such as diagnosis, debugging and repair, interpretation, monitoring, control, design, planning and instructions. The function of the expert system for this research is to accomplish the following:

- Collect input data, arrange and pick questions according to user’s answer
- Store and distribute required input to other modules
- Receive feedback from other modules and update database
- Analysis users preferences
- Rank output based on users preferences
- Give explanations of reasoning and/or guide users for helpful references

There are many free and/or commercially available products called expert system shell that can be used as an expert system building tool. To be more specific, a shell is a piece of software which contains the user interface, a format for declarative knowledge in the knowledge base, and an inference engine. There are a number of shell features which will be needed for the purpose of this research:

- Backward Chaining (Goal Driven Reasoning) - an inference technique which uses IF-THEN rules to repetitively break a goal into smaller sub-goals which are easier to prove.
- Forward Chaining (Data Driven Reasoning) - an inference technique which uses IF-THEN rules to deduce a problem solution from initial data.
- Data Representation - the way in which the problem specific data in the system is stored and accessed.
- User Interface - that portion of the code which creates an easy to use system to ask user for input and interact with user;
- Explanations - the ability of the system to explain the reasoning process that it used to reach a recommendation.
- Coping with Uncertainty - the ability of the system to reason with rules and data which are not precisely known or sometimes with conflict information. Ranking algorithm is required while dealing with uncertainty.

The targeted users of this expert system application are pavement engineers. For those experienced engineers, this expert system program will serve as an evaluation tool for their design candidates and step-by-step guide for remediation strategies. Also, this expert system can be used as a training tool for new or inexperienced engineers to help them get familiar with commonly encountered flexible pavement distresses, feasible remediation strategies and cost-benefit analysis procedures. The users are expected to be familiar with the subject domain, and they will use the expert system software occasionally. The user-interface has to be easy to understand, clear and simple. The estimated size of the expert system is based on different pavement design scenarios and is supposed to have more then 300 if-then rules. The expert system shell selected should have the ability to call outside executable programs and

communicate with database. It will contain mathematical, mechanistic-empirical relationships, and the expected response time frame is within 20 minutes. It will run under Windows operating systems (2000, XP or vista) and will be able to deal with uncertain data and knowledge. The knowledge for the system is scattered and different design considerations and criteria have to be incorporated into the reasoning process to reach feasible solutions. The expert system also needs to be able to provide backward explanations and references for the recommended design alternatives.

Wanyan (2003) compared more than sixty commercially available expert system shells and identified EXSYS 8.1 as an easy to use tool. Continuing with her search and comparison, the newer version from EXSYS Inc. called CORVID was identified and selected as the first step developmental tool for this research based on the following key features:

- CORVID uses an "object-structure" approach to system design. Many of the advantages of a full object-oriented approach are provided without having to understand complex programming. This nature of CORVID allows it to provide the optimum balance between power, flexibility and ease of use.
- The CORVID Inference Engine supports both backward (goal driven) and forward (data driven) chaining, or combinations of the two approaches.
- Probabilistic logic ("fuzzy logic") is supported with many ways to combine confidence factors, allowing systems to find the "best" solution, and probabilistically rank multiple possible solutions in case of uncertainty.
- CORVID has a very open interface. It has built-in capabilities allowing a single system to be run in multiple languages. It can be integrated with database and external executable programs.

2.5.4. Expert System Applications in Pavement

In the past two decades, many Expert System applications were developed for pavement design, construction, management and inspection. All of these expert systems are highly domain specific, each focusing on solving one of the many problems. There are several Expert Systems developed for pavement maintenance and rehabilitation which focus on construction management, budgeting and prioritization. Another category is pavement distresses identification, diagnosis and inspection. The third group of ES applications in pavement is designing of pavements based on some structural criteria. For example, Khedr & Mikhail (1999) developed an ES for flexible pavement and overlay design. Their knowledge included: properties of pavement materials, pavement structures, and tolerable pavement behavior as it related to its structural performance and rutting prediction and fatigue performance programs.

However, there is no ES program developed so far to incorporate structural and performance analysis, remediation strategies recommendation and cost-benefit comparison in one package,

2.6. COST ANALYSIS

2.6.1. Cost Analysis

Cost analysis (also called economic evaluation, cost allocation, efficiency assessment, cost-benefit analysis, or cost-effectiveness analysis by different authors) is currently a somewhat controversial set of methods in project evaluation due to the fact that it is often quite difficult to accurately quantify benefit. There are three basic types of cost analysis evaluation: cost allocation, cost-benefit analysis and cost-effectiveness analysis.

Cost allocation is a simpler concept than the other two. At project or agency level, it basically means setting up budgeting and accounting systems in a way that allows program managers to determine a unit cost. Conventionally, road costs are estimated by either constructed costs or historical bids or a combination of both. The constructed-cost method utilized production rates, labor and equipment costs, profit and risk, taxes and material costs to estimate the unit price. The R.S. Means Construction Cost Guides are commercially available to estimate the unit price. The historical-bid approach derives the unit price by the weighted average of bids submitted by contractors over some period of time. A cost trend factor can be used to adjust and reflect the cost at the time when the project is constructed. Ou and Swarthout (1986) concluded that the bid price is a function of the effort required to complete a job item and the size of the project. Less effort and large projects tend to lower the unit price and vice versa.

Cost-benefit analysis deals with questions like “Do the economic benefits of doing this outweigh the economic costs” and ‘Is it worth doing at all”? The basic idea behind cost-benefit analysis is that if all inputs and outputs of a proposed alternative can be reduced to a common unit of impact (namely dollars), they can be aggregated and compared. In practice, however, assigning monetary values to inputs and outputs is rarely so simple, and it is not always appropriate to do so (Weimer and Vining, 1992). One important tool of cost-benefit analysis is the benefit-to-cost ratio, which is the total monetary cost of the benefit (e.g. output) divided by the total monetary costs of obtaining them (input). Another tool for comparison in cost-benefit analysis is the net rate of return, which is basically total cost minus the total value of benefit.

Cost-effectiveness analysis assumes that a certain benefit or outcome is desired, and that there are several alternative ways to achieve it. The basic question asked is “Which of these alternatives is the cheapest or most efficient way to get this benefit?” By definition, cost-

effectiveness analysis is comparative, while cost-benefit analysis usually considers only one program at a time. Another important difference is that while cost-benefit analysis always compares the monetary costs and benefits of a program, cost-effectiveness studies often compare programs on the basis of some other common scale for measuring outcomes (Sewell and Marczak, 1997). For this study, we are aiming to find feasible flexible pavement design(s) that can provide better over all performance yet stay within budget constrains. So cost-effectiveness analysis approach will be used, although it will be referred by the customary "cost and benefit analysis" term.

2.6.2. Life Cycle Cost Analysis

LCCA is an engineering economic analysis tool. It calculates the cost of a system or product over its entire life span. By considering all of the costs—agency and user—incurred during the service life of a pavement system, this analytical process helps transportation officials to select the lowest cost option. The typical LCCA for pavement system includes costs for initial design and construction, operation and maintenance, rehabilitation and salvage. In September 1998, the US Department of Transportation (DOT) introduced risk analysis, a probabilistic approach to account for the uncertainty of the inputs of the cost/benefit evaluation of pavement projects, into their decision-making policies. The traditional (deterministic) approach, did not consider the variability of inputs. It is useful in comparing the relative merit of competing project implementation alternatives. Additionally, LCCA introduces a structured methodology that accounts for the effects of agency activities on transportation users and provides a means to balance those effects with the construction, rehabilitation, and preservation needs of the system itself.

There are two basic models commonly used in infrastructure asset management:

Present Worth Value (PWV): $PWV = Cost_{Initial} + \sum Cost_{Future}\left(\frac{1}{(1+i)^{n_k}}\right)$ (2.10)

Equivalent Uniform Annual Cost (EUAC): $EUAC = PWV \times i \times \left[\frac{(1+i)^m}{(1+i)^m - i}\right]$ (2.11)

where: i = discount rate; n = number of year to the year of expenditure; k = total number of cost items used in the analysis, k = 1 to j; m = number of years into the future (analysis period).

US DOT and FHWA published a Life-Cycle Cost Analysis Primer in 2002. This primer provided background for transportation officials to investigate the use of life-cycle cost analysis (LCCA) to evaluate alternative infrastructure investment options. Additionally, the Primer demonstrated the value of such analysis in making economically sound decisions. This primer outlines in detail the LCCA methodology for establishing design alternatives, determining activity timing, estimating costs, computing Life-Cycle costs and analyzing results determining. A trial version of excel based LCCA software package called RealCost is available for download from http://www.fhwa.dot.gov/infrastructure/asstmgmt/lcca.htm. This software is very flexible and may be adapted to the needs of this study.

2.7. SUMMARY

The discussion and review presented above covered commonly used laboratory tests and models to characterize variations of expansive subgrade susceptible to environmental fluctuations, remediation strategies, design procedures and their limitations for low-volume roads. Expert system, an artificial intelligent approach to mimic human expert can be used to help reaching feasible solutions and ensure the quality of problem solving. Different cost analysis methods were compared and discussed. The following sections of this dissertation describe the development of an expert system design program for low-volume roads over

problematic subgrade soils, results analysis and comparison obtained from case studies, and future implications of this research.

CHAPTER THREE - RESEARCH APPROACH

The literature review suggests that expansive subgrade problem and traditional mechanistic design procedures which do not take into consideration the drastic expansive subgrade property variations contribute to low-volume road premature failure. This chapter will identify the most prevalent flexible pavement distress problems and describe a more realistic design approach for low classification roads on highly expansive subgrade to minimize cost and maximize performance.

3.1. DISTRICT SURVEY OF FLEXIBLE PAVEMENT DISTRESS PROBLEMS

As any pavement build on expansive subgrade, low-volume roads may experience many different types of distresses such as longitudinal cracking, fatigue (alligator) cracking, mix rutting, subgrade rutting, shoving, excessive roughness, shoulder erosion and other problems such as raveling, stripping, bleeding, water pumping etc. A one-page questionnaire (see Appendix A) was sent to all 25 districts. This questionnaire included four main questions: (1) Subgrade type; (2) Observable distress problems and probable causes; (3) geosynthetic usage; (4) stabilization methods. Responses were received from 23 districts. Among these districts 18 reported having high PI clay subgrades. Abilene district reported soils in the district are not high PI clays (95% of soils are less than PI of 20) but still severe droughts can cause cracking in soils with some clay. The responses of each district are summarized in this section. Each of the questions presented in the text below is followed by a figure and a detailed discussion of the answers provided.

Question 1— Do you have high PI clay subgrades?

18 districts reported they have high PI clay subgrades. Abilene, El Paso, Laredo, Lubbock and Odessa districts do not seem to have high PI clay subgrades.

Question 2— Types of Distress

Question 2 is about the most prevalent distress problems on high-PI clay subgrades. As shown in Figure 3.1, longitudinal cracking is the most common distress where 89% of the districts with high-PI clay subgrades encounter this problem. Other distress problems are reported by Dallas, Houston and Wichita Falls district including server longitudinal and transverse cracking due to high sulfates combined with clays, extensive use of PG76-22 and/or low asphalt content in the surface mixes and combined distress problems due to inadequate structures, poor constructions and improper or no stabilization.

Figure 3.1—Most Prevalent Distress Problems

For each distress, the causes are summarized below.

Longitudinal Cracking:

Figure 3.2 indicates that moisture migration and variation are the main reason perceived as causing longitudinal cracking. Inadequate structure built many years ago and designed for low traffic volumes is the second reason. Vegetation such as large trees and vegetations growth on the edge of the roadway plays the third main cause, together with steep shoulders and steep front slopes. Improper stabilization, poor constructions at joints, poor drainage or large drainage ditches are also common causes. Other causes include lack of shoulders, lack of subgrade support and expansive subsoils.

Transverse Cracking:

Figure 3.3 shows that the districts perceive transverse cracking is mainly caused by improper stabilization such as stabilizer content being too high or over stabilization with cement. Many districts reported transverse cracking as a minor distress problem compared to longitudinal cracking. Change in moisture is the second main reason. Inadequate structure for heavy traffic comes as the third reason. Other reasons such as thermal related cracking and semi-rigid overlays also cause this type of distress. For poor construction, one example is no sufficient mellowing period with quick lime that lead to cracking because of the hydration.

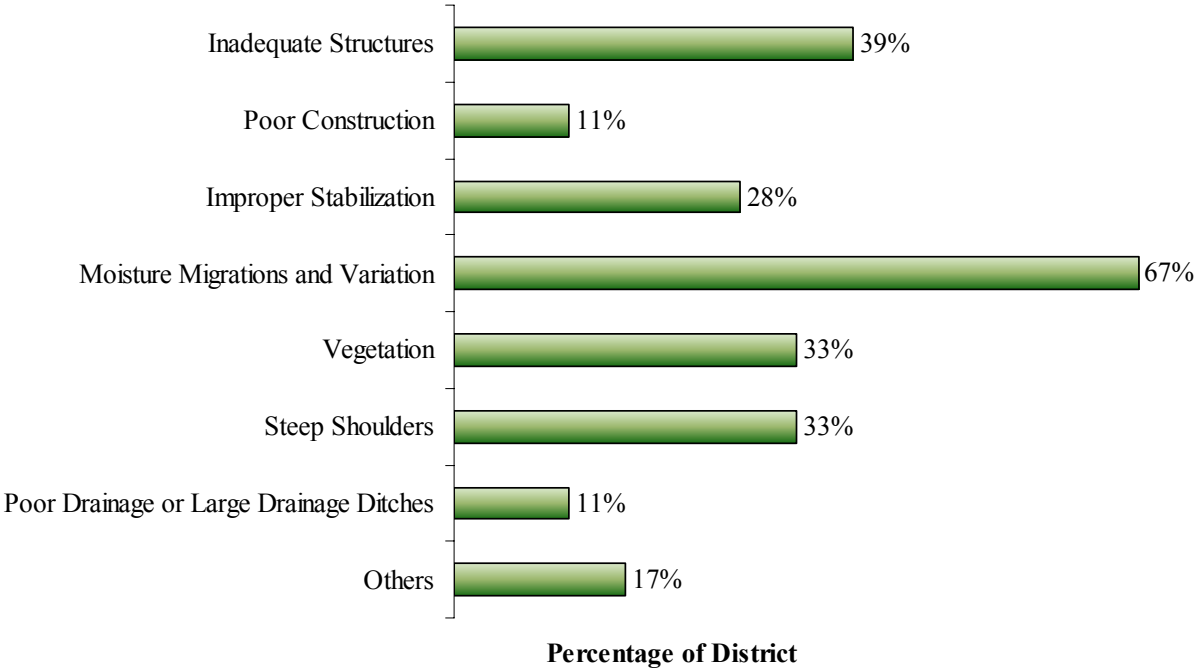

Figure 3.2—Causes for Longitudinal Cracking

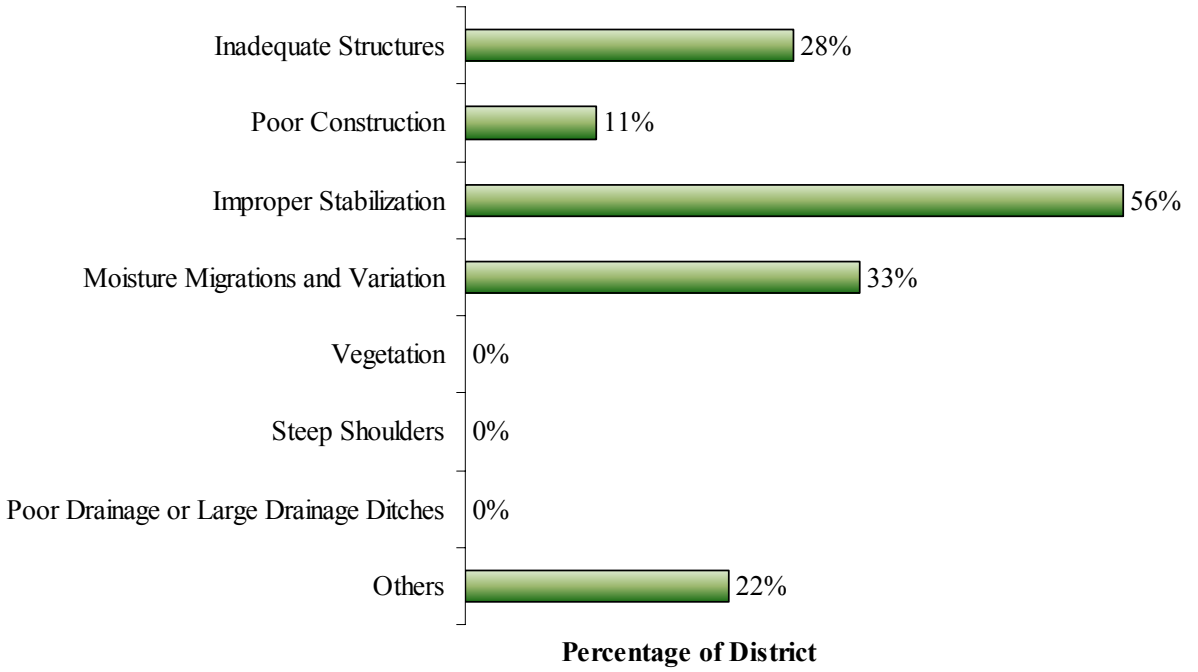

Figure 3.3—Causes for Transverse Cracking

Rutting:

Survey responses given in Figure 3.4 indicate that rutting is perceived to be mainly caused by inadequate structure. Many roads and highways are deteriorating and increasing volume and weight of traffic cause load-related rutting. Other causes include heavy loads such as oilfield trucks, no shoulders, soft ACP binder, improper compaction, moisture infiltration and lack of subgrade support. Poor construction and improper stabilization come equally as the third level reasons. Moisture migrations and variation count for 11% of the answers and steep shoulders counts for 6%.

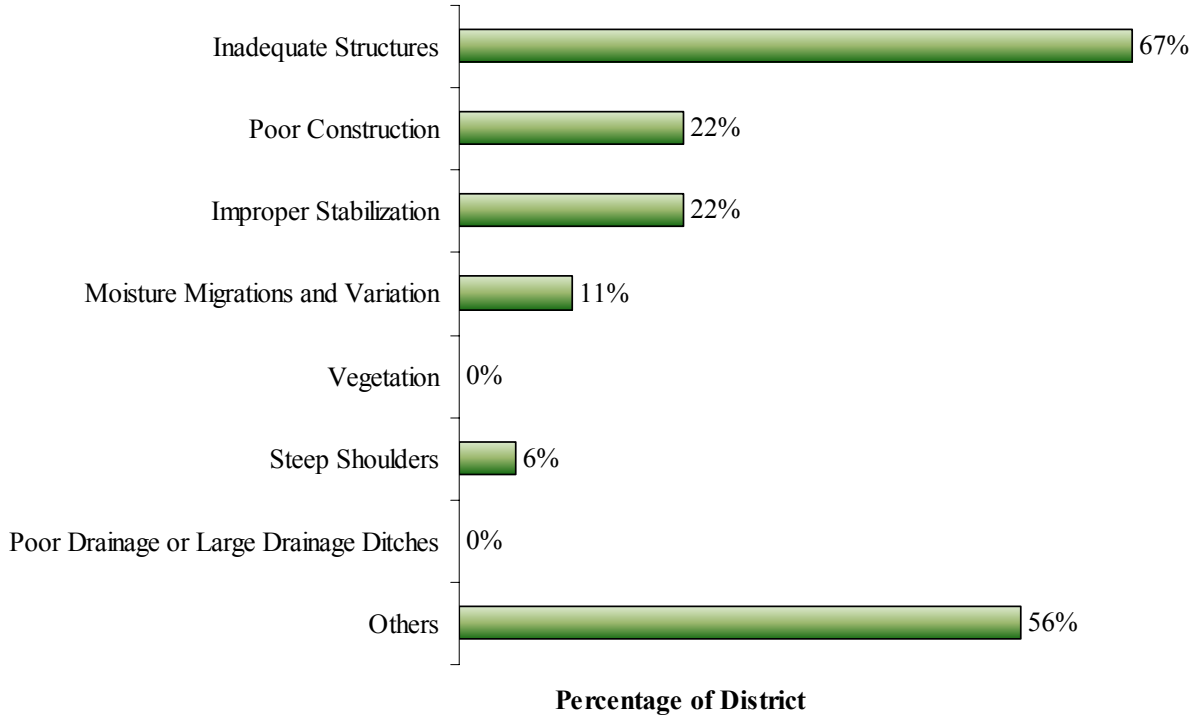

Figure 3.4—Causes for Rutting

Shoving:

Figure 3.5 shows that the main cause for shoving are heavy loads, slow and heavy traffic at intersections, excessive asphalt and bituminous stripping, poor tack coating, trapped water

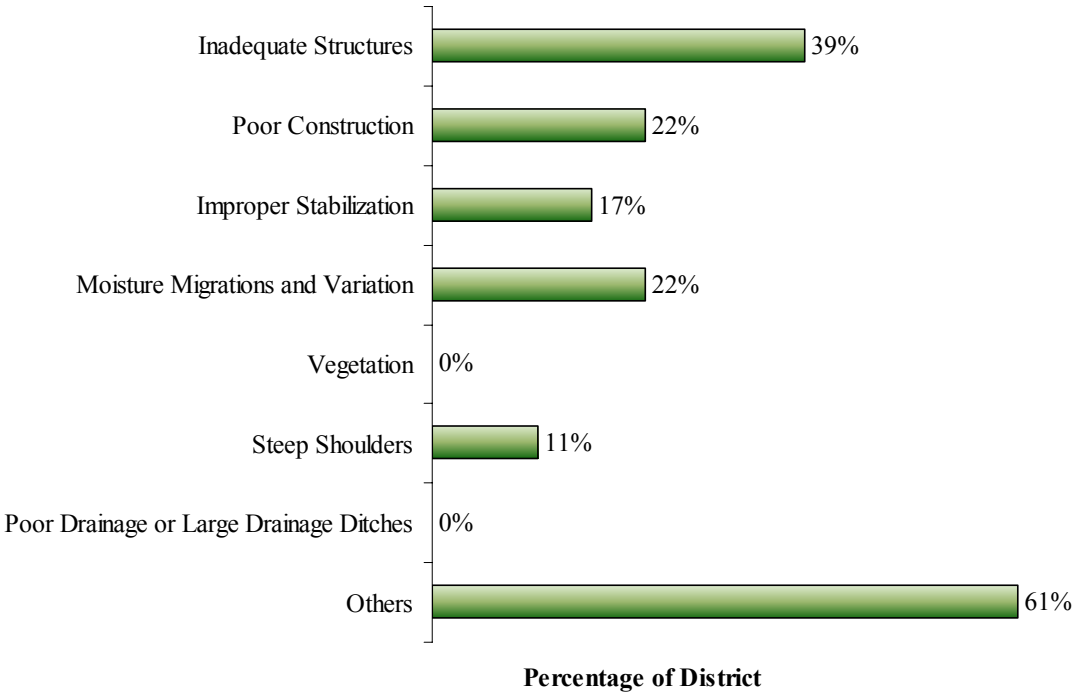

Figure 3.5—Causes for Shoving

over bedrock, moisture infiltration and no shoulders. Inadequate structure counts for the second main cause. Poor construction and moisture migration and variation share the third reason. Improper stabilization is also mentioned by 17% of the district as a cause for shoving, so does steep shoulder that reported by 11% of the districts.

Excessive Roughness:

According to Figure 3.6, 50% of the districts with high-PI clay subgrades experience excessive roughness due to moisture migrations and variation. 28% of the districts report other causes such as standing water, thermal expansion and contraction, extensive patching, inadequate compaction and expansive soils as the cause for excessive roughness. Inadequate structure and improper stabilization are reported by 22% of the districts, and poor construction is considered a cause by 17% of the districts. Vegetation counts for 11% and steep shoulder and poor drainage or large drainage ditches are reported equally by 6% of the districts.

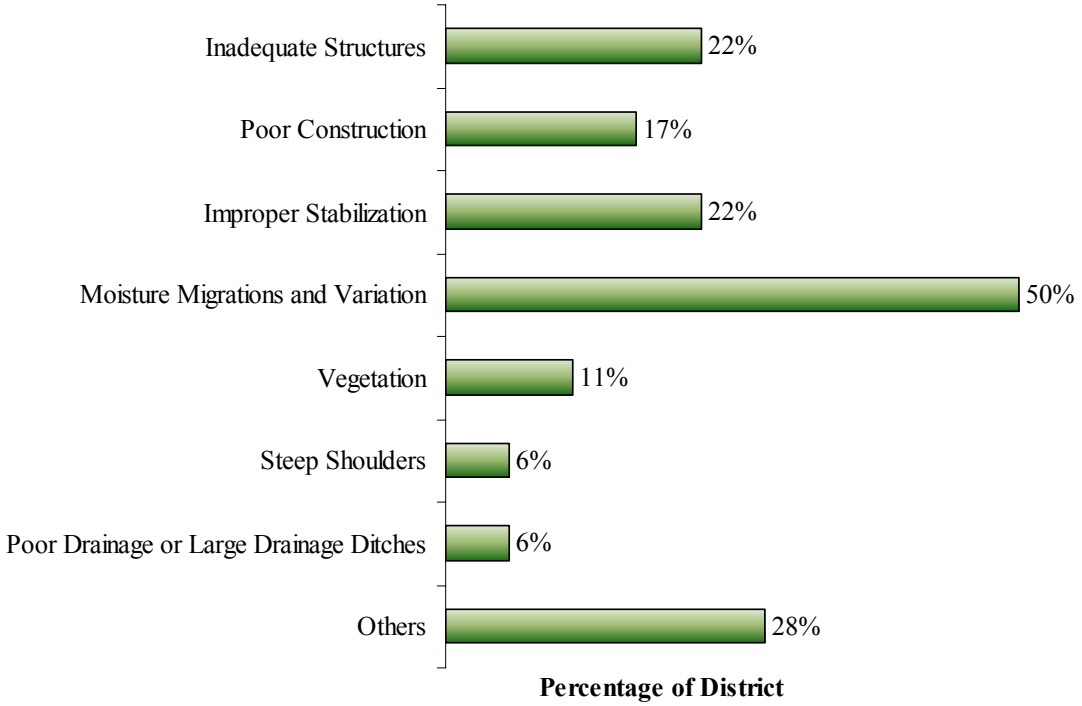

Figure 3.6—Causes for Excessive Roughness

Shoulder Erosion:

Not as many districts experience shoulder erosions as they experience other distresses mentioned above. As shown in Figure 3.7 the most important reasons for shoulder erosion reported by the districts are narrow roads, lack of shoulder, traffic run off edge and high rainfall events. 17% of the districts consider moisture migration and variation and steep shoulders to be main causes for shoulder erosion. Poor construction is reported by 11% of the districts and 6% of the districts indicate the following four reasons may also be responsible for shoulder erosion: inadequate structure, improper stabilization, vegetation and poor drainage or large drainage ditches.

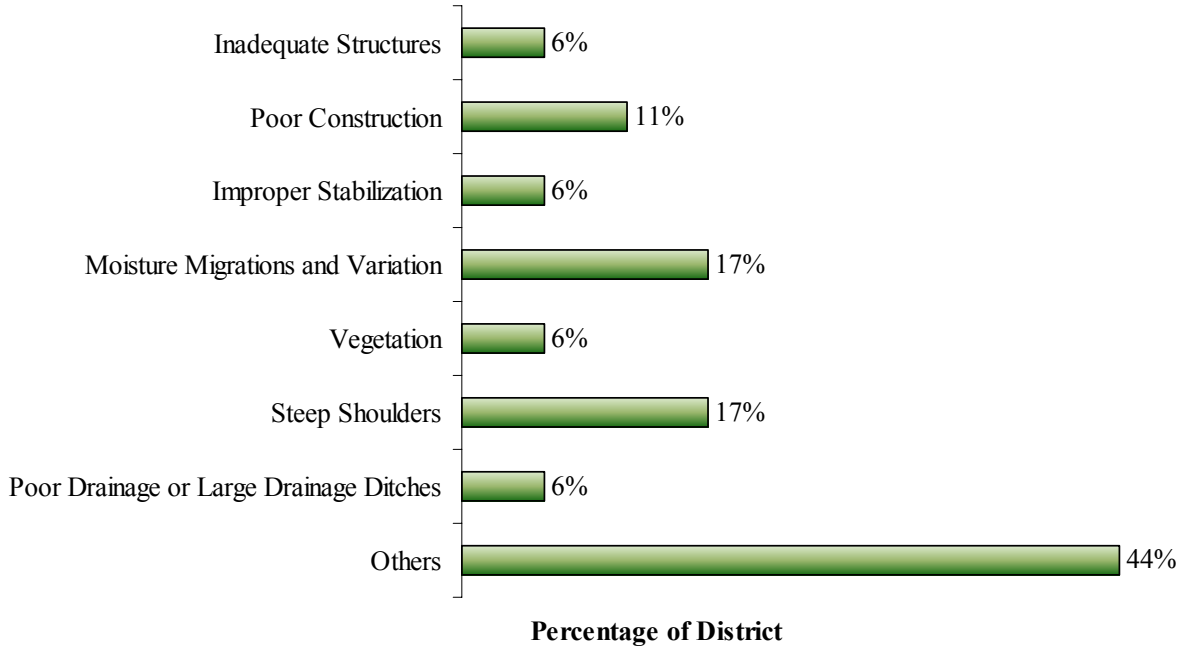

Figure 3.7—Causes for Shoulder Erosion

Other Distresses:

Other distress types are reported by Dallas, Houston and Wichita Falls district including server longitudinal and transverse cracking due to high sulfates combined with clays, extensive use of PG76-22 and/or low asphalt content in the surface mixes and combined distress problems due to inadequate structures, poor construction and improper or no stabilization.

Question 3—Do you use geo-synthetics for low volume roads on high PI clays?

Among the 23 districts (Figure 3.8), more than half reported they never used geo-synthetics on low volume roads. 32% mentioned they use it sometimes.

Question 4—What type of stabilizer do you use?

Figure 3.9 indicates all districts with high PI-clay subgrade use lime as stabilizer if they do stabilization. Cement has been used by 72% of the districts and fly ash has been used by 28%

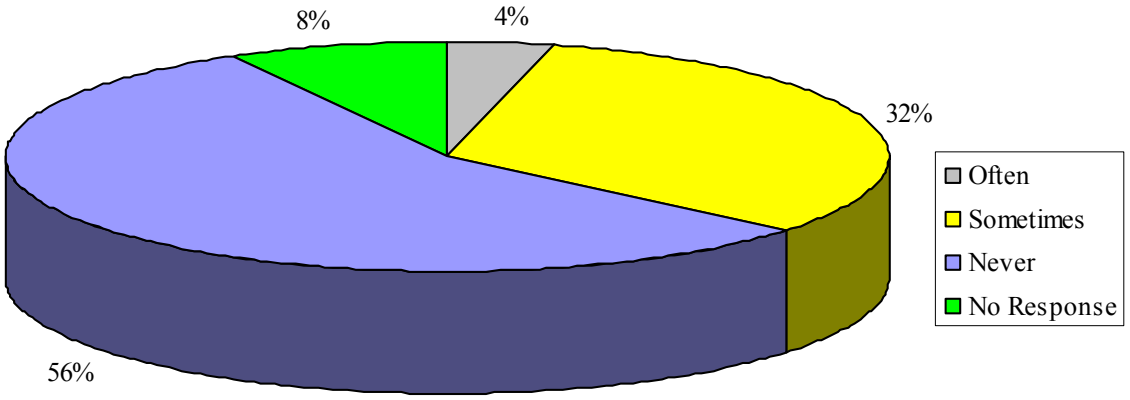

Figure 3.8—Use of Geo-synthetics for Low Volume Roads

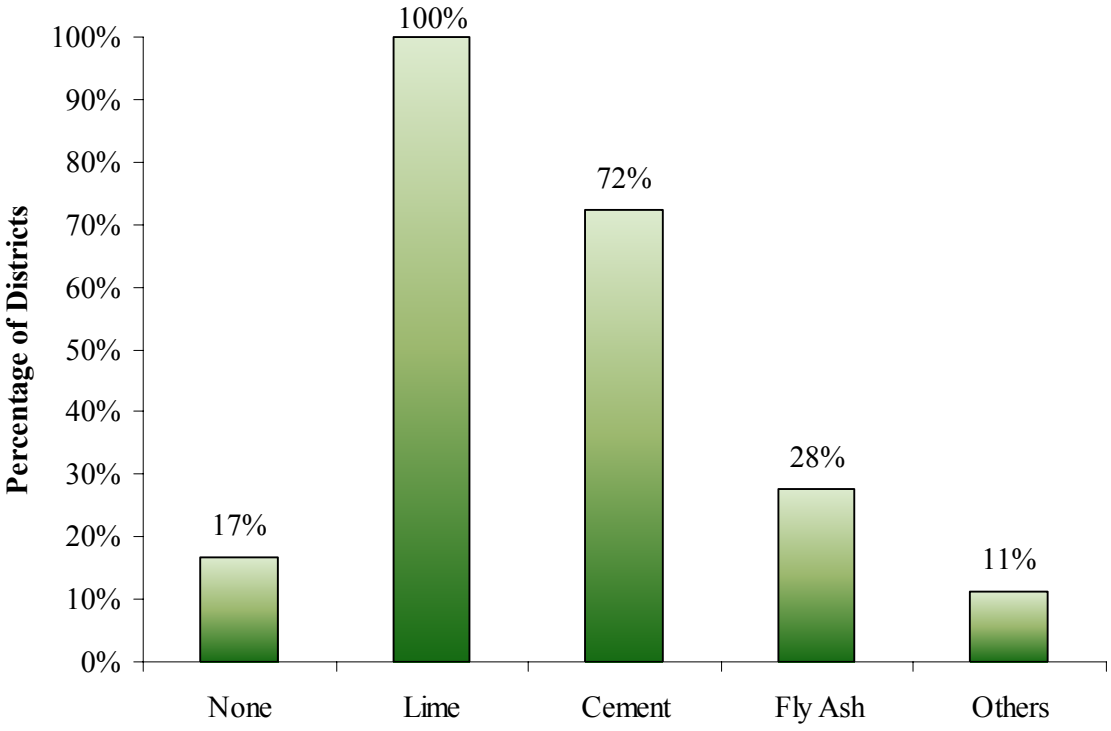

Figure 3.9—Type of Stabilizer Used for High PI Clay

of the districts. Dallas and Atlanta districts reported they use other stabilizer such as emulsion. 17% of the district indicated that sometimes they do not use any type of stabilizer for certain projects.

3.2. CONCEPTUAL DESIGN

The focus of this research is to improve current designs and remediation strategies for low-volume road which minimize construction cost and optimize performance. This section describes the conceptual design of the **Ex**pert **S**ystem for **P**avement **R**emediation **S**trategies (ExSPRS) program that consists of four main modules: ***Input***, ***Evaluation Models***, ***Remediation Strategies*** and ***Cost-Benefit Analysis***. As shown in Figure 3.10, user will be asked to provide original design, together with other inputs. The original desgin will first be evaluated and then recommendations of feasible remediation strategies will be assessed. Based on cost and benefit analysis of original design and recommended remediation strategies, the alternatives will be compared according to cost/benefit analysis. Appropriate remediation strategies are summarized and compared. Cost and benefit analysis results can be used as a guidance of feasible design alternatives for pavement engineers, especially those dealing with low classification flexible roads built on expansive subgrade soils. The ExSPRS program uses an expert system approach which manages and incorporates concepts derived from experts and uses structured knowledge to provide analysis to users as an expert would do. A realistic low-volume road design relies on many factors. Following section will discuss research methodologies for each of these modules in more details.

3.3. METHODOLOGY

3.3.1. Input Data Acquisition

The program interacts with the user to obtain the necessary input such as user-defined original design, traffic, climatic data, design preference, material properties, construction constrains, budget constraints etc. The user is encouraged to use mechanistic and/or empirical

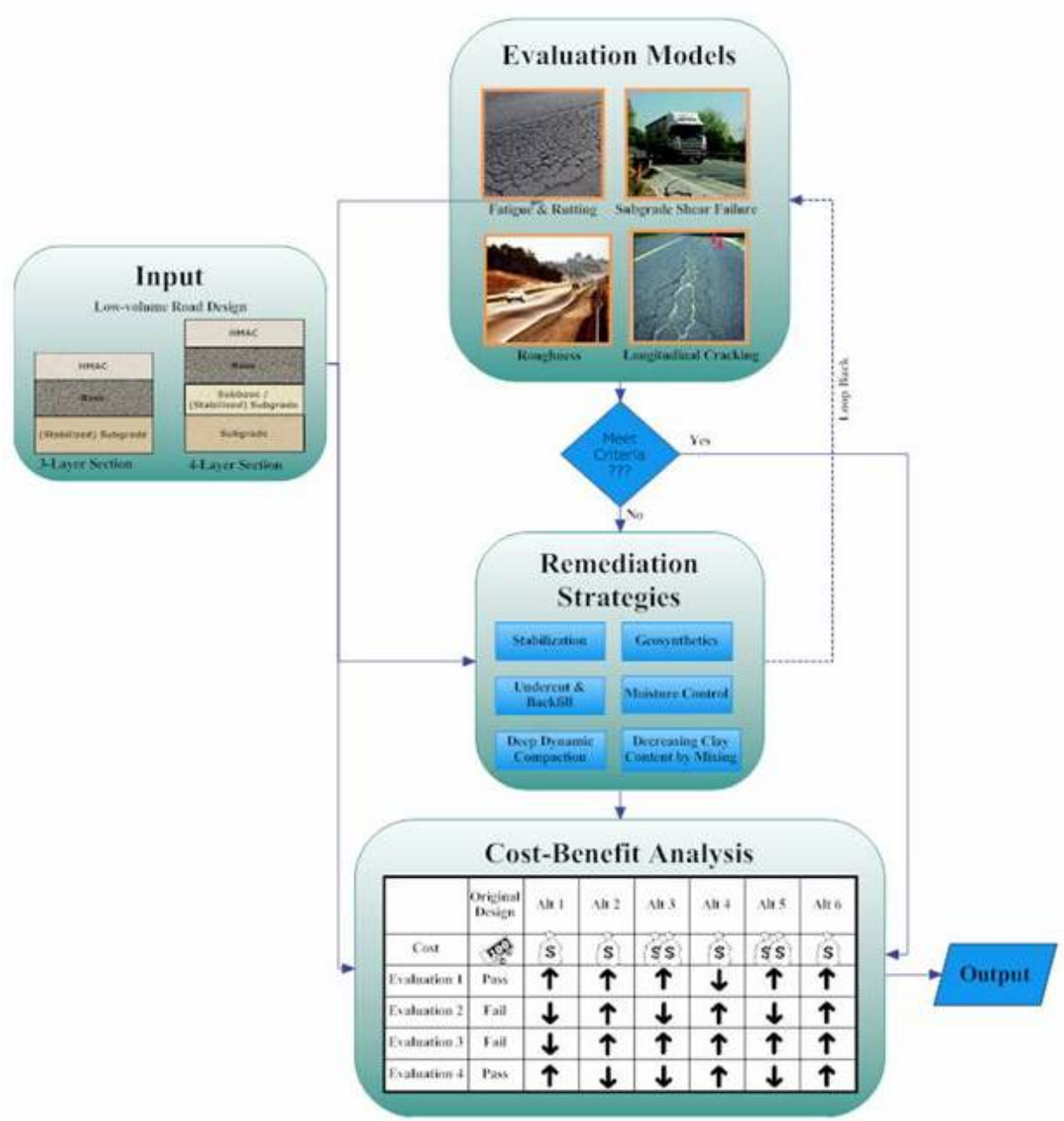

Figure 3.10—Conceptual Design

design method of his choice to arrive an original desgin before using the software. The input parameters are categorized and stored in the program database to be distributed by the ES brain to other modules. The input acquisition will be carried out with controlled detail levels for more information regarding remediation strategies and cost-benefit analysis assumptions when needed.

The objective of the ***Input*** module is to collect as much information as possible from the user without making it too tedious. There are two types of input required from the user: (1) basic input which includes layer properties, design properties and subgrade properties; (2) evaluation considerations, where the user can select appropriate evaluation checks based on his/her preference. Different questions will asked for more specific input besides those already asked in the basic input section. Basic inputs include:

- Layer Properties: This part collects basic information of the section, including description of layers, thicknesses, and material properties.
- Design Properties: Traffic related input is collected along with analysis years, service index, reliability and other design parameters.
- Soil Properties: Basic lab testing results of subgrade soil are collected in this group, including Atterberg limits, sieve analysis results, moisture content and dry density of soil samples.

Evaluation Models include four checks, which can be performed on the original design. Structural-wise, the fatigue and rutting check is mandatory, and the subgrade shear failure check is optional. Performance-wise, longitudinal shrinkage cracking check and roughness check are provided as options. In case no consideration is selected, fatigue cracking and rutting will be the only criterion checked using basic input information.

Two types of questions are used in ***Input*** module. The user is asked to either provide numeric values or answer judgmental "yes/no" type of questions. If-then rules are used to control detail levels of each input group. Default values collected from laboratory testing and literature search are provided for typical cases and software demonstration purposes.

3.3.2. Evaluations for Low-Volume Pavements

Based on the user's selection, different questions will be asked to collect required lab testing data and/or subjective judgments from the user. For example, if the user decides to check for the subgrade shear failure, the Texas Triaxial Test (Tex-117E) results will be asked for. However, if some of the test data are not available, more general questions will be asked to help the user decide which set of default values to use as substitute. Similarly, when roughness check is selected, environmental related questions will be asked.

Based on the district survey and literature review, the most prevalent distresses for low volume flexible pavements are longitudinal cracking, rutting, shoving and excessive roughness. Main causes for these distress problems can be categorized into two reasons: (1) inadequate support, which is caused by inadequate layer thicknesses, poor constructions and improper stabilization; and (2) problematic soils susceptible to moisture variation, which include subgrade volume change, shoulder problems, poor drainage or other combined effects. One or more ***Evaluation Models*** will be used to determine whether the user defined pavement design meets both criteria.

3.3.2.1. STRUCTURAL CHECK – FATIGUE CRACKING AND RUTTING

A layered linear elastic model that computes pavement responses under static loads is incorporated in the program to check for the pavement fatigue cracking and subgrade rutting. The Asphalt Institute (1982) and Shell (1978) design methods, which relate the strains to the allowable number of load repetitions, are selected as shown in the following:

$$N_f = f_1(\varepsilon_t)^{-f_2}(E_1)^{-f_3} \quad (3.1)$$

$$N_d = f_4(\varepsilon_c)^{-f_5} \quad (3.2)$$

where N_f and N_d = allowable number of load repetitions for fatigue and rutting respectively, ε_t = horizontal tensile strain at the bottom of the HMA, ε_c = vertical compressive strain on top of the subgrade, E_1 = HMA modulus, f_1 to f_5 are empirical coefficients.

3.3.2.2. STRUCTURE CHECK – SUBGRADE SHEAR FAILURE

On many Farm-to-Market (FM) roads where the expected traffic is low, it is very common to expect higher percentage of heavy trucks with wheel loads that exceed the standard 18-kip single axle load. These occasional overloads could give rise to subgrade shear failure, particularly under conditions where the pavement is build on problematic expansive soils and the subgrade is wet. Thus, it is recommended to check the design against the Texas triaxial design procedure (TEX-117-E) to ensure that the design thickness provides adequate cover to protect the subgrade against occasional overstressing. Figure 3.11 shows the TxDOT Triaxial Test TEX-117-E flexible base design chart originally developed by McDowell (1955).

This chart gives required cover depth for different design wheel load and triaxial classes. TEX-117-E described detailed steps to acquire the classification by comparing Mohr-Coulomb failure envelopes with the classification chart for subgrade and flexible base material. The depth of cover obtained here is based on keeping the wheel load stresses within the failure envelope of the subgrade material. The required cover depth from this method can be over-conservative in districts where the climate is drier, or where the soils are not as moisture susceptible (Fernando, *et al.*, 2001). To account for this conservatism, the modified triaxial design method (MTRX) is provided to double-check the cases when the pavement structure fails the Texas triaxial check.

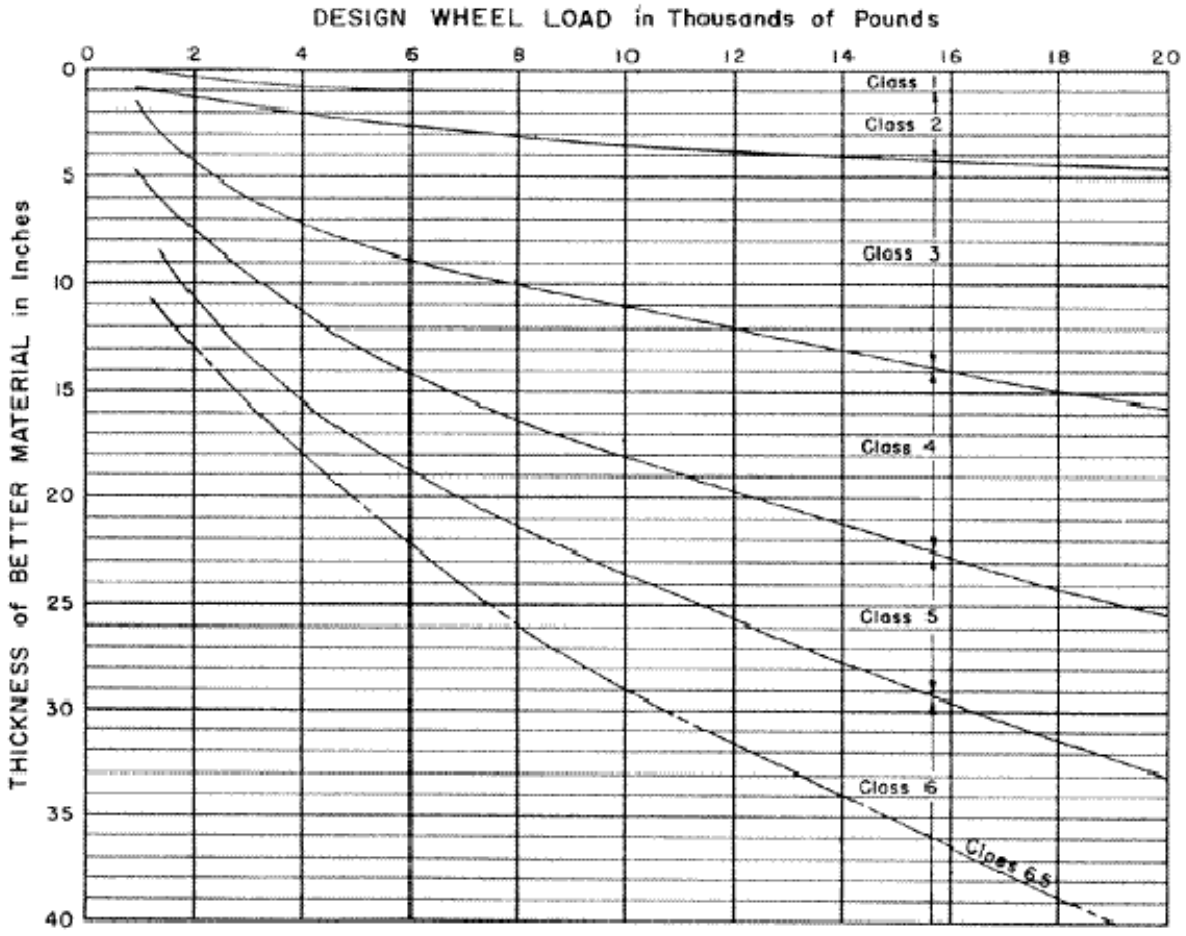

Figure 3.11—TEX-117-E Flexible Base Design Chart

3.3.2.3. PERFORMANCE CHECK – LONGITUDINAL SHRINKAGE CRACKING (LSC)

Both the district survey and literature review shown the longitudinal cracking is the predominant mode of failure for flexible pavements, especially low-volume roads. An evaluation model is needed to reveal the mechanism of the failure, the conditions that make the pavement susceptible to this type of distress, and to predict when and where this type of failure may happen for the original design. As indicated by the district survey, moisture migration and variation are the main reasons perceived as causing longitudinal cracking. Desiccation induced cracking in unsaturated expansive soil occurs due to the presence of tensile stresses, which exceed the tensile strength of the soil. The cracks resulting from this mechanism are generally initiated from the

subgrade and propagate through the base course and asphalt layer to form cracks along the pavement edges or covered shoulders (Komornik *et al.*, 1969). Transverse cracking due to shrinkage is also possible but is mostly associated with local structures contained in the pavement or in the subgrade such as ditches, and culverts. The influence of shrinkage cracks on all aspects of geotechnical engineering is considerable and hence a clear understanding of different phases of shrinkage and mechanics of longitudinal cracking formation are always important for better characterization of expansive soils (Puppala *et al.*, 2004b).

In the propagation mechanism of the longitudinal shrinkage cracking, the cracks in the asphalt layer are believed to be initiated in the subgrade. The subgrade cracks under the combined action of shrinkage by drying and the resistance to shrinkage due to base layer on one hand, and to the deeper, constant-moisture layers of the clay, on the other hand. Resistance to the shrinkage results in shear stresses at the interface of subgrade and base which in turn produce compression stresses in the granular courses and tension stresses in the clay. When the tensile stress equals the tensile strength, cracking sets in. With further drying, the crack propagates through the base course towards the asphalt layer. This upward climb of cracks is due to the bond between the subgrade and the base and to the low tensile strength of the base course. If the tensile strength of the asphalt layer is also inadequate, the crack may propagate through to the surface, after which another new cracking cycle begins. (Uzan, *et al.*, 1972; Bell and Wright, 1991)

Expansive subgrade soils may develop cracks from moisture variation and would cause tensile stresses as a function of its elastic modulus. Consider a pavement base layer that restrains the subgrade. The subgrade usually develops shrinkage tensile stress, σ_{ss} under shrinkage. If the tensile stress exceeds the tensile strength of the subgrade material, a fracture will develop. The

fracture amount (Δl) due to shrinkage in the subgrade length (l) can be estimated by shrinkage strain (ε_{ss}). The simplified relationship is:

$$\sigma_{ss} = \varepsilon_{ss} \cdot E = \frac{\Delta l}{l} \cdot E \tag{3.3}$$

where E = modulus of subgrade soil; and ε_{ss} = shrinkage tensile strain of subgrade soil.

Finite element analysis method can be used to evaluate the resulting tensile stress (σ_{ss}) of the expansive clay for a known shrinkage strain (ε_{ss}) and modulus (E). Empirical or theoretical relationships can be used to get those two parameters. Laboratory tests can be performed to get subgrade tensile strength (σ_{design}). To prevent longitudinal cracking from happening, design considerations should be taken with a safety factor so that the predicted tensile stress is always less than the tensile strength of the expansive subgrade. The design criterion is:

$$\sigma_t \leq \frac{\sigma_{design}}{f} \tag{3.4}$$

where f is the safety factor.

3.3.2.4. PERFORMANCE CHECK – ROUGHNESS

Environmental changes cause subgrade volume change induced by swelling and/or shrinking. The roughness of pavement is the result of the cumulative deformation and differential volumetric change of the problematic subgrade soils. The use of roughness as a direct quantitative measure of pavement performance is evident in the literature. The development of this evaluation module depends on two steps: (1) find an appropriate volumetric change prediction model, and (2) find a quantitative way to evaluate pavement roughness caused by such volumetric change and deterioration.

The international roughness index (IRI) model derived from AASHTO design guide by Lytton *et al*. (2004) is incorporated in the software. The model has the following format:

$$IRI = IRI_0 + (4.2 - IRI_0)\exp\left[-\left(\frac{\rho_i}{t}\right)^{\beta_i}\right] \quad (3.5)$$

where IRI_0 = initial *IRI* in m/km or in/mile, and ρ_i, β_i = roughness parameters.

If the original design passes the evaluation, it will be sent to the cost and benefit analysis module directly. On the other hand, if the original design fails one or more of the criteria, remediation module will carry on the task of providing possible mitigation strategies to improve the design.

3.3.3. Remediation Strategies Module

The ***Remediation Strategies*** module investigates possible mitigation strategies for the original design based on the outcome from the evaluation module. Based on the literature search, main remediation strategies include: stabilization, moisture control, geosynthetics and other methods. Both qualitative and quantitative methods are necessary to develop the frame work of this module. Development approaches of these remediation methods will be discussed in the following section.

Depending on which criteria the original design fails, commonly used remediation strategies are categorized into two types: (1) strategies dealing with failure caused by inadequate support, which include stabilization, using geosynthetics and undercut and backfill method, and (2) strategies dealing with failure caused by moisture variation, which include all strategies in the first category plus moisture control, decreasing clay content by soil mixing and deep dynamic compaction. The logic flow is controlled by If-Then rules following Figure 3.12.

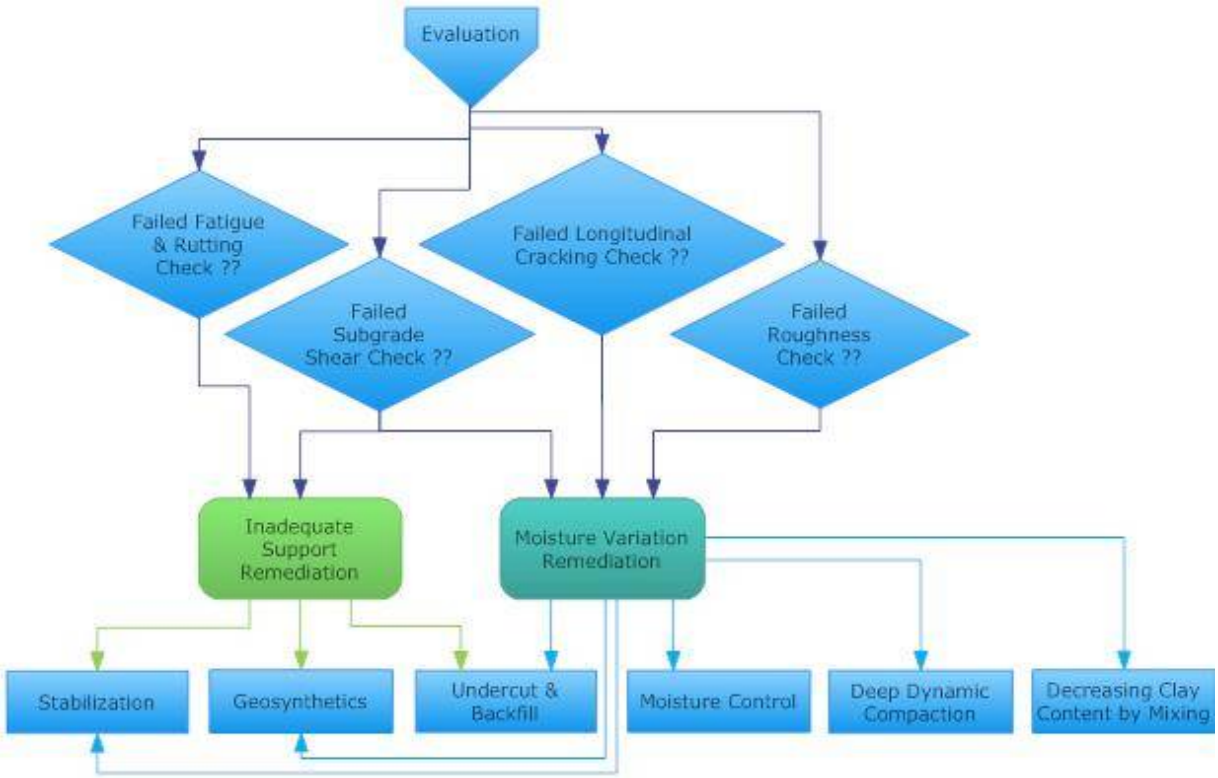

Figure 3.12— Schematic of Remediation Strategies

To select appropriate stabilization methods for subgrade, three aspects are considered: regular stabilization, sulfate rich soils and organic rich soils. TxDOT stabilization guide for soils and sulfate rich soils are used as guidelines. For organic rich soils, additional test of organic content (ASTM-D 2974) is required. It is well understood that organic soils can inhibit the cementitious reactions between the stabilizers and the soil. Special addictives such as bentonite and high aluminum cement will be suggested to the user, special considerations and techniques will also be recommended based on subgrade soil properties.

As discussed in Section 2.3.3, geosynthetic reinforcement will be placed near the base-subgrade interface to maximize the benefit. A subroutine using the FHWA design method (by Holtz *et al.*, 1998) is used in this module.

Moisture control subroutine is further divided into three categories, e.g. usage of moisture barriers, improving surface drainage and vegetation control. Most of the moisture control methods are illustrative. This subroutine will focus on providing information such as design details, construction methods, and useful references.

There are other remediation methods aiming at maintain the moisture content of the subgrades or improve subgrade strength, such as deep compaction, undercut and backfill, decreasing clay content, widening the right of way, etc. These case specific modifications are included when appropriate in the program.

The motivation to have remediation module is to offer the user as much help as possible by providing appropriate remediation strategy scenarios. The expert system brain may ask the user more questions to help selecting these strategies. A logic control is added to send the selected remediation strategies to cost analysis module for further analysis of benefit and performance improvement.

3.3.4. Cost-Benefit Analysis Module

Life cycle cost analysis (LCCA) is a process for evaluating the total economic worth of a usable project segment by analyzing initial costs and discounted future cost, such as maintenance, user, reconstruction, rehabilitation, restoring, and resurfacing costs, over the life of the project segment (National Highway System Designation Act Section 303, 1995). The primary purpose of an LCCA is to quantify the long-term implication of initial pavement design decisions on the future cost of maintenance and rehabilitation activities necessary to maintain some pre-established minimum acceptable level of service for some specified time.

Since this research focuses on low volume pavements, which typically have low daily traffic, the user costs (i.e., vehicle operating costs, user delay costs, and crash costs) can be considered minimal and omitted. For the same reason, construction activity timing of low-volume roads is not critical. Construction time estimation is omitted assuming cost to be the control parameter. The remediation scenarios are given as different alternatives, however, except the initial construction costs for each alternative, future agency costs are hard to quantify due to limited information on how much long-term improvement can be achieved. This makes LCCA not a feasible option. To compare recommended alternatives economically, simple ***Cost-Benefit*** analysis suits our need better.

The agency costs are calculated by using the unit price information obtained from the RS Means CostWorks Data for Heavy Construction (R.S. Means, 2007). The productivity rates of the pavement construction activities found in RS Means database can be exported into a spreadsheet for convenience. Cost analysis part is responsible to communicate with the exported excel sheet and assemble initial construction costs accordingly. Benefit analysis part is carried out using "before-and-after" analysis. The user will need to provide improved laboratory test results for selected remediation strategies. With these improved parameters the evaluation modules are executed again to compare structure and performance improvement with the newly recommended approach.

The output of ***Cost-Benefit*** analysis module extracts the cost estimations and benefit comparisons of original design together with the selected modification alternatives that were recommended by ExSPRS. An attractive feature of expert system is its ability to mimic the reasoning procedure of human experts. Efforts are made to enable the ExSPRS program to interact with the user: that is, hints, references and simple explanations are provided throughout

the program. For ease of comparison, tabulated output is used to indicate benefit (structure and performance improvement) vs. cost (increasing cost).

CHAPTER FOUR - STRUCTURE AND PERFORMANCE EVALUATION MODELS

4.1. OVERVIEW

Expansive soils are noted for their problematic characteristics. They exhibit exceptionally low strength and tend to swell when they become wet; and they are highly brittle and shrink when they become dry. Their susceptibility to moisture variation results in two main types of damage through seasonal wetting and drying cycles: (1) Fatigue cracking, rutting and subgrade shear failure due to inadequate support; (2) Excessive roughness, swelling and severe longitudinal shrinkage cracking due to volume change. This chapter explains in detail four types of performance models used to check the integrity of the low-volume roads.

4.2. FATIGUE CRACKING AND RUTTING MODELS

The horizontal tensile strain (ε_t) at the bottom of an asphalt layer is due to bending of the layer under the traffic load. After many load repetitions these flexural tensile strains may lead to fatigue cracking. For thin surfacing, this fatigue cracking starts at the bottom of the asphalt layer, gradually propagates upward and finally appears at the road surface. An asphalt pavement structure must be designed in such a way that this type of damage does not occur too early. On the other hand, rutting can initiate in any layer of the structure, making it more difficult to predict than fatigue cracking. For low-volume roads, subgrade rutting which is attributed mostly to a weak pavement structure is mostly considered. The subgrade rutting is calculated in terms of the vertical compressive strain (ε_c) at the top of the subgrade layer. It is important to design the flexible pavement in such a way that the relevant stress levels remain sufficiently low to limit the fatigue and rutting failure.

Many computer programs are available to calculate the theoretical stresses, strains, and deflections anywhere in a pavement structure. For low-volume roads, the layered linear elastic models require a minimum number of inputs to adequately characterize a pavement structure and its response to loading. These models can yield results rapidly and will serve the evaluation purpose well. Layered elastic models assume that each pavement structural layer is homogeneous, isotropic, and linearly elastic. The modulus of each layer is considered to be a constant value independent of the state of the stress applied.

The linear elastic multi-layer program WES5 is adopted and modified to conduct this check. The original program WESLEA (Van Cauwelaert, *et al.*, 1989) was developed for the Waterways Experiment Station (WES) of the US Army Corps of Engineers. The WES5 version can handle a maximum of five layers with the subgrade counting as one layer. The number of circular loads is assumed to be one, and can be further modified to simulate up to a maximum of 20 loads. The tire load is set at 18 kips (90 KN) for standard loading conditions. The required inputs for this subroutine include: total number of layers, modulus of each layer (E), thickness (h) and Poisson's ratio (μ) for each layer. The allowable number of load repetitions (remaining life in ESALs) to cause fatigue cracking (N_f) and rutting (N_d) are calculated using The Asphalt Institute and Shell equations (Equations 3.1 and 3.2) based on predicted horizontal tensile strain ε_t and vertical compressive strain ε_c at critical locations. Constants f_1 through f_5 are empirically-derived parameters. In this module, values of 0.0796, 3.291, 0.854, 1.365×10^{-9}, and 4.477 are used, respectively. The outputs give allowable load repetitions directly. Parameters N_f and N_d are compared with final estimated design traffic and a "Failure" flag will be displayed if either one is less than the targeted design traffic.

4.3. SUBGRADE SHEAR FAILURE MODELS

It is common for low-volume roads to expect higher percentage of heavy trucks among their daily traffic. These occasional overstressing scenarios could give rise to subgrade shear failure, particularly under conditions where the road is built on moisture susceptible fat clay subgrades. This model checks pavement to ensure adequate cover thickness over subgrade to prevent such failure using the Texas triaxial method and software LoadGage (Fernando, *et al.*, 2007). Figure 4.1 shows the subgrade shear failure check algorithm. The details related to the use of these models are provided later.

The Texas triaxial design method is based on a stress analysis to establish the depth of cover required to keep the load induced stresses in the subgrade within the material's failure envelope (as defined by its Texas triaxial class). TxDOT later adopted McDowell's load-thickness design curves in the traditional Texas triaxial design method TEX-117-E. McDowell also provided a thickness reduction chart for stabilized layers of 8 in. or greater based on the cohesiometer value of the stabilized material. An external stand-alone program called "TriaxialCheck.exe" was developed with digitalized thickness design curves (Figure 3.11 in Chapter 3) to perform this check. The required inputs are: design wheel load, Texas triaxial test results of soil class or cohesion as well as angle of internal friction. This subroutine gives the required cover depth above subgrade as an output.

Fernando, *et al.* (2007) pointed out that the subgrade material tested in TEX-117-E is under capillary saturation to define the Texas triaxial class. It can be notably conservative in districts where the climate is drier, or where the soils are not as moisture susceptible. They also reported it is not rationale to use a safety factor of 1.3 as in McDowell's curves to account for differences in pavement damage potential between single and tandem axle configurations.

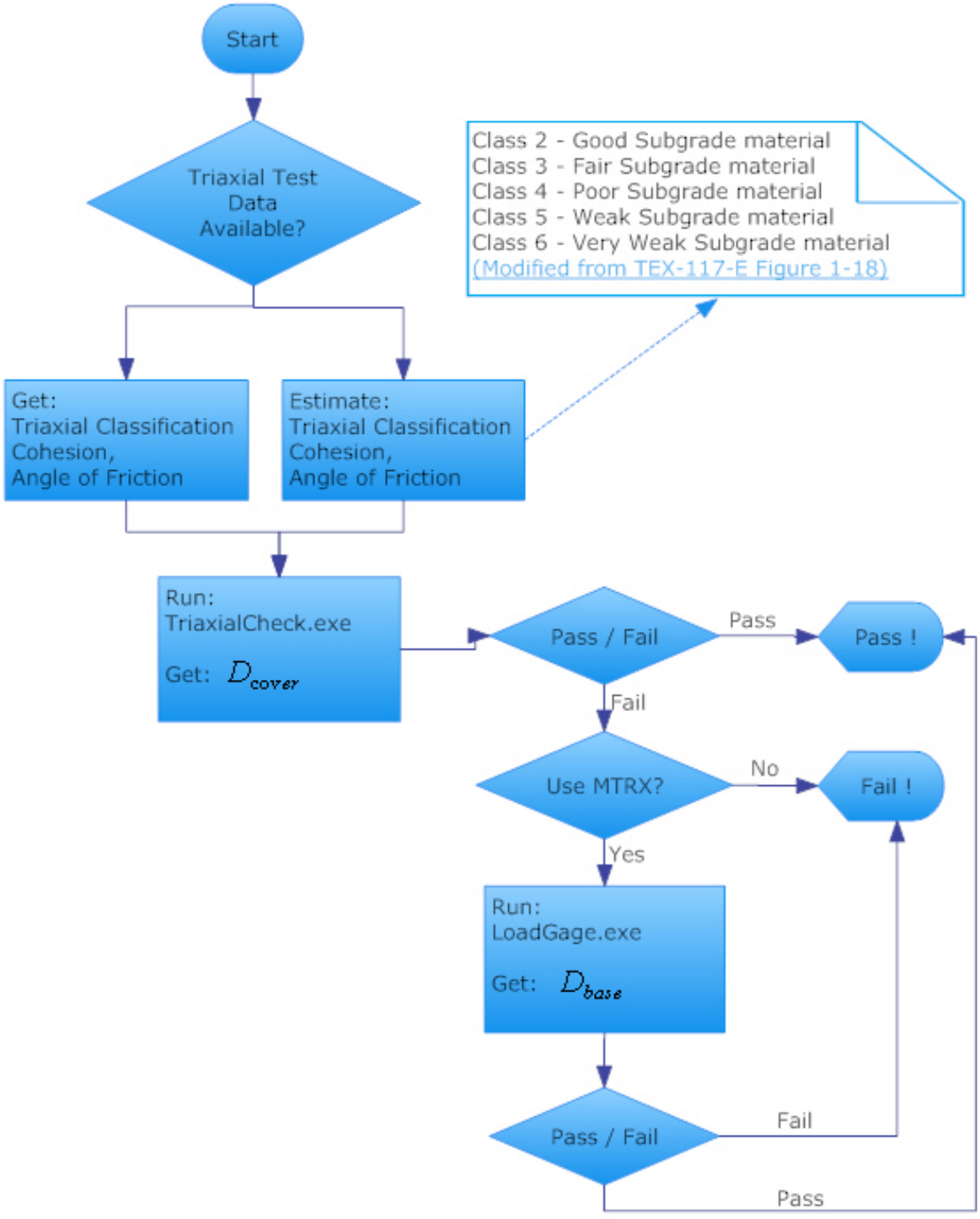

Figure 4.1—Subgrade Shear Failure Check Flowchart

The updated modified triaxial design method (MTRX) which is capable of considering regional climatic differences and soil conditions is recommended for a more realistic assessment

of pavement thickness requirement. They also developed a computer program called LoadGage to automate the modified MTRX process. This modified process is incorporated in the subgrade shear failure check and can be selected to accommodate Texas triaxial check based on user's preference.

4.4. ROUGHNESS MODELS

Two types of roughness models are considered in this study: (1) differential distortion caused by heaving and/or shrinking; and (2) small irregularities in pavement surface due to pavement deterioration. After evaluating more than a dozen differential heaving prediction models, the potential vertical rise (PVR) method is selected to estimate the differential movements. The international roughness index (IRI) is selected to quantify the second concern.

4.4.1. Comparison of Volumetric Change Prediction Models

Since the project mandate was not to develop new models for this task but to rely on existing models, a number of existing models developed in Texas or elsewhere were identified and evaluated. The literature shows that the prediction of heaving has received more attention than shrinking of expansive soil due to moisture fluctuation. Numerous prediction methods have been developed based either on one-dimensional oedometer test results or on direct matric suction measurements (Fredlund and Rahardjo, 1993). In this section, literature findings on how to predict volumetric change behavior of expansive soils will be compared and discussed.

Parameters that are useful for identifying the swell/shrinkage potential include liquid limit (LL), plasticity index (PI), coefficient of linear extensibility (COLE), the natural total suction and physicochemical test. Table 4.1 gives estimations of probable soil expansion degrees based on simple classification tests.

Table 4.1—Probable Expansion as Estimated from Classification Test Data (from Holtz and Kovacs, 1981)

Degree of Expansion*	Probable Expansion (as a percent of the total volume change)	Colloidal Content (percent less than 1μm)	Plasticity Index	Shrinkage Limit
Very High	> 30	> 28	> 35	< 11
High	20 - 30	20 - 31	25 - 41	7 - 12
Medium	10 - 20	13 - 23	15 - 28	10 - 16
Low	< 15	< 15	< 18	> 15

*Under a surcharge of 1 psi

Several other models have been reported in the literature by McKeen (1980), Hamberg (1985), Snethen, *et al.* (1977), Mitchell and Avalle (1984), Jayatilaka and Lytton (1997), and Lytton, *et al*. (2004). Direct tests (such as free vertical swell strain test, volumetric swell strain test and suction potential measurements) are typically carried out to characterize the swelling potential of clays. Alternatively, indirect parameters such as Atterberg limits, activity or cation exchange capacity can be used to assess swell potentials of expansive subsoils. Instruments such as tensiometer or thermal conductivity sensors or filter paper method can be used to measure matric suction, whereas psychrometer or filter paper method can be used to measure total suction in soils. Swell properties such as swell strain and swell pressure of expansive soils are dependent on three factors: (1) soil properties such as compaction or natural moisture content variation, dry density, and plasticity index, (2) environmental conditions including temperature and humidity and (3) natural overburden pressure. Because of the influence of these factors, several expansive soil characterization methods have been developed (Puppala *et al*., 2004a). These methods are mainly based on (1) swell strain and pressure measurements, (2) plasticity properties, and (3) other correlations using activity and compaction properties.

4.4.1.1. OEDOMETER TEST METHOD

Based on oedometer tests, volume change can be estimated by applying the consolidation theory in reverse.

$$\frac{\Delta H}{H} = \frac{\left|e_f - e_0\right|}{1 + e_0} \tag{4.1}$$

where ΔH= heave; H = layer thickness; e_0 and e_f are initial and final void ratios, respectively. As the oedometer test results usually overestimate the vertical swell, Al-Shamrani and Al-Mhaidib suggested a lateral restraint factor and a moisture factor to be used in analyses when using the results of oedometer tests.

4.4.1.2. VAN DER MERWE (1964) METHOD

This method is based on empirical relationships between the degree of expansion, PI, percent clay fraction, and the surcharge pressure. The total heave at the ground surface is found from:

$$\Delta H = \sum_{D=1}^{D=n} F \times PE \tag{4.2}$$

where ΔH = total heave (in.); D = depth of soil layer in increments of 1 ft; n = increment at the deepest level; F = reduction factor for surcharge pressure, $F = 10^{-D/20}$, PE = potential expansion (in./ft.), which is a function of the PI and the minus 2μ fraction (as shown in Figure 4.2). The PE values are based on consolidometer swell test results and field observation. This method does not consider variations in initial moisture conditions.

4.4.1.3. HAMBERG (1985) METHOD

Hamberg (1985) evaluated available testing procedures for characterizing expansive soils. He developed a method for predicting total heave on specified sites with shallow depth moisture changes and light structural loading. His relationships are in the form of

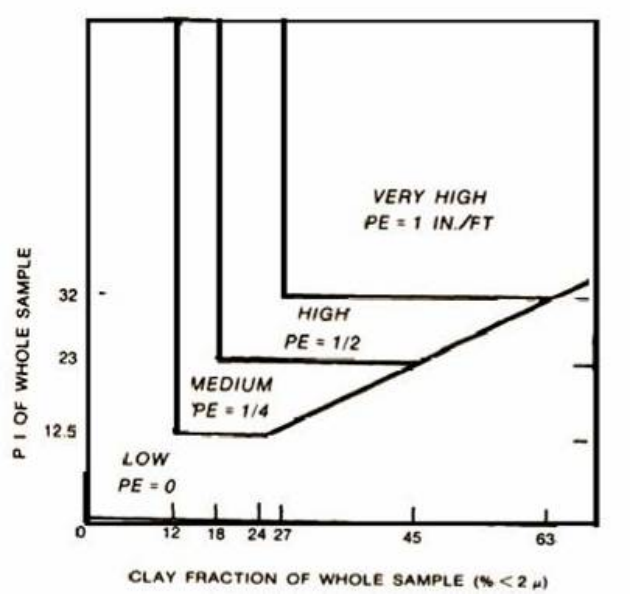

Figure 4.2—Van De Merwe (1964) Method for Potential Volume Change Prediction

$$\Delta H = \sum_{i=1}^{N}\left[\frac{H_i}{(1+e_0)}\right]\times\left[C_h \times \Delta\log(h)\right]_i \tag{4.3}$$

$$\Delta H = \sum_{i=1}^{N}\left[\frac{H_i}{(1+e_0)}\right]\times\left(C_w \times \Delta w\right)_i \tag{4.4}$$

where ΔH = vertical movement; N = number of layers to depth of active zone; H_i = thickness of layer i; e_0 = initial void ration of layer i; C_h = suction index with respect to void ratio (slope of void ratio verses soil suction in logarithmic scale); h = soil suction (total or matric); C_w = modulus ratio (slope of void ratio versus water content); Δw = change in water content.

4.4.1.4. SNETHEN (1977) METHOD

Snethen *et al*. (1977) proposed a model to predict potential heave as following:

$$\frac{\Delta H}{H} = \frac{C_\tau}{1+e_0}\left[\left(A - Bw_0\right) - \log\left(\tau_{mf} + \alpha\sigma_f\right)\right] \tag{4.5}$$

where ΔH = heaving (ft);H = stratum thickness (ft); C_x = suction index, $C_x=\alpha G_s/100B$, G_s is the specific gravity, e_0 = initial void ratio; w_0 = initial moisture content (%); τ_{mf} = final matrix soil

suction (tsf); α= compressibility factor. In the absence of measured data, α can be roughly estimated from the PI by: *PI<=5,* α*=0*; *5<PI<40*, α*=0.0275PI-0.125*; *PI>=40*, α*=1*; σ_f = final applied pressure (overburden plus external load) (tsf), *A, B* = constants of suction vs. water content relationship.

4.4.1.5. MITCHELL AND AVALLE (1984) METHOD

Mitchell and Avalle derived a simple method to predict soil expansion movement from soil suction changes. They termed instability index as the relationship between soil linear strain and moisture characteristic of unconfined undisturbed samples which are allowed to dry from moisture content above the shrinkage limit. They proposed shrinkage test to obtain this index.

$$\Delta H = \sum_{i=1}^{N} \left(I_{pt} \times \Delta u \times H_i \right) \tag{4.6}$$

where ΔH = vertical movement; N = number of layers to depth of active zone; I_{pt} = instability index; Δu = soil suction change, and H_i = thickness of layer i.

4.4.1.6. LYTTON (2004) METHOD

Lytton *et al*. (2004) developed a procedure for determination of swell potentials based on suction measurements and diffusion models of soils with various scenarios. The Thornthwaite moisture index, which is derived from the moisture balance procedure developed between rainfall and evapotranspiration (Thornthwaite, 1948), can be used to characterize climatic effects. Lytton, *et al.* (2004) procedure accounts for this and other parameters including topography and presence of localized water sources.

$$\frac{\Delta H}{H} = f\left(\frac{\Delta V}{V} \right) \tag{4.7}$$

Where $\Delta H/H$ = vertical strain; f = the crack fabric factor, can be calculated as $f=0.67-0.33\Delta pF$, $1/3 \leq f \leq 1$.

$$\Delta H = \sum_{i=1}^{N} f\left(\frac{\Delta V}{V}\right)_i \times \Delta z_i \tag{4.8}$$

where Δz_i = the i^{th} depth increment; N = number of layers to depth of active zone.

$$\left(\frac{\Delta V}{V}\right)_{i,swelling} = -\gamma_h \log\left(\frac{h_f}{h_i}\right) - \gamma_\sigma \log\left(\frac{\sigma_f}{\sigma_i}\right) \tag{4.9}$$

$$\left(\frac{\Delta V}{V}\right)_{i,shrinkage} = -\gamma_h \log\left(\frac{h_f}{h_i}\right) + \gamma_\sigma \log\left(\frac{\sigma_f}{\sigma_i}\right) \tag{4.10}$$

where $\Delta V/V$ = volume strain; γ_h = suction compression index, which can be expressed as: $\gamma_h = -(\Delta V/V_i)/(\log_{10}(h_f/h_i))$; h_i, h_f = initial and final suction; γ_σ = compressibility constant (mean principal stress compression index), and σ_i, σ_f = initial and final mean principal stresses respectively.

Several test methods can be used to determine the values of γ_h. McKeen (1980) indicated that filter paper and thermocouple psychrometer could be interchangeably used in laboratory studies. Filter paper method has several advantages: simplicity, low cost, and the wide range of suction values that it can measure.

Although Lytton's method is considered as an improvement when compared to current PVR method, it is still limited by a few problems and concerns. The influence or impacts of various boundary conditions on swell property variations need more investigation. The method also uses several empirical relationships with different degrees of coefficient of correlation. Such practice can lead to compounding of errors, which may limit the practicality of such expressions for routine use. Once thoroughly evaluated and modified if necessary, this suction based method can be confidently used for estimating swell properties of site soils in the design of pavements.

4.4.1.7. POTENTIAL VERTICAL RISE (PVR) METHOD (TEX-124-E)

The potential vertical rise method (PVR) is widely used in Texas for the estimation of volume change behavior of expansive soils. The PVR is the latent or potential ability of a soil material to swell, at a given density, moisture, and loading condition, when exposed to capillary or surface water, and thereby increase the elevation of its upper surface, along with anything resting on it.

Field heaves are estimated based on the swell test results of compacted soils. The potential heave of each soil stratum is estimated from a family of curves using the LL, PI, surcharge pressure on the soil stratum, and initial water content. The initial water content is compared with maximum (0.47LL + 2) and minimum (0.2LL + 9) water contests to evaluate the percent volumetric change. The PVR of each stratum is found from a chart using the percent volumetric change and the unit load bearing. Heave down depths of up to 30 ft are summed to evaluate the total PVR. PVR method will be further discussed in Section 4.4.2.

4.4.1.8. SUMMARY OF OTHER METHODS

There are usually two quantitative parameters for swelling characteristic: (1) Percentage swelling which is the vertical swelling strain under the applied load, and (2) Swelling pressure which is the maximum vertical stress required to keep the soil sample at the initial volume when the sample is inundated with water and full swell occurs (Ofer and Blight, 1985).

Hussein (2001) derived a constitutive model to represent the visco-plastic behavior of an expansive soil upon wetting and drying. The model takes into account the current stress, water content and clay content as well as environmental factors. The time-dependent deformation and stress changes are associated with pore-water migration and the swelling and viscous nature of

the material. The magnitudes of percent swell and swelling pressure are influenced by a large number of other factors, such as:

- Compositional factors, which include the type and amount of clay mineral present in the soil as well as the pore fluid characteristics.
- Environmental factors, such as initial moisture content, initial density, initial degree of saturation, initial soil structure, stress history, availability and composition of ambient water and temperature.
- Procedural factors in laboratory testing e.g. size and shape of soil sample, degree of disturbance and testing procedure and techniques used.
- Climate, depth of active zone, location and thickness of the expansive soil layer, applied loads (weight of structure and soil overburden), vegetation, site topography, surface drainage and confinement

Budge, *et al*. (1966) used one-dimensional consolidometer test to determine the swell characteristics of an expansive subgrade soil. This method was specifically applied to stiff, fissured clay shale which served as subgrade. Due to overburden removal and moisture increase, the subgrade in question caused pavement heave in the order of several inches. In their research, a new sampling equipment was designed which contained a series of liners. This enable the test specimens to remain confined in linear rings. Complete lateral confinement prevents stress relief accompanied by premature expansion during transfer of the sample into the consolidometer. The samples were loaded and unloaded in single increments to determine the expansion characteristics. The portion of total heave resulting from moisture increase was obtained in a similar swell test in which the soil was given free access to water while under full overburden pressure. Total surface heave was estimated from pressure release and soil moisture increase.

Their validation study showed surface heave predictions close to the field measured heave on the test pavement in the first five years since construction. This study also showed it was possible to estimate the potential heave of increments of soil at any sampling depth. But as expected, the layers of soil immediately beneath the pavement contributed more to heave of the pavement than increments at greater depth.

For design purposes, empirical prediction methods are generally inadequate. Holland and Cameron (1981) suggested swell testing in conventional consolidometer with a moisture correction factor provided better predictions. Various correlations have been suggested for predicting the swell pressure and percent swell, they are summarized in Appendix B.

4.4.1.9. SELECTION OF VOLUMETRIC CHANGE PREDICTION MODEL

In order to select the most feasible volumetric change prediction model, the estimated vertical movements from the seven models discussed in previous sections (Section 4.4.1.1 to 4.4.1.7) using our laboratory test results and field results are studied. An excel file was developed to automate the calculation process.

Table 4.2 summarizes parameters used and results obtained. Prediction results do not show any trends or correlations. For a 6-ft soil stratum, the predicted vertical volumetric change (heaving) varies widely from 0.1 in. to 6.3 in. Snethen (1977) method gives the minimum estimation yet Lytton (2004) reaches the maximum result. PVR method yields an estimated vertical rise of 2.4 in. It is very difficult to give an exact estimate of volumetric change behavior for different subgrade soils that an engineer may encounter in situ. The information and discussions presented thus far in this section suggests that these empirical relationships are only valid for certain conditions and they become less representative for our high PI subgrade

Table 4.2—Comparisons of Volumetric Change Prediction Models from Literature (Paris)

Parameters		Values	Volumetric Change Prediction Models						
			Oedometer	Van Der Merwe (1964)	Hamberg (1985)	Snethen (1977)	Mitchell & Avalle (1984)	Lytton (2004)	PVR
Liquid Limit (%)	LL	60						x	x
Plastic Limit (%)	PL	24						x	x
Plasticity Index (%)	PI	36							x
Passing No. 200 (%)	P200	100						x	x
Passing No. 40 (%)	P40	100						x	
Fine clay content (<2μm) (%)	<2μm	70					x	x	
Specific gravity	Gs	2.7				x		x	x
Initial void ratio	e_0	0.65	x		x	x		x	
Final void ratio	e_f	0.62	x						
Initial moisture content (%)	w_0	15				x			
Final moisture content (%)	w_f	23				x			x
Change in moisture content	Δw	8			x		x		
Mean principal stress compression index $\gamma_\sigma = C_c/(1+e_0)$	γ_σ	0.2125						x	
Compressibility factor (0<α<1)	α	0.865				x			
Compression index	C_c	0.35						x	

Table 4.2—Comparisons of Volumetric Change Prediction Models from Literature (Paris) (Continued)

Parameters		Values	Volumetric Change Prediction Models						
			Oedometer	Van Der Merwe (1964)	Hamberg (1985)	Snethen (1977)	Mitchell & Avalle (1984)	Lytton (2004)	PVR
Suction index with respect to void ratio $C_h = C_w \cdot D_h$	LL	60						x	x
Modulus ratio $C_w = \Delta e / \Delta w$	C_w	-0.325			x				
Suction index $D_h = \Delta w / \Delta u$	D_h	0.049							
Soil suction change (pF)	Δh	1.645			x		x		
Initial suction (pF)	h_i	4.092			x			x	
Final suction (pF)	h_f	2.447			x			x	
Suction compression index	γ_h	-5.24						x	
Intercept of SWCC (1)	A	4.88				x			
Slope of SWCC	B	10.57				x			
Initial mean principal stress (psi)	σ_i	0.58						x	
Final mean principal stress (psi)	σ_f	2.58				x		x	
Predicted vertical movement (in.)			**1.1**	**6.0**	**0.1**(2) **1.1**(3)	**0.1**	**5.8**	**6.3**	**2.4**

Note: (1) SWCC – Soil Water Characteristic Curves; (2) Result from Eq. 4.3; (3) Result from Eq. 4.4.

analysis. It is not appropriate to extend the usage of these site-specific prediction models towards more generalized analysis. PVR method is finally selected as it is widely accepted, more generalized and more suitable for subgrade soils encountered in Texas.

4.4.2. Potential Vertical Rise

The PVR calculations are carried out manually in accordance with Test Method TEX-124-E. Following information is needed to perform PVR calculation:

- Total subgrade depth subjects to moisture fluctuation.
- LL, PI, MC and percent material passing No. 40 sieve (P40)
- PVR limiting criteria.

A typical PVR analysis is depicted for Paris soil in Table 4.3. Following are the steps to perform the calculation.

1) Enter soil layer thickness (column 1), LL (column 3), MC (column 6), P40 (column 8), and PI (column 9), for each soil layer.
2) Determine the overburden average load for each soil layer and tabulate in the appropriate row (column 2).
3) LL value for each layer (column 3) is used to calculate moisture content of Dry (column 4) and Wet (column 5) conditions by provided equations.
4) Record percent moisture values from the field samples in column 6. Determine whether the layers are "wet," "dry," or "average" by comparing actual moisture content with "dry" (column 4) and "wet" (column 5) values. The layer is considered "average" if the moisture content is closer to the average of the "wet" and "dry" conditions.

Table 4.3—PVR for Natural Subgrade in Paris District (Dry Soil Conditions)

1	2	3	4	5	6	7	8	9	10	11	12	13	14	15	16	17
Depth (ft)	Avg. Load (psi)	LL	Dry (0.2LL +9)	Wet (0.47LL +2)	MC (%)	Dry Avg Wet	P40	PI	% Vol. Swell	% Free Swell	PVR top	PVR bottom	Diff.	Mod. Factor for No.40	Mod. Factor for Density	PVR in Layer (in.)
0-2	1	60	21	30.2	23	Dry	100	36	10.5	13.8	0	1.1	1.1	1	1	1.1
2-4	3	60	21	30.2	23	Dry	100	36	10.5	13.8	1.1	1.9	0.8	1	1	0.8
4-6	5	60	21	30.2	23	Dry	100	36	10.5	13.8	1.9	2.4	0.5	1	1	0.5
6-8	7	60	21	30.2	23	Dry	100	36	10.5	13.8	2.4	2.8	0.4	1	1	0.4
8-10	9	60	21	30.2	23	Dry	100	36	10.5	13.8	2.8	3.0	0.2	1	1	0.2
10-12	11	60	21	30.2	23	Dry	100	36	10.5	13.8	3.0	3.2	0.2	1	1	0.2
																Total PVR = 3.2

5) Record the P40 in column 8 and PI in column 9.

6) Estimate the percent volumetric change for 1 psi overburden for each layer based on the PI and moisture condition of the each layer using Figure 4.3. Enter estimated percent volumetric change value for each layer in column 10.

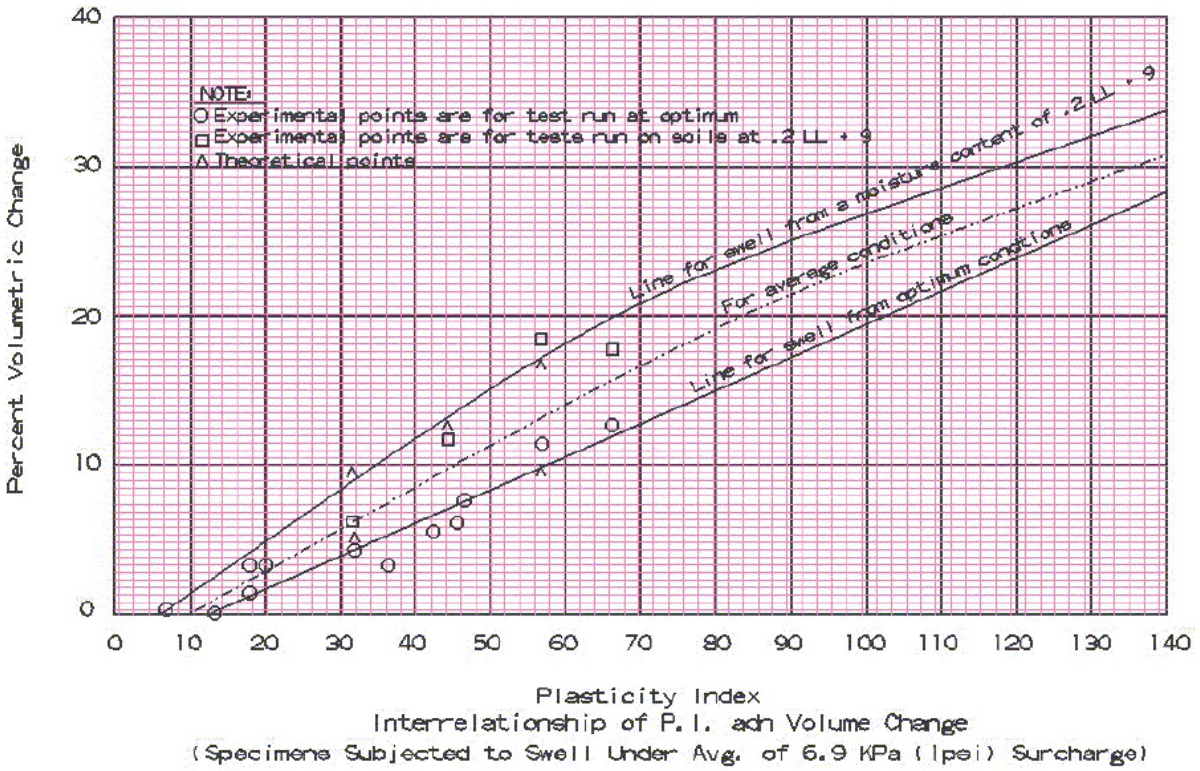

Figure 4.3—Interrelationship of PI and Percent Volume Change (Tex-124-E)

7) Convert the value in column 10 to the free swell (column 11) using: % Free Swell = (% Vol. Swell @ 6.9 kPa)* (1.07) + 2.6.

8) Estimate the PVR from the corresponding percent free swell curve in Figure 4.4 for the top (column 12) and bottom (column 13) of each layer and estimate the difference from the two (column 14).

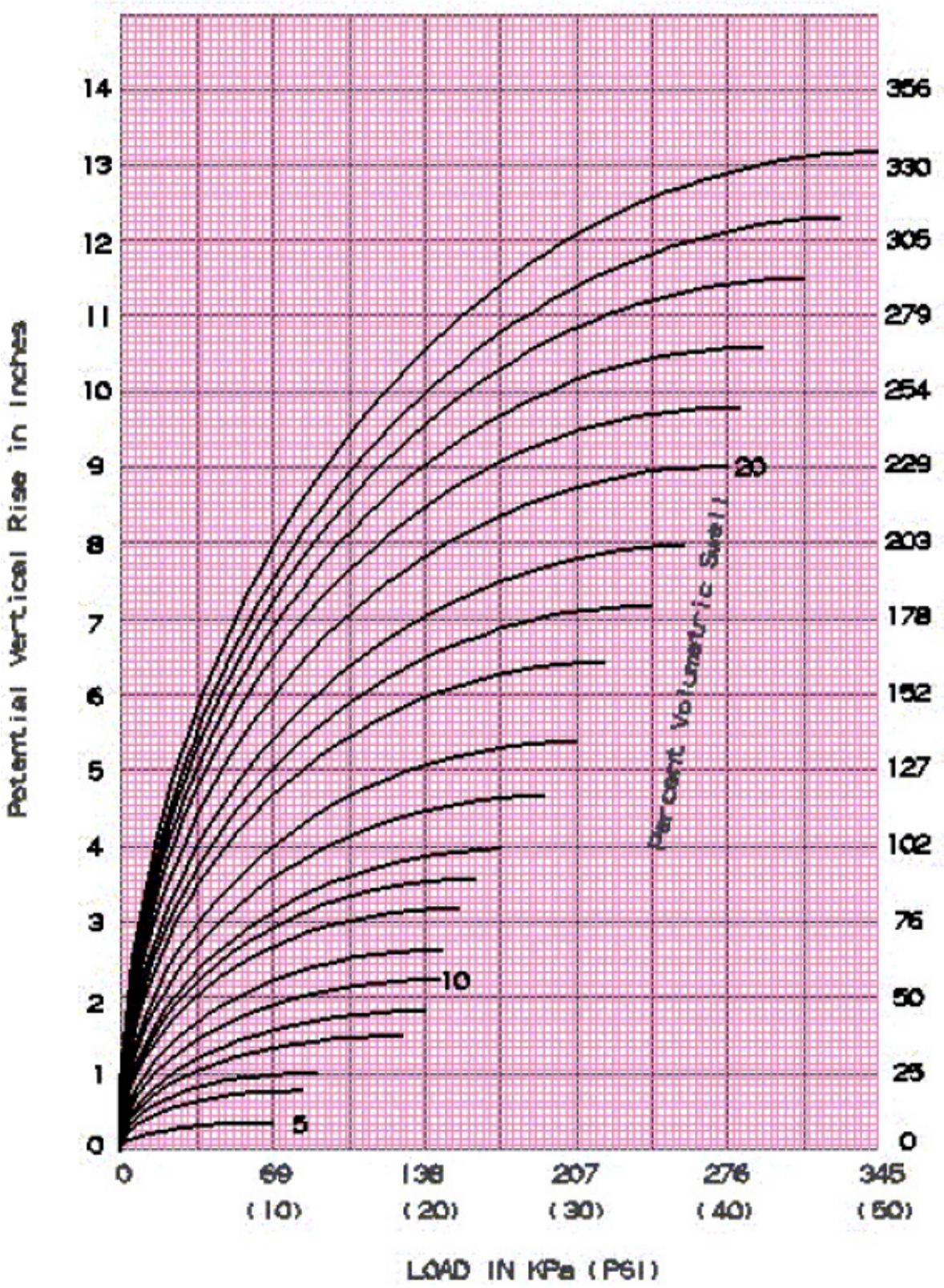

Figure 4.4—Relation of Load to Potential Vertical Rise (Tex-124-E)

9) Estimate the modification factor for the PVR values in column 14 based on P40 (column 8) is greater than or equal to 25% (the modification factor is equal to P40 divided by 100). Record the correction factor in column 15.
10) Estimate the modification factor for the wet density (the modification factor is equal to 125 pcf divided by the actual wet density of each layer). Enter this correction factor in column 16.
11) Multiply the difference in PVR (column 14) by the two modification factors (columns 15 and 16) and record the results in column 17.
12) Sum the PVR values for all layers. In this example, the Paris soil has a PVR of 3.2 in. without any pavement structure surcharge under dry condition.

In order to automate PVR calculation, TxDOT developed an Excel spreadsheet with newly generated curve equations. Upon the entry of necessary soil properties, the Excel software program provides the PVR value at both top and bottom of each layer and the total PVR value. Puppala and Reddy (2006) studied the new TxDOT excel sheet and found some discrepancies between the manual calculation and the automated excel results, especially at higher volumetric swell (25%-35%). To more accurately reproduce Figure 4.4 and automate PVR estimates in this project, extensive digitalization and curve-fitting were performed. A simple equation to calculate PVR based on volumetric swell is developed in the form of:

$$PVR = \sqrt{C_1 \cdot P + C_2 \cdot P^2} \tag{4.11}$$

where P = average load of the analyzed layer (psi), C_1, C_2 = curve-fitted constants that are a function of percentage volumetric swell (α) as shown below:

$$C_1 = (a_1 + c_1(\alpha - 5)^{0.5} + e_1(\alpha - 5)/(1 + b_1(\alpha - 5)^{0.5} + d_1(\alpha - 5)) \tag{4.12}$$

$$C_2 = (a_2 + c_2(\alpha - 5)^{0.5} + e_2(\alpha - 5))/(1 + b_2(\alpha - 5)^{0.5} + d_2(\alpha - 5)) \tag{4.13}$$

Table 4.4 summarizes the curve-fitted constants to calculate C_1 and C_2.

Table 4.4—Curve-Fitted Constants for PVR Calculation

Parameter	$i = 1$	$i = 2$
a_i	0.024553	-0.00134
b_i	-0.42373	-0.41504
c_i	0.028175	-0.00109
d_i	0.047329	0.046243
e_i	0.009891	7.05E-05

Since the amount of volume change in expansive soils is directly related to the changes in moisture content or soil suction, the maximum potential vertical movement at the edge of a pavement should be higher than that of the interior of the pavement. The magnitude of vertical movement in a pavement is not uniform everywhere even when the subgrade soil properties are similar. PVR method does not consider horizontal difference. Also, PVR method does not consider topography, vegetation and drainage effects. The consensus of the practitioners is that the method described above gives overly conservative estimations of swell potentials for low plasticity soils and under conservative estimations for high PI soils. TxDOT is currently attempting to implement an alternate approach for better swell property characterization (Lytton *et al*., 2004).

4.4.3. International Roughness Index

IRI is used to define characteristic of the longitudinal profile of a traveled wheel track and constitutes a standardized roughness measurement. It is based on the average rectified slope (ARS), which is a filtered ratio of a standard vehicle's accumulated suspension motion divided by the distance traveled by the vehicle during the measurement. The commonly recommended units are meters per kilometer (m/km). IRI is then equal to ARS multiplied by 1,000. Figure 4.5 re-plots the physical interpretation of the open-ended IRI scale (from Sayers *et al.*, 1986).

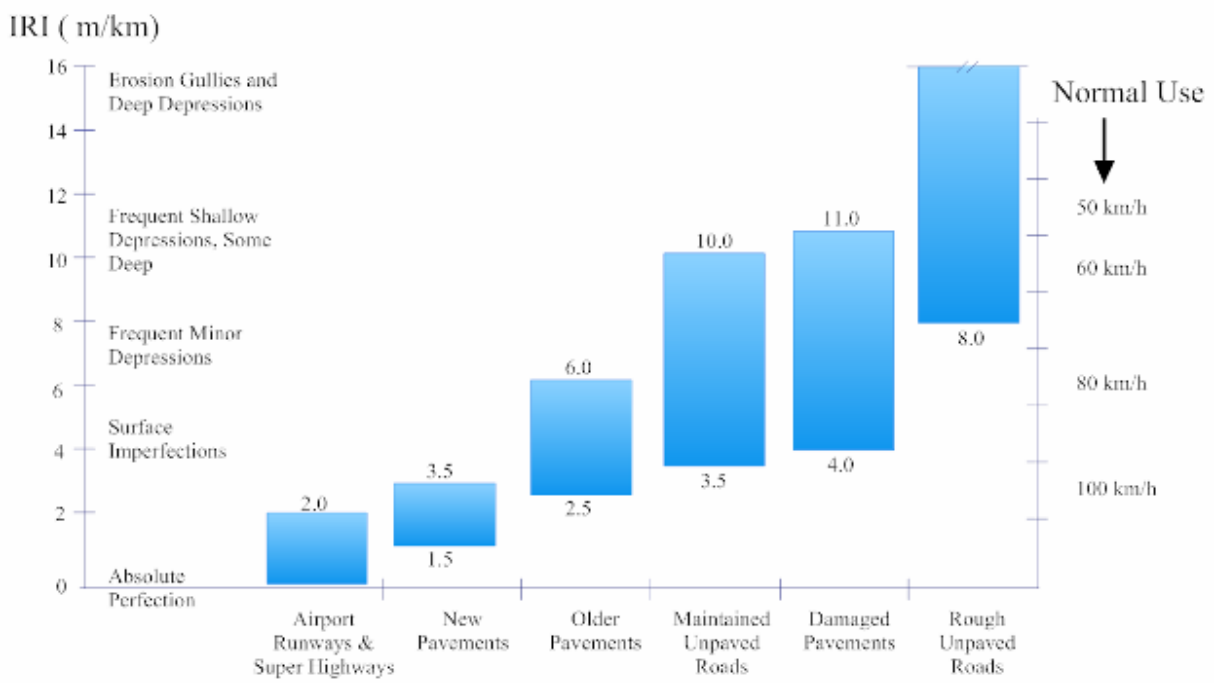

Figure 4.5—Physical Interpretation of the Open-Ended IRI Scale (Replotted from Sayers, et al., 1986)

Non-traffic-related pavement roughness is caused mainly by differential heaving, thermal or shrinkage cracking and loss of bearing capacity. Moisture variation is the major factor contributing to the unevenness of subgrade heaving/shrinking which in turn, is the major factor contributing to pavement roughness.

Lytton *et al*. (2004) used AASHTO (1993) design equations in their two-dimensional analysis to predict roughness in terms of IRI caused by both traffic and expansive clay movements as follows:

$$IRI = IRI_0 + (4.2 - IRI_0)\exp\left[-\left(\frac{\rho_i}{t}\right)^{\beta_i}\right] \tag{4.14}$$

where IRI_0 = initial *IRI* in m/km, β_i = regression roughness coefficient = 0.56, ρ_i = roughness parameter that can be calculated from:

$$\rho_i = A_i - B_i \Delta H \tag{4.15}$$

where ΔH = total vertical movement (mm) considering both shrinking and swelling, A_i = parameter that is a function of traffic, structural number (SN) of the pavement section, and resilient modulus of subgrade soil (M_R). Lytton *et al*. (2004) derived A_i as:

$$A_i = t\left[\log_e\left(\frac{3.01}{8.4183\exp\left(-0.4664\left(4.2-2.7\left(10^{\lambda}\right)\right)\right)-1.19}\right)\right]^{\left(\frac{1}{0.56}\right)} \quad (4.16)$$

where t = 480 months, which is assumed to be the time required for the roughness due to expansive clays to be complete, λ = parameter that is a function of accumulated ESALs (W_{18}), standard normal variable (Z) corresponding to the assigned reliability, SN, M_R and standard deviation (S_0 = 0.35). λ is also estimated for 40 years from

$$\lambda = \left[0.4+\frac{1094}{(SN+1)^{5.19}}\right]\times\left[\log_{10} W_{18} - 9.36\log_{10}(SN+1)+8.27-2.32\log_{10} M_r + ZS_0\right] \quad (4.17)$$

where B_i = statistical constant = 35.817+8.758Z.

In roughness check module, the PVR value predicted as described in Section 4.4.2 is used as ΔH. This value only takes into consideration the maximum possible heaving. Since high PI subgrade is also subject to vertical shrinking, in reality the combined total vertical movement (ΔH) should be much less. As a result, this evaluation gives an over estimate of IRI.

4.5. LONGITUDINAL SHRINKAGE CRACKING (LSC) MODELS

4.5.1. Overview

During a dry weather cycle, subgrade shrinkage will cause lateral forces which may exceed its tensile strength. The increase in the lateral shrinkage stress of soil is the main reason for the development of longitudinal cracks. Currently TxDOT does not design pavement for mitigation of longitudinal cracks. Extensive laboratory investigation and modeling were carried out to address this issue. Figure 4.6 presents the conceptual flowchart of LSC model developmental steps. Firstly, laboratory tests were conducted to develop generalized

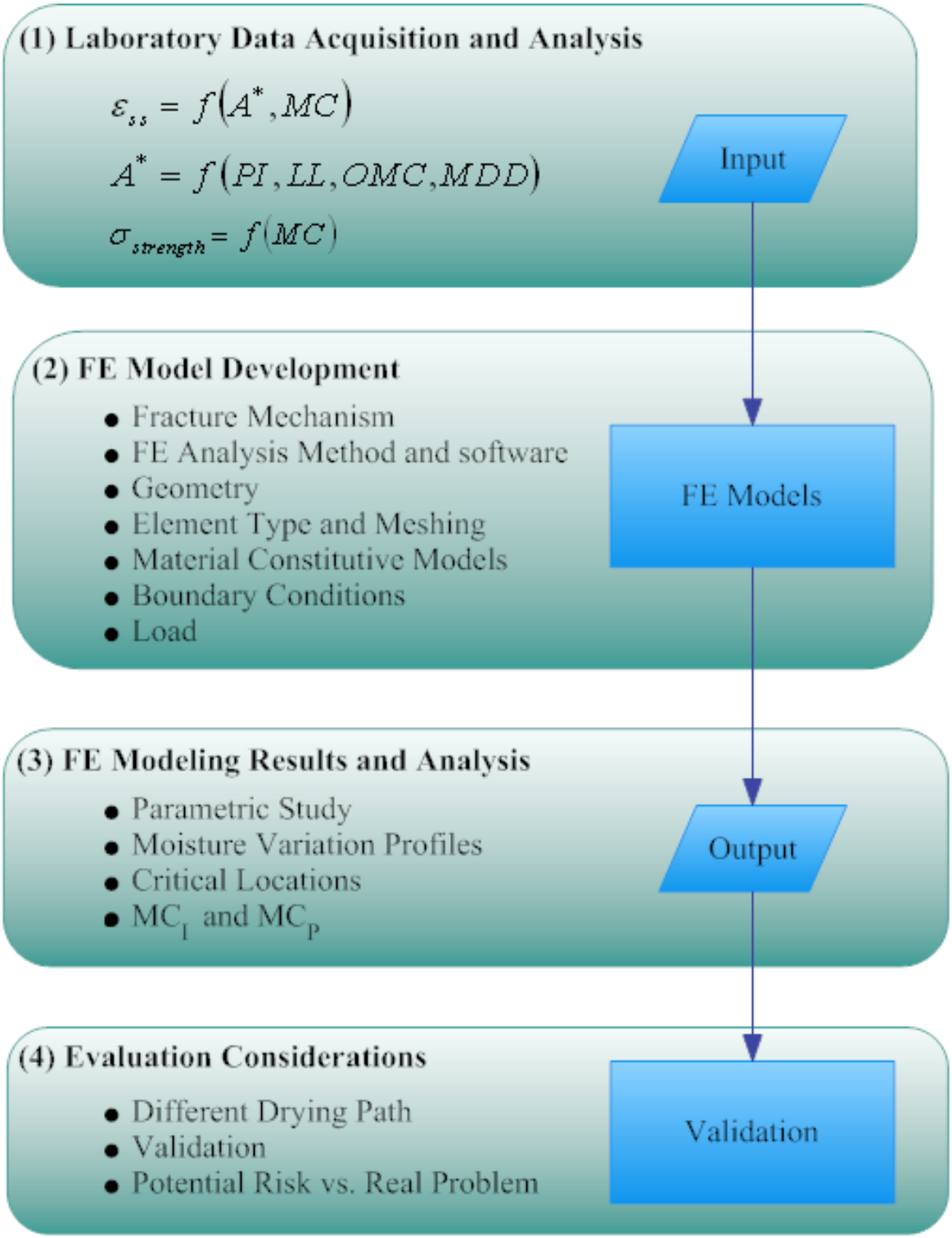

Figure 4.6—Conceptual Flowchart of LSC Model Development

mathematical models which can predict the variation in subgrade soil shrinkage strain (ε_{ss}), tensile strength ($\sigma_{strength}$) and modulus (M_R) as a function of subgrade moisture content (MC) variations. To be specific, three mathematical relationships will be concluded as: (1) ε_{ss} as a function of MC and parameter A^*; (2) A^* as a function of index properties; and 3) $\sigma_{strength}$ as a function of MC. These models are used as input in finite element analysis (FEA) modeling to estimate the moisture content thresholds for the initiation (MC_I) and propagation (MC_P) of longitudinal cracks in the pavement structure. The FEA code also estimates the most likely location for such cracking. Following sections describes the methodology of each step to perform the LSC check under moisture variation. Finally evaluation considerations and validations will be discussed.

4.5.2. Laboratory Data Acquisition and Analysis

4.5.2.1. Laboratory Tests Overview

Extensive laboratory tests were conducted to determine the shrinkage strain, strength and stiffness properties of several clays at different moisture conditions. The reader is referred to Sabnis *et al.* (2008) for details of this aspect of the project. These properties were used as inputs and constraint in the LSC check module. A brief explanation is provided below.

Six different clay materials, consisting of five high-PI clays (PI > 25) and one low-PI clay (PI = 17), were tested. The high-PI clays were brought from Houston, Forth Worth, San Antonio, Paris and Bryan Districts, whereas the low-PI clay was from El Paso. Among these, Paris clay showed the most drastic change in property with moisture variation and El Paso the least. In the following section, Paris clay will be used in discussion as an example for the worst case scenario. Several index tests, consisting of hydrometer (Tex-110-E) and Atterberg limits (Tex-104-E and Tex-105-E), were carried out on the clay materials. Moisture density tests were also performed

on all materials to obtain their optimum moisture contents (OMC) and maximum dry densities (MDD) following Tex-114-E. Strength tests performed include unconfined compressive strength (UCS) tests (Tex-117-E) and indirect tensile strength (IDT, Tex-226-F) tests. The free-free resonant column tests (FFRC, Tex-149-E), resilient modulus tests (MR, AASHTO-T-307) and permanent deformation (PD) tests were carried out to quantify the stiffness properties of each clay material.

Three moisture conditioning regimes were used for above tests. In the first set of tests, the specimens were prepared and tested at their corresponding OMC. The second set involves drying specimens from OMC to constant weights (DFO). The third set of specimens was saturated from their OMC (SFO). In following discussions, the relationships developed for specimens that were dried from optimum (DFO) are included for brevity.

4.5.2.2. SHRINKAGE STRAIN AND MOISTURE CONTENT RELATIONSHIP DEVELOPMENT

The volumetric shrinkage strain tests measured the variations in the absolute values of vertical, lateral and volumetric shrinkage strains with time. Figure 4.7 shows the typical results of Paris clay. In this case, the specimen shrunk equally in lateral and vertical direction with the maximum shrinkage strain of 6.8%. The volumetric strain had a maximum value of 18.8%. Since the development of general relationships between moisture variation and shrinkage strain was of interest, the moisture contents were normalized by dividing the individual moisture contents by the OMC, as shown in Figure 4.8 for Paris clay. Based on extensive curve fitting analysis, a relationship in the form of Equation 4.18 was selected:

$$\varepsilon_{ss} = \left[A^* \left(1 - NMC^2\right)\right]^2 \tag{4.18}$$

where ε_{ss} is shrinkage strain; A^* is the parameter that was obtained from curve fitting.

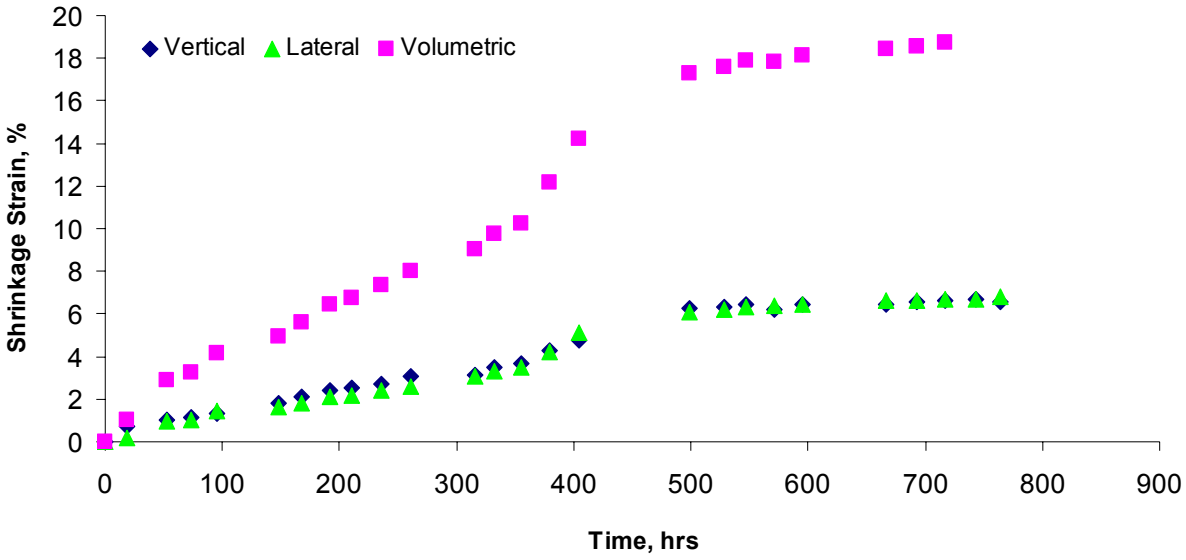

Figure 4.7—Shrinkage Strain Variations with Time (Paris, DFO)

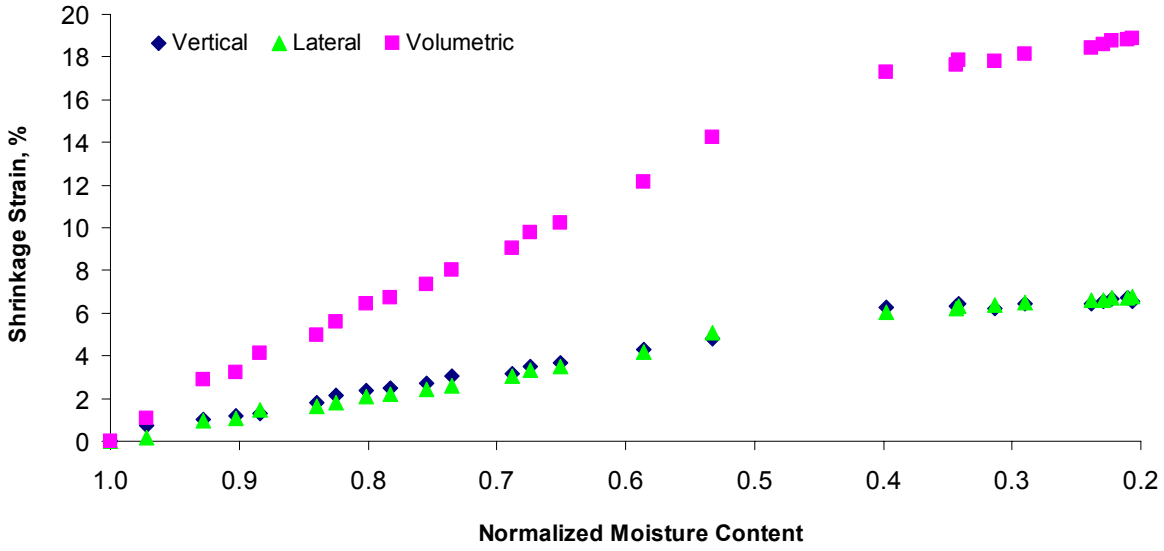

Figure 4.8—Shrinkage Strain Variations with NMC (Paris, DFO)

For each site, three identical specimens were prepared and tested. Table 4.5 summarizes parameter A^* in Equation 4.18 for lateral, vertical and volumetric shrinkage strains of Paris clays. All three shrinkage strains correlated well with the NMC for each specimen curve-fitted individually ($R^2 > 0.9$).

Table 4.5—Best-fit Parameter A^* for Shrinkage Strain vs. NMC (Paris, DFO)

Specimen	Lateral		Vertical		Volumetric	
	A*	R^2	A*	R^2	A*	R^2
Specimen 1	2.83	0.96	2.83	0.96	4.76	0.96
Specimen 2	2.75	0.98	2.66	0.99	4.57	0.99
Specimen 3	2.68	0.93	2.65	0.97	4.50	0.95

4.5.2.3. SHRINKAGE STRAIN AND INDEX PARAMETERS RELATIONSHIP DEVELOPMENT

Parameter A^* is highly site specific. An attempt was made to develop relationships that can predict the fitted parameter A^* in Equation 4.18 from the index properties of the material. In that manner, the variations in shrinkage strain can be readily predicted by knowing the index properties of the soil. The relationships between A^* values and their corresponding index properties for all soils except Houston[1] are plotted in Figure 4.9.

Best fit curves between Parameter A^* and these index properties of all clay materials (except Houston) are shown in Table 4.6. Based on R^2 values, A* is correlated or marginally correlated to PI, LL, MDD and OMC; whereas PL and seismic modulus at OMC are poorly correlated to A*. In general, PI and OMC are the two parameters that most favorably correlate with parameters A*.

To strengthen the relationship between index properties and A^*, the use of all four index parameters was advocated using Equation 4.19.

$$A^* = \frac{A_{PI} \times W_{A-PI} + A_{LL} \times W_{A-LL} + A_{OMC} \times W_{A-OMC} + A_{MDD} \times W_{A-MDD}}{W_{A-PI} + W_{A-LL} + W_{A-OMC} + W_{A-MDD}} \quad (4.19)$$

[1]The results from the Houston clay were used for validation purposes, since it is not appropriate to validate a relationship with data used in the development process.

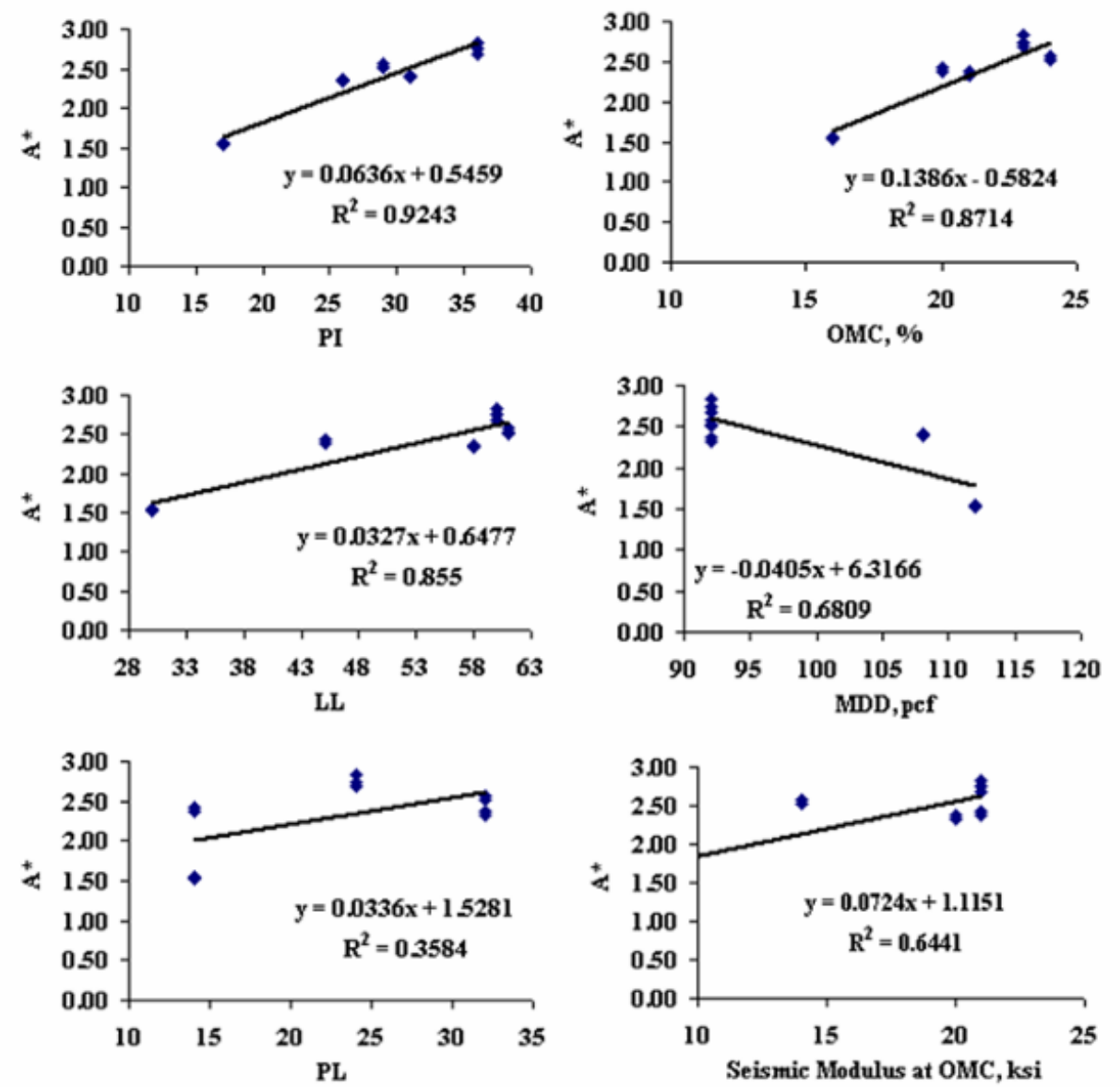

Figure 4.9—Summary of Correlations between Parameter A* and Index Properties (DFO)

where A_i is parameter A^* obtained from single index parameter *i* in Table 4.6; $W_{A\text{-}i}$ is the weighting factor for index parameter *i*; *i* refers to one of the four selected index parameters of PI, LL, OMC and MDD.

To make the model versatile so that it can be used with any missing data, the R^2 value from each of the relationships in Table 4.6 was used as a weighting multiplication factor. To get

Table 4.6—Correlation Analysis Results of Parameter A_i and Index Properties (DFO)

Index Property (i)	Equation	Parameter A_i^*		
		Lateral	Vertical	Volumetric
PI	Slope	0.06	0.25	0.59
	Intercept	0.55	-2.59	-3.32
	R2	0.92	0.83	0.83
LL	Slope	0.03	0.13	0.28
	Intercept	0.65	-2.57	-1.70
	R2	0.85	0.93	0.90
OMC	Slope	0.14	0.47	1.02
	Intercept	-0.58	-5.42	-8.20
	R2	0.87	0.93	0.95
MDD	Slope	-0.04	-0.17	-0.32
	Intercept	6.32	21.13	44.82
	R2	0.68	0.84	0.73

the weighted parameter A^*, the weighting factor for each of the index parameters, $W_{A\text{-}i}$ can be calculated using

$$W_{A-i} = \frac{G_i}{\sum G_i} \tag{4.20}$$

where G_i is the contribution factor, which is calculated based on $(R^2)_i$ values:

$$G_i = \begin{cases} (R^2)_i \times 4 & if \quad (R^2)_i \geq 0.8 \\ (R^2)_i \times 2 & if \quad 0.8 > (R^2)_i \geq 0.6 \\ (R^2)_i \times 1 & if \quad (R^2)_i \leq 0.6 \end{cases} \tag{4.21}$$

For R^2 values equal to or greater than 0.8, a factor of 4 is multiplied to get G_i. Similarly, for R^2 values between 0.6 and 0.8 a factor of 2 is multiplied to obtain G_i. For the R^2 value less than 0.6 a multiplication factor of 1 was used. As a general rule, the more complete index properties used, the better the correlation will be. Figure 4.10 summarized the steps used in developing ε_{ss} versus index properties relationship in flowchart format.

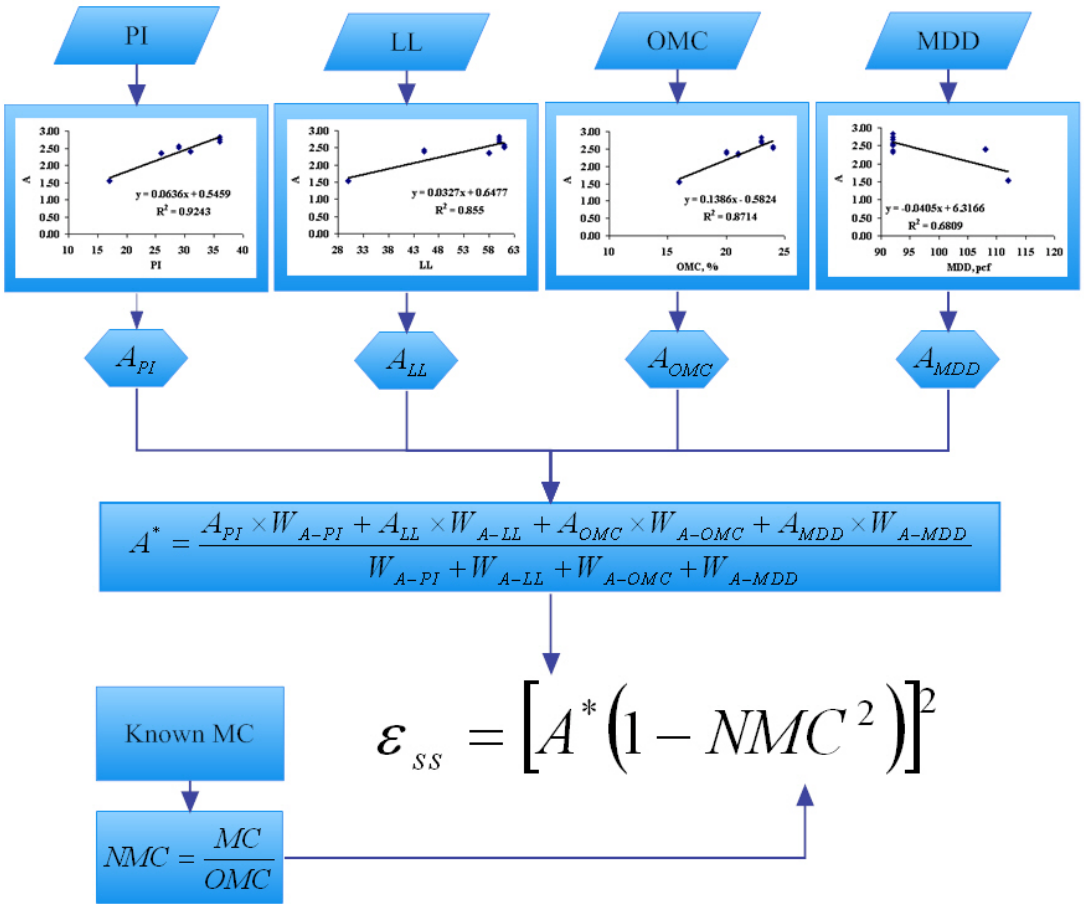

Figure 4.10—Flowchart of Shrinkage Strain Prediction Relationship Based on Index Properties

4.5.2.4. TENSILE STRENGTH AND MOISTURE CONTENT RELATIONSHIP DEVELOPMENT

IDT tests were performed on two specimens of each clay sample at six different moisture content levels from optimum to dry conditions. The variations in the average IDT strengths and normalized moisture contents for all soils are shown in Figure 4.11. All soils, except Bryan, follow a unique trend with approximately 25 psi peak strength under dry condition and decrease smoothly to approximately 5 psi at OMC. Given the number of soil tested, and to build in conservatism in the model, the results from Bryan were excluded from curve-fitting process. The mathematical relationship to estimate soil tensile strength $\sigma_{strength}$ from NMC is in the form of:

$$\sigma_{strength} = 35.7e^{-2.779 \times NMC} \quad (R^2 = 0.89) \tag{4.22}$$

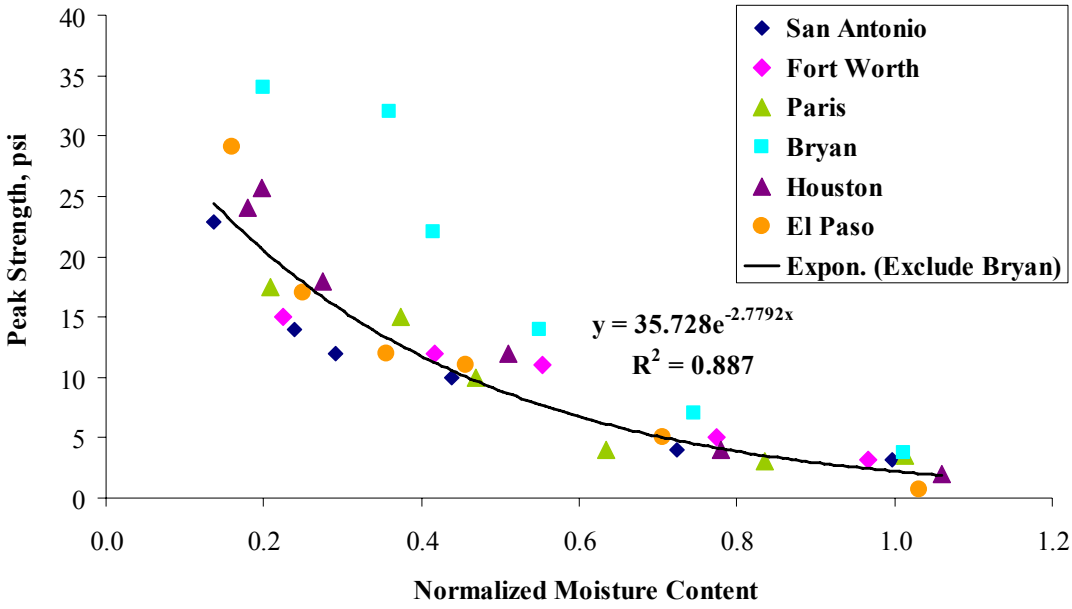

Figure 4.11—Indirect Tensile Strengths of Clays at Different Normalized Moisture Content

4.5.3. Finite Element Models Development

Two FEA models are used for the purpose of LSC check. Results from FEA models help pavement engineers determine the critical locations, moisture variation and possible design modifications to meet design criteria. In this section, the development procedures are introduced. First, FEA modeling algorithm is discussed. Then a brief overview of fracture mechanics and subgrade shrinkage cracking propagation mechanism are presented. The selection of appropriate FEA model and software, as well as FEA modeling details such as geometry, element type, meshing, material constitutive equations, boundary conditions and loading are discussed in Appendix C.

4.5.3.1. Longitudinal Shrinkage Cracking Model Algorithms

Figure 4.12 summarizes the LSC check algorithm. Normalized moisture content (NMC) is used as a controlled input (by iteration rules) to calculate $\sigma_{strength}$ using Equation 4.22. The same NMC value is also used to predict shrinkage strain, ε_{ss} by Equation 4.18. The representative

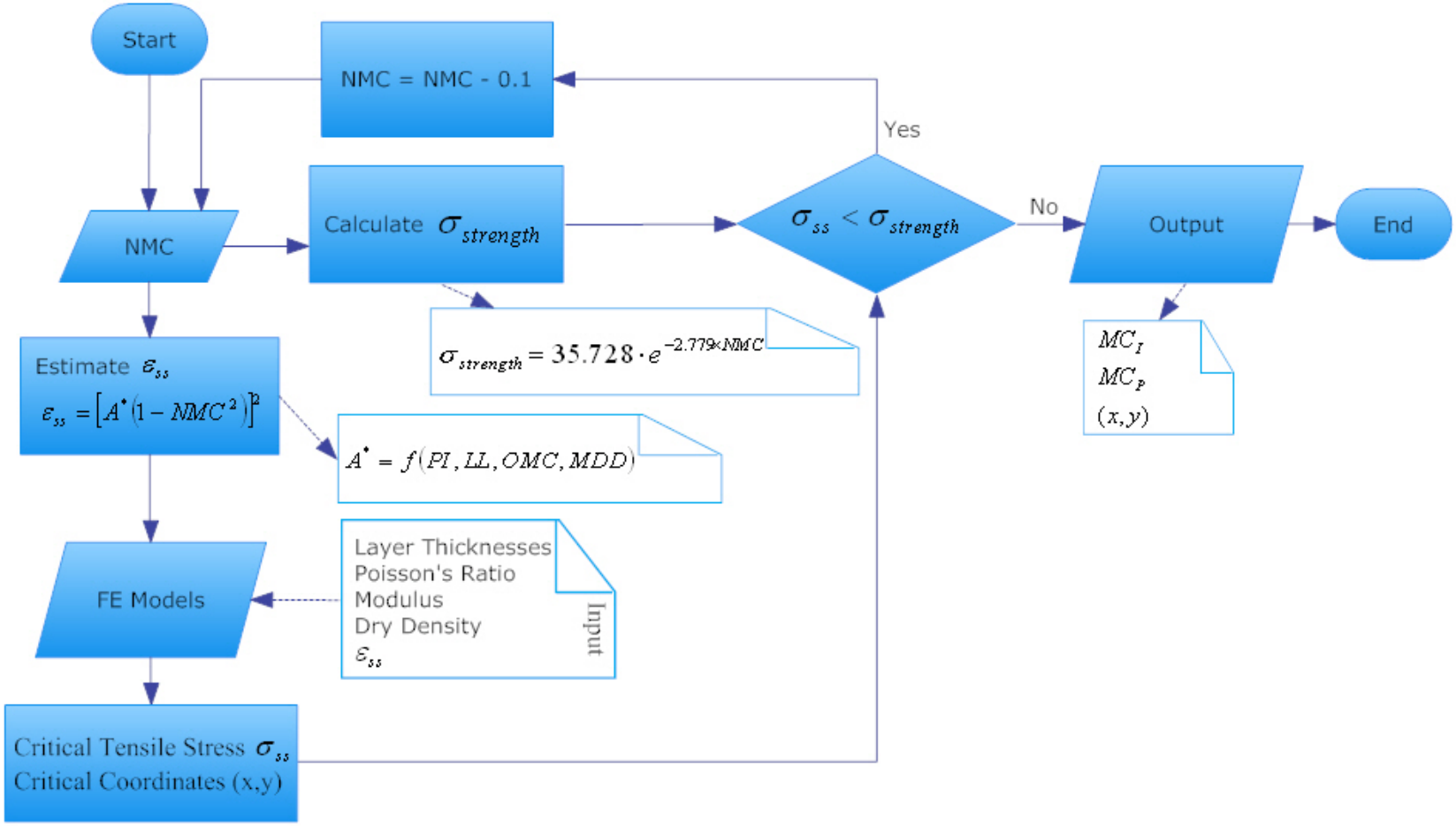

Figure 4.12—Longitudinal Shrinkage Cracking Model Algorithms

shrinkage strain induced tensile stress value (σ_{ss}) and the coordinates of critical stress points are then reported. If $\sigma_{ss} < \sigma_{strength}$, the crack has not yet initiated at the specified moisture content, and drying process is further simulated by reducing *NMC* . The FEA model stops when the critical moisture content that initiates cracking (e.g. $\sigma_{ss} >= \sigma_{strength}$) is identified. This moisture content that corresponds to the threshold of subgrade crack initiation is reported as MC_I. Based on further fracture mechanics analysis, the moisture content threshold to prevent cracking propagation through the pavement structure can also be estimated and reported as MC_P. Final outputs of LSC check include the two moisture thresholds MC_I and MC_P, and the coordinates of critical locations for longitudinal cracking. As a special note, the LSC model is based on drying from optimum. Although ε_{ss} prediction model for drying from saturation has also been studied, it is not incorporated in the model.

4.5.3.2. FRACTURE MECHANISM

Cohesive soil fracture behavior is rather complex. It is helpful to have a brief overview of fracture mechanics and cracking propagation mechanism to better understand subgrade shrinkage cracking behavior.

4.5.3.2.1. Types of Fractures

Two typical behaviors are anticipated for pavement materials under tension. A ductile material is characterized through plastic deformations which occur when the stress exceeds the yield strength (σ_y). In this case, the ultimate stress at fracture (σ_f) can only be attained after sufficiently large inelastic deformations. A brittle material, in contrast, exhibits no significant inelastic deformations prior to fracture. Thus, for brittle materials to fail, it is assumed that the maximum stress must be equal to or larger than the tensile strength ($\sigma_{strength}$) of the material. To simplify, linear elastic fracture mechanics is used in the FEA modeling. For a crack in a linear

elastic body, there are three different fractures commonly referred to as Mode I, II, and III (Figure 4.13).

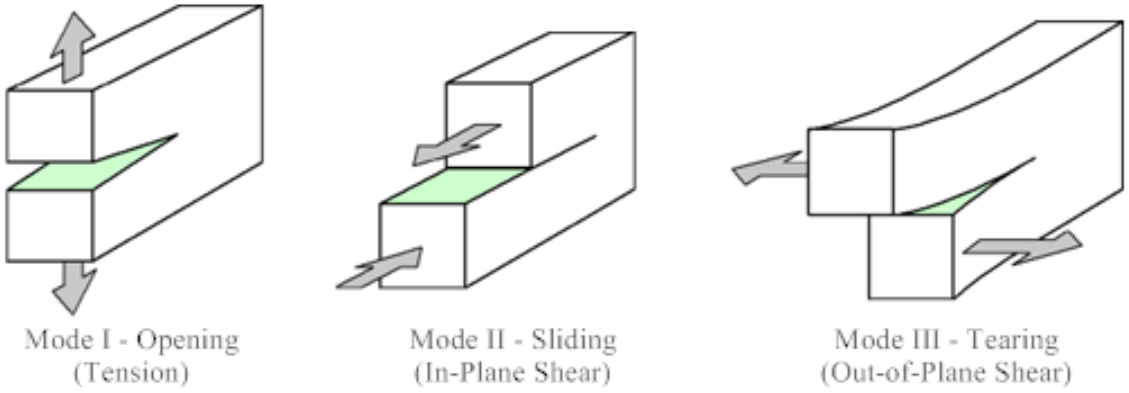

Figure 4.13—Three Fracture Modes

Mode I is the principal mode of fracture that occurs when two surfaces of a crack are being separated by tensile forces which are applied perpendicularly to the plane of the crack. Mode II is also referred to as the sliding mode of fracture and occurs when in-plane shear forces are applied to a body containing a crack. Mode III is sometimes called the tearing mode of fracture. This mode has out-of-plane shear forces acting on a plate the same manner that one uses to tear a sheet of paper. In the case of the shrinkage cracks, Mode I is assumed.

4.5.3.2.2. Fracture Toughness and Stress Intensity Factor

According to Griffith's fracture theory (1920), for ideally brittle materials, the growth of a crack requires creation of surface energy, which is supplied by the loss of strain energy accompanying the relaxation of local stresses as the crack advances. Failure occurs when the loss of strain energy is sufficient to provide the increase in surface energy. Irwin (1957) and his colleagues modified Griffith's theory and reformulated it in terms of stress, rather than energy. They introduced a new materials property: fracture toughness (K_{IC}) to quantitatively express a material's resistance to brittle fracture when a crack is present. If a material has large fracture

toughness, it will probably undergo ductile fracture. Brittle fracture is very characteristic of materials with a low fracture toughness value. The K_I value is a quantity which gives the magnitude of the elastic stress field called the stress intensity factor, subscript *I* refers to Mode I fracture. The general form of the stress intensity factor K_I is:

$$K_I = f(a/W) \cdot \sigma\sqrt{\pi a} \tag{4.23}$$

where *f(a/W)* is a dimensionless parameter which is also referred to as geometric factor. As its name implies, *f(a/W)* depends on the geometries of both the specimen and the crack. Parameter 2a is the through-thickness crack length; σ is the applied stress (remotely, not on crack tip). The crack tip stress and displacement fields, in a 2D rectangular coordinate system are shown in Figure 4.14. Equation 4.24 shows the stress intensity factor components for Mode I fracture.

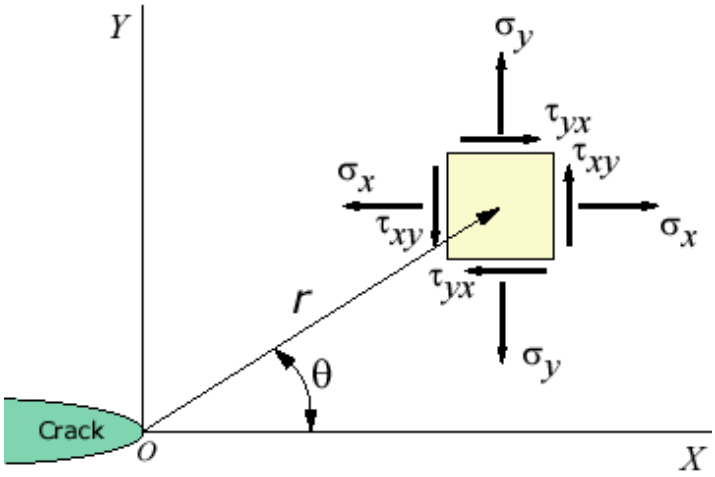

Figure 4.14—Two Dimensional Crack Tip Stress Components

$$K_I = \sqrt{2\pi r} \cdot \lim_{r \to 0} \sigma_{ij} \cdot \frac{1}{f_{ij}^{(I)}(\theta)} \tag{4.24}$$

4.5.3.2.3. Weight Function Method to Determine Stress Intensity Factor

A large number of methods are advocated in the literature to obtain stress intensity factor. Among these methods, the weight function method is especially suited for a given geometry, when a large number of stress intensity factor solutions for complex loadings are desired. The well-defined knowledge of a two-dimensional elastic crack solution as a function of crack length

for any loading enable one to determine the stress intensity factor for the same body under any other loading. Details of the development of simple-form generalized weight functions to obtain the geometric factor (*f*) are available in Wu and Carlsson (1991). Based on their calculation, for an edge crack in a semi-infinite plane which is subject to linear tensile stress σ as shown in Figure 4.15, the corresponding $f = 1.12$ when $C = a$, where C is the loading length and a is the crack length. This f can be used in Equation 4.23 to obtain K_I. Similarly the fracture toughness K_{IC} can be obtained using the same equation with different f and laboratory measured $\sigma_{strength}$. The four-point bend test was performed for this purpose, and the details can be found in Sabnis *et al.* (2008).

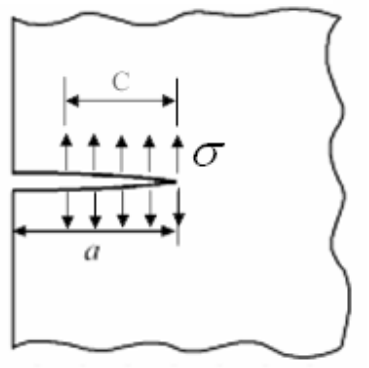

Figure 4.15—Semi-infinite Plane with an Edge Crack under Tension

4.5.3.2.4. Progression Criterion of Initial Shrinkage Crack

The crack initiation criterion described earlier ($\sigma_{ss} >= \sigma_{strength}$) in FEA algorithm determines the moisture content MC_I at which the onset of the shrinkage crack in the clayey subgrade may occur. After the crack initiates in the subgrade, the fracture mechanics model is used to further examine whether the initial shrinkage crack is stable or whether it will propagate through the pavement structure. To simplify calculation, initial crack is assumed to be very small (a = 1 in.) and applied linear tensile stress is uniform. Parameters K_I and K_{IC} can be compared using same Equation 4.23 but different applied linear tensile stresses (σ_{ss} vs. $\sigma_{strength}$) and

different geometry factors (semi-infinite vs. laboratory set up dimensions) respectively. When $K_I < K_{IC}$ the crack is stable and will not grow. On the other hand however, when $K_I >= K_{IC}$, the crack will start to propagate up. The progression of the initial shrinkage crack is critical to the development of the surface longitudinal crack.

4.5.3.3. FINITE ELEMENT ANALYSIS MODEL DEVELOPMENTAL DETAILS

A typical low-volume pavement section, consisting of a thin asphalt layer over base and subgrade is represented in Figure 4.16. Each pavement layer is assumed to be homogenous, isotropic, and fully bonded to the underlying layer. Pavement shoulder is modeled as a uniform block fully bounded at the pavement interface. Because of symmetry, a half-wide pavement (12 ft wide) with shoulder (4 ft wide) was studied to reduce calculation efforts. As few as three layers and as many as necessary layers can be introduced to the FEA program.

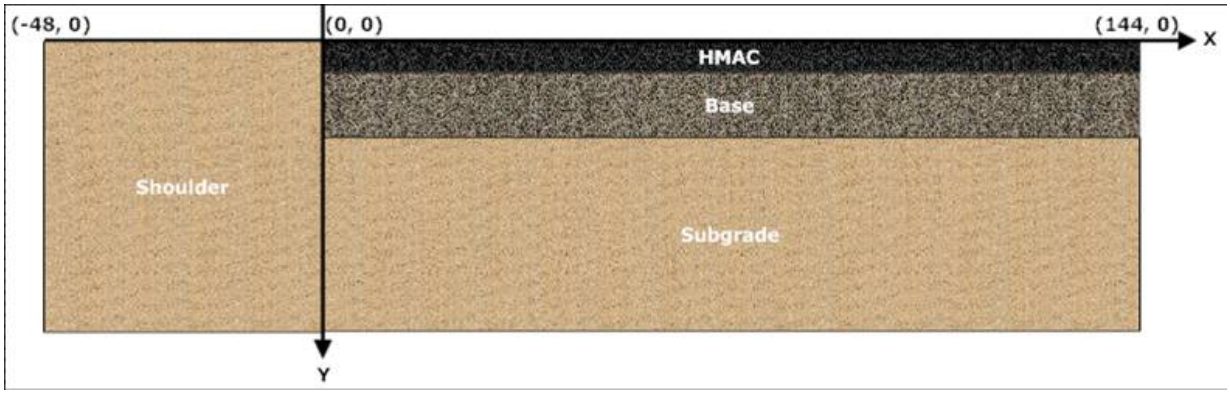

Figure 4.16—Typical Pavement Section Geometry Setup in FE Modeling

After considering the computational time limitation and required level of accuracy of FEA output, two FE models are developed: (1) Elastic Model: a two-dimensional plane strain linear model developed in Matlab is used to estimate the initialization of longitudinal cracks. (2) Fracture Model: a more sophisticated nonlinear plastic-elastic FE model developed in LS-Dyna is used to further study the crack propagation into the pavement structure. Developmental details are included in Appendix C.

4.5.4. Finite Element Modeling Results and Analysis

Typical 3- and 4-Layer low-volume pavement sections were studied by both FEA models. Table 4.7 summarizes typical material properties used in the Fracture Model. Figure 4.17 shows the labeling details for variable layer thicknesses and moduli cases. In this section, results from both Elastic Model and Fracture Model are discussed, followed by parametric study comparisons. Finally conclusions are made and the results from both models are combined together to answer the question of "when" and "where" will longitudinal shrinkage cracking happen for a given pavement.

Table 4.7—Typical Material Properties Used for Finite Element Modeling

Layer	Mass Density		Modulus		Poisson's Ratio	Yield (Compressive) Strength		Fracture (Tensile) Strength	
	kg/m^3	pcf	MPa	ksi		KPa	psi	KPa	psi
AC	2243	140	3450	500	0.35	1380	200	827	120
Base	2042	128	345	50	0.35	345	50	207	30
Lime Stab. SG	1762	110	207	30	0.40	207	30	-	-
SG/SB	1762	110	69	10	0.40	69	10	-	-

4.5.4.1. Finite Element Analysis Modeling Results

4.5.4.1.1. Elastic Model Results

Figure 4.18 shows the typical stress contours of the 3L Home case for Paris at 0.9NMC level. Top figure includes compressive and tensile stresses. The subgrade and part of the shoulder develops tensile stresses while the AC and base layer are under compression. The largest tensile stress in x-direction develops along the subgrade and base interface. Bottom figure is scaled to show tensile stress contour only. Maximum tensile stress happens underneath pavement towards centerline. Figure 4.19 shows the typical stress contours for the 4L Home case

3L Cases Label Details

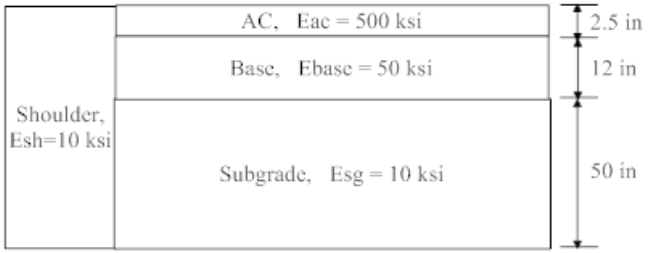

3L Home Case

Layer Thickness Analysis Cases

Label	AC (in.)	Base (in.)	Subgrade (in.)
3L_Home	2.5	12	50
3L_AC0.5	0.5	12	50
3L_AC4.5	4.5	12	50
3L_Base6	2.5	6	50
3L_Base18	2.5	18	50
3L_SG30	2.5	12	30

Layer Property Analysis Cases

Label	Eac (ksi)	Ebase (ksi)	Esg (ksi)
3L_Home	500	50	10
3L_Eac300	300	50	10
3L_Eac700	700	50	10
3L_Ebase20	500	20	10
3L_Ebase80	500	80	10
3L_Esg5	500	50	5
3L_Esg15	500	50	15

4L Cases Label Details

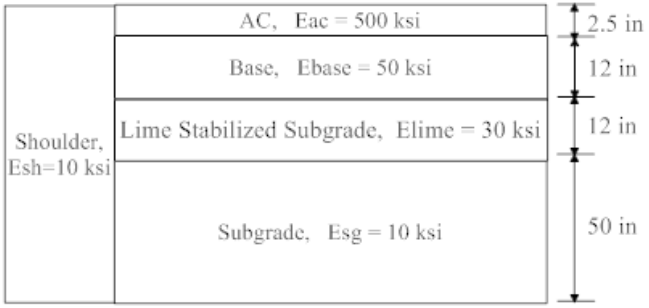

4L Home Case

Layer Thickness Analysis Cases

Label	AC (in.)	Base (in.)	Lime Stab. Sg (in.)	Subgrade (in.)
4L_Home	2.5	12	12	50
4L_AC0.5	0.5	12	12	50
4L_AC4.5	4.5	12	12	50
4L_Base6	2.5	6	12	50
4L_Base18	2.5	18	12	50
4L_SG30	2.5	12	12	30

Layer Property Analysis Cases

Label	Eac (ksi)	Ebase (ksi)	Elime (ksi)	Esg (ksi)
4L_Home	500	50	30	10
4L_Eac300	300	50	30	10
4L_Eac700	700	50	30	10
4L_Ebase20	500	20	30	10
4L_Ebase80	500	80	30	10
4L_Esg5	500	50	30	5
4L_Esg15	500	50	30	15

Figure 4.17—Finite Element Modeling Cases Label Details

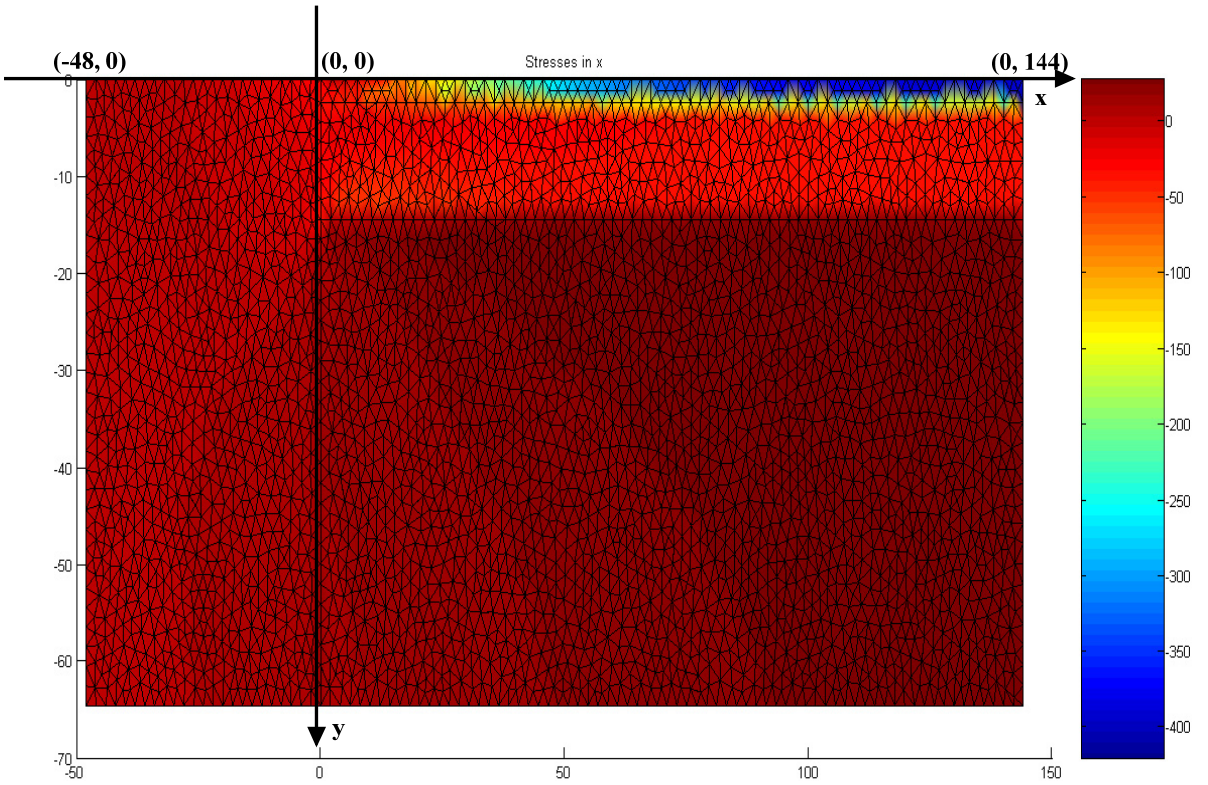

3-Layer Home Case Full Range Stress Contour (Paris 0.9 NMC)

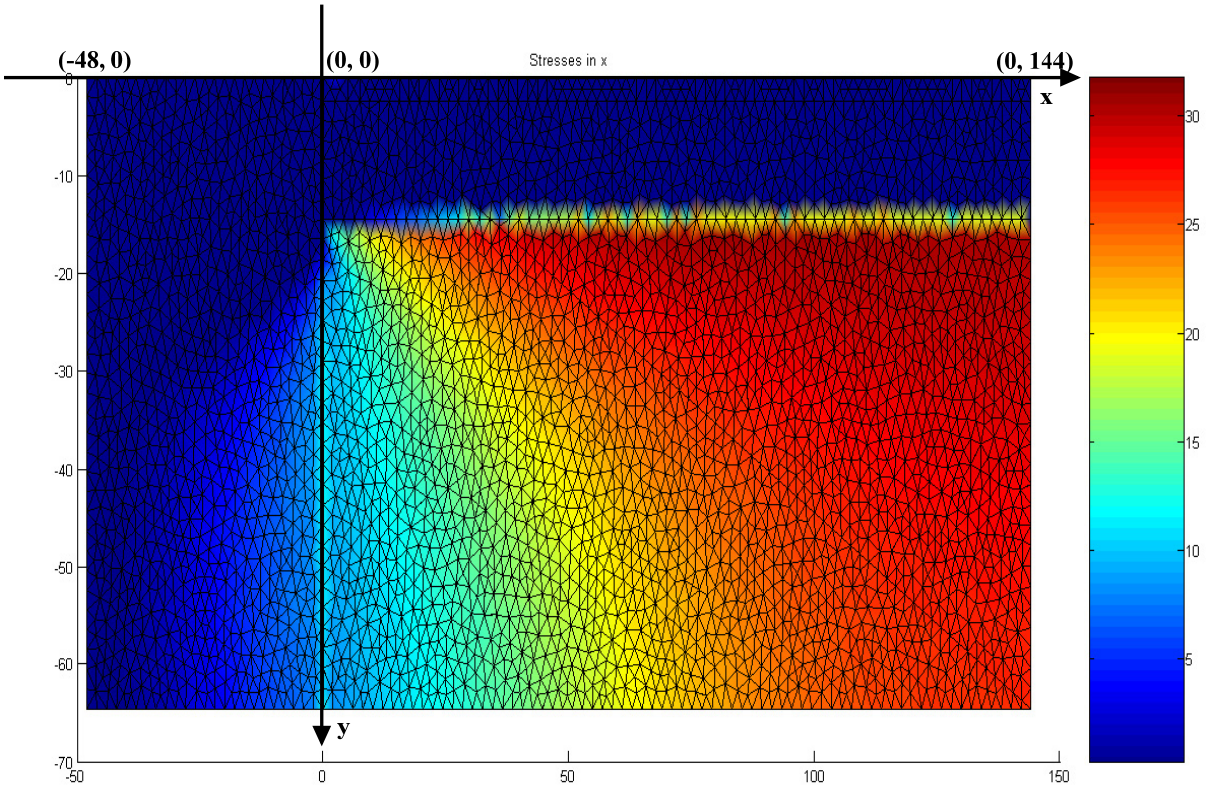

Figure 4.18—Elastic Model 3-Layer Home Case Stress Contours (Paris, 0.9NMC)

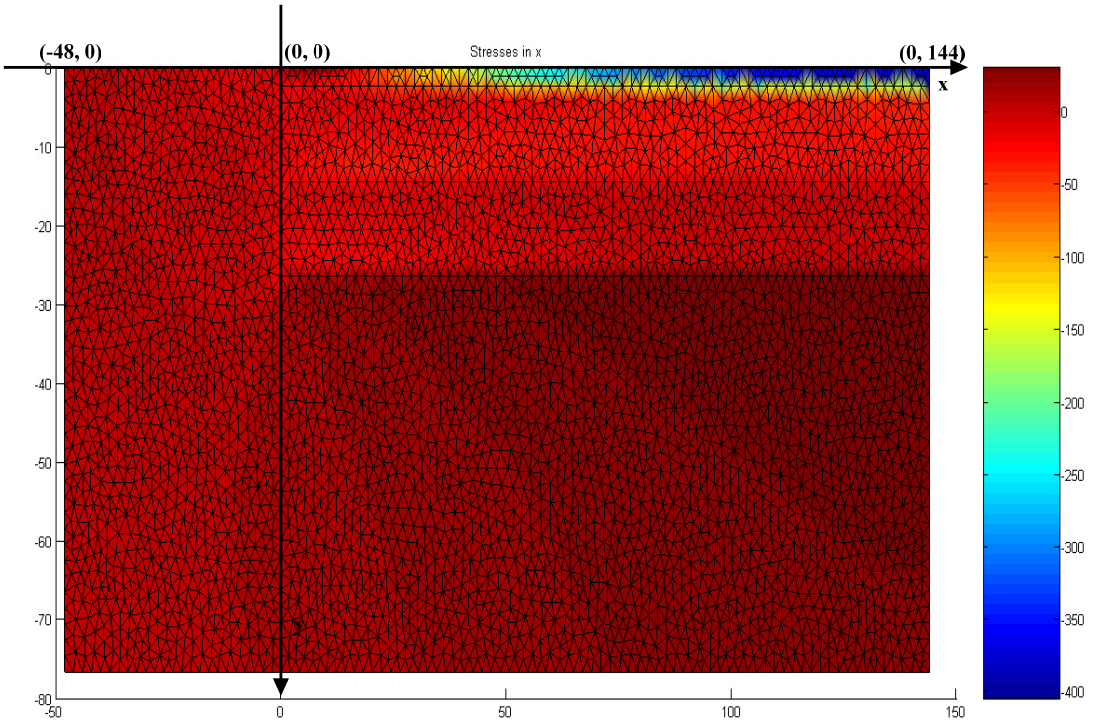

4-Layer Home Case Full Range Stress Contour (Paris 0.9 NMC)

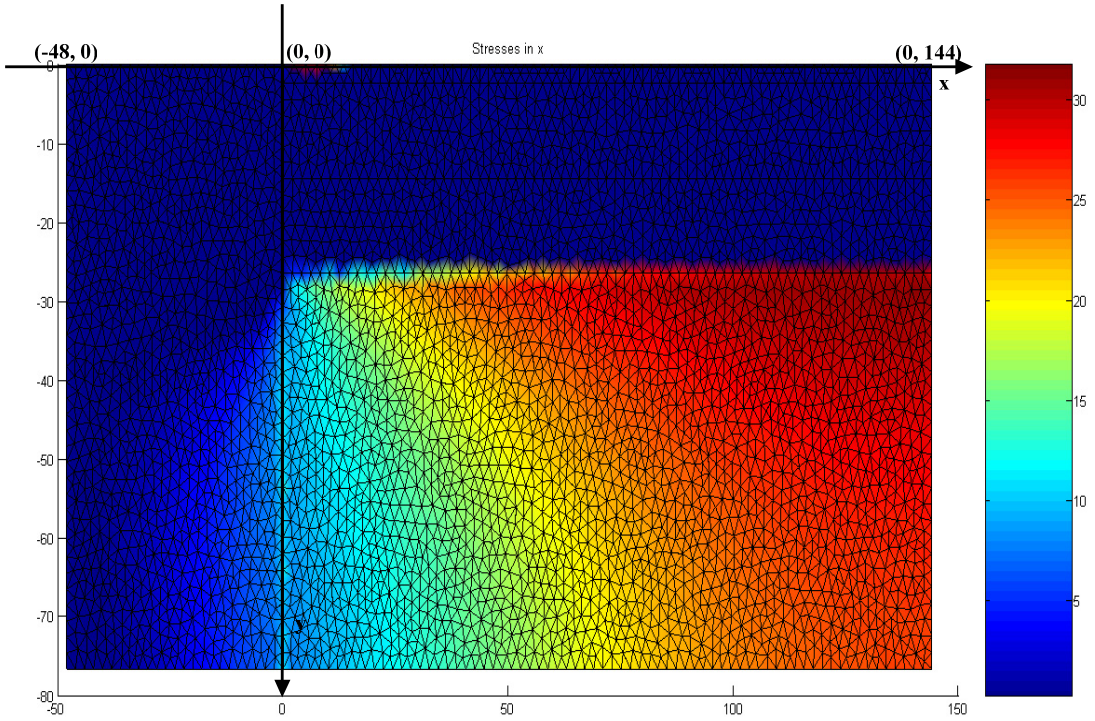

4-Layer Home Case Scaled Tensile Stress Contour (Paris 0.9 NMC)

Figure 4.19—Elastic Model 4-Layer Home Case Stress Contours (Paris, 0.9NMC)

under same moisture change (Paris, drying from optimum to 0.9NMC). Similar results to the previous case are observed. With one added layer of lime stabilized subgrade, the magnitude of maximum tensile stress does not change much, however, the overall contour shifted slightly toward the pavement centerline as compared to the 3-layer case.

The Elastic Model is programmed to sort and print out the top 50 tensile stresses within subgrade and shoulder. These points are plotted on top of the pavement section as shown in Figure 4.20. The base-subgrade interface has a higher frequency of being under greatest tension. All 50 points fall within the top 5-in. of subgrade layer. By comparing the 3-layer and 4-layer data series, the overall location shifted towards centerline when cover thickness above subgrade increases. Figure 4.21 plots the magnitude of top 50 largest tensile stress points across pavement. The resulting shrinkage induced tensile stresses are close for the 3-layer and 4-layer pavement (31±0.5 psi), that is, the controlling shrinking stresses are not sensitive to the cover depth above subgrade. This conclusion will be further discussed in the following parametric study section 4.5.4.2.

4.5.4.1.2. Fracture Model Results

Figure 4.22 shows typical snapshots of tensile stress contours and fractured elements for the 3L Home case of Paris. Top figure shows at 0.9NMC, base starts to fracture. Although the maximum tensile stresses in subgrade are located along the middle of the lane towards pavement centerline, fracture first progresses at the shoulder-pavement interface due to the fact that the pavement shoulder is a much weaker material compared to base and ACP layer and thus the interface between shoulder and pavement is more critical than that between base and subgrade. This trend is further confirmed by the bottom figure as subgrade and shoulder continue dry out.

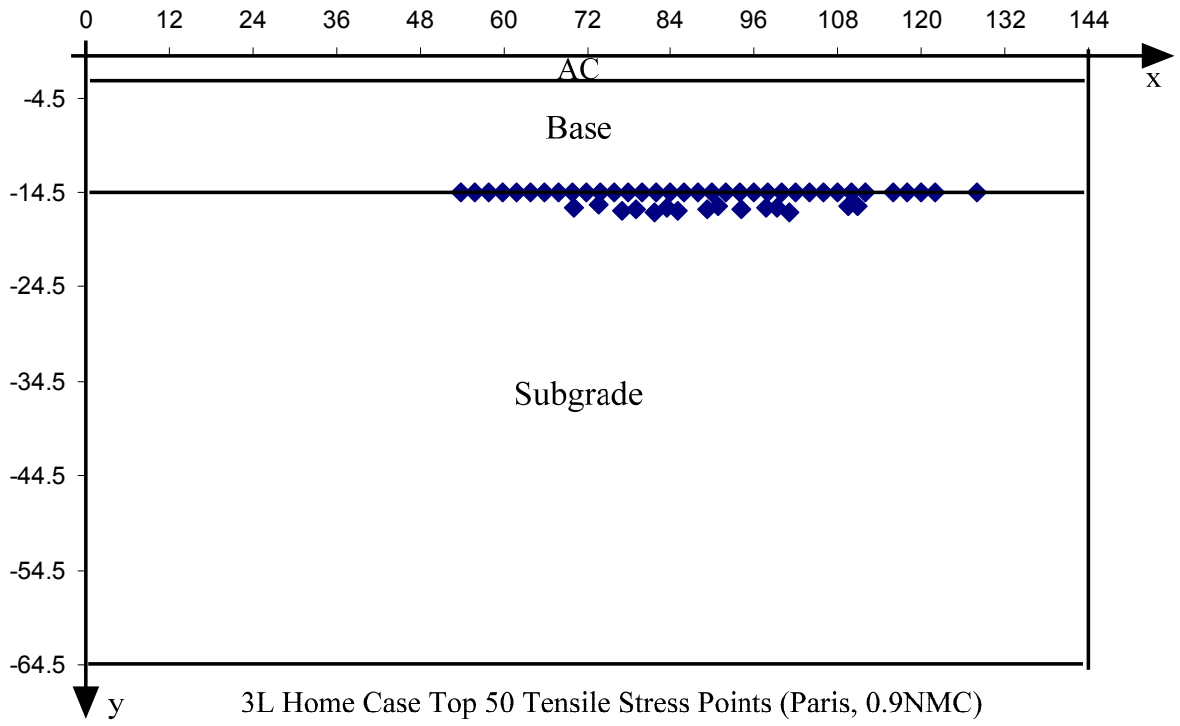

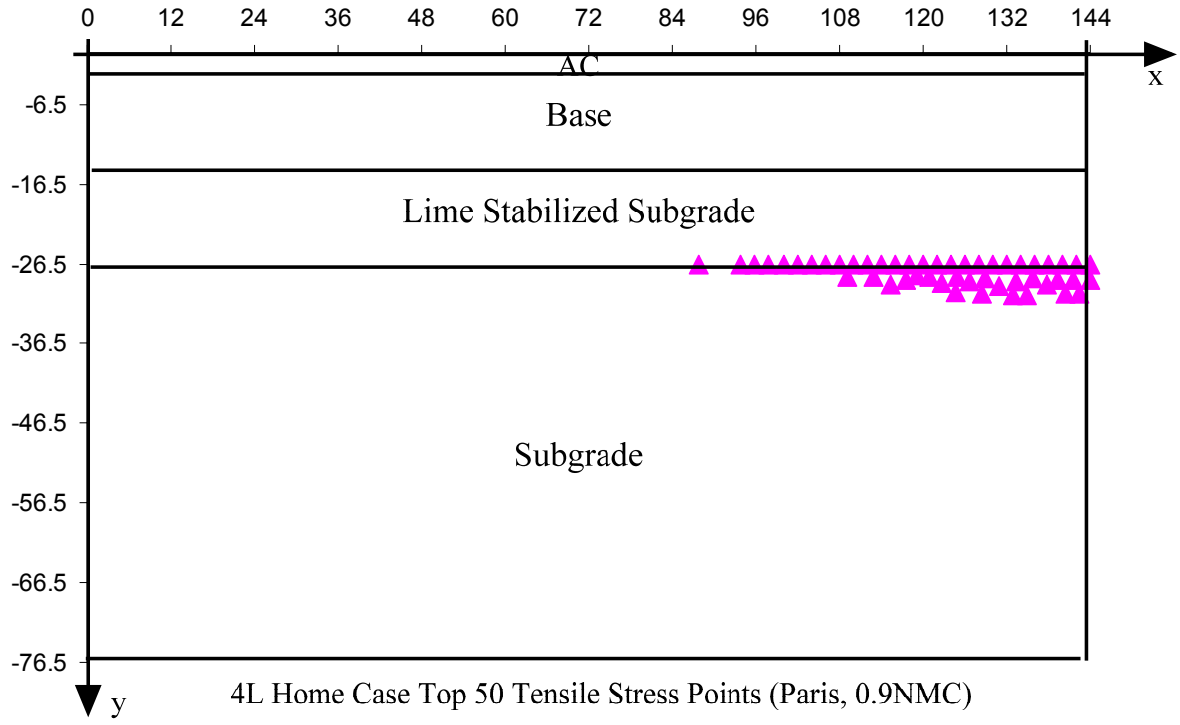

Figure 4.20—Locations of Top 50 Tensile Stress Points (Paris, 0.9NMC)

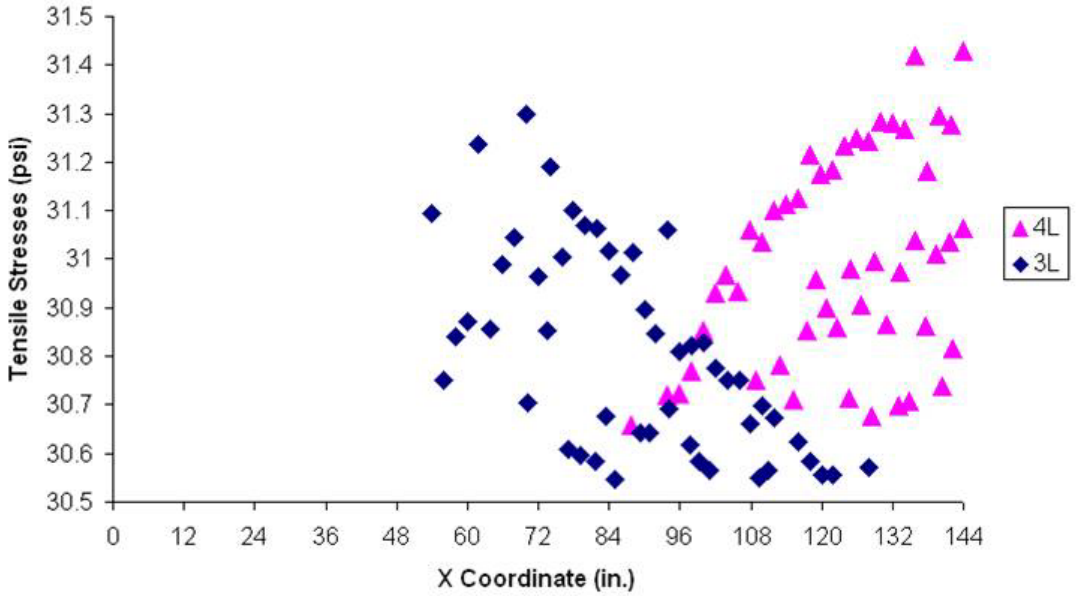

Figure 4.21—Top 50 Largest Tensile Stress Points (Paris, 0.9NMC)

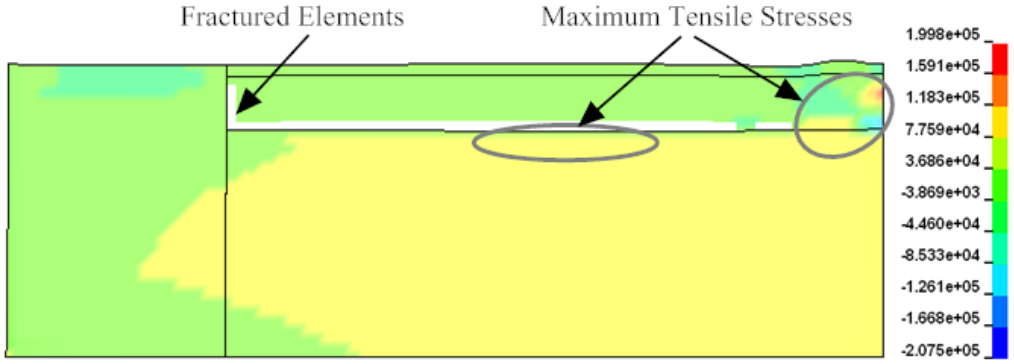

Snap Shot of Tensile Stress Contours and Fractured Elements at 0.9NMC

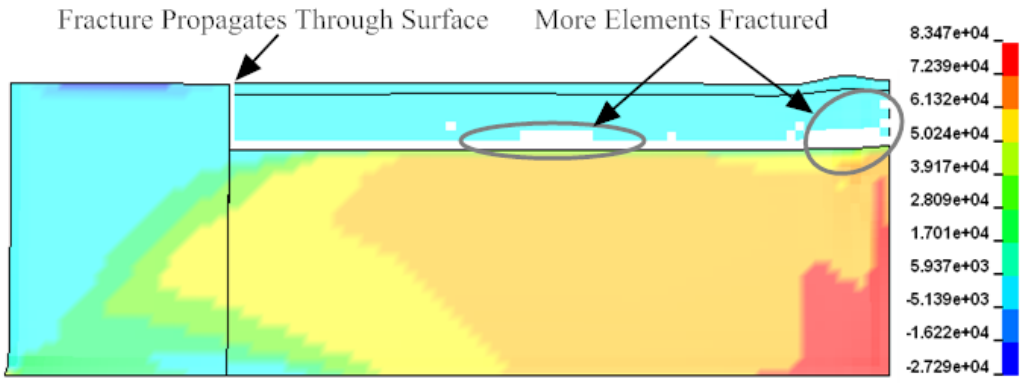

Snap Shot of Tensile Stress Contours and Fractured Elements at 0.8NMC

Figure 4.22—Fracture Model 3-Layer Home Case Stress Contours and Fractured Elements (Paris, Drying from Optimum to 0.8NMC)

At 0.8NMC, the crack propagates up through shoulder-pavement interface and reaches the surface. Base further cracks at those locations where tensile stresses are larger. Subgrade and part of the shoulder develop tensile stresses (positive) while the ACP and base layer are essentially under compression (negative). Results of largest tensile stresses developed within subgrade agree with those from the Elastic Model. When fracture happens in an element, that element is removed, resulting in the redistribution of the stresses and a new equilibrium state. In the bottom figure, the bottom-right corner in red means the material starts to show ductile property (starts to stretch). This discrepancy is caused by the assumption that the subgrade material is a thermo-elastic-plastic material and that bottom right corner is fixed in all directions by boundary conditions.

Figure 4.23 shows typical snapshots of tensile stress contours and fractured elements for 4L Home case of Paris under same moisture change (drying from optimum to 0.8NMC). Similar results as discussed earlier for the 3-layer case are observed. However, with the more sophisticated Fracture Model, the benefit of the added layer of lime stabilized subgrade stands out. Even though the magnitude of maximum tensile stress in subgrade does not change much, and the controlling NMC level is the same as for 3-layer case, the actual damage caused by the subgrade shrinking is less severe. The critical tensile stress points shift further toward the pavement centerline as compared to the 3-layer case. This trend also agrees with the trend from Elastic Model.

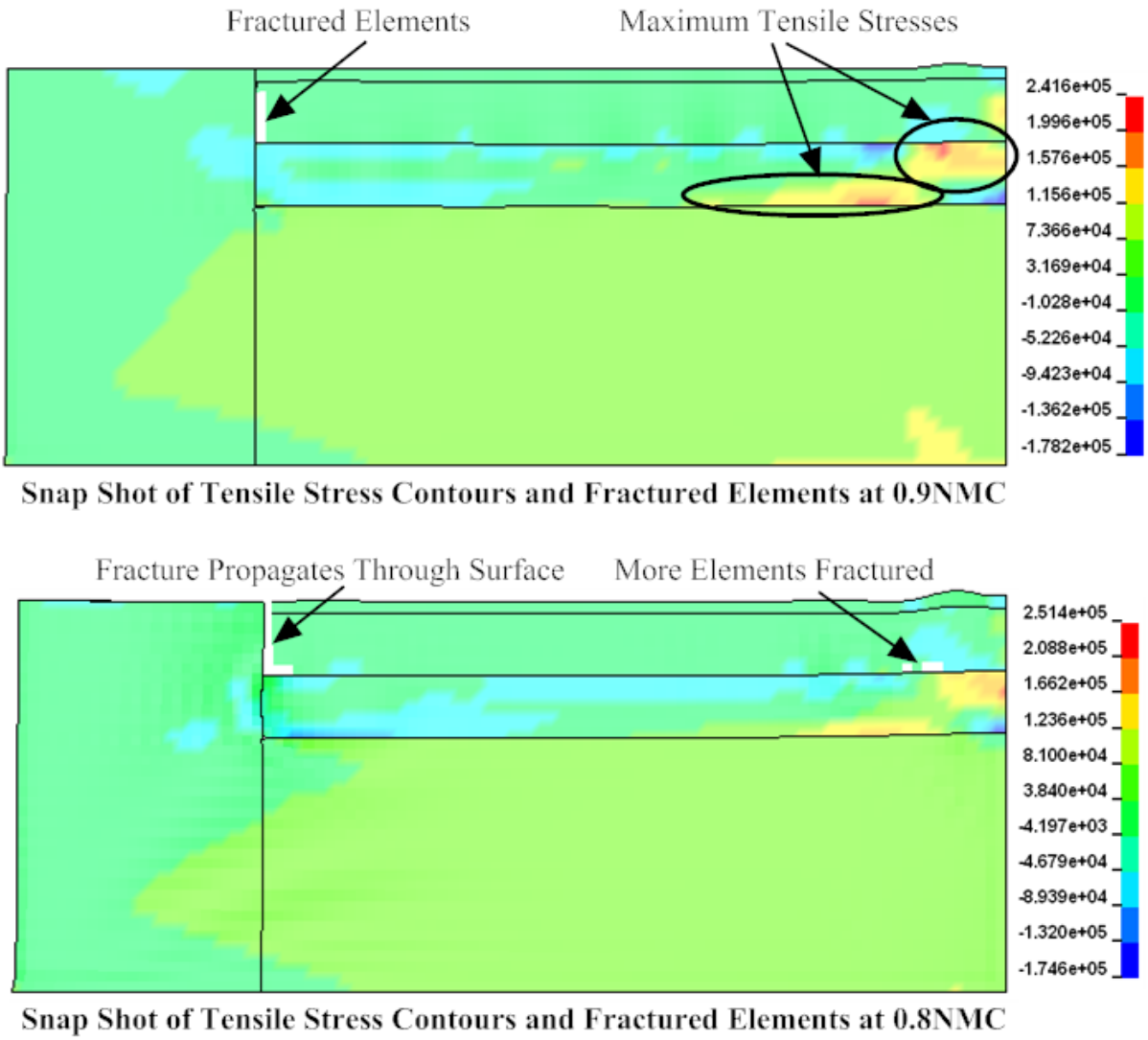

Figure 4.23—Fracture Model 4-Layer Home Case Stress Contours and Fractured Elements (Paris, Drying from Optimum to 0.8NMC)

4.5.4.2. PARAMETRIC STUDIES

The computation effort for Elastic Model is much less than that for the Fracture Model due to their different setup. The average time to execute one case in the Elastic Model is about 2 minutes. On the other hand, it takes from 5 to 40 minutes to execute the Fracture Model for one case. Elastic Model is mainly used to study the effects of layer thickness and modulus variation on resulting average value of top 50 shrinkage induced tensile stress points (σ_{avg}). Fracture

Model is used to identify relationship between shrinkage cracking initiation and propagation. Appendix D contains the detailed parametric study results using the Elastic Model.

4.5.4.2.1. Elastic Model Results

The parametric study on different ACP, base and subgrade layer thicknesses and moduli for both 3- and 4-layer sections gave close results and same trend. For low-volume roads, it seems that the lime-stabilized layer does not provide superior performance with respect to prevent subgrade shrinkage cracking from happening. However as mentioned earlier, it does help to reduce the severity of such distress and delay the propagation process. With the increased ACP and base thicknesses, the resulting σ_{avg} increases. The ACP layer thickness has bigger effects on σ_{avg} as compared to the base thickness. On the other hand, subgrade thickness shows slightly opposite effect, i.e., with a thicker subgrade subject to shrinking, the resulting σ_{avg} decreases. The increase in ACP, base and subgrade layer moduli increased σ_{avg}. The subgrade layer modulus has bigger impact on σ_{avg} as compared to the ACP and base layers.

Above analysis is based on the assumption that the shoulder and the subgrade have same material properties and are subject to the same level of moisture change, i.e., the shrinkage induced tensile stresses are uniform throughout shoulder and subgrade. However, in reality the subgrade soil is under a flexible impermeable asphalt layer, the moisture variation under the pavement centerline is different from that under the pavement edge or the shoulder. Many studies have attempted to analytically predict such differences (Mitchell, 1979; Lytton, *et al.*, 2004; Luo and Prozzi, 2007). Generally speaking, the closer the location is to the pavement centerline, and the deeper is the pavement structure, the less moisture change in the subgrade soil will be observed.

The effects of the horizontal and vertical moisture variations are simulated by applying different profiles of initial shrinkage induced strains (ε_{ss}) to subgrade and shoulder of 3- and 4-layer Home cases (Paris, 0.9NMC). When the vertical moisture variation decreases with depth, the distribution of the top 50 tensile stress points remains unchanged but shifts slightly towards centerline. The resulting σ_{avg} increases by about 6% for both 3- and 4-layer cases when more sub-layers are introduced.

Interesting results are observed when horizontal moisture variation decreases underneath the pavement. The top 50 tensile stress points are distributed into two groups: one still falls within the subgrade, while the other appears at the shoulder-pavement interface. This change implies two critical locations worth monitoring. When moisture variation within subgrade (underneath impermeable pavement) is less than that in the shoulder (directly exposed to environment), the critical location within subgrade shifts toward the centerline, and the shoulder-pavement interface also becomes critical. This result agrees with our field observation, which will be discussed further in Section 4.5.5.1, Section 7.1.3 and Appendix E. When only shoulder is susceptible to drying, all 50 points are located near shoulder-pavement interface. Overall, when the moisture variation in subgrade becomes smaller with depth and horizontally closer to the pavement centerline, the longitudinal cracks tend to occur near the middle of the lane and near the shoulder-pavement interface.

4.5.4.2.2. Fracture Model Results

Different ACP, base and subgrade layer thickness cases are studied for both 3- and 4-layer pavement sections for two different case scenarios: worst case (Paris) and best case (El Paso). From the contours shown in Figure 4.22 and 4.23, a range of cracks can progress as subgrade dries out. It is therefore necessary to relax the assumption of a single crack on the

pavement region. The first crack always initiates in subgrade at shoulder-pavement interface while more cracks emerge at the location where subgrade has maximum tensile stresses. These cracks relieve some of the linear shrinkage tension and result in new equilibrium. As moisture level decreases, the initial small cracks propagate upward and grow in width.

Table 4.8 and 4.9 summarize the two controlling moisture content levels labeled as "Initiation" and "Propagation" as a percentage of normalized moisture content for 3- and 4-layer sections, respectively. When comparing same pavement cross-section over different subgrade soils (worst vs. best), pavements with lower PI subgrade withstand drying better. That is, same pavement built on high PI subgrade is more susceptible to longitudinal cracking under same moisture variation.

Table 4.8—Summary of Controlling Moisture Content Results for 3-Layer Pavement Sections (Represented in NMC values)

Worst Case (Paris)		
	Initiation	**Propagation**
Home	0.9	0.8
AC0.5	0.9	0.8
AC4.5	0.9	0.8
Base6	0.9	0.8
Base18	0.9	0.8

Best Case (El Paso)		
	Initiation	**Propagation**
Home	0.9	0.8
AC0.5	0.8	0.6
AC4.5	0.9	0.7
Base6	0.8	0.7
Base18	0.9	0.7

Table 4.9—Summary of Controlling Moisture Content Results for 4-Layer Pavement Sections (Represented in NMC values)

Worst Case (Paris)		
	Initiation	**Propagation**
Home	0.9	0.8
AC0.5	0.9	0.8
AC4.5	0.9	0.8
Base6	0.9	0.8
Base18	0.9	0.8

Best Case (El Paso)		
	Initiation	**Propagation**
Home	0.8	0.7
AC0.5	0.8	0.7
AC4.5	0.8	0.6
Base6	0.8	0.7
Base18	0.8	0.7

For worst cases (Paris), 3- and 4-layer sections give exactly the same results: first set of longitudinal cracks always initiate in top of subgrade at 0.9NMC, progress along shoulder-

pavement interface and become visible near shoulder-pavement interface at 0.8NMC. Another set of cracks initiates in where subgrade develops the maximum tensile stress due to shrinking, usually in the middle of the traffic lane, propagate upward toward the surface and grow in width. However, these cracks underneath the pavement may not daylight at the surface as fast as the pavement edge-shoulder crack. Layer thicknesses do not seem to play significant roles in critical results of controlling moisture levels.

For best case (El Paso, low PI subgrade) scenarios, 4-layer sections have clear advantage over 3-layer sections in withstanding subgrade drying induced longitudinal cracking. Comparing best case results in Table 4.8 and 4.9, longitudinal cracking initiates at 0.8NMC for most cases with exception of 3L_Home, 3L_AC4.5 and 3L_Base18. The controlling moisture content level for crack propagation is 0.7NMC for most cases except 3L_Home, 3L_AC0.5 and 4L_AC4.5.

Increased layer thicknesses do not seem to guarantee better performance, especially for high PI clays. For Paris case (PI = 36), no changes in controlling moisture levels are observed with increased AC or base thicknesses. For El Paso (PI = 17), 3-layer cases with thinner AC and base (Table 4.8, 3L_AC0.5 and 3L_Base6) performs better than thicker-layer alternatives, this may due to interface/boundary condition assumptions which oppose less restrains when the layer is thinner, and thus more flexibility can be expected. It is to be noted for low PI subgrade, 4-layer cases perform better than 3-layer cases (best cases in Table 4.9 vs. Table 4.8), which agrees with common consensus that thicker pavements outperform thinner ones.

Overall, subgrade soil property plays a much more important role in low-volume pavement longitudinal cracking distress than cross-section differences (number of layers, and thickness of each layer).

4.5.4.3. CRITICAL LOCATIONS AND LIMITING MOISTURE LEVELS

To estimate the critical limiting moisture levels to prevent pavement longitudinal cracking, two critical values are worth mentioning: (1) MC_I, which identifies the moisture level below which subgrade starts to develop shrinkage cracks; and (2) MC_P, which limits the moisture level to prevent crack growth. There are also two critical locations in analyzing longitudinal cracking: (1) Pavement edge-shoulder interface where will show the first sign of cracking; and (2) Underneath the pavement where maximum resulting tensile stress happens in the subgrade. These locations can be identified by both the Elastic Model and Fracture Model. The moisture level to initiate cracking from the Elastic Model agrees well with the Fracture Model results. The moisture level to limit shrinkage crack from daylighting at the pavement surface can be only obtained from the Fracture Model, which cannot be automated. To simplify the problem, MC_P will be estimated from generalized relationship of:

$$NMC_P = NMC_I - 0.2 \tag{4.25}$$

where NMC_P and NMC_I are the normalized MC_P and MC_I, respectively.

4.5.5. Evaluation Considerations

In this section, the LSC check module is validated. To simplify our model, assumptions are made that all drying starts from optimum moisture content. In reality, however, drying and wetting cycles may start at any moisture content. Constrains and limitations of LSC module are also identified.

4.5.5.1. VALIDATION OF PROGRAM

Verification and validation of the LSC check is carried out in two steps:

1) Comparison of LSC check results with field measurements
2) Comparison of LSC check results with recent research

4.5.5.1.1. Comparison of LSC Check Results with Field Measurements

To evaluate and validate the LSC check results, field observations were carried out at test sites with the following preferred attributes: (1) Reasonably newly constructed; (2) Design records are available: (3) Construction records are reasonably completed; (4) Contain some areas with typical distresses encountered due to high-PI clay; and (5) Clay subgrade is reasonably uniform. After thorough considerations, five sites including Fort Worth, Houston, San Antonio, Paris and Atlanta were selected. To ascertain the soil properties, soils were first sampled and shipped to laboratories for traditional and advanced characterization tests. Details of these tests and results are covered in Sabnis *et al.* (2008). At each site, gravimetric moisture content, matric suction values, rainfall and pavement conditions (cracks and elevations) were collected.

Two types of field sensors were embedded at the test sites. One type is moisture sensors together with data logger and the other one is field matric suction sensors. Both types of system were carefully placed close to each other to ensure that the data from both systems represent the same soil conditions. All sensors were embedded 1.0 to 1.5 feet below the ground surface. Prior to the placements, a 0.5 in. depression was made at the bottom of the hole, in which the sensor was carefully placed to eliminate air gaps between the sensor and soil. The excavated soil was then filled onto the hole and compacted in the approximate 4-in. lifts. Extreme care was taken to ensure that the compaction was similar to the adjoining subsoils. Figure 4.24 depicts typical site schematic with three sensors implanted away from the shoulder. For all sites, the monitoring period was from January 2007 to June 2008 except for Atlanta site which was from March 2008 to June 2008. Moisture contents were measured continuously by data loggers. Matric suction pressures were gathered manually at each site visit. Pavement elevation surveys, photographing of pavement cracks and recording of any field conditions were collected at each site visit.

Rainfall data were collected from National Environmental Satellite, Data and Information Service (NESDIS) at (http://www.ncdc.noaa.gov/oa/climate/).

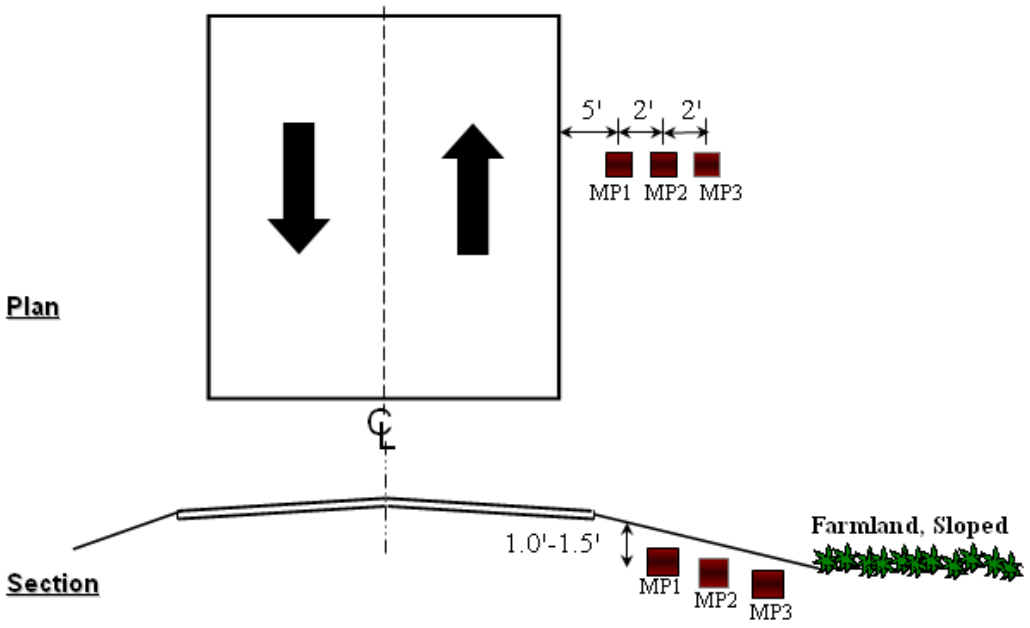

Figure 4.24—Typical Site Schematic for Field Measurements (by UTA)

Paris site is used here as an example to validate the program. This site was selected to study the influence of a poor drainage ditch and large trees near the pavement section and their location impacts on adjacent pavement cracking. This site is considered to have the worst pavement condition since the cracks were not only large but also long and deep. Figure 4.25 shows some pictures taken during field visits. This road had been rehabilitated in April 2007 and then in July 2007; minor cracks still reappeared on the pavement surface shortly after the rehabilitation. Figure 4.26 summarizes Paris site field measurement details.

Figure 4.25—Pavement Surface Conditions for FM 910

As discussed earlier, the LSC check model predicted that for Paris site at 0.9 NMC subgrade cracking initiates and at 0.7 NMC cracks will propagate up to surface and become visible. Laboratory test results indicate that the OMC of Paris is 23%. As such, the threshold moisture content for the appearance of the longitudinal cracks is: MC_P = 16% (0.7 times 23%). This corresponds very well with field observations, as shown in Figure 4.25 and 4.26, new cracks observed on September 2007 with an average moisture content of 15% to 17%. Elevation survey data also reached lowest near that period of time which indicates significant shrinkage behavior in the underlying and adjacent soil.

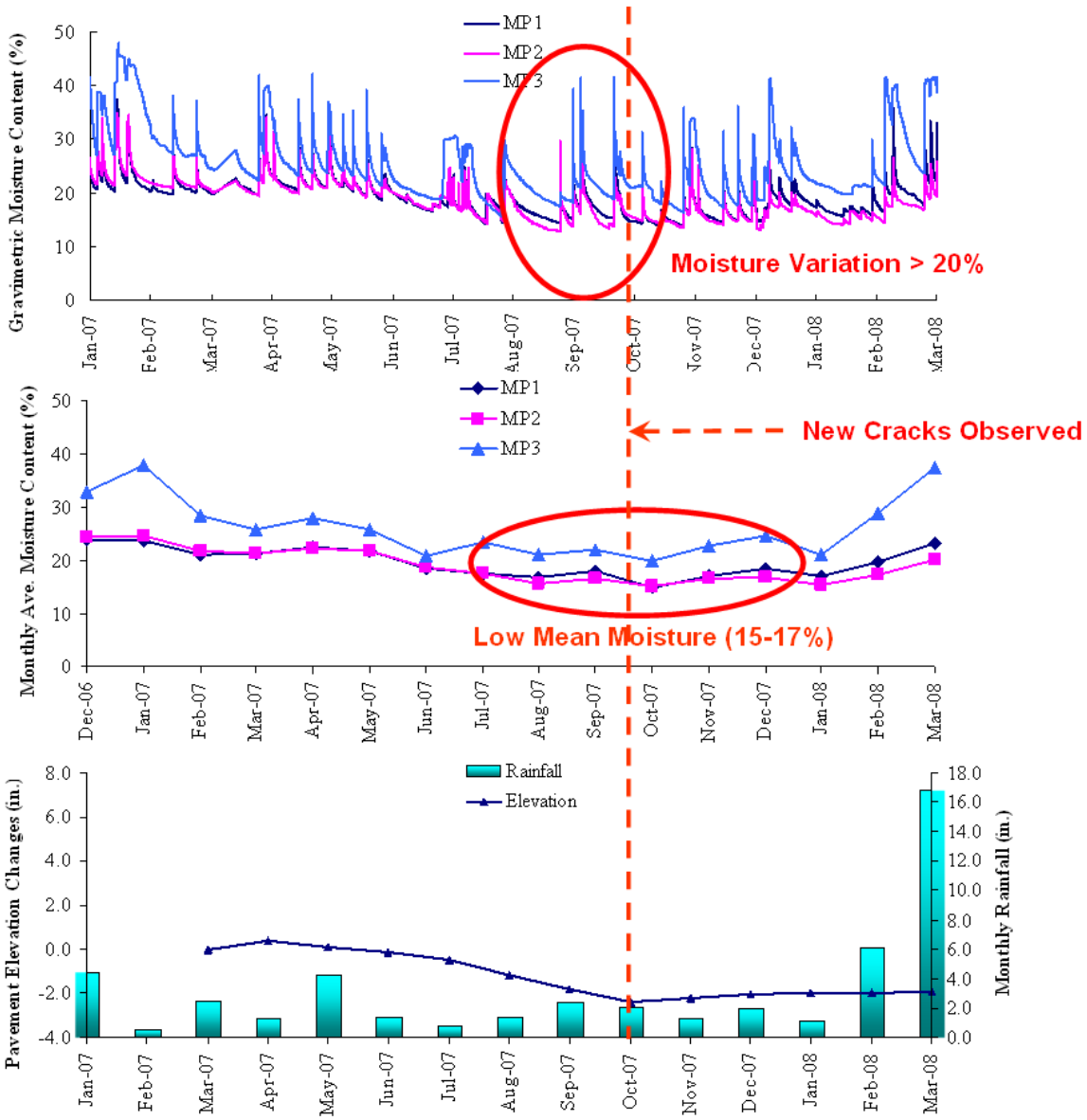

Figure 4.26—Field Data Measurements for Paris Site, FM910 (by UTA)

Similar practices were performed to compare results for other sites. All results of LSC check model show good correlation with field measurements. Complete details are further discussed in Chapter 7.

4.5.5.1.2. Comparison of LSC Check Results with Recent Research

Zornberg, *et al.* (2008) developed a 2D plane strain linear elastic fracture model in ABAQUS to study crack development in pavement structure due to moisture change in expansive subgrade. The conceptual idea behind this model (will be referred to as Zornberg's model in later discussion) is very similar to the LSC models developed for this research except that they utilized matric suction change instead of moisture content change as a means to predict resulting shrinkage strain (ε_{ss}).

A typical 3-layer section was analyzed by both models with same layer thicknesses, moduli and Poisson's ratios as shown in Table 4.10. Subgrade layer was further divided into 7 sub-layers with different moisture change profiles as used by Zornberg's model. Since vertical moisture variation is implemented in our LSC model but horizontal-wise is limited, only vertical shrinkage strains are calculated and used. Table 4.11 summarizes subgrade shrinkage strains (ε_{ss}) applied in the analysis. Zornberg's model used a 157-inch-wide pavement with a 472-inch-wide subgrade, extending part as natural shoulder.

Table 4.10—Pavement Section Information used for Validation Study

Layer	Thickness (in)	Modulus (ksi)	Poisson's Ratio
AC	1	363	0.35
Base	10	51	0.35
Subgrade	240	11	0.35

Table 4.11—Subgrade Information used for Validation Study

Sublayer	Thickness (in)	ε_{ss} (%)
1	20	-0.466
2	20	-0.226
3	20	-0.111
4	20	-0.055
5	20	-0.027
6	20	-0.013
7	20	-0.007
8	20	-0.003
9	80	0.000

The two studies yielded comparable results. Figure 4.27 compares the contours of the two programs. Both stress contours show the largest tensile stress (positive) in the subgrade presented in the area close to the pavement shoulder and close to the base-subgrade interface. This area has the highest possibility to generate cracks. In Zornberg's research the initial crack was determined to be at 24-inch horizontally away from the pavement shoulder, 6-inch deep in the vertical direction from base-subgrade interface. Initial crack length was assumed to be 1 inch. The stress intensity factor (K_I) at the tip of the initial crack was 82 psi-in$^{1/2}$. Our calculation gives K_I = 109 psi-in$^{1/2}$ based on the assumption of a 1-in. initial edge crack in a semi-infinite plane which is subject to linear tensile stress that was calculated by the Elastic Model. For this specific case, both analyses reached the same conclusion that shrinkage induced longitudinal cracking is going to propagate up (because $K_I > K_{IC}$, see Section 4.5.3.2.4). Reasons for the differences between LSC check and Zornberg's study may include: (1) Geometry differences: Zornberg's model has wider pavement and a much wider (10 times wider) shoulder; (2) Boundary and constrain differences: In our LSC model, shoulder is considered as one single isotropic and homogenous block, it cannot be further divided into sublayers for different moisture profile. Also, our model only enables ε_{ss} variations in vertical direction, but not in horizontal direction.

4.5.5.2. PREDICTION MODELS FOR DIFFERENT DRYING PATH

In our laboratory tests, three compaction moisture conditioning paths were used. The three moisture conditioning paths are: dry from optimum (DFO), saturate from optimum (SFO) and dry from saturation (DFS). Section 4.5.3.1 mentioned that ε_{ss} prediction model used in LSC check was performed for specimens drying from optimum (DFO). When soil specimens are dried through different path, the correlations between moisture content and soil property parameters (such as ε_{ss}, M_R) change. Figure 4.28 depicts trend changes in M_R vs. MC and Figure

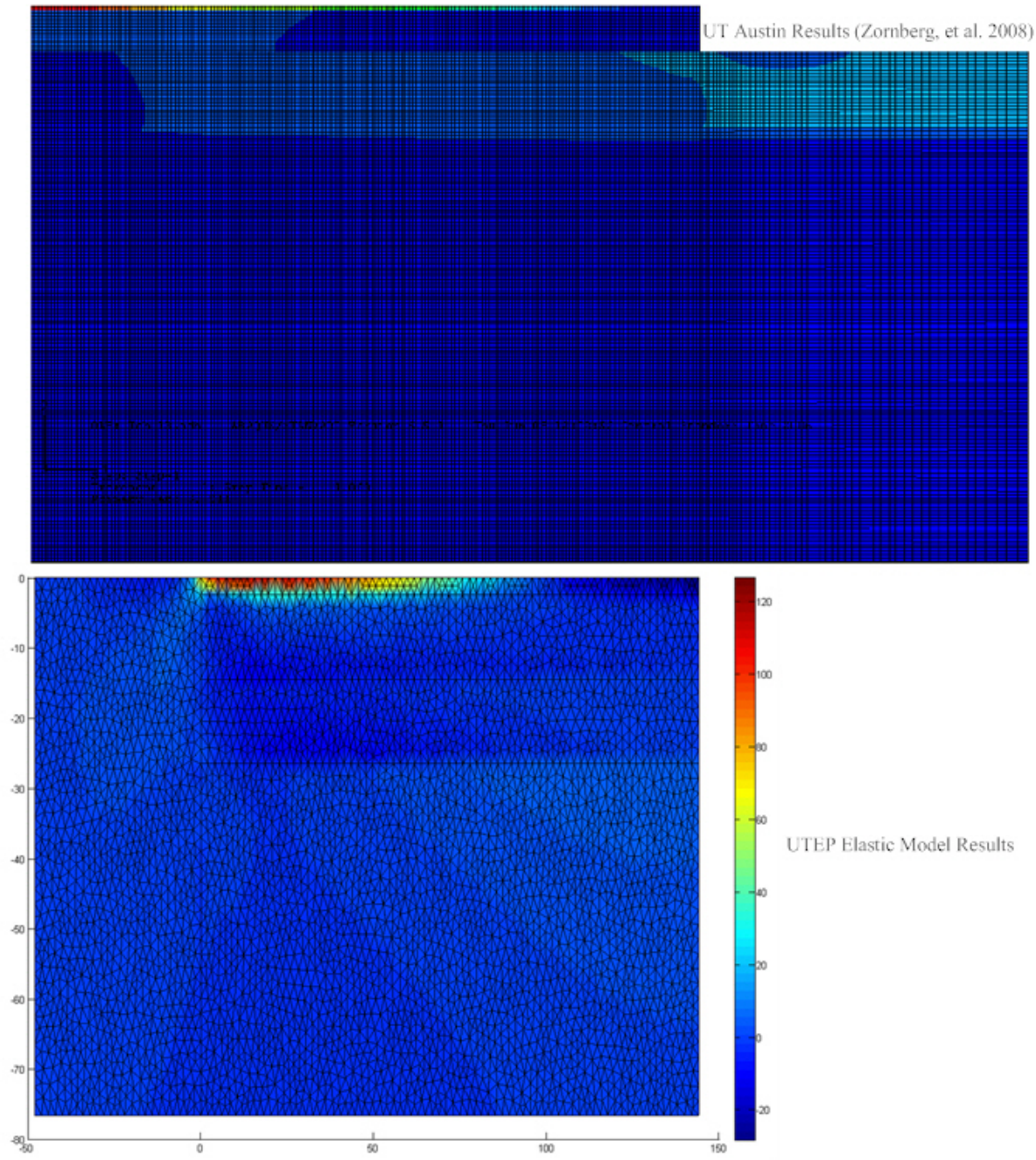

Figure 4.27—Comparisons of Tensile Stress Contours for Validation Study

4.29 shows the trend difference in ε_{ss} vs. MC, respectively. In the drying case, for example, same Paris soil has bigger M_R value but smaller ε_{ss} value at same final MC when comparing DFO to DFS..

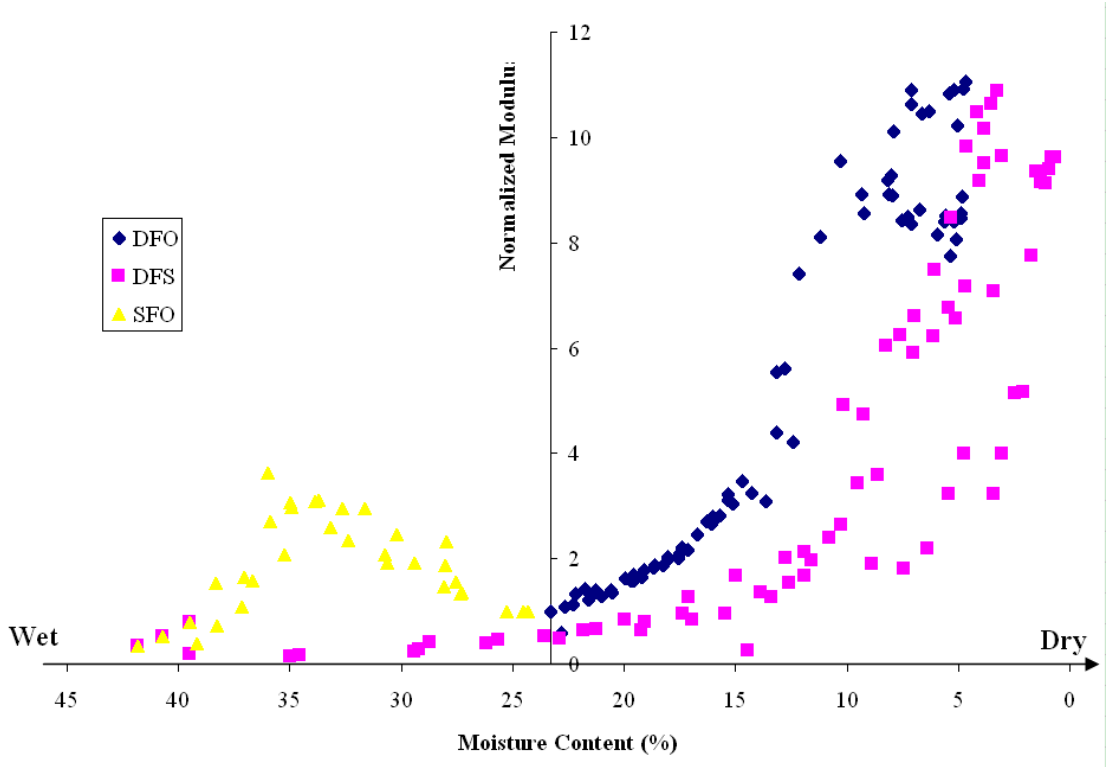

Figure 4.28—Normalized Modulus vs. Moisture Content for Different Moisture Conditioning Paths (Paris)

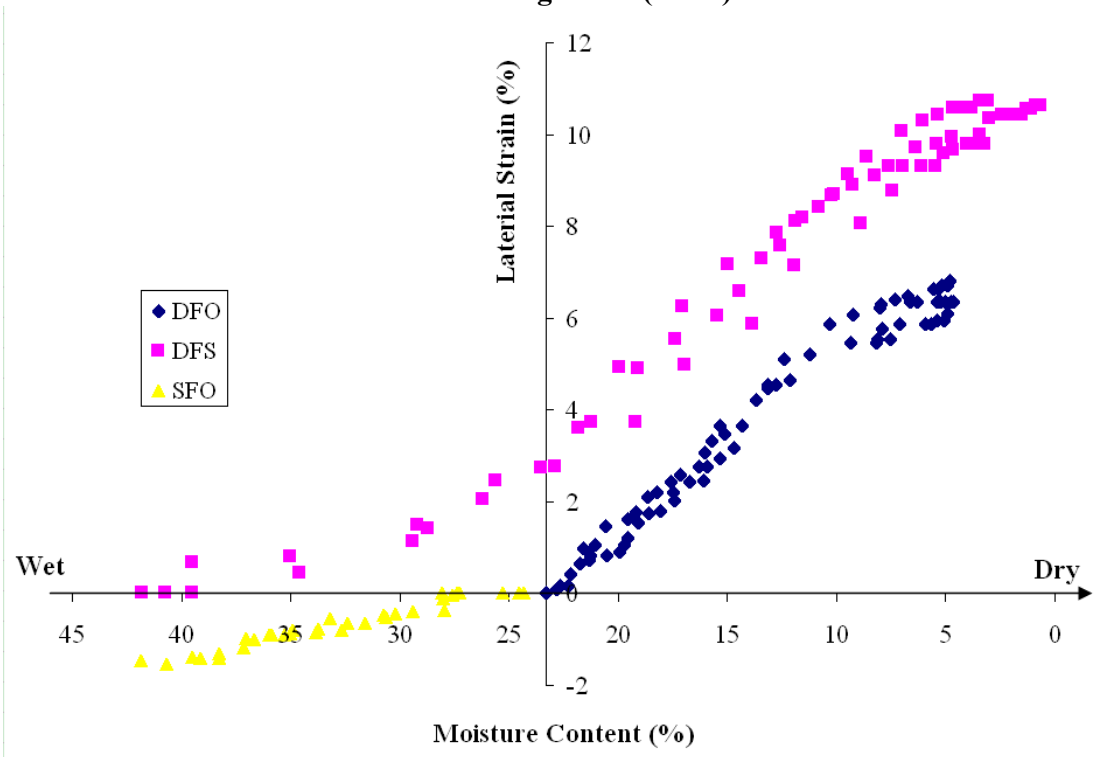

Figure 4.29—Lateral Strain vs. Moisture Content for Different Moisture Conditioning Paths (Paris)

CHAPTER FIVE - DEVELOPMENT OF REMEDIATION STRATEGIES

5.1. OVERVIEW

Many remediation strategies can be used to improve the detrimental properties of expansive soils, such as shrink-swell and low shear strength. In the ***Remediation Strategies*** module, six modification strategies are grouped into two categories: (1) To improve subgrade strength and stiffness, which include stabilization, geosynthetics reinforcement, undercut and backfill; and (2) To minimize moisture variation induced swell/shrink problems, which include moisture control, deep dynamic compaction and decreasing clay content in addition to those three included in category (1). Appropriate methods will be recommended from either or both categories following the algorithm flow chart shown in Chapter 3, Figure 3.12. The user has the choice to decide which one(s) to be considered and analyzed for the original design. Each remediation method will be discussed in details in the following sections.

5.2. STABILIZATION

Clayey soils are often stabilized with calcium based stabilizers to improve their engineering properties including strength, volumetric change potential and permeability. This method is recommended for all failure cases discussed in Chapter 4. TxDOT has standardized guidelines for Modification and Stabilization of Soils and Base for Use in Pavement Structures (2005) and Guidelines for Treatment of Sulfate-Rich Soils and Bases in Pavement Structures (2005). Those two documents provide the main decision making guidance for this subroutine. Three components are involved in the Stabilization subroutine: Part I. Regular Subgrade Stabilization; Part II. Sulfate-Rich Subgrade Stabilization; and Part III. Organic-Rich Subgrade

Stabilization. Figure 5.1 describes the decision making process with three logic blocks identified on top. From start, the block-arrows indicate the main logic flow of the subroutine. We only consider materials with more than 25% passing the No. 200 sieve. For coarser aggregate base materials, the program ends with an informative screen, which guides the user according to the TxDOT guidelines. For subgrade stabilization, the program goes to Part I, following the decision tree and gets recommended stabilizer(s). Results are temporarily stored in the knowledge database. Then the program continues to Part II to get another set of results. The logical "AND" operation will be performed on the two sets of results, meaning only those stabilizers selected in both Part I and Part II will be selected and stored. Similarly, the program continues to Part III and replace the temporary stored stabilizer(s) again with another "AND" operation. The subroutine selects appropriate stabilizer(s) and gets useful references or comments by following the decision making algorithm. Final results are stored in the knowledge base and reported to the user on ExSPRS screen. Each part will be discussed in details in the following sections.

5.2.1. Regular Subgrade Stabilization Methods

TxDOT guidelines use PI as the primary input to select appropriate stabilizers. For low PI subgrade (PI<15), asphalt, lime-Fly ash or cement can be used. For medium PI (15<=PI<=35), cement, lime, lime-cement and lime-fly ash can be used. For high PI (PI>35), lime, fly ash or mixed lime-cement, lime- Fly ash can be used. As stated in ExSPRS, stabilizer(s) selected in this program serves as a rule of thumb in stabilization considerations. Validation tests and other factors such as material availability, construction costs and time should be considered whenever it is possible.

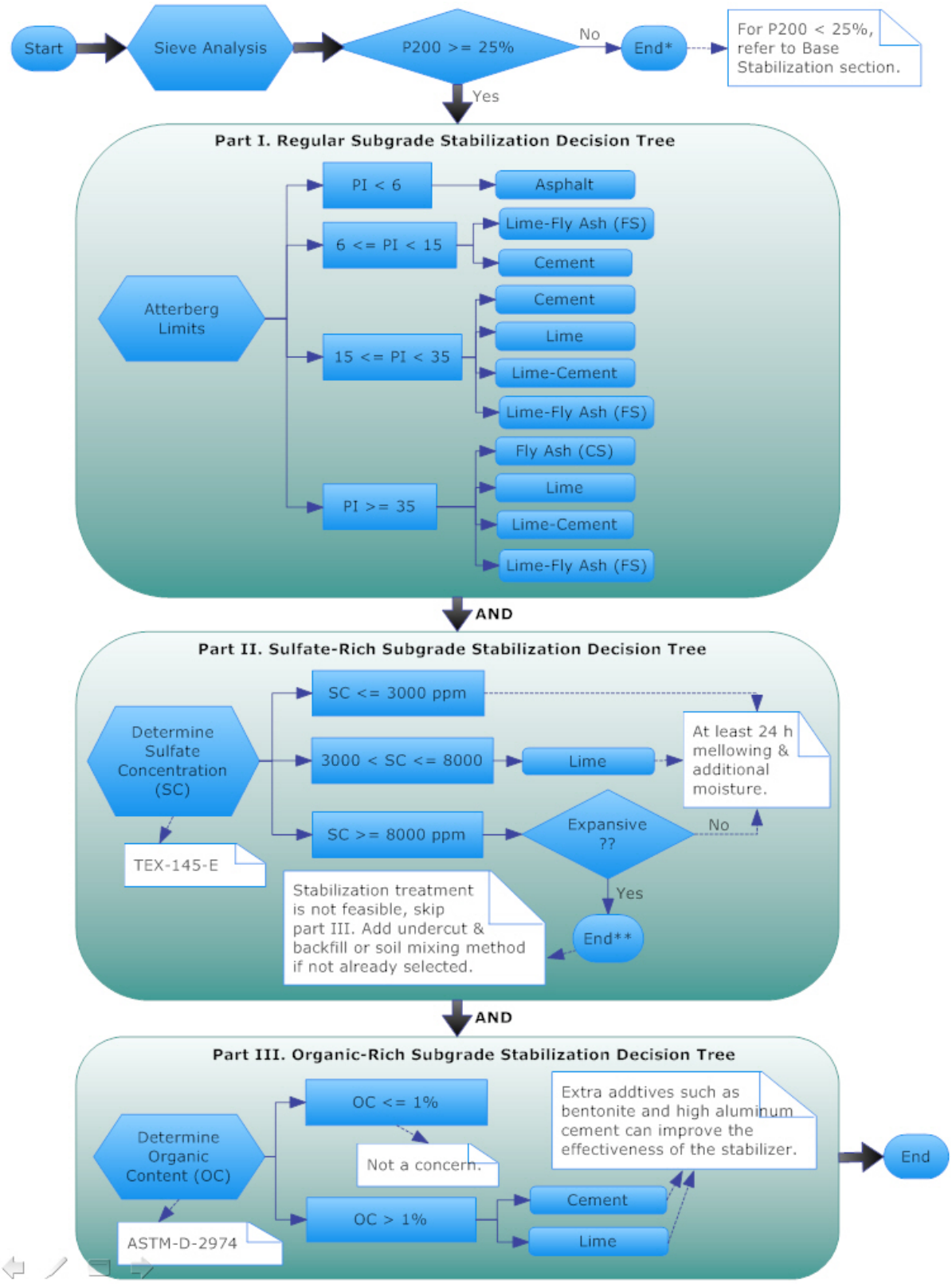

Figure 5.1—Stabilization Subroutine Flowchart

5.2.2. Sulfate Rich Subgrade Stabilization Methods

Sulfate rich subgrade has the potential of sulfate-induced heave. The first step in this block is to determine the sulfate attack risk. According to the TxDOT guidelines, certain soil formations have a higher probability to possess significant sulfate sources, like gypsum, than others. The guideline identified potential areas of sulfate-rich subgrade in a colored map as shown in Figure 5.2. Green highlighted areas have severe heaves associated with Eagle Ford formation and gold areas shows high risk potentials.

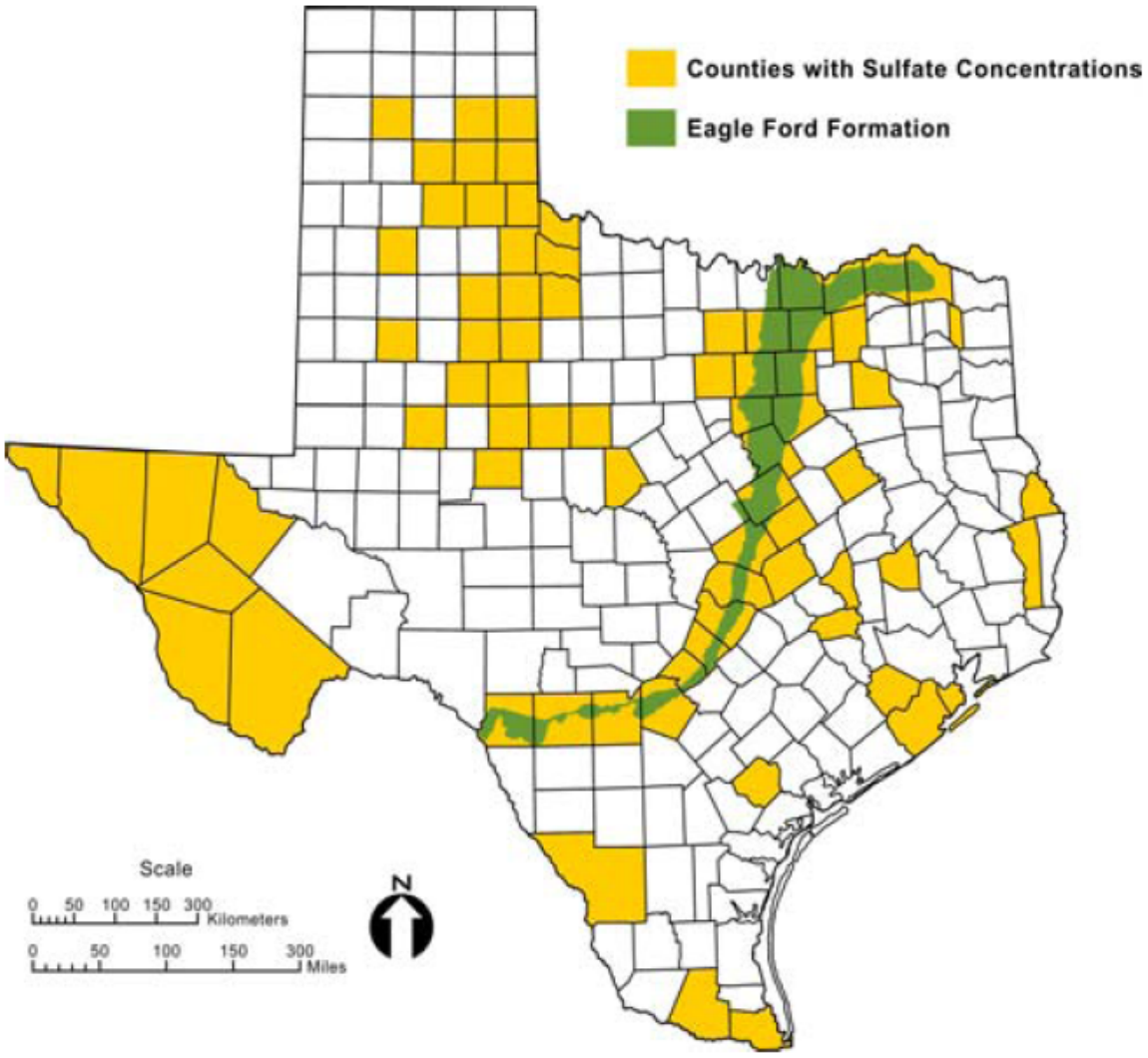

Figure 5.2—Texas Counties with Sulfate-Heave Potentials

Several techniques have been proposed to reduce the sulfate-induced potential heave. TxDOT guidelines recommend mellowing and moisture treatment. Mellowing is the process of allowing the lime treated soil to remain in an uncompacted state for a period of time in order for the lime to react with the clay particles and sulfates. Double application of lime is one of the commonly used technique which consists of an initial application of about half of the total amount of lime required for stabilization. A mellowing period of 72 hrs to 7 days is required prior to compaction. Then the rest of the lime is applied and the soil-lime mixture is compacted (Kota *et al.*, 1996; Little and Petry, 1992). Another popular technique is to use low calcium stabilizers such as portland cement Types I/II, V, Class F fly ash or non-calcium improvement methods such as using geosynthetics, undercut & backfill and decreasing clay content. Pre-treating sulfate-bearing soils with barium hydroxide also help improving stabilization effectiveness (Ferris *et al*., 1991; Kota *et al.*, 1996).

Part II procedure starts from quantifying the sulfate concentration (SC) by following TEX-145-E procedure to see whether there is a potential sulfate-induced risk. Several measurements should be taken along the project alignment and the highest SC should be used. For SC < 3000 ppm, no additional considerations beyond traditional stabilization treatment (Part I) are needed but mellowing is required. For 3000 ppm <= SC <= 8000 ppm, lime is recommended with mellowing and additional moisture. For SC > 8000 ppm, if the subgrade is expansive, no traditional stabilization is feasible and the program stops without going further to Part III. It is recommended to use undercut & backfill method or blending with non-plastic soils as substitute remediation strategies. Part I results can be used for very high SC (SC > 8000 ppm) only if the subgrade shows no significant swell potential..

5.2.3. Organic Rich Subgrade Stabilization Methods

Different tests methods can be used to determine the organic content. TxDOT practices recommend using a "Loss on Ignition" method. (ASTM-D-2974 – Standard Test Methods for Moisture, Ash, and Organic Matter of Peat and Organic Soils) This test is performed to determine the organic content of soils. The organic content is the ratio, expressed in percentage, of the mass of organic matter in a given mass of soil to the mass of the dry soil solids. Soil samples are dried in an oven at 220ºF (105ºC) prior to be placed in the ignition oven to burn off the organic matter. The ignition oven is set to 840ºF (450ºC) and soil samples are left until constant weight is achieved. The weight lost is attributed to organics. Chikyala *et al.* (2006) pointed out that the limitation of this method comes from the fact that it does not discriminate between organic carbon and inorganic carbon. Results from this method give higher organic content (OC) estimation.

It is well understood that organic soils can inhibit the cementitious reactions between the stabilizers and the soil. Many additives have been tried to improve the effectiveness of calcium based stabilization. The supply of extra admixtures may react with minerals on the surface of cement particles and water-immiscible hydration products may result. On the other hand, the addition of extra admixtures could accelerate cement hydroxylation and hydration in which calcium hydroxide, calcium silicate hydrate, sodium silicate hydrate and calcium aluminate hydrate may form. The most commonly used additive is bentonite. The addition of a small amount of high aluminum cement appears to increase the compressive strength further (Hampton and Edil, 1998).

Organic soils are often stabilized with lime or cement with additives as mentioned earlier. Benefits of special mixing techniques such as deep mixing and dry jet mixing are investigated by

many researchers and improvement of engineering properties has been reported (Yang *et al*., 1998; Ahnberg and Holm, 1999).

Part III algorithm is relatively simple. After the OC is determined, the program will recommend cement and lime as stabilizer if organic matter is a concern (OC >= 1%). It will also remind the user to use additives such as bentonite or high aluminum cement if possible. In case OC < 1%, no further consideration is needed.

5.3. USE OF GEOSYNTHETICS

Geosynthetics have proven to be among the most versatile and cost-effective ground modification materials with many advantages. They take up less space compare to soil or aggregate layers; can be customized and installed very easily; most of them are manufactured homogeneous with minimal material variations. Overall using geosynthetics is a cost effective remediation strategy. This method will be recommended for all failure cases discussed in Chapter 4. For the scope of this research, geosynthetics reinforcement is assumed to be targeted for subgrade improvement. The reinforcement is placed at the top of subgrade near aggregate base course interface. Based on literature review, the FHWA design method developed by Holtz *et al*. (1998) is selected. Figure 5.3 shows the steps of the geosynthetics design subroutine. Figure 2.15 through 2.17 mentioned in Chapter 2 were digitalized and curve fitted for this purpose. An external executable program is developed to collect required input which includes subgrade shear strength (C_u), bearing capacity factor (N_c) and maximum wheel load. To calculate C_u Equation 5.1 through 5.3 are used. Since CBR value is not commonly tested by TxDOT districts, the empirical equation 5.2 (Powell *et al*., 1984) which relates CBR to subgrade resilient modulus (M_R) can be used to estimate C_u directly from tested subgrade resilient modulus. Since

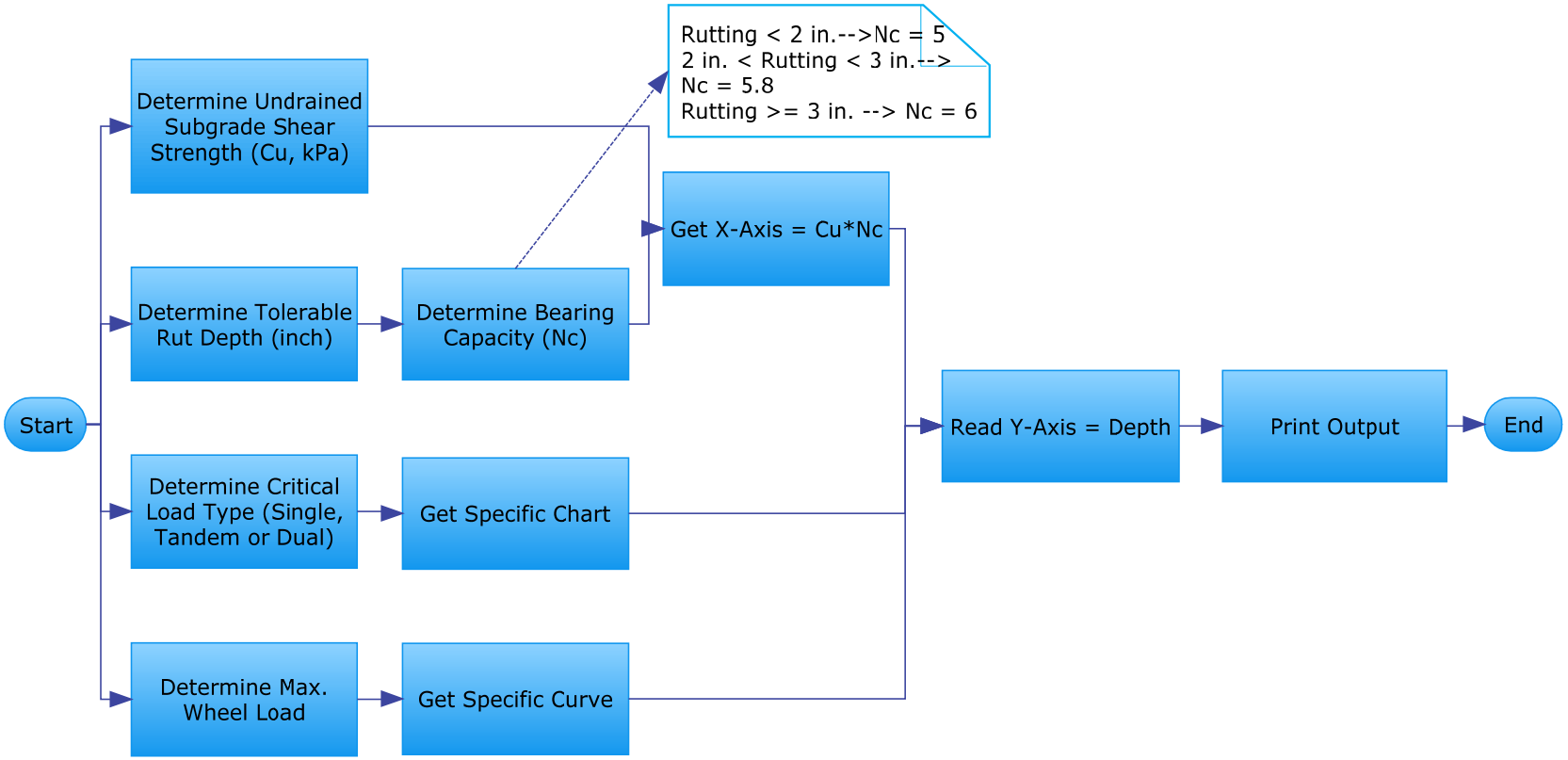

Figure 5.3—Geosynthetics Subroutine Flowchart

the unit for C_u required is in kPa, unit conversion is needed and final calculation can be expressed in Equation 5.3.

$$C_u = 30 \times CBR \tag{5.1}$$

$$M_R = 2555 \times CBR^{0.64} \tag{5.2}$$

$$C_u = 30 \times \left(\frac{Mr}{2555} \right)^{\frac{1}{0.64}} \tag{5.3}$$

where C_u = subgrade undrained shear strength (kPa), which can be measured by Vane shear test or estimated using empirical relationship; M_R = subgrade resilient modulus (psi), for design purpose, the worst case scenario will be considered. The minimum resilient modulus measured throughout the year (M_R under wet condition) will be used in the program; CBR = California bearing ratio. N_c is determined by maximum tolerable rut depth. The ExSPRS program will ask user for load type and maximum wheel load information. Then the subroutine automatically gets the minimum required cover depth based on the digitalized design charts and printout the results.

After executing the Geosynthetics subroutine, the minimal required depth of cover will be compared to original design. If the original design does not meet the minimal requirement, updates will be made to increase original design base layer thickness to meet the requirement. This step ensures the insertion of geosynthetic at recommended location (near top of subgrade) will be fully functional without losing its anchorage strength. If the original design meets the required cover depth, no further modification on layer thicknesses is needed. The program leaves the geosynthetics selection to the user. To tailor appropriate geosynthetics type and properties to a specific project, many properties should be considered such as physical properties, which include type of geosynthetics, thickness, specific gravity and mass per unit area. Mechanical properties are another group of criteria which concerns about tensile strength, tear strength, puncture strength, stiffness, pull-out resistance etc. Hydraulic properties such as porosity and

permeability of geosynthetics are also important when used as drainage materials to convey or prevent the water flow.

Table 2.4 and 2.5 in Chapter 2 provide some general guidelines for geotextile selection. Useful information can be found from free downloadable geosynthetic design softwares such as SpectraPave2™ (http://www.tensarcorp.com) and Propex's RACE program (http://www.geotextile.com).

Although many projects have shown successful results of improved pavement performance due to geosynthetics utilization, there is still a lack of understanding about the behavior of the composite system, especially accurately quantifying the structural benefit by geosynthetics and incorporating a generalized improvement factor into design methodology. For the purpose of this research, an improvement factor of 2 is recommended to approximately estimate the geosynthetics remediation benefit (Gurung, 2003; Abd El Halim *et al.*, 1983; Steward *et al.*, 1977; Giroud *et al.*, 1984; Giroud and Noiray, 1981; Montanelli, *et al.*, 1999; Koerner, 2005).

5.4. MOISTURE CONTROL METHODS

Many pavement distress problems are caused by moisture variation and migration. The ExSPRS program categorizes failure into two reasons: (1) Inadequate support; and/or (2) Moisture variation induced swell/shrink problem such as differential heaving, longitudinal cracking and roughness. The moisture control subroutine will be offered to the user for longitudinal shrinkage crakcing and excessive roughness discussed in Chapter 4. This remediation strategy focuses on measurements that directly deal with minimizing moisture change in subgrade. Figure 5.4 displays the hierarchy of moisture control methods included in

this subroutine. There are three main groups: (1) Use moisture barriers; (2) Improve drainage; and (3) Treat nearby vegetations. This subroutine is illustrative rather than analytical. Detailed information that is provided to the user is discussed in the following sections.

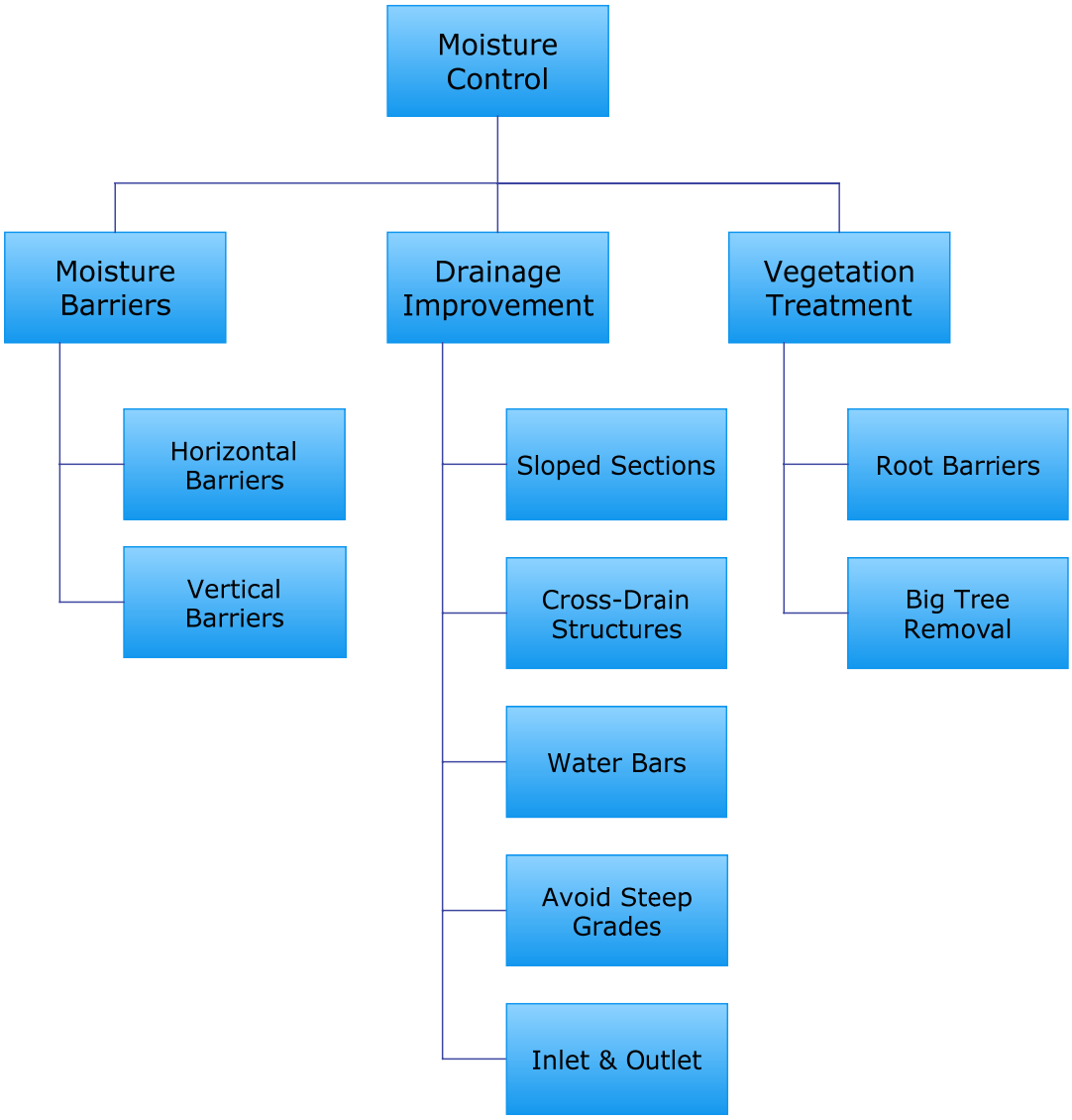

Figure 5.4—Hierarchy of Moisture Control Subroutine

5.4.1. Moisture Barriers

From literature review, it is suggested that the vertical barriers provide better results in maintaining subgrade moisture level constant (Browning, 1999; Steinberg, 1992). The placement

of a vertical moisture barrier is to isolate the subsoils from the climatic changes and thus minimize moisture variations. In drier season when most of the new pavement is constructed, the role of the vertical moisture barrier is to prevent subgrade access to free water. On the other hand, under wet conditions, the barrier will prevent excessive drying of the subgrade soil, especially under pavement shoulders, and thus to prevent longitudinal shrinkage cracking from happening.

Field trials to evaluate the effect of barrier depth have shown that the deeper barriers (8 ft) outperformed the shallow barriers (6 ft) in maintaining a more constant moisture regime, thereby further reducing vertical movements (Gay and Lytton, 1988). However, the deeper the barrier is, the more expensive the construction will become. Thus, using vertical moisture barriers has usually only been reserved for major highways. To successfully implement vertical barriers to lower classification roads, Evans and McManus (1999) developed a new economical barrier construction method that consist of a spray seal surface over low-quality base and subgrade.

According to Evans and McManus (1999), moisture barriers constructed in the United States over the last 20 years has led to cheaper barriers, but still too expensive for low-volume road applications and have several disadvantages. The rounded gravel backfill commonly used in Texas (TxDOT Special Specification No. 5431) is not an ideal material since this kind of backfill provides an "easy" moisture path to the bottom of the barrier, and thus would promote deep-seated swelling. In cases of flat terrain, where there is poor drainage, it would act like a storage reservoir next to the expansive clay subgrade. Evans and McManus's method involved the design of equipment to (1) excavate a deep and narrow slit trench (Figure 5.5a); (2) install plastic

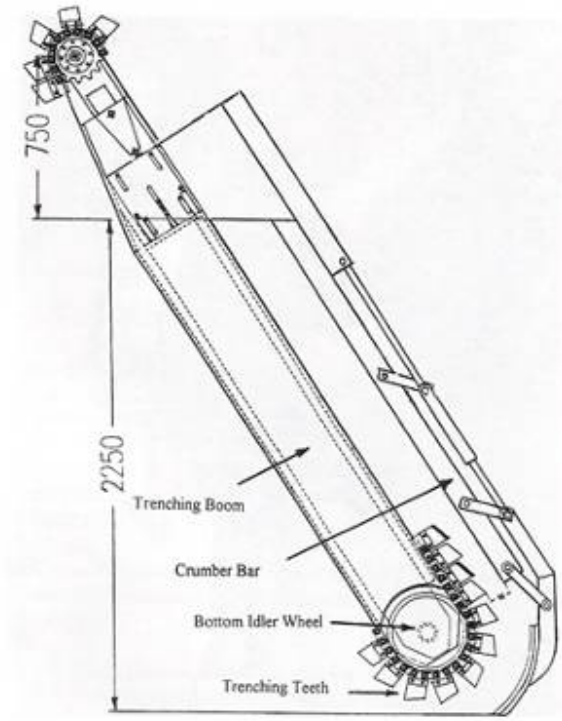

Figure 5.5a - Slim-line Trenching Boom and Crumber Bar Design

Figure 5.5b - Membrane Dispenser and Membrane Held by Polystyrene Wedges

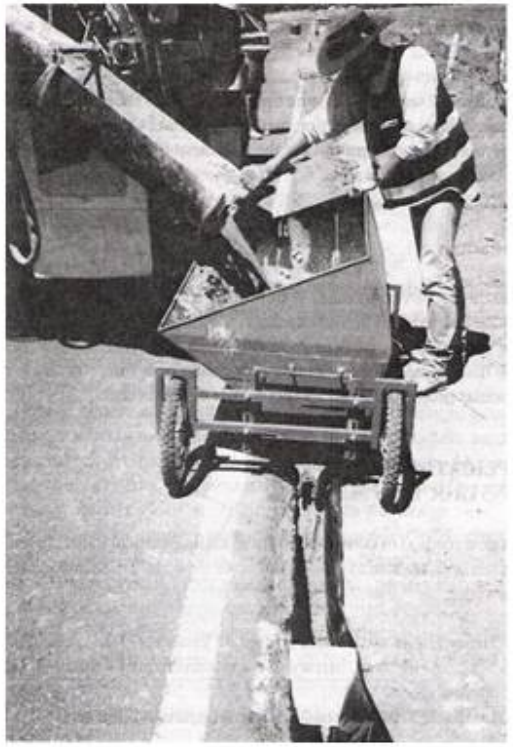

Figure 5.5c - Membrane, Polystyrene Wedges, and Placement of Flowable Fill

Figure 5.5—Vertical Moisture Barriers for Low-Volume Roads (from Evans and McManus, 1999)

sheeting into the trench without damaging it (Figure 5.5b) and (3) discharge a flowable cementitious backfill into the trench (Figure 5.5c). The cost of this new barrier is about $3.10 per lineal foot, which can be used in cost estimation if more accurate unit cost information is not available.

5.4.2. Positive Drainage Improvement Measurements

The most important aspect of road design is drainage (Cedergren, 1974). The adverse effects of poor drainage include premature rutting, cracking, increased roughness and decrease in serviceability. The use of specially designed drainage systems will significantly reduce the time moisture is retained in the pavement system. They also help in minimizing moisture change in the subgrade and make it more stable. Lack of adequate surface drainage is one of the critical factors leading to problems with expansive subgrade soils. Excess water enters pavement sections primarily from rainfall and also from other surface infiltration cause serious pavement damage. Unless high permeability drainage layers are installed in the full width of the pavement, excessive water often remains in the subgrade or within the layers for days, or even months after it stops raining. As a result, pavement life is shortened and annual costs of pavements increased (Rollings and Christie, 2002; Cedergren, 1974). Some obvious drainage problem signs, such as water ponding in the drainage ditches, soft spots in the ditch, or the presence of plants and weeds that grow best in saturated or submerged environments should be closely monitored.

Keller and Sherar (2003) provided detailed drainage design information specially targeted to low volume roads. Table 5.1 compares the pros and cons of different drainage improvement measures discussed in their work.

Table 5.1—Comparisons of Typical Drainage Improvement Strategies (from Keller and Sherar, 2003)

Name	Pros	Cons
Outsloped Roads	• Best way to disperse surface water; • Minimize road width; • No need for inside ditches; • Minimize cost.	• Requires surface and slope stabilization; • Unsafe; • Slippery during rainy periods.
Insloped Roads	• Efficiently controls road surface water.	• Require ditches or cross-drains; • Need extra road width; • Costly.
Crown Section Roads	• Provide higher standard of drainage.	• Less effective for rural roads, especially narrow ones; • Require ditches or cross-drains.
Culvert Cross-Drains	• Most common type for road surface drainage; • Provide a smooth road surface profile.	• Pipes are expensive; • Smaller pipes are susceptible to plugging and require cleaning.
Rolling Dip Cross-Drains	• Cost less; • Easier maintenance.	• Only suitable for low volume, low to moderate speed roads (< 30 mph).
Water Bars	• Customizable for high clearance vehicles or to block traffic; • Better erosion control.	• Only for inactive roads, 4WD roads, skid roads and trails.
Inlet & Outlet Control	• Prevent erosion, plugging.	• Extra cost.

Following recommendations are displayed to the user if this specific remediation strategy is selected. Design details are copyrighted by Keller and Sherar (2003).

- For outsloped, insloped, or crown roadway sections use 3 - 5 % cross slopes (up to 5% is best) (Figure 5.6).
- Use roadway cross-drain structures (rolling dips, pipe culverts, or open top culverts) to move water across the road from the inside ditch to the slope below the road (Figure 5.7 and 5.8).
- Space the cross-drain structures frequently enough (Table 5.2) to remove all surface water. Use culvert cross-drains on roads with an inside ditch and moderately fast vehicle speeds.

Construct rolling dips rather than culvert cross-drains for typical, low volume, low speed roads with grades less than 12%.

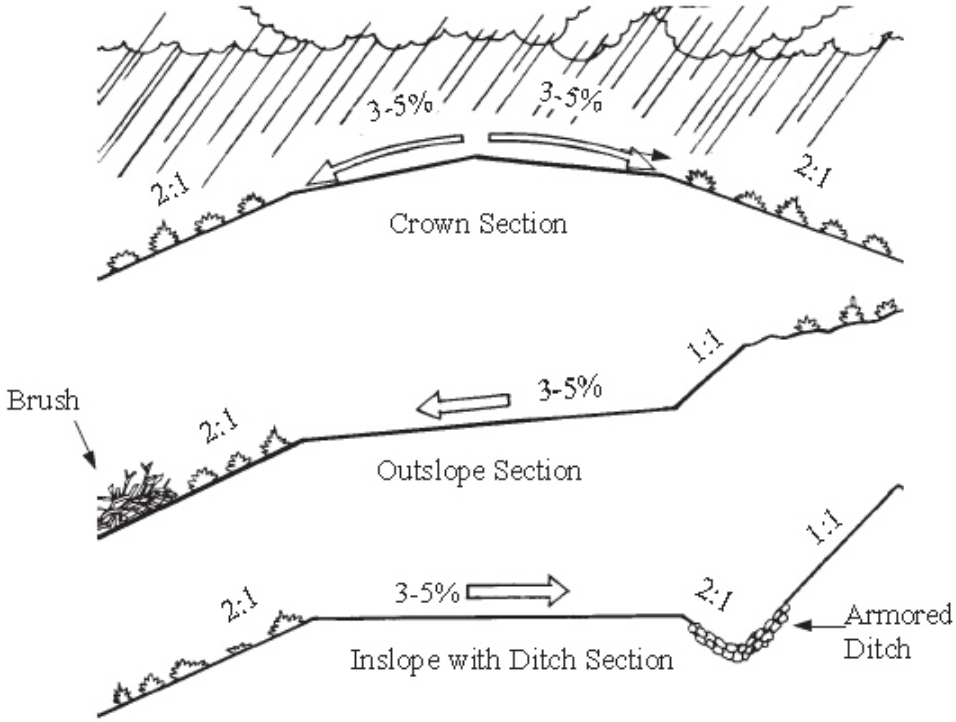

Figure 5.6—Sloped Surface Drainage Options

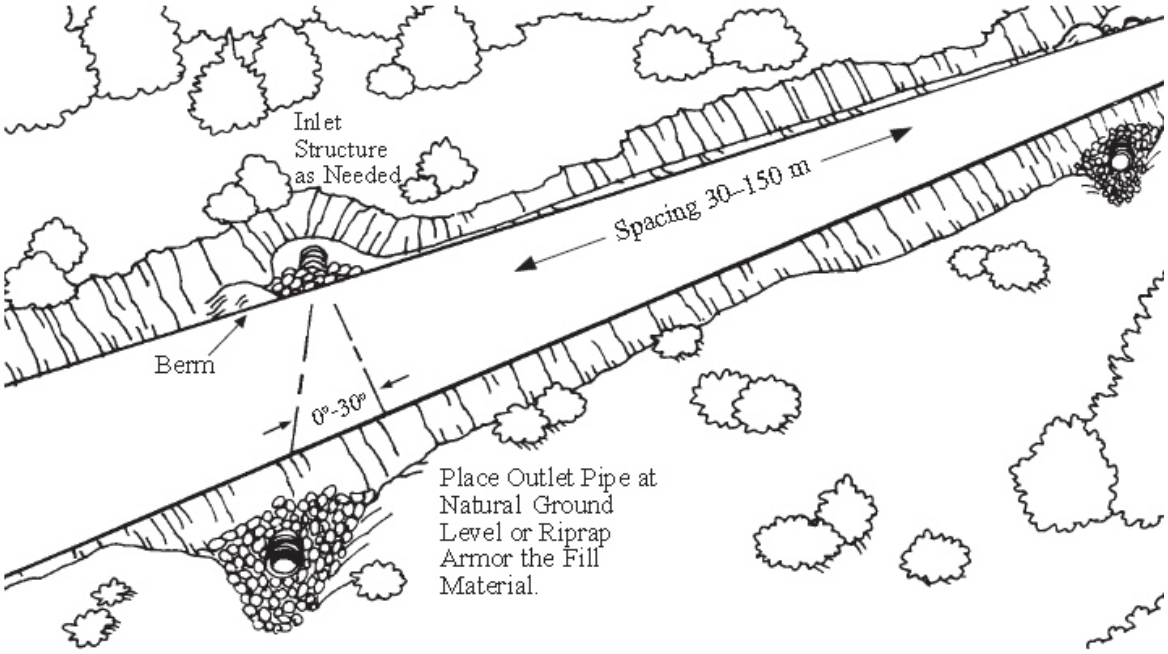

Figure 5.7—Details of Culvert Cross-Drains

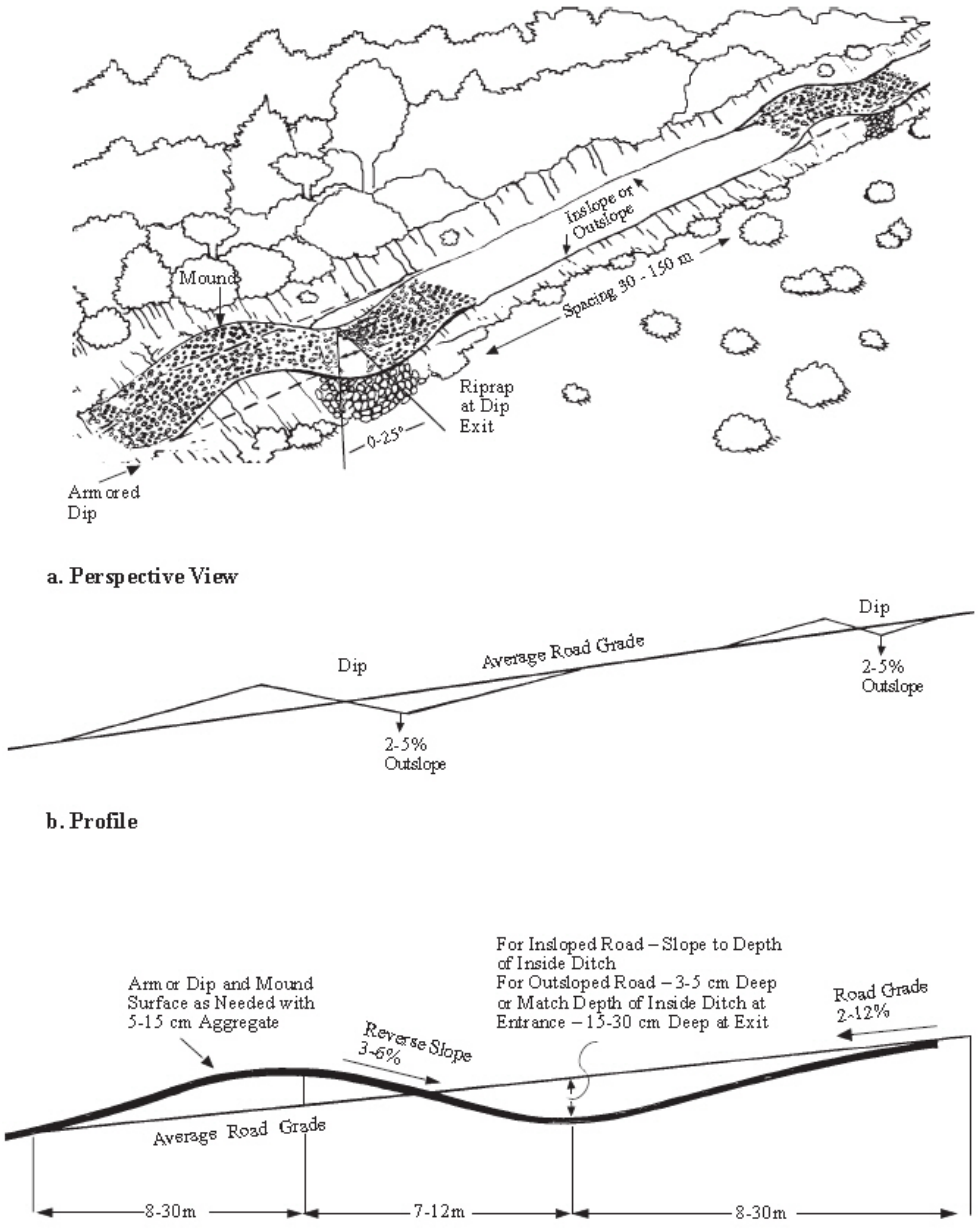

Figure 5.8—Details of Rolling Dip Cross-Drains

Table 5.2—Recommended Maximum Distance for Cross-Drains (Meters)

Road Grade %	Low to Non-Erosive Soils*	Erosive Soils**
0-3	120	75
4-6	90	50
7-9	75	40
10-12	60	35
12+	50	30

- Construct water bars on infrequently used roads or closed roads to control surface runoff. Construct frequently spaced water bars (follow recommendation as shown in Table 5.3) angled at 0-25 degrees with an outslope of 3-5% and a depth of 1 to 2 ft (0.3 to 0.6 meters). Install water bars as shown in Figure 5.9.

Table 5.3—Recommended Water Bar Spacing (Meters)

Road Grade %	Low to Non-Erosive Soils[1]	Erosive Soils[2]
0-5	75	40
6-10	60	30
11-15	45	20
16-20	35	15
21-30	30	12
30+	15	10

Note: 1) Coarse rocky soils, gravel and some clay; 2) Fine, friable soils, silt, fine sands.

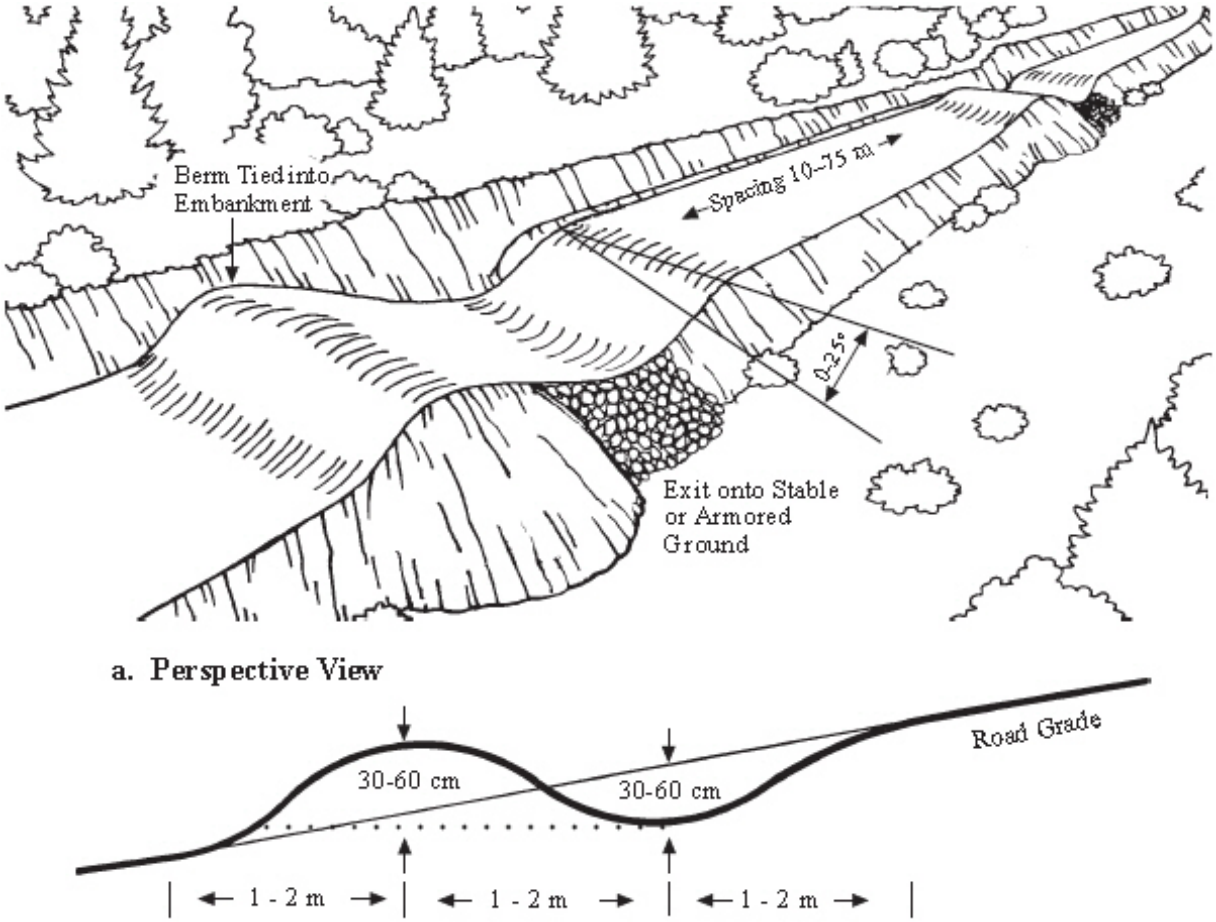

Figure 5.9—Details of Water Bars

- Avoid steep road grades in excess of 12 to 18%. It is very difficult and expensive to properly control drainage on steep grades. Roll grades or undulate the road profile frequently to disperse water, particularly into and out of stream crossings.
- When ditch grade control is needed, use drop inlet structures with culvert cross-drains to prevent ditch down-cutting or where space is limited against the cut bank. Figure 5.10 shows typical culvert drop inlet structures. Alternately, use catch basins excavated into firm soil. Discharge culverts and cross-drain dips at natural ground level, on firm, non-erosive soil or in rocky or brushy areas. If discharged on the fill slopes, armor outlets with riprap or logging slash, or use down-drain structures. Extend the pipe 0.5 to 1.0 meters beyond the toe of the fill slope to prevent erosion of the fill material.

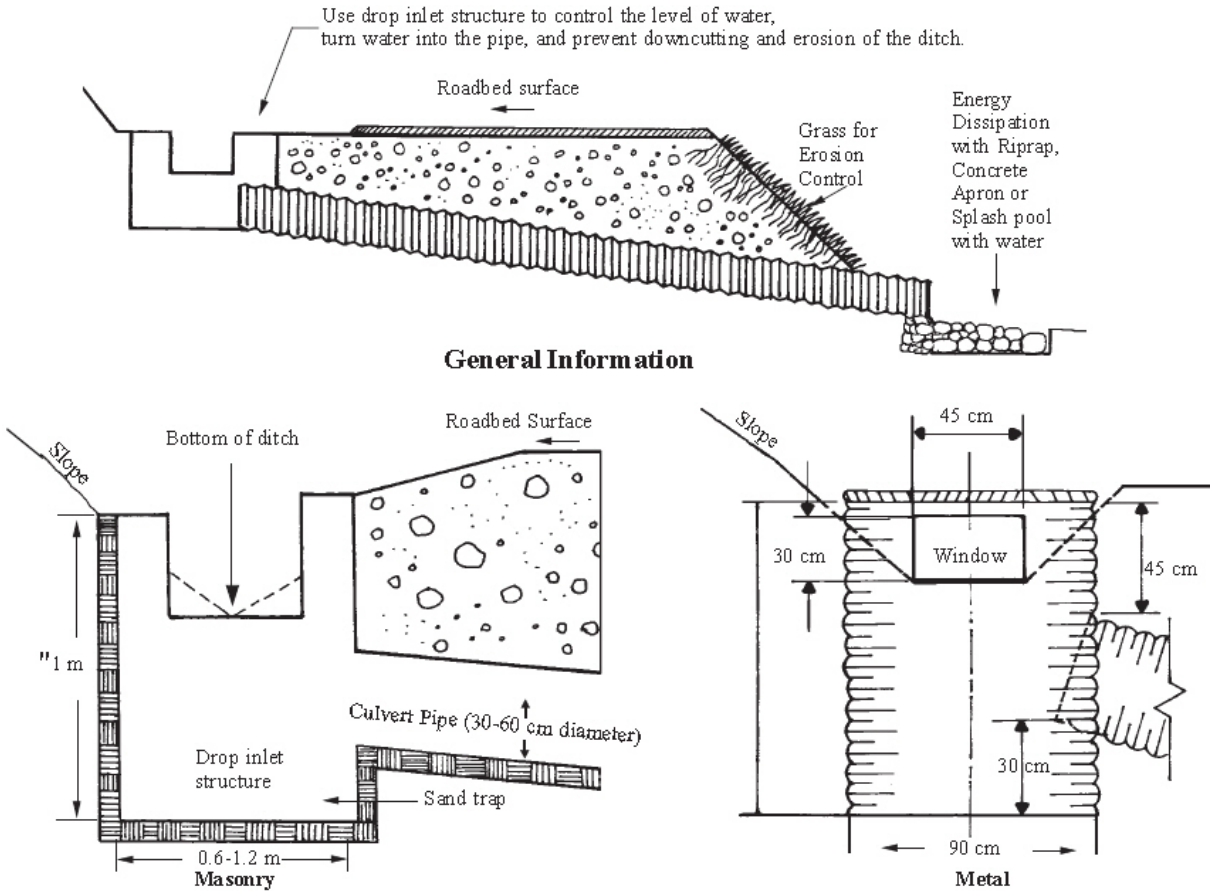

Figure 5.10—Typical Drop Inlet Structure Types with Culvert Cross-Drains

- In erosive soils, armor roadway ditches and leadoff ditches with rock riprap, masonry, concrete lining or, at a minimum, grasses. Ditch dike structures can also be used to dissipate energy and control ditch erosion.
- Use inlet and outlet control. Water should be controlled, directed, or have energy dissipated at the inlet and outlet of culverts, rolling dips, or other cross-drainage structures. This can ensure that water and debris enters the cross-drain efficiently without plugging, and that it exits the cross-drain without damaging the structure or causing erosion at the outlet. Figure 5.11 depicts culvert outlet protection.

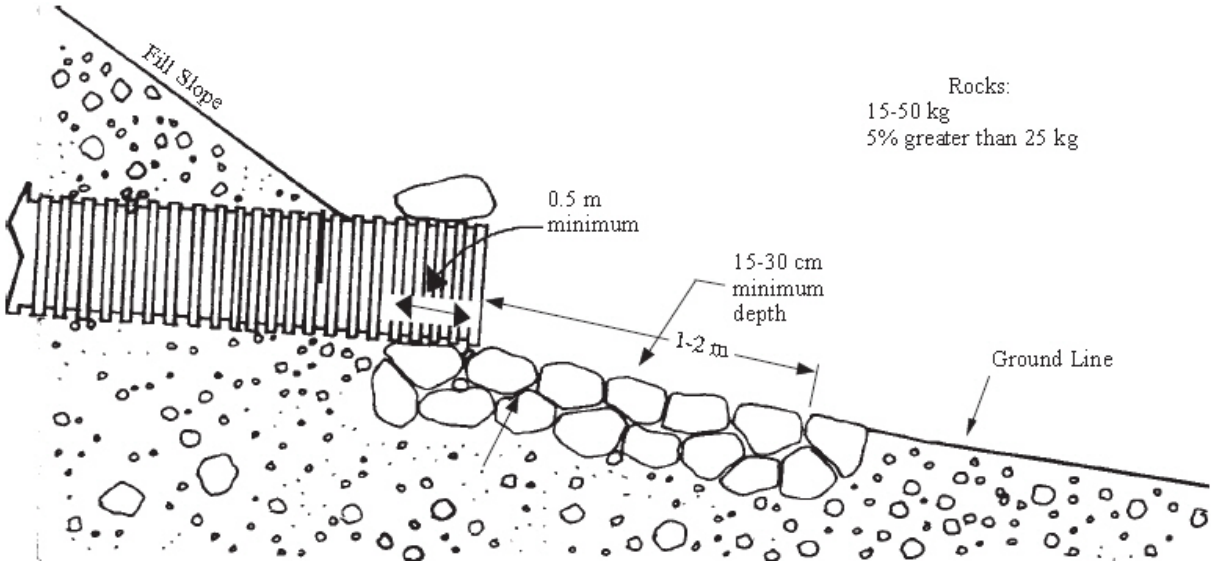

Figure 5.11—Typical Culvert Outlet Protection

5.4.3. Vegetation Treatment

Plant transpiration (water extraction by roots) is generally more significant than subgrade soil evaporation due the low pavement surface permeability, especially for newly constructed roads. In addition, roots from trees near pavements are known to grow under and take advantage of cracks in pavement, resulting in additional cracking or lifting of the pavement (D'Amato *et al.* 2002). Dissimilar soil moisture withdrawal from tree root zones in volumetrically sensitive clays

frequently results in differential settlements due to shrinkage (Ravina, 1984). The cost of the damage is in excess of $100 million per year in the United States (McPherson, 2000). Vertical root barrier is one treatment that has been found to redirect root growth to lower levels of the soil, thus reducing damage (Costello *et al*., 1997). Big tree removal provides another choice for vegetation treatment. A rule of thumb to avoid soil shrinkage and damage to pavement is to keep the distance to height of tree ratio (D:H) greater than 1.0-1.5 and remove big trees within that range (Ward, 1953; Biddle, 1983 and 2001; Tucker and Poor, 1978).

5.5. OTHER METHODS

When it is necessary to build pavement over weak and expansive soils, other methods are available to improve subgrade performance beside previously mentioned ones.

Poor subgrade soil can simply be removed and replaced with high quality fill. This method, which is also called "undercut & backfill," is a simple procedure that does not require any specialized equipment. However, unless a suitable backfill material is available near the job site, removal and replacement is generally much more expensive than the use of additives. For this reason, removal and replacement is mostly used in urban areas, where dust and environmental impacts make the use of additives less desirable. Removal and replacement may also be the best option in areas where deep deposits of peat and muck (organic rich soils) cannot be treated with the use of additives. For lower classification roads, economic constrains have to be taken into account. Table 5.4 shows typical over-excavation (undercut) depths recommended by the Colorado Asphalt Pavement Association (CAPA).

Table 5.4—Undercut Depth Recommended by CAPA

Subgrade Plasticity Index	Depth of Over-Excavation Below Normal Subgrade Elevation (ft)
10 - 20	2
20 - 30	3
30 - 40	4
40 - 50	5
More than 50	6

Above recommended values are used as the lower limit of undercut depth and Equation 2.7 presented in Chapter 2 by Ahlvin (1962) is programmed in the remediation subroutine to calculate the upper limit. Values between these two ranges are recommended to the user for further consideration.

When undercut and backfill is not economically feasible, another method which is referred to as "decreasing clay content" provides an alternative. As the name implies, this process is to dilute expansive soils with non-expansive fill. It is less time consuming and cheaper compared to undercut & backfill when quantities of non-expansive fills are limited. When this method is selected, the user needs to know the targeted PI. By using Equation 2.8, the volume of required mixing sand can be calculated. If swelling characteristic tests were performed, Equation 2.9 can be used to quantify the swell potential change by using this method.

Deep dynamic compaction is one of the most economical ground modification methods. This technique involves repeatedly raising and dropping a large weight in a prescribed pattern to densify the potentially unstable or weak underlying materials with high-energy impacts. The weight may range from 6 to 25 tons and the drop height typically varies from 30 to 60 ft. The degree of densification achieved is a function of the energy input (i.e., weight and drop height) as well as the saturation level, fines content and permeability of the material. As mentioned by

several researchers, (Mowafy *et al*., 1985; Rollins and Christie, 2002), this method is not appropriate for saturated clayey soils and the solution may be temporary due to water infiltration.

CHAPTER SIX - COST-BENEFIT ANALYSIS

6.1. OVERVIEW

In this chapter, assumptions and procedures to perform cost assessment are discussed. "Before and after" analyses are incorporated to quantify the benefits of the alternate remediation strategies. Cost-effectiveness comparisons between original design and alternatives are provided. Following three questions are answered:

1) How to determine unit costs for original design and selected remediation strategies?
2) How to estimate benefit of selected remediation strategies?
3) How to use cost and benefit comparison results?

6.2. COST ASSESSMENT ASSUMPTIONS

Due to the lack of data, relationships and models to perform complete life cycle cost analysis (LCCA), ***Cost-Benefit Aanalysis*** is used instead to perform the pavement cost assessment. Many assumptions are made to simplify the procedure without compromising the results accuracy. Following sections discuss these assumptions in detail.

6.2.1. Basic Assumptions

For a typical pavement cost analysis, both user cost and agency cost components need to be included. User cost consists of vehicle operating cost (fuel, tires, maintenance, repair and depreciation of the vehicle) and non-vehicle operating cost (travel time delays, cargo damage, driver/passenger discomfort or injury, and so on). Small reduction in user cost may result in substantial benefit when traffic volumes are high. However, the focus of this research is on low-volume roads, which typically have low daily traffic. The user costs can be considered minimal

and thus omitted from cost assessment. For the same reason, delay costs due to construction activities of low-volume roads are not critical. Construction time estimation is also omitted assuming cost to be the controlling parameter.

The agency cost can be estimated based on the measurements of the physical quantities involved in construction, such as length, area, volume, weight, work hours, individual items or bundles, and lump sums of money. Once the number of units required is calculated, it can be multiplied by the unit cost to compute the total cost. The calculated cost can be further adjusted for agency's administration and construction overhead as well as contractor's overhead to estimate the final agency costs. Unit price information for this study was obtained from the RS Means CostWorks Data for Heavy Construction (R.S. Means, 2007). All productivity rates of the pavement construction activities are exported from R.S. Means database into excel spreadsheets. These unit cost data can be easily updated with most current information as they become available.

Cost analysis is only considered for road lanes, and shoulders are excluded. User needs to provide total number of lanes in both directions, road length and lane width. By default, the roadway section being analyzed is a one-mile, two-lane low-volume road with 12-ft-wide lanes.

New pavement is assumed for planning construction activities. Only main construction activities are considered, which include, but not limited to excavation, backfill, compaction, and preparation of subbase, base, and ACP layers. Minor activities such as underground utility removal, drainage and manhole installation, bridge or culvert construction, surface detailing and finishing are eliminated for simplification.

R.S. Means differentiates productivity rates and unit costs for same construction activity with different lift thickness. User defined layer thicknesses are interpolated/extrapolated based on available lift thickness information. Total activity cost which includes cost of bare materials, bare labor, bare equipment, overhead and profit is used in our unit cost approach. One crew with one shift is used for all activities since expediting with more crew members or shifts results higher unit cost. For each activity, normal or ideal set of working conditions are considered. No variability is considered to account for changes in weather or other factors during the construction.

6.2.2. Remediation Strategies Assumptions

For each remediation strategy the cost is considered separately. The assumption made in this study is that these remediation measurements are independent of each other. The final cost is reported with a "+" sign for each modification strategy. The user should expect to spend extra cost as specified for that alternative in addition to the original design cost. A special screen allows the user to select/input assumption details for suggested remediation strategies. Following sections discuss these assumptions in detail.

R.S. Means gives cost information on three stabilizers: asphalt, cement and lime. For fly ash, or mixed lime-cement, lime-fly ash, the price of lime stabilization is used as substitute. If unit price information is available on those stabilizers, the excel sheet can be updated so the program will have that information available.

The selection of appropriate geosynthetics type and optimum location has been discussed in earlier chapters (Section 2.3.3 and Section 5.3). To estimate the cost, the heavy duty geotextile used for soil stabilization and reinforcement is assumed. Only information the user needs to

provide is the target tensile strength for the geosynthetics. R.S. Means 2007 reports the tensile strength per fabric sheet in terms of pounds (lb). The available options are 120-lb, 200-lb and 600-lb. Other associated installation costs are not considered due to lack of information.

If moisture control methods are suggested, the user will first have to decide which one(s) out of the three categories they want to implement (see Figure 5.4 in Chapter 5). All encountered costs will be added up together for the final cost estimation of moisture control methods.

For moisture barriers, regular drainage geotextile is assumed. The user will be asked for the geotextile film thickness (in).

There may be several ways to improve drainage. Additional costs considered by the program include grading sloped sections and the use of culvert by either build cross-drain structures, water bars or inlet and outlet. The user needs to provide culvert diameter (in), spacing (ft) and slope description (gentle or steep).

When vegetation treatment is selected, the user needs to select from drop-down lists of following information: diameter of big trees (bigger than 12-inch); number of big trees to be removed per mile; Number of trees less than 12-inch per acre (range in hundreds); percentage of hardwoods and roadside width for smaller trees (those less than 12-inch) (ft/side)

Undercut & backfill depth will be used to govern the cost of this remediation method. The calculated depth (upper limit as discussed in Section 5.5) is automatically loaded from previous calculations (Chapter 2, Equation 2.7). The unit cost consists of two parts: excavation and backfill. Same rules of interpolation/ extrapolation are applied in this case. No extra input is needed.

Due to the lack of cost data for deep dynamic compaction, airport subgrade compaction is used as a substitute. The user need to select percentage of standard proctor density (ASTM D698—Moisture Density Relationship for Soils, Standard Method) from R.S. Means' available pool: 80%, 85%, 90% and 95%.

The agency cost for decreasing clay content method includes three parts: excavation, backfill and mixing. Due to lack of information, it is estimated the same way as undercut & backfill, with half the depth entered by the user (meaning a partial mix and replacement).

6.3. COST DATA AQUIREMENT

RS Means offers different productivity rates for detailed lists of work items according to current market and location of the project. To select the productivity rate for a specific activity, the project location has to be first selected before entering the spreadsheet screen. Costs are adjusted by location factors. Figure 6.1 shows a location setup screen with detailed location factors information for Fort Worth district (zip code prefix 760).

As an example, the local productivity rates for lime stabilized subgrade in Fort Worth district could be found by using the drop-down list as shown in Figure 6.2. Under "Site Construction" category, the "Earth Work" and "Soil Stabilization" could be found as highlighted. The productivity rates are differentiated by lift thickness. It breaks the total activity cost into four cost components (Figure 6.3): bare materials, bare labor, bare equipment, and overhead and profit.

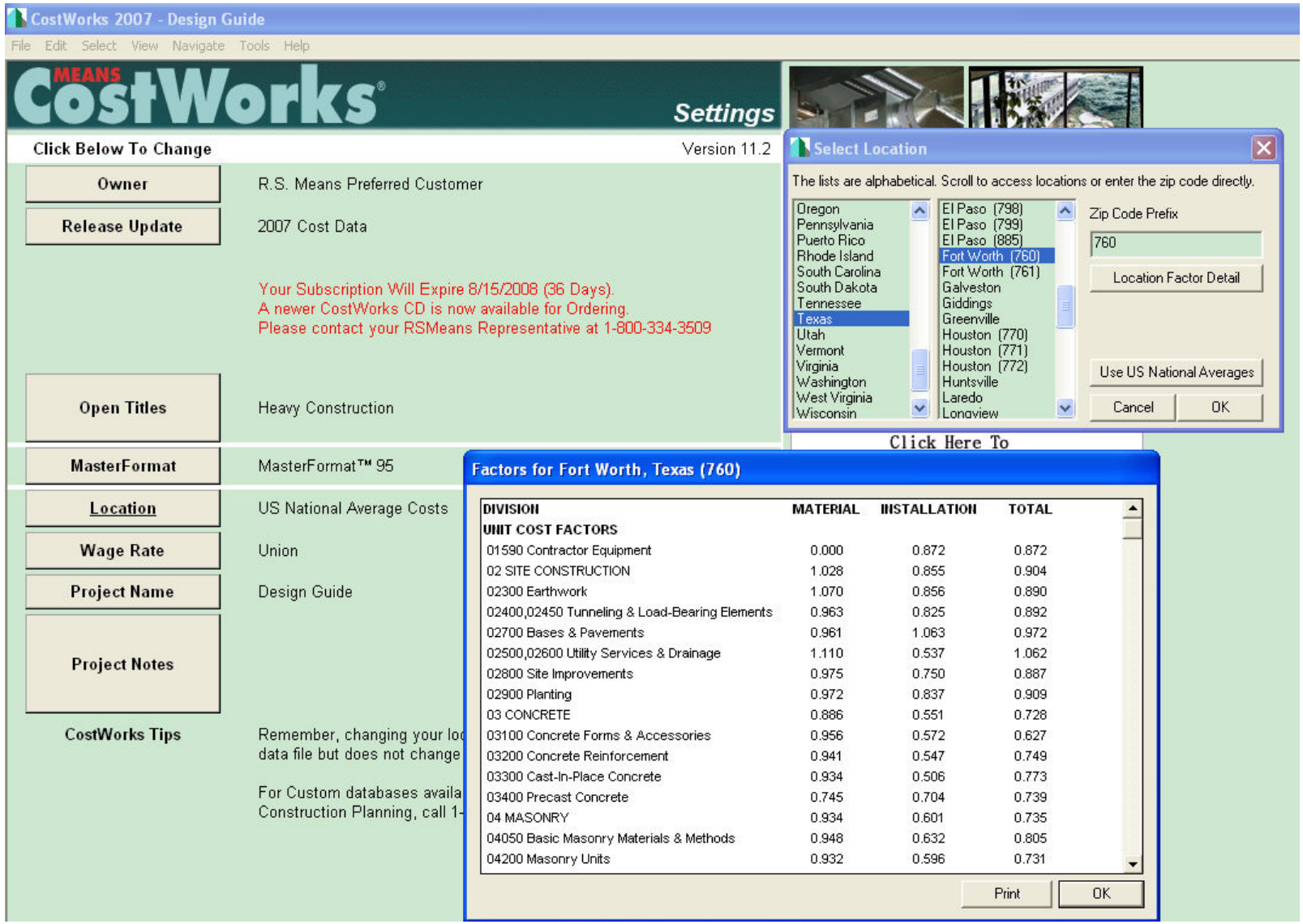

Figure 6.1—RS Means CostWorks Location Setup (Fort Worth)

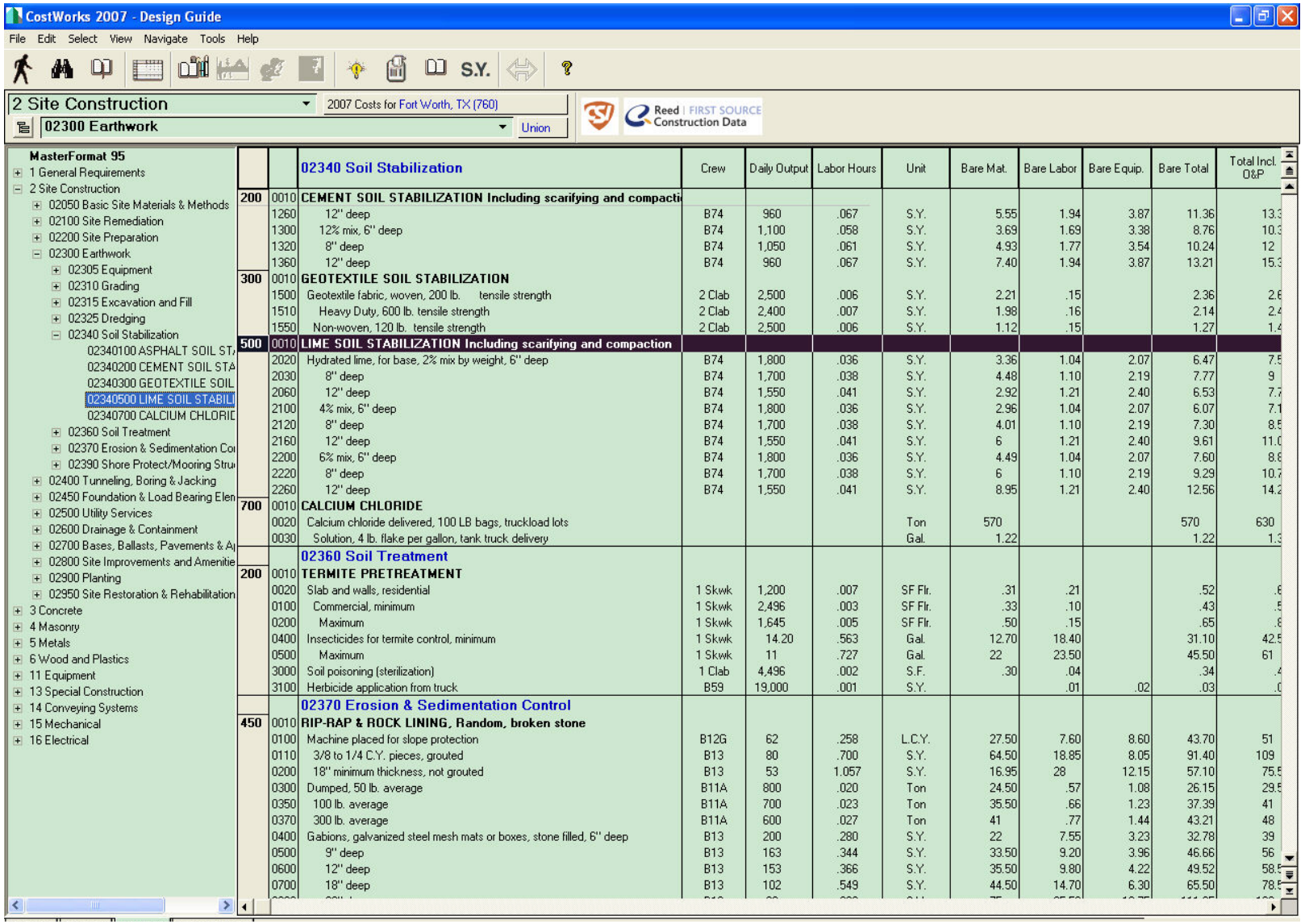

		02340 Soil Stabilization	Crew	Daily Output	Labor Hours	Unit	Bare Mat.	Bare Labor	Bare Equip.	Bare Total	Total Incl. O&P
200	0010	CEMENT SOIL STABILIZATION Including scarifying and compacti									
	1260	12" deep	B74	960	.067	S.Y.	5.55	1.94	3.87	11.36	13.3
	1300	12% mix, 6" deep	B74	1,100	.058	S.Y.	3.69	1.69	3.38	8.76	10.3
	1320	8" deep	B74	1,050	.061	S.Y.	4.93	1.77	3.54	10.24	12
	1360	12" deep	B74	960	.067	S.Y.	7.40	1.94	3.87	13.21	15.3
300	0010	GEOTEXTILE SOIL STABILIZATION									
	1500	Geotextile fabric, woven, 200 lb. tensile strength	2 Clab	2,500	.006	S.Y.	2.21	.15		2.36	2.6
	1510	Heavy Duty, 600 lb. tensile strength	2 Clab	2,400	.007	S.Y.	1.98	.16		2.14	2.4
	1550	Non-woven, 120 lb. tensile strength	2 Clab	2,500	.006	S.Y.	1.12	.15		1.27	1.4
500	0010	LIME SOIL STABILIZATION Including scarifying and compaction									
	2020	Hydrated lime, for base, 2% mix by weight, 6" deep	B74	1,800	.036	S.Y.	3.36	1.04	2.07	6.47	7.5
	2030	8" deep	B74	1,700	.038	S.Y.	4.48	1.10	2.19	7.77	9
	2060	12" deep	B74	1,550	.041	S.Y.	2.92	1.21	2.40	6.53	7.7
	2100	4% mix, 6" deep	B74	1,800	.036	S.Y.	2.96	1.04	2.07	6.07	7.1
	2120	8" deep	B74	1,700	.038	S.Y.	4.01	1.10	2.19	7.30	8.5
	2160	12" deep	B74	1,550	.041	S.Y.	6	1.21	2.40	9.61	11.0
	2200	6% mix, 6" deep	B74	1,800	.036	S.Y.	4.49	1.04	2.07	7.60	8.8
	2220	8" deep	B74	1,700	.038	S.Y.	6	1.10	2.19	9.29	10.7
	2260	12" deep	B74	1,550	.041	S.Y.	8.95	1.21	2.40	12.56	14.2
700	0010	CALCIUM CHLORIDE									
	0020	Calcium chloride delivered, 100 LB bags, truckload lots				Ton	570			570	630
	0030	Solution, 4 lb. flake per gallon, tank truck delivery				Gal.	1.22			1.22	1.3
		02360 Soil Treatment									
200	0010	TERMITE PRETREATMENT									
	0020	Slab and walls, residential	1 Skwk	1,200	.007	SF Flr.	.31	.21		.52	.6
	0100	Commercial, minimum	1 Skwk	2,496	.003	SF Flr.	.33	.10		.43	.5
	0200	Maximum	1 Skwk	1,645	.005	SF Flr.	.50	.15		.65	.8
	0400	Insecticides for termite control, minimum	1 Skwk	14.20	.563	Gal.	12.70	18.40		31.10	42.5
	0500	Maximum	1 Skwk	11	.727	Gal.	22	23.50		45.50	61
	3000	Soil poisoning (sterilization)	1 Clab	4,496	.002	S.F.	.30	.04		.34	.4
	3100	Herbicide application from truck	B59	19,000	.001	S.Y.		.01	.02	.03	.0
		02370 Erosion & Sedimentation Control									
450	0010	RIP-RAP & ROCK LINING, Random, broken stone									
	0100	Machine placed for slope protection	B12G	62	.258	L.C.Y.	27.50	7.60	8.60	43.70	51
	0110	3/8 to 1/4 C.Y. pieces, grouted	B13	80	.700	S.Y.	64.50	18.85	8.05	91.40	109
	0200	18" minimum thickness, not grouted	B13	53	1.057	S.Y.	16.95	28	12.15	57.10	75.5
	0300	Dumped, 50 lb. average	B11A	800	.020	Ton	24.50	.57	1.08	26.15	29.5
	0350	100 lb. average	B11A	700	.023	Ton	35.50	.66	1.23	37.39	41
	0370	300 lb. average	B11A	600	.027	Ton	41	.77	1.44	43.21	48
	0400	Gabions, galvanized steel mesh mats or boxes, stone filled, 6" deep	B13	200	.280	S.Y.	22	7.55	3.23	32.78	39
	0500	9" deep	B13	163	.344	S.Y.	33.50	9.20	3.96	46.66	56
	0600	12" deep	B13	153	.366	S.Y.	35.50	9.80	4.22	49.52	58.5
	0700	18" deep	B13	102	.549	S.Y.	44.50	14.70	6.30	65.50	78.5

Figure 6.2—Typical RS Means Data Spreadsheet

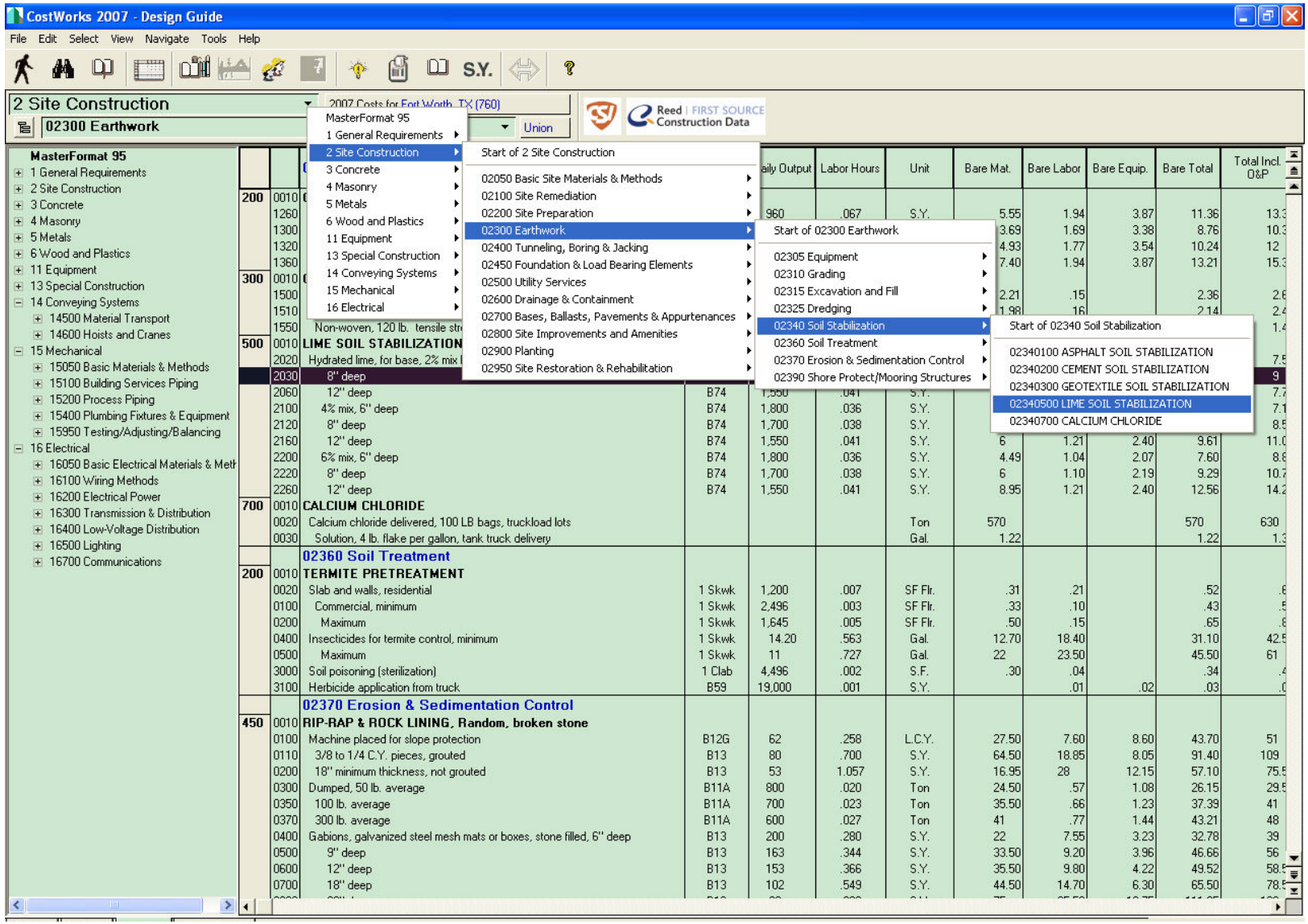

Figure 6.3—Layout of Construction Activity Drop-Down List

Construction activities in R.S. Means are identified by “Activity Number”, “General Description”, “Productivity Units” and “Crew Code” among other descriptors. Detailed information such as crew, daily output, labor hours, unit and cost for different categories are listed according to lift thickness of the layer and material used for stabilization. The detailed crew information can be viewed in a pop up window by double clicking the crew number. Figure 6.4 shows detailed crew information for the crew labeled B74.

Crew Lookup - based upon National Average Costs

File

Crew No.		Bare Costs		Incl. Subs O&P		Cost Per Labor-Hour	
Crew B74 (Union)		Hr.	Daily	Hr.	Daily	Bare Costs	Incl. O&P
1	Labor Foreman (outside)	$30.75	$246.00	$47.86	$382.90	$34.03	$51.91
1	Laborer	$28.75	$230.00	$44.75	$358.00		
4	Equip. Oper. (med.)	$38.40	$1,228.80	$57.85	$1,851.20		
2	Truck Drivers (heavy)	$29.55	$472.80	$45.65	$730.40		
1	Grader, 30,000 Lbs.		$505.40		$555.95		
1	Ripper, beam & 1 shank		$76.40		$84.05		
2	Stabilizers, 310 H.P.		$2,530.00		$2,783.00		
1	Flatbed Truck, Gas, 3 Tor		$185.20		$203.70		
1	Chem. Spreader, Towed		$44.20		$48.60		
1	Roller, Vibratory, 25 Ton		$565.60		$622.15		
1	Water Tanker, 5000 Gal.		$121.20		$133.30		
1	Truck Tractor, 195 H.P.		$235.60		$259.15	$66.62	$73.28
64 L.H., Daily Totals			$6,441.20		$8,012.40	$100.64	$125.19

Figure 6.4—Crew Information Details

6.3.1. Exporting and Updating Cost Data

Cost data acquired from R.S. Means for each construction activity with different lift thicknesses are added to R.S. Means estimator list. These unit costs are grouped and exported in to different excel spreadsheets. Figure 6.5 shows exported lime stabilization data. Some columns are hidden in order to show parameters of interest. The CSI number is the identification number used in R.S. Means for each activity. Description column shows detailed information of the activity including lift thickness, material properties, machinery and other description. Crew

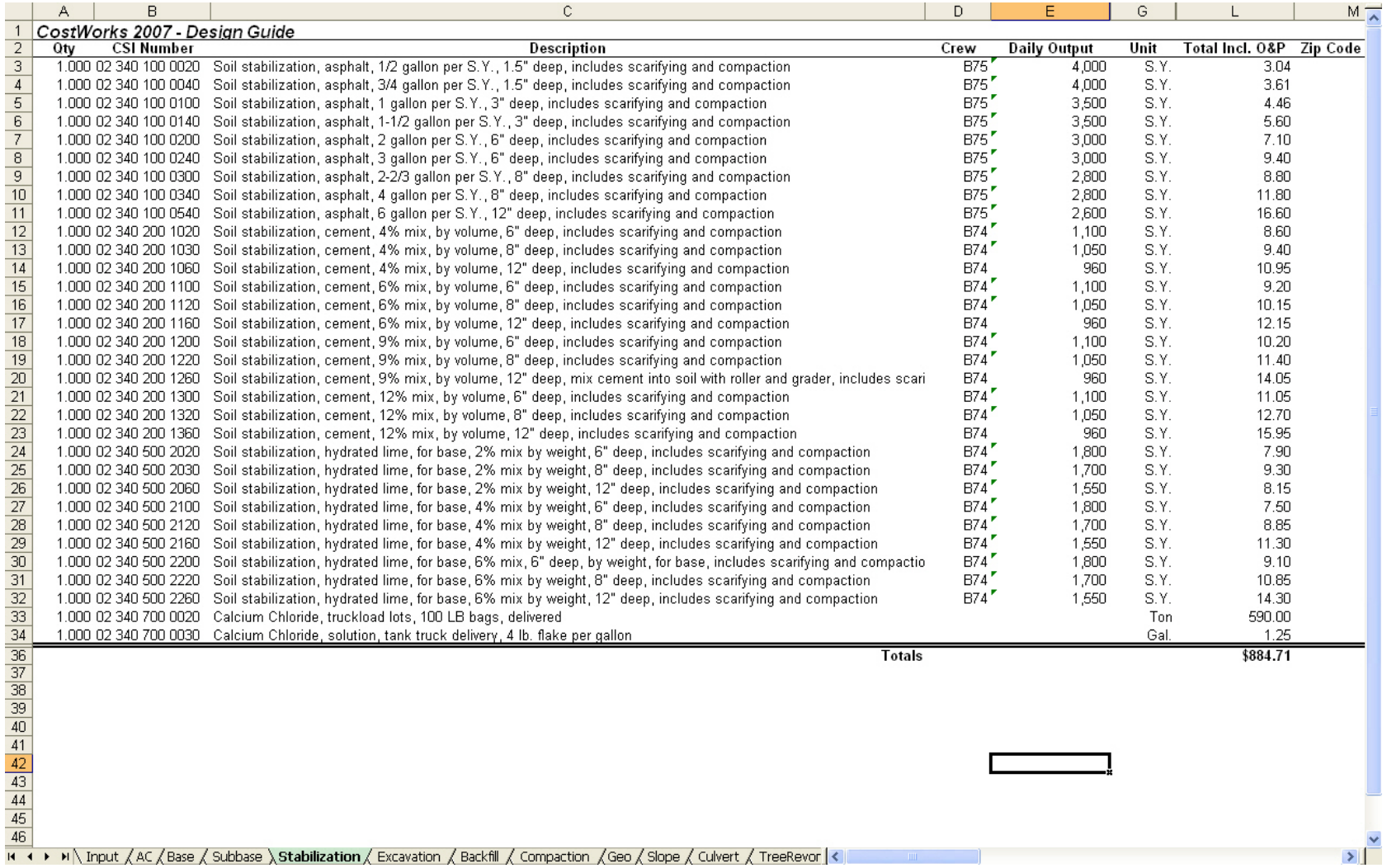

	A	B	C	D	E	G	L	M
1	*CostWorks 2007 - Design Guide*							
2	**Qty**	**CSI Number**	**Description**	**Crew**	**Daily Output**	**Unit**	**Total Incl. O&P**	**Zip Code**
3	1.000	02 340 100 0020	Soil stabilization, asphalt, 1/2 gallon per S.Y., 1.5" deep, includes scarifying and compaction	B75	4,000	S.Y.	3.04	
4	1.000	02 340 100 0040	Soil stabilization, asphalt, 3/4 gallon per S.Y., 1.5" deep, includes scarifying and compaction	B75	4,000	S.Y.	3.61	
5	1.000	02 340 100 0100	Soil stabilization, asphalt, 1 gallon per S.Y., 3" deep, includes scarifying and compaction	B75	3,500	S.Y.	4.46	
6	1.000	02 340 100 0140	Soil stabilization, asphalt, 1-1/2 gallon per S.Y., 3" deep, includes scarifying and compaction	B75	3,500	S.Y.	5.60	
7	1.000	02 340 100 0200	Soil stabilization, asphalt, 2 gallon per S.Y., 6" deep, includes scarifying and compaction	B75	3,000	S.Y.	7.10	
8	1.000	02 340 100 0240	Soil stabilization, asphalt, 3 gallon per S.Y., 6" deep, includes scarifying and compaction	B75	3,000	S.Y.	9.40	
9	1.000	02 340 100 0300	Soil stabilization, asphalt, 2-2/3 gallon per S.Y., 8" deep, includes scarifying and compaction	B75	2,800	S.Y.	8.80	
10	1.000	02 340 100 0340	Soil stabilization, asphalt, 4 gallon per S.Y., 8" deep, includes scarifying and compaction	B75	2,800	S.Y.	11.80	
11	1.000	02 340 100 0540	Soil stabilization, asphalt, 6 gallon per S.Y., 12" deep, includes scarifying and compaction	B75	2,600	S.Y.	16.60	
12	1.000	02 340 200 1020	Soil stabilization, cement, 4% mix, by volume, 6" deep, includes scarifying and compaction	B74	1,100	S.Y.	8.60	
13	1.000	02 340 200 1030	Soil stabilization, cement, 4% mix, by volume, 8" deep, includes scarifying and compaction	B74	1,050	S.Y.	9.40	
14	1.000	02 340 200 1060	Soil stabilization, cement, 4% mix, by volume, 12" deep, includes scarifying and compaction	B74	960	S.Y.	10.95	
15	1.000	02 340 200 1100	Soil stabilization, cement, 6% mix, by volume, 6" deep, includes scarifying and compaction	B74	1,100	S.Y.	9.20	
16	1.000	02 340 200 1120	Soil stabilization, cement, 6% mix, by volume, 8" deep, includes scarifying and compaction	B74	1,050	S.Y.	10.15	
17	1.000	02 340 200 1160	Soil stabilization, cement, 6% mix, by volume, 12" deep, includes scarifying and compaction	B74	960	S.Y.	12.15	
18	1.000	02 340 200 1200	Soil stabilization, cement, 9% mix, by volume, 6" deep, includes scarifying and compaction	B74	1,100	S.Y.	10.20	
19	1.000	02 340 200 1220	Soil stabilization, cement, 9% mix, by volume, 8" deep, includes scarifying and compaction	B74	1,050	S.Y.	11.40	
20	1.000	02 340 200 1260	Soil stabilization, cement, 9% mix, by volume, 12" deep, mix cement into soil with roller and grader, includes scari	B74	960	S.Y.	14.05	
21	1.000	02 340 200 1300	Soil stabilization, cement, 12% mix, by volume, 6" deep, includes scarifying and compaction	B74	1,100	S.Y.	11.05	
22	1.000	02 340 200 1320	Soil stabilization, cement, 12% mix, by volume, 8" deep, includes scarifying and compaction	B74	1,050	S.Y.	12.70	
23	1.000	02 340 200 1360	Soil stabilization, cement, 12% mix, by volume, 12" deep, includes scarifying and compaction	B74	960	S.Y.	15.95	
24	1.000	02 340 500 2020	Soil stabilization, hydrated lime, for base, 2% mix by weight, 6" deep, includes scarifying and compaction	B74	1,800	S.Y.	7.90	
25	1.000	02 340 500 2030	Soil stabilization, hydrated lime, for base, 2% mix by weight, 8" deep, includes scarifying and compaction	B74	1,700	S.Y.	9.30	
26	1.000	02 340 500 2060	Soil stabilization, hydrated lime, for base, 2% mix by weight, 12" deep, includes scarifying and compaction	B74	1,550	S.Y.	8.15	
27	1.000	02 340 500 2100	Soil stabilization, hydrated lime, for base, 4% mix by weight, 6" deep, includes scarifying and compaction	B74	1,800	S.Y.	7.50	
28	1.000	02 340 500 2120	Soil stabilization, hydrated lime, for base, 4% mix by weight, 8" deep, includes scarifying and compaction	B74	1,700	S.Y.	8.85	
29	1.000	02 340 500 2160	Soil stabilization, hydrated lime, for base, 4% mix by weight, 12" deep, includes scarifying and compaction	B74	1,550	S.Y.	11.30	
30	1.000	02 340 500 2200	Soil stabilization, hydrated lime, for base, 6% mix, 6" deep, by weight, for base, includes scarifying and compactio	B74	1,800	S.Y.	9.10	
31	1.000	02 340 500 2220	Soil stabilization, hydrated lime, for base, 6% mix by weight, 8" deep, includes scarifying and compaction	B74	1,700	S.Y.	10.85	
32	1.000	02 340 500 2260	Soil stabilization, hydrated lime, for base, 6% mix by weight, 12" deep, includes scarifying and compaction	B74	1,550	S.Y.	14.30	
33	1.000	02 340 700 0020	Calcium Chloride, truckload lots, 100 LB bags, delivered			Ton	590.00	
34	1.000	02 340 700 0030	Calcium Chloride, solution, tank truck delivery, 4 lb. flake per gallon			Gal.	1.25	
36			**Totals**				**$884.71**	

Input | AC | Base | Subbase | **Stabilization** | Excavation | Backfill | Compaction | Geo | Slope | Culvert | TreeRevor

Figure 6.5—Sample Excel File Used for Cost Analysis

column gives crew number, detailed information of the crew can be found as discussed earlier. Daily output is used to estimate activity time, and based on our assumptions, is omitted from our calculation. Unit column identifies the unit and conversion is carried out by the ExSPRS program if necessary. Column L (Total Incl. O&P) is the unit cost value used to assemble final costs.

As shown in this example, main activities considered in cost analysis include ACP, base, subbase layer construction, stabilization, excavation, backfill, compaction, geosynthetics, slope, culvert, tree removal and barriers.

The ExSPRS program has a handler to retrieve information from the excel file and use it in cost estimation calculation. It is recommended to keep using the original exporting format to avoid any confusion and to mobilize easy update when new data become available.

6.3.2. Assembling Costs

Cost estimation is carried out for original design and every suitable remediation strategies separately. Cost for each activity is calculated by multiplying the unit cost by the quantity with correct corresponding unit. Total cost is obtained by summing the cost of individual activities. The excel handler is responsible for comparing and picking up correct unit cost record from the exported excel file for each activity. These unit costs are reported to the user for convenience. By default the reported unit cost value is cost in dollars per lane per mile. Final cost estimation is adjusted for actual length and width the user has provided. The agency's administration and construction overhead are already included in the estimation. The ExSPRS program assembles relevant activities together and put final estimation in thousand dollars in tabulated form.

For original cross-section design, calculations require descriptions of each layer and their thickness. The surface area (in S.Y.) of each layer is used to multiply unit cost for according lift thickness. Thus the total cost equals the summation of ACP, base, subbase (if any) and subgrade (either compaction or stabilization).

Different remediation strategies may require other quantities such as number of big trees per mile to estimate the additional costs accrued. Final cost to implement certain remediation strategy is the cost summation of every activity selected under that method by the user. For example, moisture control has three categories: moisture barriers, drainage improvement and vegetation treatment. Final additional cost the user can expect to spend depends on which one(s) of those three categories he wants to implement. In this case, the more categories selected the better moisture control improvement can be expected, as well as higher expenses.

6.4. BENEFIT ANALYSIS

To conduct a reasonably complete cost-benefit analysis the relevant costs and benefits were assumed to be measurable, quantifiable and comparable in dollar terms. However, for a given strategy, assigning monetary values to benefit is rarely simple. Each remediation strategy will change certain soil properties and/or pavement characteristic parameters. Further field observations and full scale tests are required to quantify the benefits for the recommended strategies. The "before-after" analysis is proposed as an alternative to roughly justify the benefits in terms of structural and performance improvement. Thus the benefits are quantified in terms of how much improvement each remediation strategy will provide by comparing the before-and-after ***Evaluation*** module results. An important assumption made is that the benefits of different remediation strategies carried out on the original design are independent of each

other. The same assumption holds true for cost analysis. This assumption makes sure the cost & benefit analysis results are comparable in terms of effectiveness.

The changing trend of the parameters under each treatment is tabulated in Table 6.1 with "⇧" meaning increase, "⇩" meaning decrease, "⇳" meaning either increase or decrease is possible, and "—" meaning no change. This information is based on educated hypothesis and is provided only as a general guide for the user to reasonably estimate the appropriate input values. The ExSPRS asks the user to provide new input information accordingly and re-evaluate selected modification alternative(s).

6.5. COST-BENEFIT ANALYSIS RESULTS

Results of ***Cost-Benefit Analysis*** are reported to the user in tabulated format. Original design and each recommended remediation strategy are compared side by side for their cost and benefit (evaluation results) estimations. No ranking is provided due to the fact that prevailing distress problems are different for each district, and thus the concentration of the design goal changes, which in turn will yield different user preferences. A good design relies on not one single factor but many factors combined. ***Cost-Benefit Analysis*** results open the door for more in-depth understanding regarding how to reach a reasonable and satisfactory design for low-volume road built over problematic subgrade soils. The user is encouraged to explore different possibilities and compare multiple preference criteria in order to reach a better and more informed decision.

Table 6.1—Summary of Parameter Changing Trend for Remediation Strategies

Parameters	Remediation Strategies					
	Stabilization	**Geosynthetics**	**Moisture Control**	**Undercut & Backfill**	**Deep Dynamic Compaction**	**Decrease Clay Content**
Subgrade Modulus at Optimum (ksi)	⇧	⇧	—	⇳	⇳	⇳
Subgrade Modulus during Wet Season (ksi)	⇧	⇧	⇧	⇳	⇳	⇳
PI (%)	⇩	—	—	⇳	—	⇳
LL (%)	⇳	—	—	⇳	⇳	⇳
OMC (%)	⇳	—	—	⇳	⇳	⇳
IDT (psi)	⇧	⇧	—	⇳	⇳	⇳
Soil Classification from Texas Triaxial Test	⇧	⇧	—	⇳	⇳	⇳

CHAPTER SEVEN - CASE STUDIES

In this chapter, case studies are conducted to demonstrate the capabilities of ExSPRS and to evaluate its feasibility as a tool to help pavement engineers reach better and more rational pavement design. In this study, five representative sites (Fort Worth, Houston, San Antonio, Paris and Atlanta) are selected as baseline studies to verify the outcomes of ExSPRS. Laboratory tests are described with great details in Sabnis *et al.* (2008). Field data collections, which include instrumentation systems, site information and field measurements, are described. Required inputs for all cases are compiled in tabulate format. ExSPRS is followed step by step with Fort Worth case to illustrate the evaluation assessment. Possible failures/problems are predicted and feasible remediation strategies are recommended. Cost-benefit analysis is discussed to help the user reach effective solutions. Finally, other cases study results are summarized.

7.1. DATA COLLECTION

7.1.1. Baseline Study Sites Information

The test site in Fort Worth is located at Farm to Market (FM) 157, about 380 ft from the east side of US Post Office at Venus, Texas (Figure 7.1 left). Severe longitudinal and transverse cracking with local pavement settlement were already observed at the first visit of the site (Figure 7.1 right). The side slope is covered with grass on both sides of the road. The area next to the pavement shoulder is an irrigation farmland. No drainage ditch is available on both sides of the pavement.

Figure 7.1—Fort Worth FM 157 Site

The test site in San Antonio is located at FM 1052, about 2.8 miles from the city of Uvalde, Texas (Figure 7.2 left). No pavement crack was observed at the first visit (Figure 7.2 right). Pavement shoulder is almost leveled and covered slightly with grass on both sides. No drainage ditch is available next to the pavement shoulders. The area next to the pavement shoulder is supposedly farmland. However, no vegetation was observed during any site visits.

Figure 7.2—San Antonio FM 1052 Site

The test site in Paris is located at FM 910, about 2.5 miles from city of Clarksville, Texas (Figure 7.3 left). Large cracks and dipping on the pavement were observed at the first visit (Figure 7.3 right). Soil slope next to the pavement shoulder also exhibited severe cracking and

numerous potholes that were about 1 to 2-ft in diameter and 1 to 3-foot depth along the section. Several large trees exist along the road.

Figure 7.3—Paris FM 910 Site

Houston test site is located at FM 1236, about 0.5 mile from the intersection between FM 1236 and FM 422, Needville, Texas (Figure 7.4 left). Severe longitudinal cracking was observed during the first visit (Figure 7.4 right). The side slope is covered heavily with grass on both sides. On one side of the road, there is also a poorly-maintained drainage ditch that may increase the seasonal fluctuation in the moisture content and yield the problem of soils heaving and shrinking that eventually result in cracking on the pavement.

Figure 7.4—Houston FM 1236 Site

Atlanta test site is located at FM 1840, about 0.5 mile from the intersection between FM 1840 and TX 98, New Boston, Texas (Figure 7.5 left). Several transverse and longitudinal cracks were noted during the first visit (Figure 7.5 right). There are drainage ditches on both sides of the road. The site feature is similar to Houston site except the side slopes is shorter and the size of drainage ditches are smaller.

Figure 7.5—Atlanta FM 1840 Site

7.1.2. Field Instrumentation Systems

Soil samples were retrieved from each site. Laboratory tests performed include Atterberg limits, Texas triaxial tests (Tex-117-E), resilient modulus tests, permanent deformation tests, unconfined compression strength tests (UCS) and indirect tensile strength tests (IDT) tests. In addition, 3D free swell tests, volumetric shrinkage strain tests, swell pressure tests, shrinkage pressure tests and filter paper suction measurements were carried out. Sites were embedded with two types of instrumentation systems: (1) Moisture sensors together with data logger; and (2) Field matric suction sensors. Both types of system were carefully placed close to each other to ensure that the data from both systems represent the same soil conditions. The Gropoint® Moisture sensors and data logger (Figure 7.6) played an important role in understanding the variation and propagation of soil moisture in this research. They work on the principle of Time

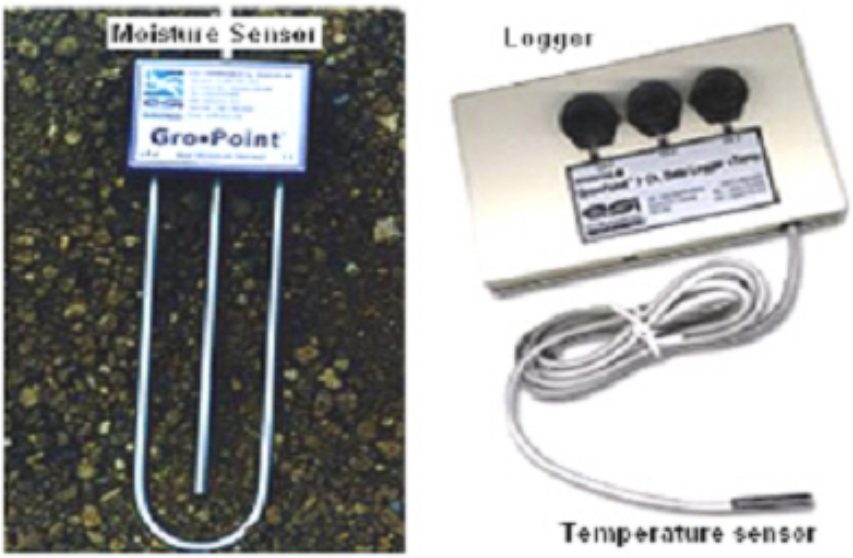

Figure 7.6—Temperature & Moisture Probes (left) and data logger (right) (from http://www.esica.com/products_gropoint.php)

Domain Transmissometry (TDT) technology to provide volumetric moisture contents. The selection of the suction sensors is based on their accurate measurements of suction potentials more than 100 kPa. The Fredlund thermal conductivity (FTC) sensor was used in this research. Although FTC sensors have certain limitations like high failure rate in the field and the fragile ceramic used in the sensor, they are reported to be able to measure field suctions that are greater than 1,500 kPa reliably. The FTC sensor consists of a cylindrical porous block containing a temperature sensing element and a miniature heater (Figure 7.7). The heater at the center of the porous block converts electrical energy to thermal energy. The temperature sensor measures the temperature rise as a function of the elapsed heating time. Since water has a much higher thermal conductivity than air, the rate of dissipation of the thermal energy within the porous block will increase with the increase in water content. Thus, higher water content will result in a lower temperature rise at the center of the porous block, and, consequently, a lower voltage output of the temperature sensor. Since the water content is corresponding to the matric suction in the surrounding soil, the voltage output of the temperature sensor (i.e., the output of the suction

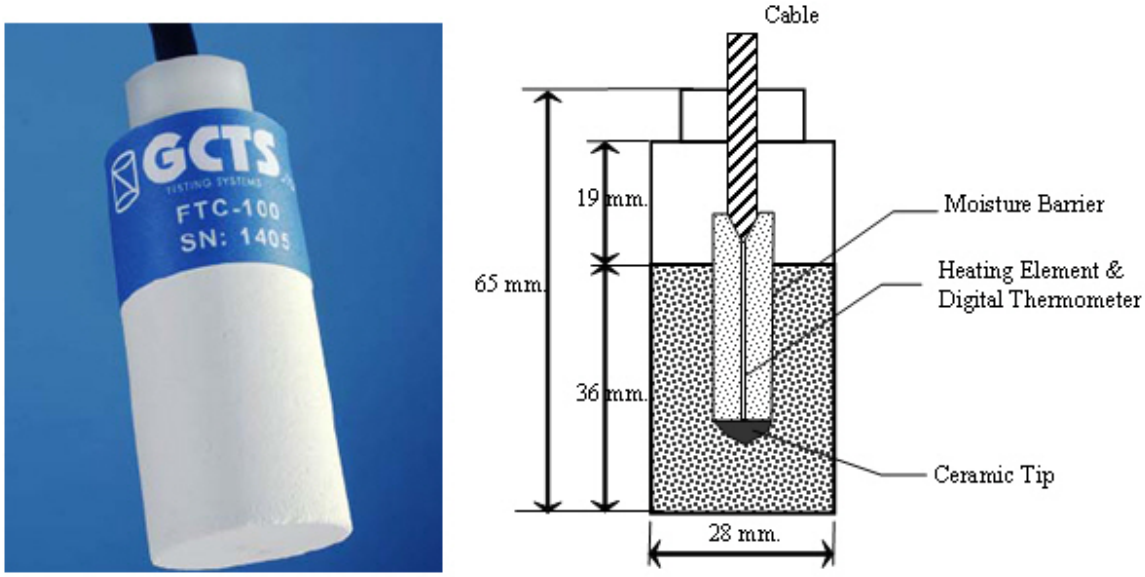

Figure 7.7—FTC sensor (left) and Schematic (right)

sensor) is calibrated to determine the matric suction (Feng *et al.*, 2002).

7.1.3. Field Measurements

After calibration and installation of these sensors, data collection was carried out every one to two months (during each site visit). A visual pavement distress survey was also carried out at each site visit. Topographic surveys were periodically conducted during moisture and matric suction data collection in the field, and then these results were used to evaluate vertical movements (swell/shrinkage volume changes) along the test sections. As shown in Figure 7.8, at each site, data for elevation survey were recorded at seven points 20 ft apart from one another. In addition, FWD and DCP were used to estimate the pavement structural parameters of the site.

Field results for each site are graphically presented in the form of soil moisture contents, monthly average soil moisture contents, rainfall amounts, and pavement elevation changes against time. This data is correlated with the new and reappearance of old pavement cracks at the site. Typical results for Fort Worth are summarized in Figure 7.9. Field measurements for other

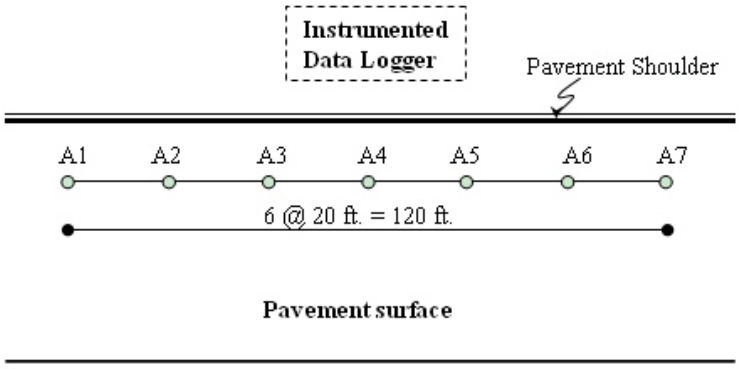

Figure 7.8—Schematic of Elevation Survey Section (by UTA)

sites can be found in Appendix E.

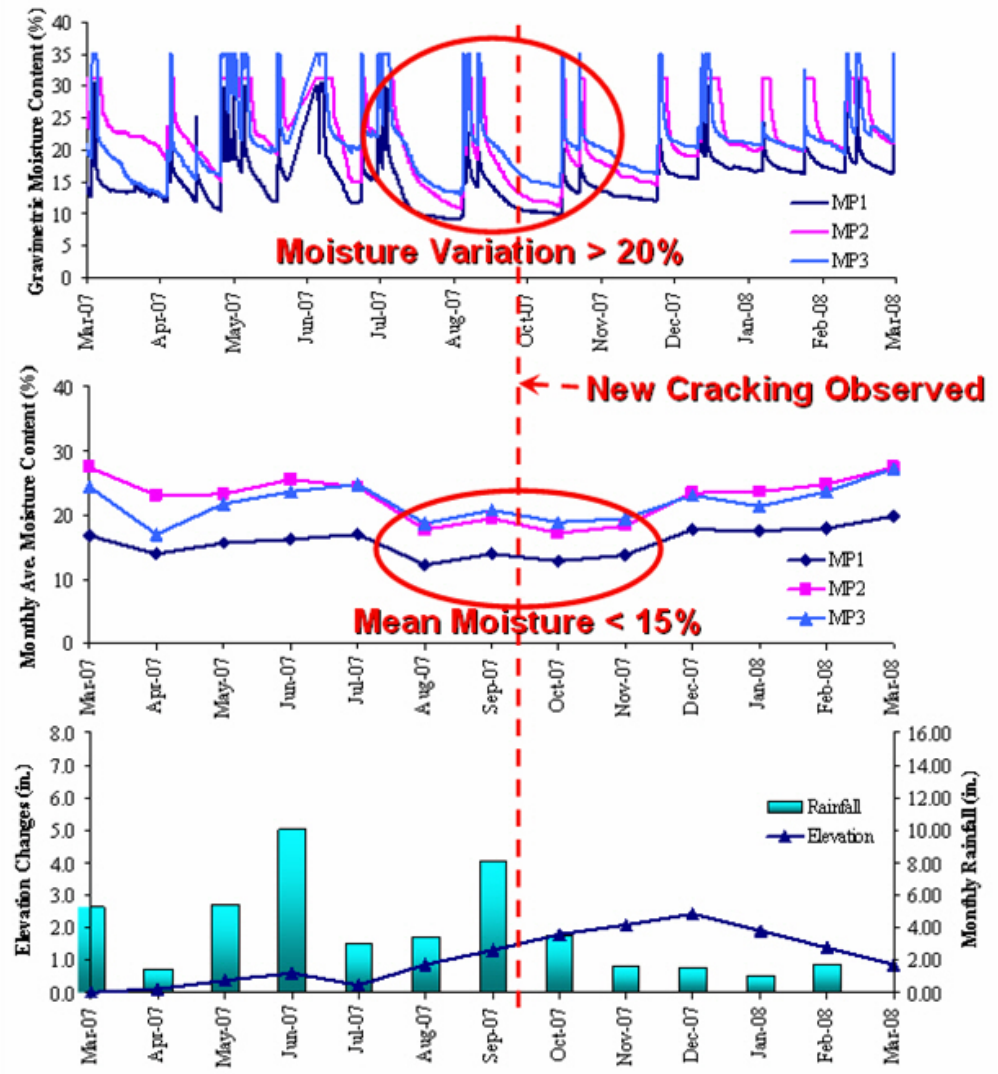

Figure 7.9—Summary of Field Data Measurements for Fort Worth Site (by UTA)

7.1.4. Summaries of Case Study Input Data

Laboratory tests data and field measurements for all five sites are summarized and compiled into Tables 7.1 through 7.5 as input for ExSPRS. Figure 7.10 shows the snap shot of the input window filled-out using Fort Worth data.

Table 7.1—Fort Worth Case Study Input Data (FM 157)

Layer Properties	Number of layers			3
	Description of layers	HMAC	Flexible Base	Compacted Subgrade
	Thickness (in.)	2	8	200
	Modulus (ksi)	350	55	12
	Poisson's ratio	0.33	0.35	0.40
Design Properties	Design ESALs (millions)			1
	Analysis period (years)			10
	Initial serviceability index			4.0
	Reliability (in decimal)			0.8
	Design wheel load (kips)			18
	Tire Pressure (psi)			100
	Road length (mile)			1
	Total number of lanes			2
	Lane width (ft)			12
	Depth of treated subgrade (in)			12
	Percent of time pavement is exposed to saturation moisture level (%)			1 to 5
	Pavement drainage quality			Good
Soil Properties	Subgrade Modulus during wet season (ksi)			7
	PI (%)			29
	LL (%)			61
	P200 (%)			85
	OMC (%)			24
	Dry MC (%)			15.1
	MDD (pcf)			91.5
	Angle of internal friction (◦)			35
	Cohesion of soil (psi)			3.6
	Classification of soil			4
	IDT at dry (psi)			15
	Design safety factor			1
	PVR limit (in)			2
	Sulfate content (ppm)			358

Table 7.2— San Antonio Case Study Input Data (FM 1052)

Layer Properties	Number of layers			3
	Description of layers	HMAC	Flexible Base	Compacted Subgrade
	Thickness (in.)	1	8	200
	Modulus (ksi)	350	67	12
	Poisson's ratio	0.33	0.35	0.40
Design Properties	Design ESALs (millions)			1
	Analysis period (years)			10
	Initial serviceability index			4.0
	Reliability (in decimal)			0.8
	Design wheel load (kips)			18
	Tire Pressure (psi)			100
	Road length (mile)			1
	Total number of lanes			2
	Lane width (ft)			12
	Depth of treated subgrade (in)			12
	Percent of time pavement is exposed to saturation moisture level (%)			1 to 5
	Pavement drainage quality			Good
Soil Properties	Subgrade Modulus during wet season (ksi)			8
	PI (%)			26
	LL (%)			58
	P200 (%)			83
	OMC (%)			21.7
	Dry MC (%)			10.5
	MDD (pcf)			91.5
	Angle of internal friction (◦)			35
	Cohesion of soil (psi)			3.6
	Classification of soil			4
	IDT at dry (psi)			22.9
	Design safety factor			1
	PVR limit (in)			2
	Sulfate content (ppm)			82

Table 7.3—Paris Case Study Input Data (FM 910)

Layer Properties	Number of layers			3
	Description of layers	HMAC	Flexible Base	Compacted Subgrade
	Thickness (in.)	3	14	200
	Modulus (ksi)	500	178	12
	Poisson's ratio	0.33	0.35	0.40
Design Properties	Design ESALs (millions)			1
	Analysis period (years)			10
	Initial serviceability index			4.0
	Reliability (in decimal)			0.8
	Design wheel load (kips)			18
	Tire Pressure (psi)			100
	Road length (mile)			1
	Total number of lanes			2
	Lane width (ft)			12
	Depth of treated subgrade (in)			12
	Percent of time pavement is exposed to saturation moisture level (%)			1 to 5
	Pavement drainage quality			Good
Soil Properties	Subgrade Modulus during wet season (ksi)			8
	PI (%)			36
	LL (%)			60
	P200 (%)			81
	OMC (%)			23
	Dry MC (%)			13
	MDD (pcf)			92.1
	Angle of internal friction (◦)			35
	Cohesion of soil (psi)			3.6
	Classification of soil			4
	IDT at dry (psi)			17.5
	Design safety factor			1
	PVR limit (in)			2
	Sulfate content (ppm)			136

Table 7.4—Houston Case Study Input Data (FM 1236)

Layer Properties	Number of layers			3
	Description of layers	HMAC	Flexible Base	Compacted Subgrade
	Thickness (in.)	4	8	200
	Modulus (ksi)	500	40	17
	Poisson's ratio	0.33	0.35	0.40
Design Properties	Design ESALs (millions)			1
	Analysis period (years)			10
	Initial serviceability index			4.0
	Reliability (in decimal)			0.8
	Design wheel load (kips)			18
	Tire Pressure (psi)			100
	Road length (mile)			1
	Total number of lanes			2
	Lane width (ft)			12
	Depth of treated subgrade (in)			12
	Percent of time pavement is exposed to saturation moisture level (%)			1 to 5
	Pavement drainage quality			Good
Soil Properties	Subgrade Modulus during wet season (ksi)			6
	PI (%)			35
	LL (%)			54
	P200 (%)			87
	OMC (%)			20.1
	Dry MC (%)			13
	MDD (pcf)			99.1
	Angle of internal friction (◦)			35
	Cohesion of soil (psi)			3.6
	Classification of soil			4
	IDT at dry (psi)			25.7
	Design safety factor			1
	PVR limit (in)			2
	Sulfate content (ppm)			247

Table 7.5— Atlanta Case Study Input Data (FM 1840)

Layer Properties	Number of layers			3
	Description of layers	HMAC	Flexible Base	Compacted Subgrade
	Thickness (in.)	6	10	200
	Modulus (ksi)	350	255	12
	Poisson's ratio	0.33	0.35	0.40
Design Properties	Design ESALs (millions)			1
	Analysis period (years)			10
	Initial serviceability index			4.0
	Reliability (in decimal)			0.8
	Design wheel load (kips)			18
	Tire Pressure (psi)			100
	Road length (mile)			1
	Total number of lanes			2
	Lane width (ft)			12
	Depth of treated subgrade (in)			12
	Percent of time pavement is exposed to saturation moisture level (%)			1 to 5
	Pavement drainage quality			Good
Soil Properties	Subgrade Modulus during wet season (ksi)			6
	PI (%)			50
	LL (%)			73
	P200 (%)			89
	OMC (%)			28.5
	Dry MC (%)			11.5
	MDD (pcf)			88.5
	Angle of internal friction (◦)			35
	Cohesion of soil (psi)			3.6
	Classification of soil			4
	IDT at dry (psi)			Not available
	Design safety factor			1
	PVR limit (in)			2
	Sulfate content (ppm)			Not available

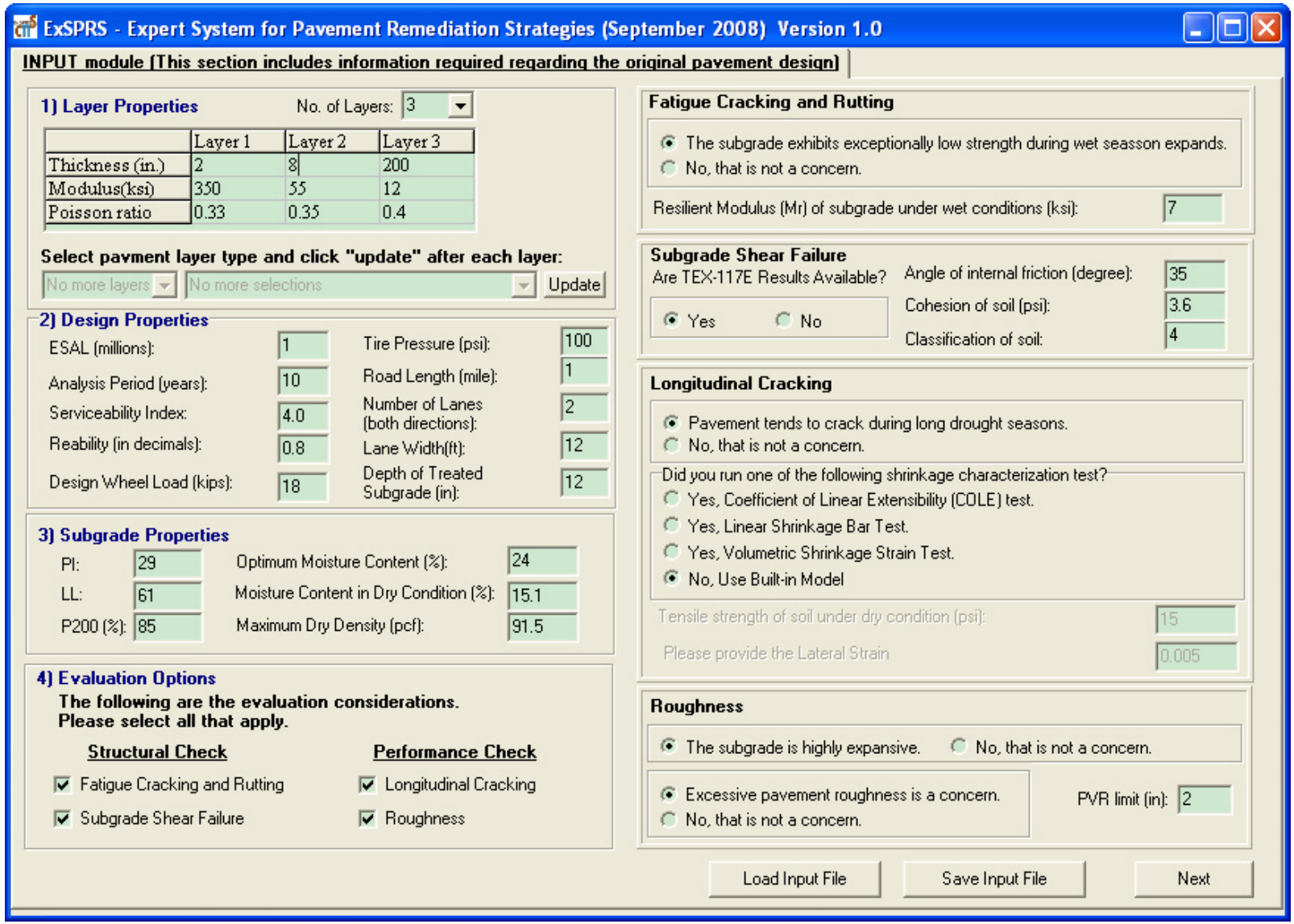

Figure 7.10—Fort Worth Case Study Input Screen

7.2. RESULTS OF EVALUATION MODULE

Only Fort Worth case study results are presented here with details. Results for other four cases are concluded in Section 7.5. As shown in Figure 7.10, all four evaluation checks are selected to fully illustrate the results for fatigue cracking & rutting, subgrade shear failure, longitudinal shrinkage cracking and roughness. The evaluation results from ExSPRS are shown in Figure 7.11. As our estimated accumulated design ESALs was 1 million, the original design passed the fatigue cracking and substantially failed the rutting criteria. Even though the cover depth (total thickness above subgrade) at the site was 10 in., the Texas triaxial check proposed minimal required depth of 15 in. The original design also failed the MTRX check, since that LoadGage software proposed a minimum required base thickness of 12 in. The total potential vertical rise (PVR) check also failed as the estimated value was 2.6 in. The IRI check gave 1.58 m/km, which passed the criteria for farm to market road (Figure 4.5 in Chapter 4).

Longitudinal shrinkage cracking check suggests that the subgrade will start to develop longitudinal shrinkage cracks when moisture content drops below 21.6%. The cracks will day light on pavement surface when the moisture content drops below 16.8%. The ExSPRS program also presents a plot of the top 50 largest tensile stress points within subgrade simulated by the FEA model, as shown in Figure 7.12. The most likely location of the crack is near 1/3 lane width. (2 to 7 ft) from the edge, where most of the top 50 largest tensile stress points are located. Although the program cannot predict exactly how long it might take for the subgrade desiccation cracks to propagate to the surface, it is safe to assume that after just one typical drying cycle (typically a few weeks according to local rainfall history data) this bottom-up shrinkage cracking will start causing problems.

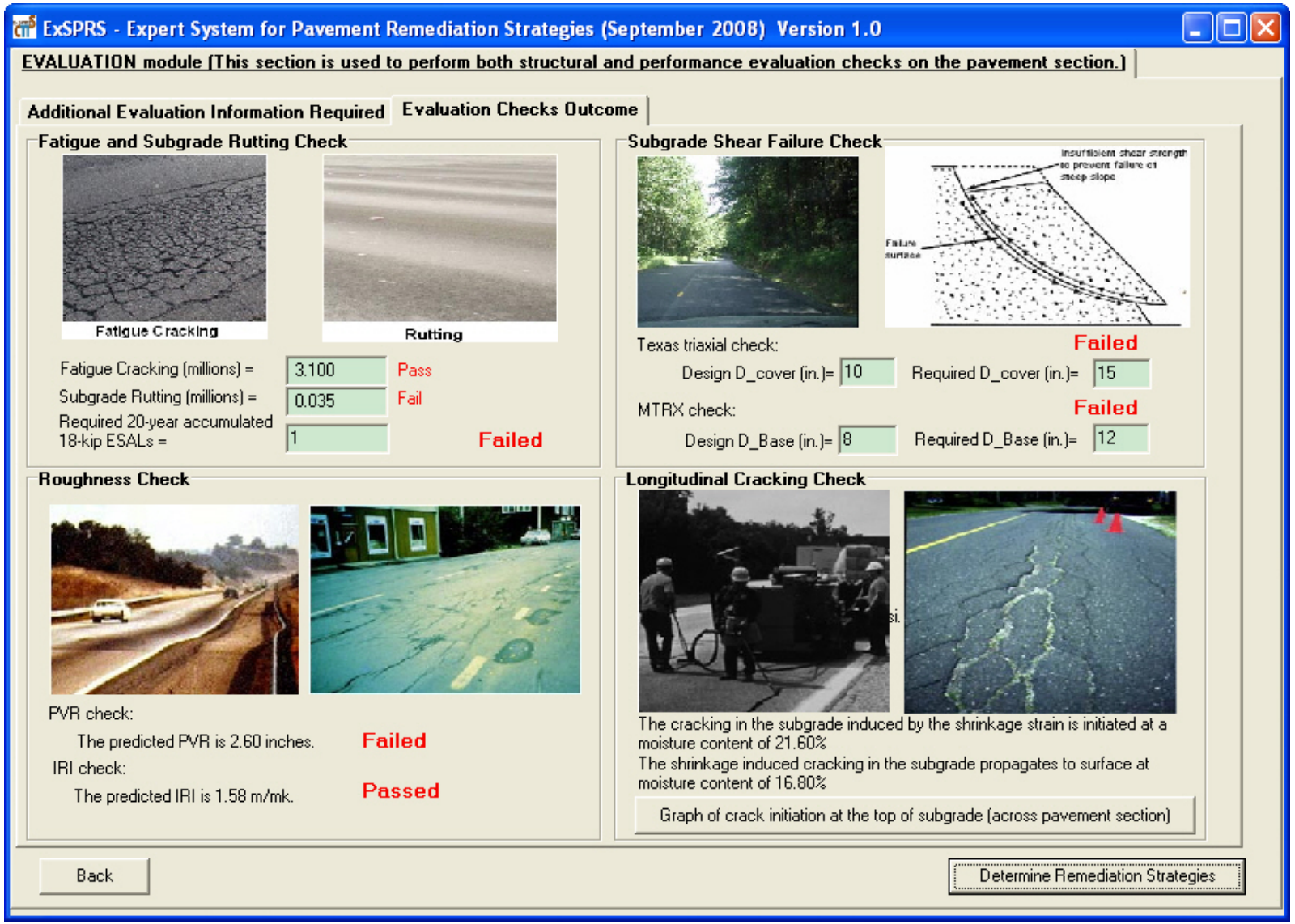

Figure 7.11—Fort Worth Case Study Evaluation Outcome Screen

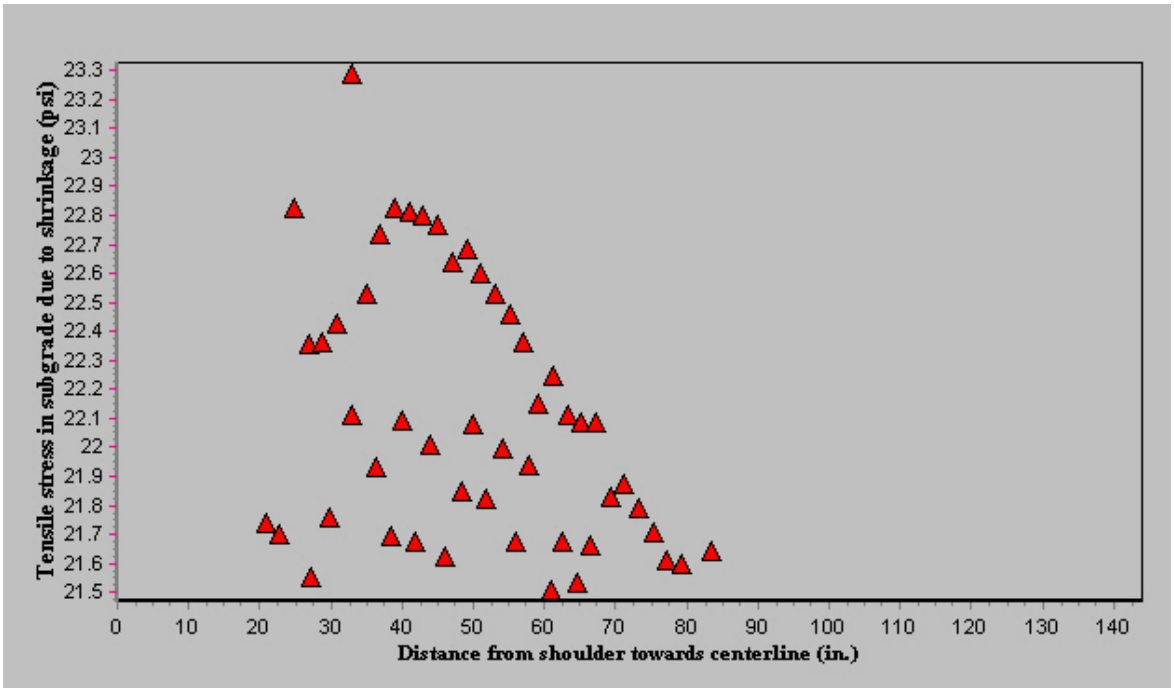

Figure 7.12—Fort Worth Case Study Plot of Top 50 Largest Tensile Stress Points in Subgrade

Field measurements of Fort Worth (Figure 7.9) indicate that the highest moisture content was around 35% and the lowest around 11%. The largest moisture fluctuation occurred during mid-July to mid-October in 2007 when the mean moisture changed by more than 20%. New longitudinal cracks were observed following the dry season in late September. The dry cycle has a mean moisture content of 15%. It can be concluded from the field measurements when subgrade moisture dropped below 15%, shrinkage cracks became visible on surface. Figure 7.13 shows pictures of the current Fort Worth site conditions. The longitudinal cracking was developed near outer-wheel lane towards pavement edge. The distressed area is about 3 feet wide. These field observations correspond very well with our model estimation.

7.3. RECOMMENDED REMEDIATION STRATEGIES

In this case, the original design is subject to both inadequate support and moisture variation problems. All six remediation strategies were selected for illustration purposes.

Figure 7.13—Fort Worth Site Current Conditions

Laboratory tests indicated a sulfate content of 358 ppm, and negligible organic content. The program recommends regular mix design and construction practices to be used with a minimum of 24 hours mellowing time. Calcium based stabilizers of lime, cement, fly-ash or mixtures can be used.

Geosynthetics can be placed near subgrade-base interface to improve pavement performance. Based on the geosynthetic design method of FHWA, original design met the requirement of aggregate thickness over geosynthetics, no modification to layer thickness is needed and the geosynthetics can be directly laid at the recommended location near base-subgrade interface.

Moisture control recommends three different types of remediation methods: using vertical moisture barriers, improving pavement drainage and applying vegetation treatment such as big tree removal or using root barriers. This part illustrates information rather than performs design/calculations. The user is strongly encouraged to read through detailed recommendations.

The program calculated the required undercut and backfill thickness to be 18 in. The key benefit and references of deep dynamic compaction and decreasing clay content are provided to the user.

7.4. COST-BENEFIT ANALYSIS RESULTS

Table 7.6 summarizes the cost analysis assumptions for this study. Table 7.7 represents the cost analysis results (regenerated in tabulated format for demonstration purpose). The original design costs about $330k/mile. Subgrade stabilization using 4% lime costs $159k/mile more, moisture control by using drainage improvement, moisture barriers and vegetation removal costs $49k/mile more, use of geosynthetics requires $33k/mile in addition. Undercut and backfill, deep dynamic compaction and decreasing clay content require addition of $11k/mile, $5k/mile and $4k/mile respectively. To justify the benefit of each remediation method, before-after analysis should be carried out.

Table 7.6—Fort Worth Case Study Cost Analysis Assumptions

Stabilization		Stabilizer	Lime
		Stabilization percent mix	4%
Geosynthetics		Geosynthetics tensile strength (psi)	600
Moisture Control	**Drainage Improvement**	Culvert diameter (in)	6
		Culvert spacing (ft)	500
		Sloped section	Gentle
	Barriers	Barrier film thickness (in)	0.8
	Vegetation Removal	Big tree diameters (≥ 12”)	12”
		Number of big trees to be removed (per mile)	5
		Number of trees less then 12" per acre	Up to 400
		Percentage of hardwoods	0-25%
		Roadside Width for smaller trees (ft./side)	6
Undercut & Backfill		Undercut and backfill depth (in)	15
Deep Dynamic Compaction		Compaction Depth (in)	12
		Percentage of standard proctor density	85%

Table 7.7—Fort Worth Case Study Cost Analysis Results (Regenerated)

Design Alternatives		Thousand Dollars
Original Design		$ 330
Stabilization	+	$ 159
Geosynthetics	+	$ 33
Moisture Control	+	$ 49
Undercut & Backfill	+	$ 11
Deep Dynamic Compaction	+	$ 5
Decreasing Clay Content	+	$ 4

Due to the limitation of our research scope, no real laboratory data were available on the changed parameters for the selected remediation strategies. Hypothetical numbers were used to demonstrate the benefit analysis results. Table 7.8 summarizes before and after analysis parameters and results. Red bold numbers are changed parameters, assumed based on literature reviews and recent research data. Table 7.8 has been color-coded for the bottom half ("*Results Comparison of Before-After Analysis"*) based on which of the updated parameters that specific result uses. Because some updated parameters are used for more than one evaluation check, the top part of the table ("*Parameters Affected in Evaluation Module"*) shows the colors in column 8, except for IRI check, the direct affected input is estimated PVR value.

Among the recommended remediation strategies, stabilization and moisture control methods are the most expensive ones (Table 7.7). However, the soundness of a pavement engineer's final selection is also dependent on benefit analysis. It is critical to select the most efficient and cost-effective remediation method base on laboratory testing and field measurements.

Different remediation strategies may improve different aspects of pavement performance. For example, stabilization (comparing Table 7.8 col.2 to col.1) increases allowable fatigue and rutting repetitions, decreases subgrade shear failure possibility, and also decreases pavement

Table 7.8—Fort Worth Case Study Benefit Analysis Parameters and Results Summary (Regenerated)

Parameters	Original	Remediation Strategies						Color Code	
		Stabilization	Geosynthetics	Moisture Control	Undercut & Backfill	Deep Dynamic Compaction	Decrease Clay Content		
	(1)	(2)	(3)	(4)	(5)	(6)	(7)	(8)	
Parameters Affected in Evaluation Module									
M_r at optimum (ksi)	12	**30**	**50**	12	**25**	**18**	**22**		
M_r at wet (ksi)	7	**15**	**50**	**14**	**15**	**9**	**10**		
PI	29	**20**	29	29	**15**	29	**20**		
LL	61	**45**	61	61	**40**	61	**50**		
OMC (%)	24	**26**	24	24	**21**	**26**	**22**		
MDD (pcf)	91.5	**100**	91.5	91.5	**110**	**100**	**100**		
IDT (psi)	2.9	**18**	**100**	2.9	**20**	**5**	**12**		
Soil Classification	4	**3.8**	**3**	4	**3.5**	**3.9**	**3.8**		
Results Comparison of Before-After Analysis									
N_f (million ESALs)	3.1	2.86	2.64	2.88	2.86	3.01	2.97		
N_d (million ESALs)	0.04	0.22	8.47	0.18	0.22	0.06	0.08		
D_{cover} (in.)	15	12	4	15	9	14	12		
D_{base} (in.)	12	13	Pass	12	Pass	12	12		
PVR (in.)	2.6	0.94	2.6	2.6	0.48	2.6	0.94		
IRI (m/km)	1.58	1.38	1.58	1.58	1.35	1.58	1.38		
MC_I (%)	21.6	23.4	21.6	21.6	18.9	23.4	19.8		
MC_P (%)	16.8	18.2	16.8	16.8	14.7	18.2	15.4		

roughness. However, the stabilized subgrade may initiate shrinkage induced cracking at MC of 23.4% while the original design is safe and sound until the MC level drops below 21.6%. On the other hand, stabilized subgrade is less susceptible to environmental moisture change and migration; the higher MC_I number doesn't necessarily mean the stabilized subgrade will experience longitudinal cracking distress earlier under the same circumstances.

Although the before-after analysis presented here is hypothetical, it provides us a different approach to quantify benefit instead of estimating pecuniary values for the modifications. This improvement wise comparison can assist us in identifying possible design inefficiencies and selecting better and more reasonable remediation strategies.

7.5. SUMMARY OF CASE STUDIES

Detailed information about all sites is included in Appendix E. Table 7.9 summarizes field measurements for the five sites. Case studies are performed using inputs summarized in Table 7.1 to 7.5 obtained from field testing and pavement evaluation. ExSPRS evaluated these designs, recommended appropriate remediation strategy candidates and estimated the cost. Due to lack of real data for benefit analysis, only Fort Worth case is demonstrated with hypothetical before-after analysis as discussed earlier in Section 7.4.

Table 7.10 summarizes the results obtained from ExSPRS. Evaluation results show different possible distress problems for each site. For San Antonio, the pavement section has a very thin ACP layer (1 in.). This case failed rutting check and subgrade shear failure check but marginally passed PVR check. The main problem for this case identified by ExSPRS is "inadequate support". So the program recommended strategies focusing on improving structure support, which include stabilization, geosynthetics reinforcement and undercut & backfill. In

Table 7.9—Summary of Field Measurements

Site Name	Site Features	New Cracks	Rainfall	Monthly Mean $MC \leq 15\%$	Moisture Variation $\Delta MC \geq 20\%$	Time New Cracks Observed
Fort Worth	Farm lands, sloped terrain.	Yes	Sporadic rainfall	Aug-Nov, 07	Aug-Oct, 07	Sep 07
San Antonio	Farm lands, flat terrain.	Yes	Long dry spells	Sep 07-Mar 08	Sep, Nov-Dec, 07; Feb 08	Nov 07
Paris	Large trees, sloped terrain	Yes	Steady rainfall	Aug-Oct, 07; Jan 08	--	Sep 07
Houston	Poor drainage ditch, sloped terrain	No	Steady rainfall	--	--	--
Atlanta	Poor drainage ditch, sloped terrain	No	Steady rainfall	--	--	--

Table 7.10—Summary of Five Baseline Sites Case Study Results

		Fort Worth	San Antonio	Paris	Houston	Atlanta
Evaluation Results	N_f (million ESALs)	3.1	115.56	123.42	1.246	633.6
	N_d (million ESALs)	0.035	0.03	12.17	0.085	9.95
	D_{cover} (in.)	15	15	15	15	15
	D_{base} (in.)	12	11	Pass	Pass	Pass
	PVR (in.)	2.6	2	4	3.8	7.7
	IRI (m/km)	1.58	2.64	1.36	1.27	2.21
	MC_I (%)	21.6	19.5	20.7	18.1	25.7
	MC_P (%)	16.8	15.1	16.1	14.1	20.0
Construction Cost Estimation		$ 330k	$ 237k	$ 562k	$ 450k	$ 592k
Recommended Remediation Strategies	Stabilization	Yes	Yes	Yes	Yes	Yes
	Geosynthetics	Yes	Yes	Yes	Yes	Yes
	Moisture Control	Yes	No	Yes	Yes	Yes
	Undercut & Backfill	18	18	18	12	18
	Deep Dynamic Compaction	Yes	No	Yes	Yes	Yes
	Decreasing Clay Content	Yes	No	Yes	Yes	Yes

Appendix E, Figures E.1 and E.2 provide a series of pictures showing the surface distresses observed at the San Antonio location in November of 2007 and June 0f 2008. As of June 2008 more distresses were visible. There was minor rutting visible along the wheel path, but increased pavement roughness, especially at the center portion of the pavement. Another major distress

was the longitudinal cracking. Longitudinal cracking was very severe along the shoulders (>1 in. wide) and minor cracks appeared close to the pavement edge. .

Paris and Atlanta have strong base (178 and 255 ksi, respectively. These are backcalculated moduli from FWD,. Also, DCP tested base stiffnesses correlate with the FWD moduli), which in turn provide sufficient support and thus the main remediation focus is to reduce moisture variation susceptibility. Thus moisture control, deep dynamic compaction and decreasing clay content are suggested in addition to stabilization, geosynthetics and undercut & backfill.

The distress survey conducted at the Paris site is documented in Figure E.4 of Appendix E. The photos show severe longitudinal cracking distress. The cracks were over 2 to 3 inches wide and in some areas over 18 inches deep. Cracks were also visible along the shoulders of the pavement and were heavily covered with brush. On one side of the pavement (right lane in the photos) the pavement exhibited more surface roughness than the left side.

The Atlanta site showed two predominant distresses, surface roughness and longitudinal cracking. The cracks were at both sides of the lane as shown in Figure E.8 of Appendix E. The cracking closer to the shoulder were new reappearance of those sealed older cracks. Newly developed cracks are the ones closer to the center of the pavement between the two lanes. There were also rutting visible along the wheel paths.

Houston case marginally passed fatigue cracking check, but substantially failed rutting check. It failed Triaxial check, which, as discussed earlier, is conservative. While using modified Triaxial check (MTRX), Houston passed the criterion. The site in Houston was unique compared to the others. DCP test suggested very weak base and subgrade as the rod almost went

all the way through. This may due to the fact that the pavement was newly resurfaced. However, the surface does not show any rutting (see Figure E.7 in Appendix E). The only visible distress was longitudinal cracking along the shoulder.

Among the five sites, Paris, Houston and Atlanta are identified with high potential for vertical rise (PVR), which corresponds to their high PI values (36, 35 and 50, respectively). Among all cases, Atlanta shows very typical damages due to high PI subgrade, which include high PVR, IRI and earlier appearance of shrinkage induced longitudinal cracking (initiates at 25.7% MC, and will propagate up at 20% MC).

Since longitudinal cracking is identified as the most prevailing distress problem for lower classification roads, results from LSC check will be further discussed here. Overall our program predictions correspond very well with our field measurements. Fort Worth and Paris have already been discussed in details in Section 7.2 and 4.5.5.1, respectively. San Antonio site was newly constructed and no cracks were observed at initial field visit. However, by the end of this project the pavement at this site has developed severe longitudinal cracking, some of which are about 1 inch wide. ExSPRS predicted longitudinal cracking will initiate when subgrade moisture level drops below 19.5%, and cracks would daylight when MC drops below 15%. Field measurements confirmed a long and dry period during September 07 to March 08. This long dry season explained the severe longitudinal cracking damage. By examining Table 7.9, Houston site should experience longitudinal cracking damage when MC drops below 14%, however, our field team did not observe any newly developed cracks. From the MC data log, it shows this site has relatively stable moisture content, with a very short period of drying during April 07. Even during the drying period, average moisture content is above 15%, which is still above ExSPRS predicted threshold. Atlanta site data was not complete due to a late start in field instrumentation

and equipment damage. However based on ExSPRS prediction, this site is highly susceptible to moisture variation, and thus is expected to experience substantial longitudinal cracking damage and differential volumetric change (high PVR) damage. This site needs more attention for premature damages.

Construction cost wise, San Antonio case is the cheapest, and Atlanta is the most expensive. Based on these case study results, it is proved the most critical decision for pavement engineers is to put the limited budget into best use and to select the most cost-effective alternative. For low volume roads build over highly expansive subgrade, thicker and better top layers do not guarantee better performance, as shown in Paris and Atlanta case.

CHAPTER EIGHT - CONCLUSIONS AND RECOMMNEDATIONS

The framework of designing lower classification roads over expansive clay subgrade is described herein. ExSPRS program is developed to assist road engineers in evaluating and improving their design to allow more miles of rehabilitation with the same amount of funding with less distress problems in the future. To fulfill the objective of this research effort, laboratory tests were conducted to characterize the shrink-swell problem and strength-stiffness variation of expansive soil. Numerical analysis and modeling were performed to predict longitudinal cracking distress, which reported by a district survey throughout Texas to be one of the most prevailing distress problems for low-volume farm-to-market roads. Other common distresses are studied and four evaluation models are programmed to check the feasibility of the user proposed pavement section. Traditional and new remediation methods are examined and appropriate ones proposed to address the problem of premature failure of low-volume roads on high-PI clays. Finally cost-benefit analysis is added to the design guide framework to complete the computer program.

Accurate predictions of possible distresses are critical for an efficient design. The conclusion of this research to address laboratory testing, data analysis, numerical modeling and design guide framework development are given below. The limitations and recommendations for future research are also presented.

8.1. CONCLUSIONS

Although the primary aim of this research was to develop a computerized low-volume road design procedure, a number of other areas related to pavement design were also examined. Among these are: (1) laboratory tests to characterize expansive soils; (2) regression data analysis

to develop relationships between soil index properties and shrinkage strains, moduli and tensile strengths; and (3) finite element modeling to predict subgrade shrinking induced longitudinal cracking. The following conclusions are drawn from this study.

- The behavior of high PI clays change dramatically with moisture content variation. All clay specimens were prepared at optimum moisture content and were subjected to different moisture conditioning (drying or wetting). Conditioning procedures were standardized and protocols were developed.
- Volumetric change and strength behaviors of subgrade clays were tested in laboratory to characterize the expansive nature of the soil. Five typical sites with high PI (PI >= 25) clays and one site with low PI clay (PI = 17) were selected to extract soil samples. Tested strength and stiffness of the dry specimens are significantly greater than the corresponding measurements at the optimum moisture content. As specimens become wet, they lose almost all of their strengths. Testing results under dry condition for UCS are 4 to 11 times greater than those under optimum, 5 to 43 times greater for IDT results, 11 to 18 times greater for four-point bending results, 6 to 31 times greater for Free-Free tests, and 4 to 12 times greater for resilience modulus tests. The volumetric changes of expansive clays between dry and optimum conditions are also considerable. The laboratory measured volumetric swell strains and shrinkage strains of high PI clays vary from 15% to 25% and 11% to 18%, respectively.
- Laboratory testing data were gathered at three different conditions, namely drying from optimum (DFO), saturating from optimum (SFO) and drying from saturation (DFS). Extensive correlation analysis was performed between curve-fitted equation parameters and index properties of clays. Multiple mathematical relationships were developed to predict shrinkage strain and modulus of clay materials at particular moisture content by using index

properties of the clay. Both sstatistical method and real data were utilized to validate the success of each relationship. All mathematical relationships showed reasonably good prediction capabilities within PI range from 15 to 40. These empirical models were utilized later in the numerical modeling of longitudinal cracking.

- Longitudinal cracking has become the prevailing mode of failure for flexible pavements build in areas with expansive subsoils. Two FEA models, referred to as the Elastic Model and Fracture Model were developed with same geometry and boundary conditions to simulate longitudinal cracking initiation and propagation. The Elastic Model results show the base-subgrade interface has a higher frequency of being under greatest shrinkage induced tension. Top 50 largest tension elements always fall within the top 5-inch of subgrade layer. Fracture Model results shown although the maximum tensile stresses in subgrade were generally located underneath the middle of the lane towards pavement centerline, fracture would also develop at the shoulder-pavement interface. This may due to the fact that the pavement shoulder is a much weaker material compared to base and AC layer, and shoulders are more susceptible to environmental moisture variations.
- FEA results shown the consideration of layering in the subgrade moisture profile (moisture variation with depth) did not have a large effect on the modeling results. However, simulation results with different moisture variation values in shoulder and subgrade changed both magnitudes and coordinates of the critical elements in tension. Although no firm conclusions could be drawn from the parametric study on the trend of such change, it was shown that longitudinal cracking is more sensitive to moisture variation gradient along transverse direction (cross pavement along x-axis) than with depth (y-axis).

- Expert system concept was employed in the development of a software package called ExSPRS. One of the objectives of this design guide is to minimize the total cost without compromising performance. R.S. Means cost data 2007 were used in developing cost estimations. Before and after comparison analysis was presented to quantify effectiveness in terms of evaluation results improvement. No ranked conclusions were provided in output, but rather comparisons of pros (benefit) and cons (cost) were tabulated for the user. It is recommended the user to carefully compare different design schemes and remediation strategies and select a more reasonable and cost-effective design based on his specific case.
- The user-friendly computer program ExSPRS was specially targeted for low-volume roads design. It puts more considerations in mitigating detrimental subgrade properties, improving subgrade strength and stiffness, and reducing subgrade moisture susceptibility. Typical baseline studies shown for lower classification roads built over high PI subsoils, thicker and stronger pavement layers do not guarantee better performance. Use of geosynthetics reinforcement in subgrade is one of the promising strategies to improve overall serviceability and performance of low-volume roads built over expansive subgrades.

8.2. RECOMMENDATIONS

Given the above conclusions, there are some limitations and recommendations to be made. The reader should differentiate between the limitations of the presented results and those of the proposed methodology. ExSPRS aims mainly to prove the workability of the developed methodology. Nevertheless it contains some limitations that could be overcome with additional testing, modeling, analyzing and programming efforts. The following recommendations are based on the findings of this study.

- For this study it was vital to have access to real laboratory and field data that was of sound quality and organization. Testing protocols were developed to standardize test procedures and conditioning steps. In this research, six sites were selected for laboratory characteristic testing and field measurements. It is recommended that more clay materials with wider range of PI values be tested. The use of these extended lower and upper PI values will definitely strengthen the mathematical prediction relationships developed in this study. It is further recommended that research can be carried out to find correlation between different conditioning models. With a bigger pool of testing data, it may be possible to relate DFS models to SFO and DFO models or even better just to develop a new model that can be used for any moisture conditions.
- The finite element analysis results of longitudinal cracking presented earlier fulfilled the scope of the study. For a given design, however, the fracture analysis was not incorporated due to license restrictions of LS-Dyna program. Rather, the generalized deduction was made based on case studies using the LS-Dyna Fracture model. Incorporating a more sophisticated finite element program with soil fracture modeling capability which can model longitudinal cracking from beginning to end would be very beneficial and more accurate results can be estimated.
- As discussed in Chapter 6, simple before-after study was conducted in lieu of preferred alternatives. With more time and resources a post-processor should be developed for the user to compare different design alternatives and remediation strategies. The post-processor would provide an easier way to study cost-effectiveness trends. It is recommended that further analysis be conducted to identify key property parameters that control low-volume

road performance. Considerations should also be given to prioritizing alternatives and remediation strategies for an overall better and more reasonable design.

REFERENCE

- AASHTO (2002) "AASHTO Design Guide 2002 (NCHRP 1-37), The Mechanistic-Empirical Design Guide" Federal Highway Administration
- AASHTO (1997) "Specification M288-96 on Geotextiles" Standard Specifications for Transportation Materials and Methods of Sampling and Testing 18th Ed. Washington, D.C.: AASHTO
- AASHTO (1993) "AASHTO Guide for Design of Pavement" Federal Highway Administration
- AASHTO (1986) "AASHTO Guide for Design of Pavement" Federal Highway Administration
- Abd El Halim, A.O., Haas, R., and Chang, W. A. (1983) "Geogrid Reinforcement of Asphalt Pavements and Verification of Elastic Layer Theory" *TRB Research Board Record No. 949* pp.55-65
- Ahlvin, R.G. (1962) "Flexible Pavement Design Criteria" *Journal of the Aero-Space Transport Division*, Proceedings of the ASCE
- Ahnberg, H. and Holm, G. (1999) "Stabilization of Some Swedish Organic Soils with Different Types of Binders" *Proceedings of the International Conference on Dry Mix Methods for Deep Soil Stabilization*, Stockholm, Sweden, pp.101-108

- Al-Shamrani, M.A., and Al-Mhaidib, A. (1999) "Prediction of Potential Vertical Swell of Expansive Soils Using a Triaxial Stress Path Cell" *Quarterly Journal of Engineering Geology, Vol. 32,* pp.45-54
- Austin, R.A. and Gilchrist, A.J.T. (1996) "Enhanced Performance of Asphalt Pavements Using Geocomposites" *Geotextiles and Geomembranes 14*. pp.175-186
- Bell, D.O. and Wright, S.G. (1991) "Numerical Modeling of the Response of Cylindrical Specimens of Clay to Drying" *FHWA/TX-92-1195*
- Biddle, P.G. (1983). "Patterns of Soil Drying and Moisture Deficit in The Vicinity of Trees on Clay Soils" *Geotechnique*, 33, 2, pp.107-126.
- Biddle, P.G. (2001). "Tree Root Damage to Buildings" *ASCE Geotechnical Special Publication*, 115, pp.1-23.
- Brown, S.F. and Pappin, J.W. (1981) "Analysis of Pavements with Granular Bases" *Transportation Research Record 810*. pp17-23
- Browning, G. (1999) "Evaluation of Soil Moisture Barrier" *FHWA/MS-DOT-RD-99-21 & 23; Final Report*
- Budge, W.D., Sampson, E. Jr., and Schuster, R.L. (1966) "A Method of Determining Swell Potential of an Expansive Clay" *Highway Research Record*
- Bulut, R., Lytton, R. L. and Wray, W.K. (2001) "Soil Suction Measurements by Filter Paper" Geotechnical Special Publication Number 115, Proceedings of Geo-Institute Shallow Foundation and Soil Properties. Houston, TX.

- Colorado Asphalt Pavement Association (CAPA), (2000) *Guideline for the Design and Use of Asphalt Pavements for Colorado Roadways*, CAPA, Englewood, Colorado.
- Carroll, R.G., Walls, J.C. and Haas, R. (1987) "Granular Base Reinforcement of Flexible Pavements Using Geogrids," *Proceedings of Geosynthetics 87th Conference, Vol. 1*, New Orleans, USA, pp. 46-57.
- Cedergren, H.R. (1974) *Drainage of Highway and Airfield Pavements*, John Wiley and Sons, Inc., New York
- Celaya, M. and Nazarian, S. (2006) "Seismic Testing to Determine Quality of Hot-Mix Asphalt" *Transportation Research Board 85th Annual Meeting*
- Cicoff, G.A. and Sprague, C.J. (1991) "Permanent Road Stabilization: Low-Cost Pavement Structures and Lightweight Geotextiles" *Transportation Research Record 1291*. pp.294-310
- Chen, L. and Tian, K. (1985) "The Effect of Vegetation Transpiration on the Deformation of High Void Ratio Expansive Soil Foundation" *Transportation Research Record 1032*. pp.68-75
- Chikyala, S.R., Saride, S., Harris, P., Puppala, A. and Hilbrich, S. (2006) "Mitigating the Effects of Organics in Stabilized Soils: Literature Review" *Technical Memorandum of TxDOT Research Project 0-5540*
- Chou, L. (Ed.) (1987) "Lime Stabilization: Reactions, Properties, Design and Construction" TRB State of the Art Report 5, *Transportation Research Board*, National Research Council, Washington DC

- Costello, L.R., Elmore, C.L. and Steinmaus, S. (1997) "Tree Root Response to Circling Root Barriers" *Journal of Arboriculture, Vol. 23, No. 6*, pp.211-218
- Croft, J.B. (1967) The Influence of Soil Mineralogical Composition on Cement Stabilization Geotechnique vol. 17, London, England, pp.119–135.
- D'Amato, N.E., Sydnor, T.D., Knee, M., Hunt, R. and Bishop, B. (2002) "Which Comes First, The Root or the Crack?" *Journal of Arboriculture, Vol. 28, No. 6*, pp.227-289
- Daleiden, J.F., Killingsworth, B.M., Simpson, A.L. and Zamora, R.A. (1994) "Analysis of Procedures for Establishing In Situ Subgrade Moduli" *Transportation Research Record 1462*. pp.102-107
- Dedier, G. (1973) "Prediction of Potential and Swelling Pressure of Soils" Proceeding of 8th International Society for Soil Mechanics and Foundation Engineering, Vol. 22
- Department of the Army USA (1983) "Foundations in Expansive Soils, 1 September 1983." *Technical Manual TM 5-818-7*
- Drumm, E.C., Boateng-Poku, Y. and Pierce, T.J. (1990) "Estimation of Subgrade Resilient Modulus from Standard Tests" *Journal of Geotechnical Engineering, Vol. 116, No. 5,* pp.774-789
- Drumm, E.C., Madgett, M.R. (1997) "Subgrade Resilient Modulus Correction for Saturation Effects", *Journal of Geotechnical and Geo-environmental Engineering, Vol. 123, No. 7*, pp.663-670.
- El-Ramli, A.H. (1965) "Swelling Characteristics of Some Egyptian Soils" *Journal of the Egyptian Society of Engineering*, Vol. 4, No. 1

- Emery, S.J. (1988) "The Prediction of Moisture Content in Untreated Pavement Layers and Application to Design in Southern Africa" *Division of Roads and Transport Technology, DRTT Bulletin 20, CSIR Research Report 644*
- Evans, R. P.; McManus, K. J. (1999) "Construction Of Vertical Moisture Barriers To Reduce Expansive Soil Subgrade Movement" *Transportation Research Record 1652, 7th International Conference on Low-Volume Roads*, pp.108-112
- Ferguson, G. (1993). "Use of self-cementing fly ashes as a soil stabilization agent." *ASCE Geotechnical Special Publication No. 36*, ASCE, New York.
- Fernando, E., Liu W. and Lee T. (2001) " User's Guide to the Texas Modified Triaxlial (MTRX) Design Program"
- Fernando, E.G., Oh, J., Estakhri, C. and Nazarian, S. (2007) "Verification of The Load-Thickness Design Curves in the Modified Triaxial Design Method" *Report No. FHWA/TX-07/0-4519-1*
- Fredlund, D. G. and Rahardjo, H. (1993). *Soil Mechanics for Unsaturated Soils*, New York: John Wiley & Sons, Inc.
- Fredlund, D.G., Bergan, A.T. and Wong, P.K. (1977) "Relation Between Resilient Modulus and Stress Conditions for Cohesive Subgrade Soils" *Transportation Research Record No. 642*, pp. 73-81
- Gay, D.A. and Lytton, R.L. (1988) "Moisture Effects on Pavement Roughness" Geotechnical Special Publication No. 15, ASCE, New York

- Giroud, J.P., Ah-Line, C., and Bonaparte, R., (1984) "Design of Unpaved Roads and Trafficked Areas with Geogrids" *Proceedings of the 3rd International RILEM Conference* Institution of Civil Engineers, pp.116-127
- Giroud, J.P. and Han, J. (2004a) "Design Method for Geogrid-Reinforced Unpaved Roads. I. Development of Design Method" *Journal of Geotechnical and Geoenvironmental Engineering*, pp.775-786
- Giroud, J.P. and Han, J. (2004b) "Design Method for Geogrid-Reinforced Unpaved Roads. II. Calibration and Applications" *Journal of Geotechnical and Geoenvironmental Engineering*, pp.787-797
- Giroud, J.P. and Noiray, L. (1981) "Geotextile-Reinforced Unpaved Road Design" *Journal of Geotechnical Engineering Division, Proceedings of the ASCE Vol. 107, No. GT9*, pp.1233-1254
- Griffith, A.A. (1920) "The Phenomena of Rupture and Flow in Solids" *Philosophical transactions of the Royal society of London, A221*, pp.163–198.
- Gurung, N. (2003) " A Laboratory Study on the Tensile Response of Unbound Granular base Road Pavement Model Using Geosynthetics" *Geotextiles and Geomembranes* 21 pp.59-68
- Hamberg, D.J. (1985) "A simplified method for predicting heave in expansive soils" MS Thesis, Department of Civil Engineering, Colorado State University, Fort Collins, Colorado.
- Hampton, M.B. and Edil, T.B. (1998) "Strength Gain of Organic Ground with Cement-Type Binders" *Proceedings of Soil Improvement for Big Digs, 81,* pp.135-148
- Hicks, R.G. (2002) "Alaska Soil Stabilization Design Guide" *FHWA-AK-RD-01-6B*

- Holland, J.E. and Cameron, D.A. (1981) "Seasonal Heave of Clay Soils" *Civil Engineering Transactions, 1981*. pp.55-67
- Holtz, R.D. and Kovacs, W.D. (1981) *An Introduction to Geotechnical Engineering*, New Jersey, Printice-Hall
- Holtz, R.D., Christopher, B.R. and Berg, R.R. (1998) "Geosynthetic Design and Construction Guidelines" *FHWA HI-95-038*
- Hopkins, T.C. and Beckham, T.L. (2000) "Influence of Clay Fraction on the Behavior of Soil Subgrades" *Proceedings, 5th International Symposium on Unbound Aggregates in Roads,* Nottingham, UK
- Hopkins, T.C., Sun, L. and Slepak, M. (2005) "Bearing Capacity Analysis And Design Of Highway Base Materials Reinforced With Geofabrics" University of Kentucky Transportation Center, College of Engineering, Research Report KTC-05-21/SPR 238-02-1F.
- Hopkins , T.C. and Sharpe, G.W. (1985) "Unstable Subgrade I-65, Hardin County" *FSP 047-0065-091-0396,* University of Kentucky Transportation Center, College of Engineering, Research Report UKTRP 85-9.
- Horak, E. (1983) "Waterbound Macadam Bases" M.E. thesis. Department of Civil Engineering, Univ. of Pretoria, Republic of South Africa.
- Horak, E. and Triebel, R.H.H. (1986) "Waterbound Macadam as a Base and a Drainage Layer" *Transportation Research Record 1055*. pp.48-51

- Hudyma, N. and Burcin Avar, B. (2006) "Changes in Swell Behavior of Expansive Clay Soils from Dilution with Sand" *Environmental & Engineering Geosciences, Vol. 12, No. 2,* pp. 137-145
- Hufenus R., Rueegger, R., Banjac, R., Mayor, P., Springman, S.M. and Brönnimann, R. (2006) "Full-Scale Field Tests on Geosynthetic Reinforced Unpaved Roads on Soft Subgrade" *Geotextiles and Geomembranes* 24, pp.21-37
- Hussein E.A. (2001) "Viscoplastic Finite Element Model for Expansive Soils" EJGE paper 2001-0122.
- Irwin, G. (1957) "Analysis of Stresses and Strains Near The End of A Crack Traversing A Plate" *Journal of Applied Mechanics 24*, pp.361–364.
- Jefferies, M.G. and Davies, M.P. (1993) "Use of CPT to estimate equivalent SPT N_{60}". *Geotechnical Testing Journal*, 16(4) pp.458-468
- Keller, G. and Sherar, J. (2003) "Low-Volume Roads Engineering Best Management Practices Field Guide" *Produced for US Agency for International Development (USAID)*
- Khedr, S.A. and Mikhail, M. (1999) "Design of Flexible Pavements and Overlay Using an Expert System." *Transportation Research Record No. 1543*, pp. 20-28.
- Koerner, R.M. (2005) *Design with Geosynthetics,* 5th Ed. Pearson Prentice Hall, Upper Saddle River, NJ
- Komornik, A. and David, D. (1969) "Prediction of Swelling Pressure of Clays" *Soil Mechanics and Foundation Engineering, ASCE, Vol. 95, No. SM1*, pp.209-225

- Komornik, A., Wiseman, G. and Ben Yaacob, Y. (1969) "Studies in In Situ Moisture and Swelling Potential Profiles" *Second Conference on Expansive Soils,* Texas A&M University, College Station, TX
- Kota, P.B.V.S., Hazlett, D., and Perrin, L. (1996). "Sulphate-bearing soils: Problems with calcium-based stabilizers." *Transportation Research Record 1546*, pp.62-69.
- Kwon, J., Tutumluer, E., Al-Qadi, I.L. and Dessouky, S. (2008) "Mechanistic Model Development and Response Validation for Geogrid Base Reinforced Flexible Pavements" *The First pan American Geosynthetics Conference & Exhibition, March, 2008, Cancun, Mexico.*
- Little, D.N.(1999) "Evaluation of Structural Properties of Lime Stabilized Soils and Aggregates, Vol. I. Summary of Findings" National Lime Association Publication
- Little, D.N. and Petry, T.M. (1992) "Recent Development in Sulfate-Induced Heave in Treated Expansive Clays" *Proceedings of the 2nd Interagency Symposium on Stabilization of Soils and Other Materials.* Metairie, Louisiana, pp.1-18
- Little, D.N., Males, E. H., Prusinski, J.R. and Stewart, B. (2000) "Cementitious Stabilization" *79th Millennium Rep. Series, Transportation Research Board*
- Luo, R. and Prozzi, J.A. (2007) "Using Geogrids to Minimize Reflective Longitudinal Cracking on Pavements over Expansive Soils," *Transportation Research Record: Journal of the Transportation Research Board, No. 2004*, Washington, DC, 2007.
- Lytton, R.L. (1997) "The Characterization of Expansive Soils in Engineering" presentation at the Symposium on Water Movement and Equilibrium in Swelling Soils, American Geophysical Union, San Francisco, CA.

- Lytton, R., Aubeny, C. and Bulut, R. (2004) "Deisgn Procedure for Pavements on Expansive Soils Volume 1, 2, 3" Texas Transportation Institute, *Project No. 0-4518, Report No. FHWA/TX-05/0-4518-1*
- McDowell, C. (1955) "Wheel-Load-Stress Computations Related to Flexible Pavement Design" *Highway Research Board, Bulletin 114,* Washington, D.C., pp. 1-20.
- McKeen, R.G. (1980) "Field Studies of Airport Pavements on Expansive Clay" *Proc. of 4th International Conference on Expansive Soils*, Denver, CO, pp 242-261
- McPherson, E.G. (2000) "Expenditures Associated with Conflicts between Street Trees Root Growth and Hardscape in California" *Journal of Arboriculture, Vol. 26, No. 6*, pp.289-297
- Mitchell, P.W., Avalle, D.L. (1984) "A Technique to Predict Expansive Soil Movements" *Proceedings of 5th International Conference on Expansive Soils*, Adelaide, Australia
- Miller, G.A., The, S.Y., Li, D. and Zaman, M.M. (2000) "Cyclic Shear Strength of Soft Railroad Subgrade" *Journal of Geotechnical and Geoenvironmental Engineering*, pp.139-147
- Montanelli, F., Zhao, A.G. and Rimoldi, P. (1999) "Geosynthetic-Reinforced Pavement System: Testing & Design" (http://www.tenax.net/)
- Mowafy, Y.M. and Bauer, G.E. (1985) "Prediction of Swelling Pressure and Factors Affecting the Swell Behavior of an Expansive Soil" *Transportation Research Record 1032*. pp.23-33
- Mowafy, Y.M., Bauer, G.E. and Sakeb, F.H. (1985) "Treatment of Expansive Soils: A Laboratory Study" *Transportation Research Record 1032*. pp.34-39

- Nagaraj, T.S. and Srinivasa Murthy, B.R. (1985) "Rational Approach to Predict Swelling Soil Behavior" *Transportation Research Record* 1032. pp.1-7
- Nazarian, S. and Yuan, D. (2003) "Comprehensive Mechanistic-based Quality Control of Flexible Pavements with NDT Methods", Non-Destructive Testing in Civil Engineering 2003, Center for Highway Materials Research, The University of Texas at El Paso.
- Nazarian, S., Baker, M.R., and Crain, K. (1993) "Development and Testing of a Seismic Pavement Analyzer". *Report SHRP-H-375*. Strategic Highway Research Program, National Research Council, Washington, D.C.
- Nelson, J.D. and Miller, J.D. (1992) Expansive Soils: Problems And Practice In Foundation and Pavement Engineering. New York: Wiley.
- Newcomb, D.E. and Birgisson, B. (1999) "Measuring In Situ Mechanical Properties of Pavement Subgrade Soils" *National Cooperative Highway Research Program Synthesis of Highway Practice 278, TRB*, Washington, D.C.
- Ofer, Z. and Blight, G.E. (1985) "Measurement of Swelling Pressure in the Laboratory and In Situ" *Transportation Research Record 1032*. pp.15-22
- Ohri, M.L. (2003). "Swelling behavior of clays and its control." *Proc. of International Conference on Problematic soils*, Nottingham, U.K, pp 427-433
- Pengelly, A. and Addison, M. (2001) "In-Situ Modificaiton of Active Clays for Shallow Foundation Remediation" *Expansive Clay Soils and Vegetative Influences*, pp.192-214
- Picornell, M. and Lytton, R.L. (1986) "Behavior and Design of Vertical Moisture Barriers" *Transportation Research Record 1137*. pp.71-81

- Poor, A.R. (1974). ‘‘Experimental residential foundation design on expansive clay soils.’’ *Rep. No. TR-3-78*, *Final Rep.*, Construction Research Center, Univ. of Texas at Arlington, Texas.
- Powell, W.D., Potter, J.F., Mayhew, H.C. and Nunn, M.E. (1984) “The Structural Design of Bituminous Roads” *Transport and Road Research Laboratory Report LR1132*.
- Puppala, A.J., Griffin, J.A., Hoyos, L.R. and Chomtid, S. (2004a) “ Studies on Sulphate-Resistant Cement Stabilization Methods to Address Sulphate-Induced Soil Heave” *Journal of Geotechnical and Geoenvironmental Engineering*
- Puppala, A.J., Katha, B. and Hoyos, L.R. (2004b) “Volumetric Shrinkage Strain Measurements in Expansive Soils Using Digital Imaging Technology” *Geotechnical Testing Journal, Vol. 27, No. 6.*
- Puppala, A.J. and Mohammad, L.N. (1997) “A Regression Model for Better Characterization of Resilient Properties of Subgrade Soils” *8th International Conference on Asphalt Pavements,* Corp. Authors/Publisher: University of Washington, Seattle. pp.859-866
- Puppala, A.J. and Reddy, T.H. (2006) “PVR Calculations and Assessments—Fort Worth District” TxDOT Sponsored Interagency Contract *Report 02-6XXIA003*
- Puppala, A.J., Wattanasanticharoen, E. and Punthutaecha, K. (2003) “Experimental Evaluations of Stabilization Methods for Sulphate-rich Expansive Soils” *Ground Improvement Vol. 7, No. 1*, 2003. pp.25-35
- Rabba, S. (1975) “Factors Affecting Engineering Properties of Expansive Soils” M.S. Thesis, Al-Azhar University, Cairo, Egypt

- Ramamurthy, T. (1971) “Discussion Of Technique For Study Of Granular Materials” *Journal of Soil Mechanics Vol. 97, No SM4,* pp.686-690
- Rao, R.R., and Smart, P. (1980) “Significance of Particle Size Distribution Similarity in Predicction of Swell Properties” *Proc. of 4th International Conference on Expansive Soils*, Denver, Colorado, pp.96-105
- Rauhut, J.B., Eltahan, A. and Simpson, A.L. (1999) “Common Characteristics of Good and Poorly Performing AC Pavements” *FHWA-RD-99-193*.
- Ravina, I. (1984) “The Influence of Vegetation on Moisture and Volume Changes” *The Influence of Vegetation on Clays*, The Institution of Civil Engineers, Billings and Son Ltd., Great Britain, pp.62-68
- Raymond, G. and Ismail, I. (2003) “The Effect of Geogrid Reinforcement on Unbound Aggregates” *Geotextile and Geomembranes 21* pp.355-380
- Rollings, K.M. and Christie, R. (2002) “Pavement and Subgrade Distress-Remedial Strategies for Construction and Maintenance (I-15 Mileposts 200-217)” Utah DOT research and development report No. UT-02.17.
- Rowe, P.W. and Barden, L. (1964) “Importance of Free Ends in Triaxial Testing” *ASCE Journal of Soil Mechanics & Foundations Div, Vol. 90 No. SM1*, pp.1-27
- Sabnis, A., Manosuthkij, T., Abdallah, I., Nazarian, S. and Puppala, A.J. (2008) “Impact of Moisture Variation on Strength and Deformation of Clays” FHWA/TX-08/0-5430-1.

- Sayers, M.W., Gillespie, T.D. and Paterson, D.O. (1986) “Guidelines for conducting and Calibrating Road Roughness Measurements” *World Bank Technical Paper No. 46*. The World Bank, Washington, D.C., U.S.A.
- Scullion, T. and Michalak, C.H.(1998) “Flexible Pavement Design System (FPS) 19: User’s Manual” Texas Transportation Institute, Texas Department of Transportation.
- Sewell, M. and Marczak, M. (1997). “Using Cost Analysis in Evaluation” USDA/CSREES and the University of Arizona, Tucson, AZ.
- Shahu, J.T., Yudhbir, K.R. (1999) “Effective Stress Behavior of Quasi-Saturated compacted Cohesive Soils” *Journal of Geotechnical and Geoenvironemtal Engineering, Vol. 125*, pp.322-329
- Shell (1978) Shell Pavement Design Manual-Asphalt Pavements and Overlays for Road Taffic, London, England.
- Snethen, D.R., Johnson, L.D. and Patrick, D.M. (1977) “ An Evaluation of Expedient Methodology for Identification of Potentially Expansive Soils” *FHWA-RD-77-94*
- Snethen, D.R. (2001) “Influence of Local Tree Species on Shrink/Swell Behavior of Permian Clays in Central Oklahoma” *Expansive Clay Soils and Vegetative Influence on Shallow Foundations*, pp.158-171.
- Steinberg, M.L. (1992) “Vertical Moisture Barrier Update” *Transportation Research Record 1362*. pp.111-117
- Steward, J., Williamson, R. and Mohney, J. (1977) “Guidelines for Use of Fabrics in Construction and Maintenance of Low-Volume Roads” *FHWA TS-78-205*

- The Asphalt Institute (1982) *Research and Development of the Asphalt Institute's Thickness Design Manual (MS-1).* 9th Ed. Research Report 82-2 (RR-82-2), Maryland, 204 p.
- Thompson, M.R., (1966), "Lime Reactivity of Illinois Soils," Journal of the Soil Mechanics and Foundations Division, ASCE, Vol. 92, No. SMS.
- Thompson, M.R. (1979) "Subgrade Stability" *Transportation Research Record 705*. pp.32-41
- Thompson, M.R.(1982) "Highway Subgrade Stability Manual" Illinois Department of Transportation, Departmental Policies, MAT-10
- Thompson, M.R. and Robnett, Q.L. (1979) "Resilient Properties of Subgrade Soils" *Transportation Engineering Journal. ASCE. 105*, *No. TE1*.
- Thornthwaite, C.W. (1948) "An Approach Toward a Ration Classification of Climate" Geographical Review, pp.54-94
- Tirado, C., Qing, Y., Carrasco, C., Nazarian, S., Osegueda, R. (2006). "A GIS Based Algorith for Estimating Damage due to Superheavy Loads" *Report FHWA/TX-05/9-1502-01-6*, Center for Transportation Infrastructure Systems, The University of Texas at El Paso, El Paso, Texas, March 2006.
- Tsai, C.H. and Petry, T.M. (1995) "Suction Study on Compacted Clay Using Three Measurement Methods" *Transportation Research Record No. 1481*. pp.28-34
- Turban, E. (1990) Decision Support and Expert Systems: Management Support Systems MacMillan Publishing Company, Second Ed.

- Tucker, R.L. and Poor, A.R. (1978) "Field Study of Moisture Effects on Slab Movements" *Journal of Geotechnical Engineer, ASCE*, 104(4), 403-415.
- Tutumluer, E., Thompson, M.R., Garcia, G. and Kwon, J. (2005) "Subgrade Stability and Pavement Foundation Requirements" *Proc. of 15th Columbian Symposium of Pavement Engineering*, March 9-12, 2005
- US Department of Transportation, Federal Highway Administration (2000) "Statement No. 34: Basic Financial Statements—and Management's Discussion and Analysis—for State and Local Governments" *FHWA IF-00-010*
- US Department of Transportation, Federal Highway Administration (2002) " Life-Cycle Cost Analysis Primer" *FHWA IF-20-047*
- Uzan. J. (1985) "Characterization of Granular Materials" *Transportation Research Record 1022,* TRB, National Research Council, Washington, D.C.
- Uzan J., Livneh, M. and Shklarsky, E. (1972) "Cracking Mechanism of Flexible Pavements" *Transportation Engineering Journal, Proceedings of the American Society of Civil Engineers*, February, 1972. pp. 17-36
- Van Cauwelaert, F.J., Alexander, D.R., White, T.D. and Baker, W.R. (1989) "Multilayer Elastic Program for Backcalculating Layer Moduli in Pavement Evaluation" *ASTM, STP 1026,* Philadelphia, PA, pp.171-188
- Van Der Merwe (1964) "The Prediction of Heave from the Plasticity Index and Percentage Clay Fraction of Soils" *Transactions, South African Institute of Civil Engineers, Vol. 6*, Jun, pp.103-107

- van Gurp, C and van Leest, A.J. (2002) "Thin Asphalt Pavements on Soft Soil" *9th International Conference on Asphalt Pavements*, ISAP, Copenhagen.
- Vijayavergiya, V. N. and Ghazzaly, O. I. (1973) "Prediction of Swelling Potential for Natural Clays" *Proc. of 3rd International Conference on Expansive Soils*, Haifa, Israel, Vol. 1, pp.227-236
- Wanyan, Y. (2003) "Expediting Rigid Pavement Construction by Using Alternate Pavement Sections" *M.S. Thesis*, Civil Engineering Department, University of Texas at El Paso.
- Ward, W.H. (1953). "Soil Movements and Weather" *Proceedings of 3rd International Conference Soil Mechanics*, Zurich, 2, pp.477-481.
- Weimer, D.L., and Vining, A.R. (1992). *Policy Analysis: Concepts and Practice* 2nd Ed. Englewood Cliffs, NJ: Prentice Hall.
- Wesseldine, M.A. (1982). "House Foundation Failures Due To Clay Shrinkage Caused by Gum Trees" *Transactions, Institution of Professional Engineers*, NZ, March, CE9(1)
- White, D.J., Harrington, D. and Thomas, Z. (2005a) "Fly Ash Soil Stabilization for Non-Uniform Subgrade Soils, Volume I: Engineering Properties and Construction Guidelines" Iowa Highway Research Board Report: *IHRB Projectc TR-461; FHWA Project 4*,.
- White, D.J., Harrington, D. and Rupnow, T. (2005b) "Fly Ash Soil Stabilization for Non-Uniform Subgrade Soils, Volume II: Influence of Subgrade Non-Uniformity on PCC Pavement Performance" Iowa Highway Research Board Report: *IHRB Projectc TR-461; FHWA Project 4*

- Wu, X.R. and Carlsson, A.J. (1991) Weight Functions and Stress Intensity Factor Solutions, Pergamon Press.
- Yang, D.S., Yagihashi, J.N. and Yoshizawa, S.S. (1998) "Stabilization of Very Soft Soils and Organic Soils" *Proceedings of Soil Improvement for Big Digs, 81,* pp.96-110
- Yuan, D. and Nazarian, S. (2002) "Variation in Moduli of Base and Subgrade with Moisture", Transportation Research Board, Center for Highway Materials Research, The University of Texas at El Paso.
- Zacharias, G. and Ranganatham, B.V. (1972) "Swelling and Swelling Characteristics of Synthetic Clays" *Proceedings of Symposium on Strength and Deformation Behavior of Soils, Vol. 1*

APPENDIX A - DISTRICT SURVEY QUESTIONNAIRE

District name: _____ Contact person: _____
Contact phone #: _____ Contact email: _____

Do you have high PI clay subgrades? (Yes / No)
If yes, please fill the following table and indicate what factors are causing these distresses.

Distress	**Yes/No**	**Probable causes (inadequate structures, poor construction, improper stabilization, large trees, steep shoulders, large drainage ditches, moisture migrations, others)**
Longitudinal cracking		
Transverse cracking		
Rutting		
Shoving		
Excessive roughness		
Shoulder erosion		
Others (please specify)		

Do you use geo-synthetics for low volume roads on high PI clays? Never / Sometimes / Often

What type of stabilizer do you use? None / Lime / Cement / fly ash / others (please specify)

_____

APPENDIX B - SUMMARY OF SWELL PRESSURE AND PERCENT SWELL PREDICTION RELATIONSHIPS

Various correlations have been suggested for predicting the swell pressure (Table B.1) and percent swell (Table B.2). The generalized form of the equations may be written as:

$$Log(P_0 / P_a) = a_0 + a_L(LL) + a_d(\gamma_d / \gamma_w) + a_w(w_0) \quad \text{(B.1)}$$

$$Log(S_0) = b_0 + b_L(LL) + b_d(\gamma_d / \gamma_w) + b_w(w_0) \quad \text{(B.2)}$$

where P_0 = swelling pressure for zero movement; P_a = atmospheric pressure; S_0 = percent swell for zero load (%); LL = liquid limit (%); γ_d = dry density of soil; γ_w = unit weight of water; w_0 = in situ moisture content (%); and a_0, a_L, a_d, b_0, b_L, b_d are coefficients.

Notations for Table B.1 and B.2:

P_s = swelling pressure (kg/cm2); γ_d = dry density (g/cm3); LL = liquid limit (%); PI = plasticity index (%);w_s = shrinkage limit (%); w_n = natural water content (%); w_0 = initial water content (%); SI = shrinkage index; S_r = degree of saturation of specimen before start of test; w^* = water content at S_r = 100%; C = clay content (%);γ_w = density of water (g/cm^3); P = overburden effective pressure; e_o/e_L = generalized initial state of soil; ρ = slope of the line joining the present state to preconsolidation pressure; S_P = percent swell (%); H = depth of soil (ft)

Table B. 1—Correlations for Swelling Pressure Prediction (Summarized from Mowafy *et al.*, 1985; Nagaraj and Murthy, 1985)

Reference	Correlations	Comments
El-Ramli (1965)	$P_s = \frac{1}{2}\gamma_d / w_s$	Does not consider the effect of initial water content
Komornik and David (1969)	$LogP_s = 2.132 + 0.0208LL + 0.000665\gamma_d - 0.0269w_n$	Insensitive to variations in dry density
Zacharias and Ranganatham (1972)	$P_s = -\frac{225}{6.4}(SI) + \frac{290}{6.4}(LL - w^*) + \frac{1.2}{6.4}(SI)(\frac{1}{S_r})$	Dry density is not included, only valid to dry densities ranging between 17 and 18 kN/m^3
Dedier (1973)	$LogP_s = 2.55\frac{\gamma_d}{\gamma_w} - 1.705$ $LogP_s = 0.0294C - 1.923$	Does not consider the effect of initial water content. Equations cannot be applied to soils having different initial water contents.
Rabba (1975)	For sandy-clay: $LogP_s = 2.17(\gamma_d + 0.084C) - 3.91$ For silty-clay: $LogP_s = 2.5(\gamma_d + 0.006C) - 4$	Use of equations limited to an initial water content of 8%
Mowafy and Bauer (1985)	$Log(10.2P_s) = 1.366(10.2\gamma_d) + 8.951\times10^{-3}C - 2.179\times10^{-2}w_n - 2.840$	For soils from Nasr city, a satellite city of Cairo, Egypt
Vijayavergiya and Ghazzaly (1973)	$LogP_s = \frac{1}{12}(0.4LL - w_n - 0.4)$ $LogP_s = \frac{1}{19.5}(\gamma_d + 0.65LL - 139.5)$	Correlations developed based on 270 test results of undisturbed natural soils at shallow depth. To predict swell pressure and percent swell under 0.1 ton/ft^2.
Nagaraj and Murthy (1985)	$P_s(kPa) = 2492 - 12811.3\left(\frac{e_0}{e_L}\right)/(5.522 - \log P_c)$ $\rho = 0.0601 - 0.0297\left[\left(\frac{e_0}{e_L}\right) + \log\left(\frac{P_s}{P}\right)\right]$ $\left(\frac{e_0}{e_L}\right) = 1.122 - (0.2343 - \rho)\log P_c - \rho\log P$	These three equations have three unknowns in P_s, P_c and ρ and the solutions could be obtained by iteration process.

Table B. 2—Correlations for Percent Swell Prediction
(after Dept. of the Army TM 5-818-7)

Reference	Correlations	Comments
Vijayvergiya and Ghazzaly (1973)	$LogS_p = \frac{1}{12}(0.44LL - w_0 + 5.5)$ $LogS = \frac{1}{19.5}(\gamma_d + 0.65LL - 130.5)$	From initial water content to saturation for 0.1-tsf surcharge pressure
Schneider and Poor	$LogS_p = 0.9\left(\frac{PI}{w_0}\right) - 1.19$	For no fill or weight on the swelling soil to saturation
McKeen (1980)	$S_p = -100\gamma_h \log\frac{\bar{\tau}_f}{\bar{\tau}_0}$	The γ_h is found from a chart using CEC, PI, and percent clay. The weighted suction is given by $\bar{\tau} = 0.5\tau_1 + 0.3\tau_2 + 0.2\tau_3$ where τ_1, τ_2, τ_3 are in situ suctions measure in the top, middle, and bottom third of the active zone.
Johnson and Stroman (1976)	$PI > 40$ $S_p = 23.82 + 0.7346PI - 0.1458H - 1.7w_0$ $+ 0.0025PI \times w_0 - 0.00884PI \times H$ $PI \le 40$ $S_p = -9.18 + 1.5546PI + 0.08424H + 0.1w_0$ $- 0.0432PI \times w_0 - 0.01215PI \times H$	For 1 psi surcharge pressure to saturation

APPENDIX C - FINITE ELEMENT ANALYSIS DEVELOPMENTAL DETAILS

C.1. FINITE ELEMENT ANALYSIS METHODS AND SOFTWARES

There are generally two types of FEA analysis that are used: 2-D modeling, and 3-D modeling. While 2-D modeling conserves simplicity and allows the analysis to be run on a relatively normal computer, it tends to yield less accurate results. 3-D modeling, however, produces more accurate results while sacrificing the ability to run on all but the fastest computers effectively. Within each of these modeling schemes, the programmer can insert numerous algorithms (functions) which may make the system behave linearly or non-linearly. Linear systems are far less complex and generally do not take into account plastic deformation. Non-linear systems do account for plastic deformation, and many also are capable of testing a material all the way to fracture. Formulation-wise, there are three commonly used types for pavement structures: plane strain, axisymmetric, and three-dimensional. Table C.1 compares these three modeling approaches. Plane strain model requires less computational time and is relatively simple. The major limitation is the inability to model the three dimensional configuration of the pavement structure, load and responses. For example, pavement discontinuities such as longitudinal and transverse cracks are difficult to be modeled with a plane strain approach.

Table C. 1—Comparison of Finite Element Modeling Method

Concerns	Axisymmetric	2D - Plane Strain	3D
Loading	Static	Static	Static/Dynamic
Loading Area	Circular	Line	Versatile
Computation Time and Memory	Lowest	Middle	Highest Intensity
Interface Modeling	No	Partial	Yes
Discontinuity Modeling	No	Partial	Yes

After considering the computational time limitation and required level of accuracy of FEA output, the two-dimensional plane strain linear model is favorable and selected to give users a quick estimation of longitudinal cracking initiation. However, non-linear plastic-elastic FE model is needed to further study cracking propagation and fracture mechanics. With a more sophisticated FEA model following two questions of interest will be answered: (1) When will the shrinkage induced subgrade cracking pose visible damage to pavement? (2) Where will be the most critical location for such damage? To achieve analysis goals and balance limitations, two commercially available softwares are selected: Matlab® is used to perform linear elastic analysis and LS-Dyna is used to perform nonlinear elastic-plastic fracture analysis.

Tirado, *et al*. (2006) developed a FE program in Matlab® to perform pavement distress analysis under traffic loading in both two- and three-dimensions. The FE program was adopted and modified specifically to deal with shrinkage induced longitudinal cracking evaluation. Matlab is utilized to carry out the main computational tasks to identify critical moisture change level and location for initial subgrade shrinkage cracking. A stand-alone executable version can be easily created by Matlab function. With the flexibility to link the executable to the main program, end users don't need to install any additional software nor acquire Matlab license to perform the check.

LS-Dyna is an advanced general-purpose finite element analysis software package developed by the Livermore Software Technology Corporation (LSTC). It is suitable for many complex, real world problems including solid mechanics, heat transfer, and fluid dynamics. It has a large and expanding material library which includes elastic, thermal elastic-plastic, elastic-plastic with failure/fracture, and soil and crushable geocomposite with failure, to name a few. LS-Dyna also offers the possibility to develop user-defined material with specific equations of state and constitutive models for greater complexity. The main constraint of using LS-Dyna is the license requirement. In order to run the analysis, end user has to install the software and acquire license. LS-Dyna is used to carry out further analysis of cracking propagation. Same geometry setup is used for parametric studies and results are compared between the Matlab model (referred as Elastic Model) and the LS-Dyna model (referred as Fracture Model).

Table C.2 summarizes and compares the two finite element longitudinal shrinkage cracking models.

Table C. 2—Comparisons of the Two Developed FEA Models

		Elastic Model	**Fracture Model**
Developmental Software		Matlab	LS-Dyna
Distribution		Stand-alone exe	Keyword file
FEA Formulation	**Developer**	Yes	Yes
	User	No	Yes
	Geometry	12-ft wide pavement with 4-ft wide shoulder, symmetric at pavement centerline.	
	Element	Constant strain triangle elements	Eight-node hexahedron solid elements
	Mesh	Medium	
	Constitutive Models	Linear elastic	Elastic-plastic, and thermal
	Boundary	All nodes along the bottom and symmetry are constrained translationally and rotationally in x, y, z directions.	
	Load	Static (as initial strain)	Quasi-static (as thermal strain)
Execution Time		< 5 minutes	5-45 minutes

Post-processor are programmed using Borland C++ to link the longitudinal shrinkage cracking check to the main program and provide analytical and graphical output to the user. The ExSPRS software automatically incorporates Elastic model with CST elements, medium size mesh, elastic constitutive model and static load applications to eliminate the interaction between the user and the finite element code. Further analysis results from the Fracture Model are generalized and a simple relationship is used to extend the FEA results from cracking initialization (Elastic Model results) to propagation (Fracture Model results). Following sections will discuss and compare development details for these two FEA models respectively.

C.2. GEOMETRY

Typical low-volume pavement section, consisting of a thin asphalt layer over base and subgrade is used in both models. Each pavement layer is assumed to be homogenous, isotropic, linearly elastic and fully bonded to the underlying layer. Pavement shoulder is modeled as a uniform block fully bounded at the pavement interface. Because of symmetry, a half-wide pavement (144-inch wide) with shoulder (48-inch wide) was studied to reduce calculation effort. Origin is set at the surface interface of shoulder and pavement. Unit used is in inches. The Elastic Model can easily handle as many layers as needed to adequately describe the pavement structure by change of a parameter. For example, a five-layer section with a top AC layer, a base and three sub-layers in subgrade has been studied: a lime stabilized subgrade over a moisture susceptible (active) subgrade on top of a non-active subgrade layer. Adding a non-active subgrade layer can minimize boundary constraint effects. More subgrade sub-layers can also be defined to present different moisture variation trend along depth. On the other hand, the Fracture Model requires manually setup for different cross-sections. In the scope of this study, only 3- and 4-layer cross-sections are studied.

C.3. ELEMENT TYPE AND MESHING

Different element types are used for Elastic Model and Fracture Model. In the Elastic Model, constant strain triangle (CTS) elements are used. The CTS contains 3 nodes per element, 2 degree of freedom (DOF) per node and 6 DOF per element. The advantage of CTS elements is their geometric flexibility: they allow modeling intricate geometries and facilitate transition from coarsely meshed zones of a grid to finely meshed zones. CTSs usually require bigger number of elements to reach reasonable accuracy, and they are suitable for areas with small strain gradients. However, CSTs in critical areas such as stress concentrations, edges and corners may cause problems and should be avoided. An open source preprocessor called GMSH is used to create these CTS elements. The Elastic Model can create either biased seed to obtain denser mesh at the point of interest or a uniform mesh throughout the modeled section. In the case for shrinkage induced initial strain simulation, both subgrade and shoulder are of interest and thus uniform meshing fits better. The CST element size is 2-in for each triangle side. For the Fracture Model, eight-node hexahedron solid elements of 2 by 2 by 2 (in^3) are used with uniform meshing. Element sizes are uniform except for very thin top layer (< 2-inch) and corners, in which the smaller elements are used to ensure proper simulation. The Fracture Model simulates subgrade shrinking as thermal contraction and will eliminate those elements that failed. In this model, explicit method is used to solve the nonlinear problem much faster without time-consuming interactions. Time steps used in this model are evaluated based on loading, material property and the size of the elements. For a typical 3 layer section with 2 by 2 by 2 in^3 eight-node hexahedron solid elements, the running time is about 2 minutes. However, when the top layer thickness is reduced to 0.5-inch the elements in top layer become smaller (0.5 by 2 by 2 in^3). Smaller elements automatically decrease analysis time steps which dramatically increase running time to about 30 minutes.

Finite element solution highly depends on element size and boundary conditions. Generally speaking, finer mesh gives more accurate estimation. However, with finer mesh, computational time may increase tremendously. Due to memory limitation and computational time constraint, medium size elements are preferred. Figure C.1 compares the different elements and meshing of the two models for a 3-layer cross-section.

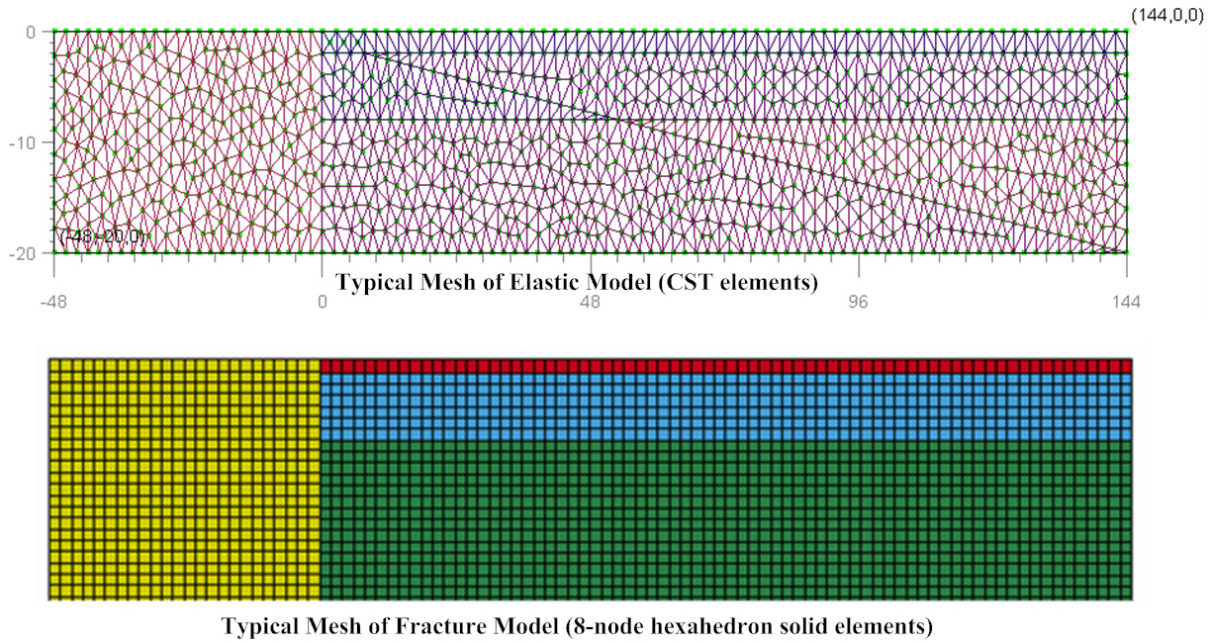

Figure C. 1—Typical Meshing in FE Modeling

C.4. MATERIAL CONSTITUTIVE MODELS

To estimate the strain/stress distribution caused by shrinkage, the generalized constitutive equation of classical elasticity (Hooke's law) is applied to each element in Elastic Model as shown in Equation C.1.

$$\sigma = D(\varepsilon - \varepsilon_0) + \sigma_0 \qquad \text{(C. 1)}$$

where ε_0 and σ_0 are the initial strain and initial stress for each element and D is the elasticity matrix containing the appropriate material properties such as modulus (E) and Poisson's ratio v. For plane strain, D matrix is:

$$D = \frac{E}{(1+\nu)(1-2\nu)} \begin{bmatrix} 1-\nu & \nu & 0 \\ \nu & 1-\nu & 0 \\ 0 & 0 & \frac{1-2\nu}{2} \end{bmatrix} \quad \text{(C. 2)}$$

Two types of materials are used in the Fracture Model: Material type 17 to simulate AC and base, and Material type 4 to model subgrade and shoulder. Since the main purpose is to study longitudinal cracking of pavement, Material type 17 is used to model AC and base which fail due to large tensile stresses. It is an isotropic elastic-plastic material which includes a failure model with an oriented crack. The failure model is based on a maximum principal stress criterion of von Mises yield condition. When the maximum principal stress exceeds the fracture stress σ_f, the element fails and the normal stress and the two shear stresses on the fracture plane are then reduced to zero. In such case, the element will not support tensile stress but will still be able to support compression stress. If the maximum principal stress subsequently exceeds the fracture stress in another direction, the element fails isotropically and behaves like a fluid. More mathematical information about this material model can be found in LS-Dyna keyword user's manual version 971 Volume II.

The von Mises yield condition Φ is given by Equation C.3.

$$\phi = J_2 - \frac{\sigma_y^2}{3} \quad \text{(C. 3)}$$

where J_2 is the second stress invariant and σ_y is the yield stress.

$$J_2 = \frac{1}{2} s_{ij} s_{ij} \quad \text{(C. 4)}$$

$$\sigma_y = \sigma_{yi} + E_p \varepsilon_{eff}^p \quad \text{(C. 5)}$$

The yield stress σ_y is a function of initial yield stress σ_{yi}, plastic hardening modulus E_p and effective plastic strain ε_{eff}^p.

When the behavior is elastic, The von Mises yield function (Equation C.3) is checked, and no changes needed. Otherwise, a scale factor f_s is used to scale back the stress deviators.

$$f_s = \frac{\sigma_y}{\left(\frac{3}{2} s_{ij}^* s_{ij}^*\right)^{1/2}} \tag{C. 6}$$

$$s_{ij}^{n+1} = f_s s_{ij}^* \tag{C. 7}$$

The plastic strain ε_{eff}^p in Equation C.5 is updated by the increment

$$\Delta\varepsilon_{eff}^p = \frac{(1-f_s)\left(\frac{3}{2} s_{ij}^* s_{ij}^*\right)^{1/2}}{G + 3E_p} \tag{C. 8}$$

where G is the elastic shear modulus.

In order to simulate shrinkage cracking, Material type 4 is used for subgrade and shoulder and the moisture change (drying in this case) induced shrinkage strain is represented as thermal shrinkage induced strain. This is a thermo-elastic-plastic material also governed by constitutive Equation C.1. The temperature dependent elasticity matrix D has following format:

$$D = \frac{E}{(1+\upsilon)(1-2\upsilon)} \begin{bmatrix} 1-\upsilon & \upsilon & \upsilon & 0 & 0 & 0 \\ \upsilon & 1-\upsilon & \upsilon & 0 & 0 & 0 \\ \upsilon & \upsilon & 1-\upsilon & 0 & 0 & 0 \\ 0 & 0 & 0 & \frac{1-2\upsilon}{2} & 0 & 0 \\ 0 & 0 & 0 & 0 & \frac{1-2\upsilon}{2} & 0 \\ 0 & 0 & 0 & 0 & 0 & \frac{1-2\upsilon}{2} \end{bmatrix} \tag{C. 9}$$

The initial shrinkage induced strain ε_0 is treated as a thermal strain, written in terms of the coefficient of thermal expansion α as:

$$\varepsilon_0 = \alpha\Delta\theta \tag{C. 10}$$

where $\Delta\theta$ is the temperature change. In the Fracture Model, thermal expansion coefficient is defined as negative one to simulate shrinking. Initial temperature of Material 4 is set to zero and moisture change is used to substitute $\Delta\theta$.

C.5. BOUNDARY CONDITIONS

The boundary conditions for both models are: 1) No horizontal displacement at the centerline of the pavement, because of symmetry; 2) No vertical displacement at the bottom of the subgrade, because the model size in depth is large enough for the subgrade to experience no significant deformation at the bottom; 3) Fully bonded interfaces with no rotational degree of freedoms. Besides, the kinematic constraints method is used by the Fracture Model for boundary and interface conditions. The input energy is integrated and included in the external work.

C.6. LOAD

In the Elastic Model, the initial strain ε_0 in Equation C.1 will be defined by average, constant values to be consistent with the constant strain conditions imposed by the prescribed displacement function. For an isotropic material in an element subject to moisture change (in this case drying), the initial strain for plane strain can be expressed as:

$$\varepsilon_0 = \begin{Bmatrix} \varepsilon_{x0} \\ \varepsilon_{y0} \\ 0 \end{Bmatrix} \tag{C. 11}$$

where ε_{x0}, ε_{y0} are initial shrinkage strain in x- and y- direction, which can be calculated using Equation 4.18 discussed in Section 4.5.2.

The nodal forces due to initial strain can be expressed as:

$$\left(f_i\right)^e_{\varepsilon_0} = -B_i^T D \varepsilon_0 t A \tag{C. 12}$$

where B is the node strain-displacement matrix, A is the area of the finite element. And t is the thickness of the element which is assumed to be 1-inch always.

$$B_i = \begin{bmatrix} \frac{\partial N_i}{\partial x} & 0 \\ 0 & \frac{\partial N_i}{\partial y} \\ \frac{\partial N_i}{\partial y} & \frac{\partial N_i}{\partial x} \end{bmatrix} \tag{C. 13}$$

For newly constructed pavements, no traffic loading is considered for the purpose of longitudinal cracking analysis, thus the initial stress caused by traffic is zero. However, if the user also wants to analyze traffic loading effects on longitudinal cracking, the Elastic Model is capable of including one-tire load, two-tire single-axle load or dual-single-axle load which contains four tires in total. The load can be placed anywhere on the pavement surface (default loading is a single tire located 6-inch from the shoulder-pavement interface). Please note although loading can be added, constitutive equations for fatigue and rutting distresses are not formulated in this FEA subroutine. For fatigue and rutting analysis, the evaluation model discussed in Section 4.2 should be used.

In order to take into consideration the accumulated body weight opposed by pavement layers, body forces are distributed to the nodes equally, in the case of CTS element, in three equal parts. The total initial stress σ_0 in Equation C.1 is simply the summation of traffic loading (if any) and body weight of pavement materials.

Since the LS-Dyna version 971 used for this study doesn't support initializing strain tensors at element center, in order to apply the shrinkage strain to subgrade and shoulder, thermal material has to be used. The moisture variation caused shrinkage strain is converted and represented as thermal expansion/contraction effects and the system is loaded with quasi-static

loading curves. Following steps described how to convert shrinkage induced strains to time-related thermal stain loading curves.

1) The shrinkage strain prediction model discussed in section 4.5.2.2 is selected (Equation 4.18 is recaptured here for demonstration purpose).

$$\varepsilon_{shrink} = \left[A^*\left(1 - NMC^2\right)\right]^2 \quad (4.18)$$

where parameter A^* can be calculated using index properties following the procedure described in Section 4.5.2.3. As an example, the Paris clay has the following index properties: PI = 36; LL = 60; OMC = 23 %; and MDD = 92 pcf. Thus, the calculated A^* = 2.61.

2) Develop shrinkage strains curves as a function of time. In order to convert the shrinkage strain versus moisture content relationship to time-dependent loading curves, it is assumed the drying time to reach every 0.1NMC change step is the same. That is, if we assume unit time for drying from OMC to 0.9NMC, then for every 0.1NMC decreasing, it takes same amount of time. It should be noted that with a longer loading time, calculation time also increases. Drying process is always assumed to start from optimum, which sets the time as zero, and the corresponding shrinkage strain as zero too. In reality, drying time vs. moisture content decrease can be correlated by laboratory curves as shown in Figure 4.7 and 4.8 in Chapter 4. Table C.3 shows four drying curves of Paris clay from optimum to 0.9NMC, 0.8NMC, 0.7NMC and 0.6NMC respectively.

3) Loading curves can be defined for the Fracture Model using shrinkage strain vs. time table developed in step 2), by plotting ε_{ss} as ordinate values and time as abscissa values. Again, if laboratory volumetric shrinkage strain tests data are available, the variations in lateral shrinkage strains with time curve as shown in Figure 4.7 should be used instead to define

corresponding loading curves. Figure C.2 shows an example of four loading curves defined for Paris clay.

Table C. 3—Example of Loading Curve Data for Fracture Model (Paris, DFO)

Optimum to 0.9NMC			**Optimum to 0.8NMC**			**Optimum to 0.7NMC**			**Optimum to 0.6NMC**		
NMC	ε_{ss} (%)	Time	NMC	ε_{ss} (%)	Time	NMC	ε_{ss} (%)	Time	NMC	ε_{ss} (%)	Time
1.00	0.00	0.0	1.00	0.00	0.0	1.00	0.00	0.0	1.00	0.00	0.0
0.99	0.00	0.1	0.98	0.01	0.2	0.97	0.02	0.3	0.96	0.04	0.4
0.98	0.01	0.2	0.96	0.04	0.4	0.94	0.09	0.6	0.92	0.16	0.8
0.97	0.02	0.3	0.94	0.09	0.6	0.91	0.20	0.9	0.88	0.35	1.2
0.96	0.04	0.4	0.92	0.16	0.8	0.88	0.35	1.2	0.84	0.59	1.6
0.95	0.06	0.5	0.90	0.25	1.0	0.85	0.52	1.5	0.80	0.88	2.0
0.94	0.09	0.6	0.88	0.35	1.2	0.82	0.73	1.8	0.76	1.21	2.4
0.93	0.12	0.7	0.86	0.46	1.4	0.79	0.96	2.1	0.72	1.58	2.8
0.92	0.16	0.8	0.84	0.59	1.6	0.76	1.21	2.4	0.68	1.96	3.2
0.91	0.20	0.9	0.82	0.73	1.8	0.73	1.48	2.7	0.64	2.37	3.6
0.90	0.25	1.0	0.80	0.88	2.0	0.70	1.77	3.0	0.60	2.78	4.0

The Fracture Model is loaded by corresponding loading curve for each NMC level, e.g. to study drying from optimum to 0.8 NMC for Paris, the top-right loading curve in Figure C.2 should be used. Cracking propagation can be studied and compared and results can be generalized as discussed in Section 4.5.3.2.4.

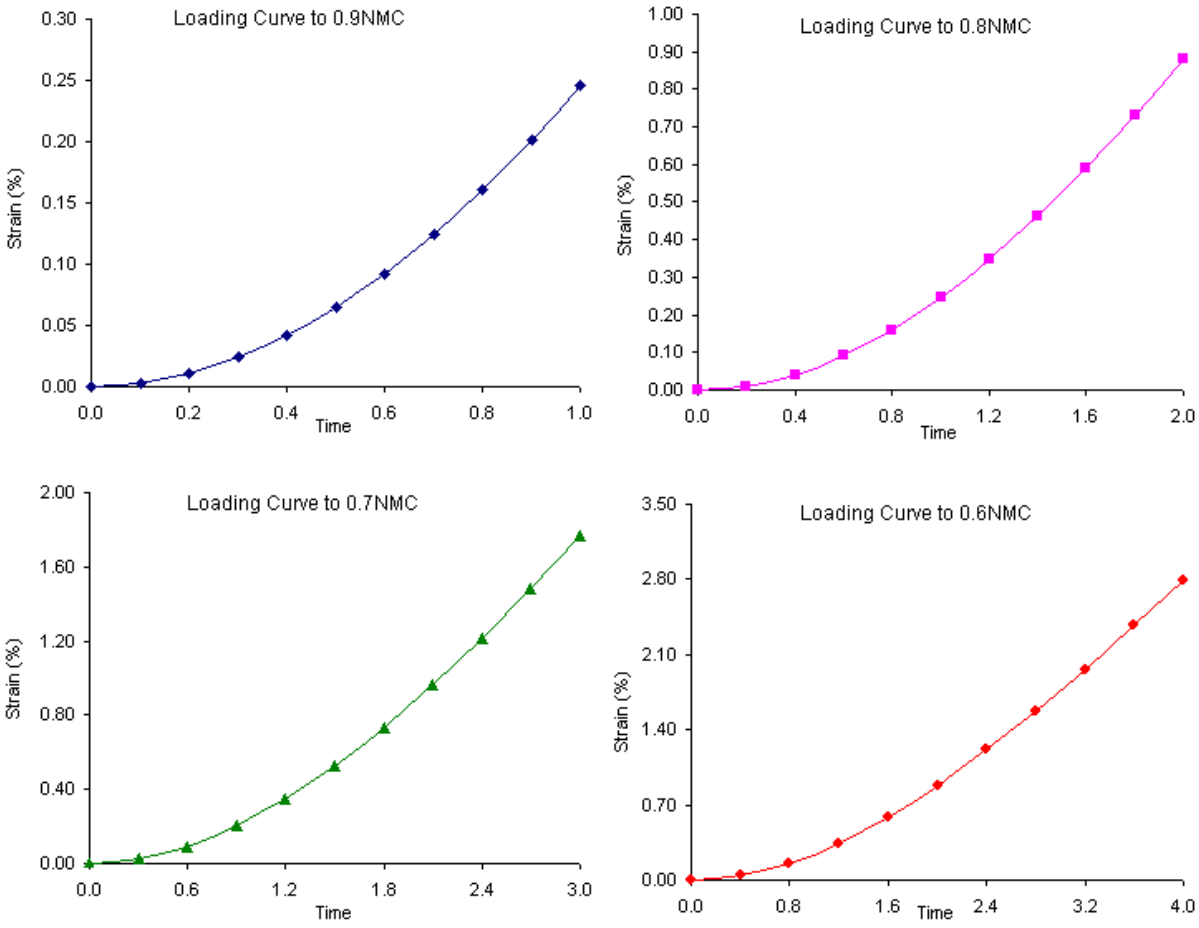

Figure C. 2—Example of Loading Curves for Fracture Model (Paris, DFO)

APPENDIX D - ELASTIC MODEL PARAMETRIC STUDY RESULTS

D.1. EFFECTS OF LAYER THICKNESSES

Figure D.1, D.2 and D.3 compare the AC, base and subgrade layer thickness effects on the average values of the top 50 largest tensile stress points (σ_{avg}) for 3-layer and 4-layer pavement sections respectively. For each comparison case, 3- and 4-layer sections have the same trend with very close resulting tensile stress values. With increased AC thickness, the resulting σ_{avg} increases. When the AC thickness changes from 0.5 inch to 4.5 inch, σ_{avg} increased from 26 psi to 33 psi for both 3- and 4-layer cases. Similarly, with increased base thickness, the resulting σ_{avg} also increases. When the base thickness changes from 6 inch to 18 inch, σ_{avg} increased from 30 psi to 32 psi for both 3- and 4-layer cases. The AC layer thickness has bigger effects on σ_{avg} compared to the base thickness. On the other hand, subgrade thickness shows slightly opposite effect, e.g. with a thicker subgrade subject to shrinking, the resulting σ_{avg} decrease. When the subgrade thickness changes from 30 inch to 70 inch, σ_{avg} decreased from 33 psi to 30 psi for both 3- and 4-layer cases.

D.2. EFFECTS OF LAYER MODULI

Figure D.4, D.5 and D.6 compare the AC, base and subgrade layer modulus effects on the average values of the top 50 largest tensile stress points (σ_{avg}) for 3-layer and 4-layer pavement sections respectively. When material modulus increases, the overall trend shows increased σ_{avg}, this trend is expected with simple Hook's law. When the AC modulus changes from 300 ksi to

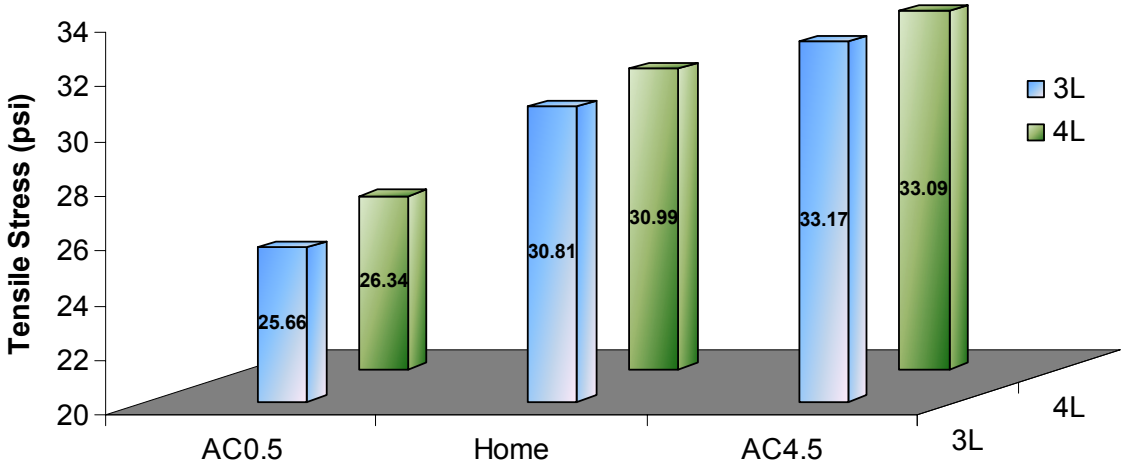

Figure D. 1— AC Layer Thickness Effects on Average of Top 50 Tensile Stresses

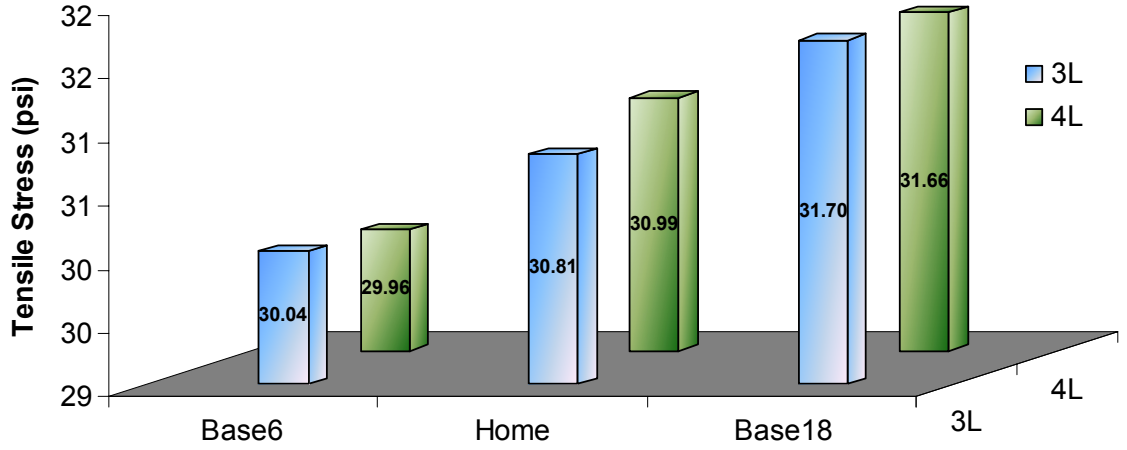

Figure D. 2— Base Layer Thickness Effects on Average of Top 50 Tensile Stresses

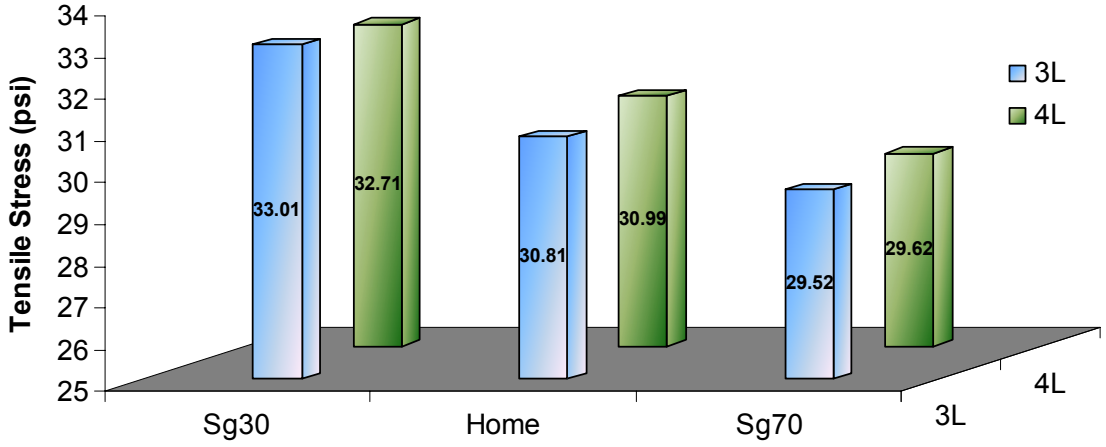

Figure D. 3— Subgrade Layer Thickness Effects on Average of Top 50 Tensile Stresses

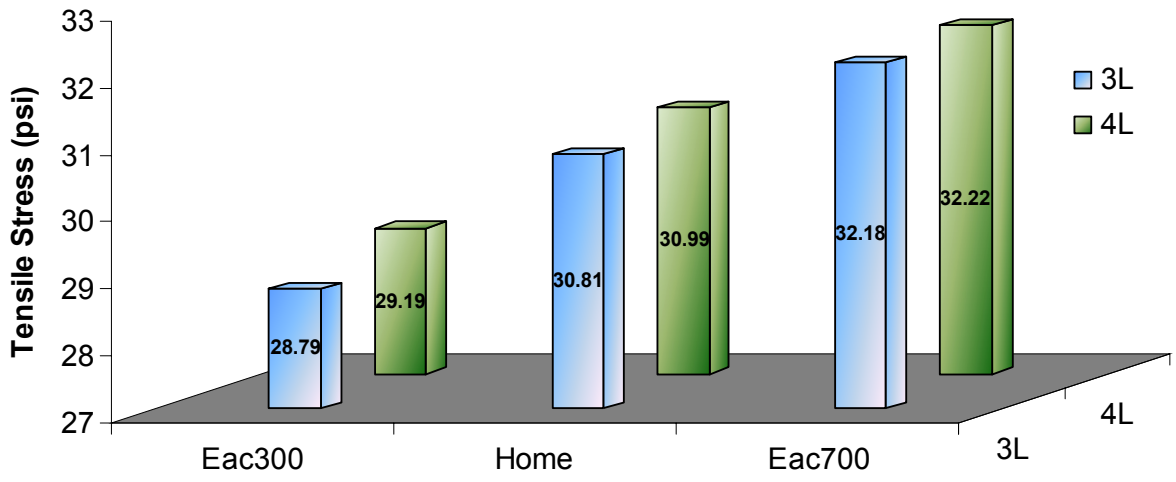

Figure D. 4— AC Layer Modulus Effects on Average of Top 50 Tensile Stresses

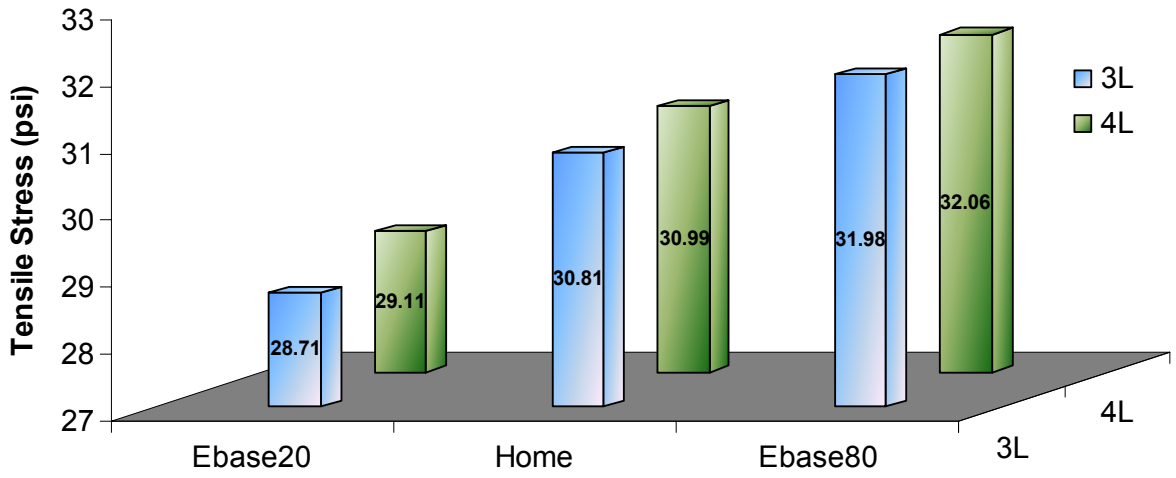

Figure D. 5— Base Layer Modulus Effects on Average of Top 50 Tensile Stresses

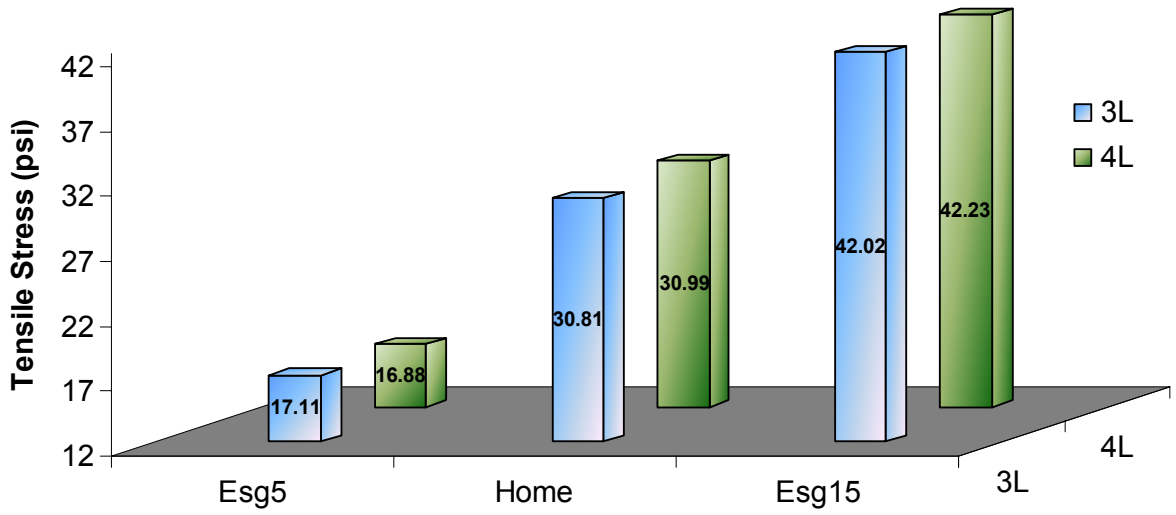

Figure D. 6— Subgrade Layer Modulus Effects on Average of Top 50 Tensile Stresses

700 ksi, σ_{avg} increased from 29 psi to 32 psi for both 3- and 4-layer cases. Same σ_{avg} values for 3- and 4-layer cases are reported when the base modulus changes from 20 ksi to 80 ksi. The subgrade layer modulus has bigger effects on σ_{avg} compared to the AC and base layer. When the subgrade modulus changes from 5 ksi to 15 ksi, σ_{avg} increased from 17 psi to 42 psi for both 3- and 4-layer cases.

From above comparison, the 3- and 4- layer sections always give very close results and same trend. For low-volume roads, it seems more layers don't provide better performance with respect to subgrade shrinkage cracking.

D.3. EFFECTS OF MESHING SIZE

The meshing size doesn't affect σ_{avg} much. Different sized elements are studied. Figure D.7 and D.8 compare the meshing size effects for 3- and 4-layer Home case respectively. When the meshing size gets smaller, the distribution of the top 50 largest tensile stress points along subgrade top becomes denser and closer to the peak. However, the peak location is not sensitive to the mesh size and is pretty stable for each case.

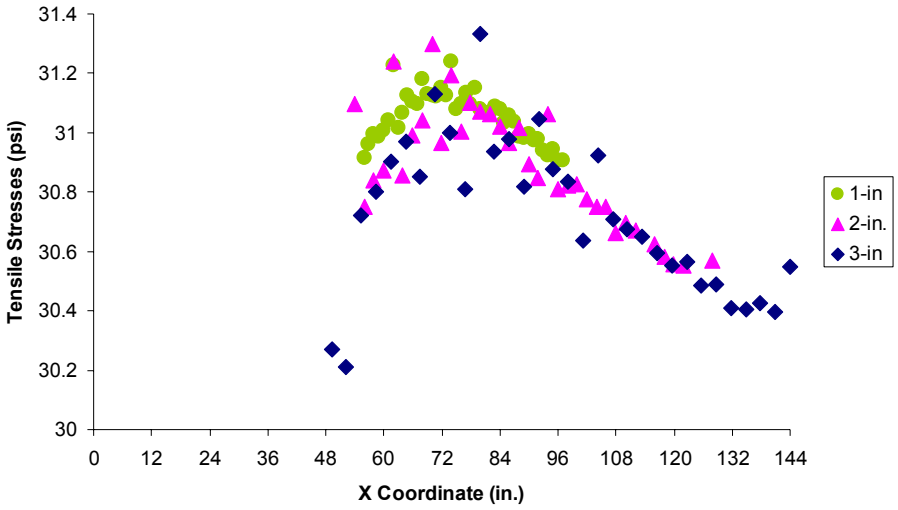

Figure D. 7—Meshing Size Effects on Tensile Stresses at Subgrade Top (3L Home)

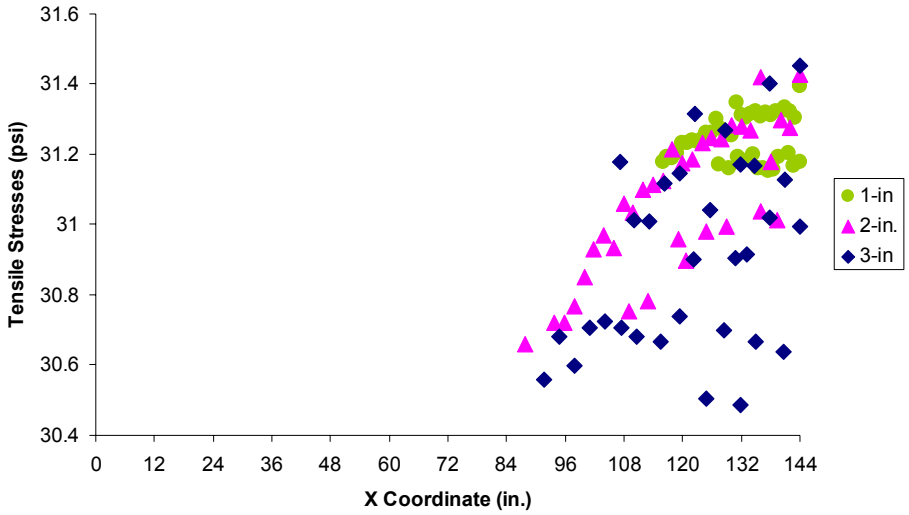

Figure D. 8—Meshing Size Effects on Tensile Stresses at Subgrade Top (4L Home)

D.4. EFFECTS OF DIFFERENT MOISTURE VARIATION PROFILES

Soil suction is a useful parameter for characterizing the effect of moisture on the volume change behavior of cohesive soil. It consists of two components: matric suction and osmotic suction. (Fredlund and Rahardjo, 1993). Matric suction comes from the capillarity, texture, and surface adsorptive forces of the soil. Osmotic suction arises from the dissolved salts contained in the soil water, which remains constant for specific soil sample. As the moisture content decreases, the matric suction increases, which results in shrinking of the soil.

Mitchell (1979) obtained an analytical relationship between soil matric suction under the impermeable cover and that at the cover edge as shown in Equation D.1.

$$u_y(x) \approx U_e + (u_y - U_e)\frac{\cosh\frac{\pi x}{2a}}{\cosh\frac{\pi L}{4a}} \qquad \text{(D. 1)}$$

where $u_y(x)$ is the matric suction at the location with a distance of x from the pavement centerline in the depth y; u_y is the matric suction at the pavement edge in the depth y; L is the pavement

width and α is soil active zone depth, under which the soil matric suction has a constant value of U_e. A number of computer programs have been developed to predict the matric suction profiles in the pavement subgrade based on Mitchell's models. Generally speaking, the closer the location is to the pavement centerline, the less matric suction change in the subgrade soil is noted. (Luo and Prozzi, 2007) Similarly, the deeper it goes, the less matric suction change is expected.

The first comparison focuses on subgrade vertical moisture change variations. All inputs remain the same for Home case except the initial strain (ε_0) caused by moisture change will be gradually decreased when it goes deeper. The subgrade layer is divided into 2, 3, 4 and 5 sub-layers. Table D.1 summarizes the case labels and strain variation details for vertical variation.

Table D. 1—Cases for Subgrade Vertical Moisture Change Variations

Label	Layer Depth (in.)	Initial Strain
3LHSg2	25, 25	$\varepsilon_0, \frac{\varepsilon_0}{2}$
3LHSg3	17, 17, 16	$\varepsilon_0, \frac{2\varepsilon_0}{3}, \frac{\varepsilon_0}{3}$
3LHSg4	12.5, 12.2, 12.5, 12.5	$\varepsilon_0, \frac{3\varepsilon_0}{4}, \frac{\varepsilon_0}{2}, \frac{\varepsilon_0}{4}$
3LHSg5	10, 10, 10, 10, 10	$\varepsilon_0, \frac{4\varepsilon_0}{5}, \frac{3\varepsilon_0}{5}, \frac{2\varepsilon_0}{5}, \frac{\varepsilon_0}{5}$
4LHSg2	25, 25	$\varepsilon_0, \frac{\varepsilon_0}{2}$
4LHSg3	17, 17, 16	$\varepsilon_0, \frac{2\varepsilon_0}{3}, \frac{\varepsilon_0}{3}$
4LHSg4	12.5, 12.2, 12.5, 12.5	$\varepsilon_0, \frac{3\varepsilon_0}{4}, \frac{\varepsilon_0}{2}, \frac{\varepsilon_0}{4}$
4LHSg5	10, 10, 10, 10, 10	$\varepsilon_0, \frac{4\varepsilon_0}{5}, \frac{3\varepsilon_0}{5}, \frac{2\varepsilon_0}{5}, \frac{\varepsilon_0}{5}$

For vertical moisture change variations, the distribution trends of top 50 tensile stress points remain unchanged as shown in Figure D.9 and D.10 for 3- and 4-layer cases simulated

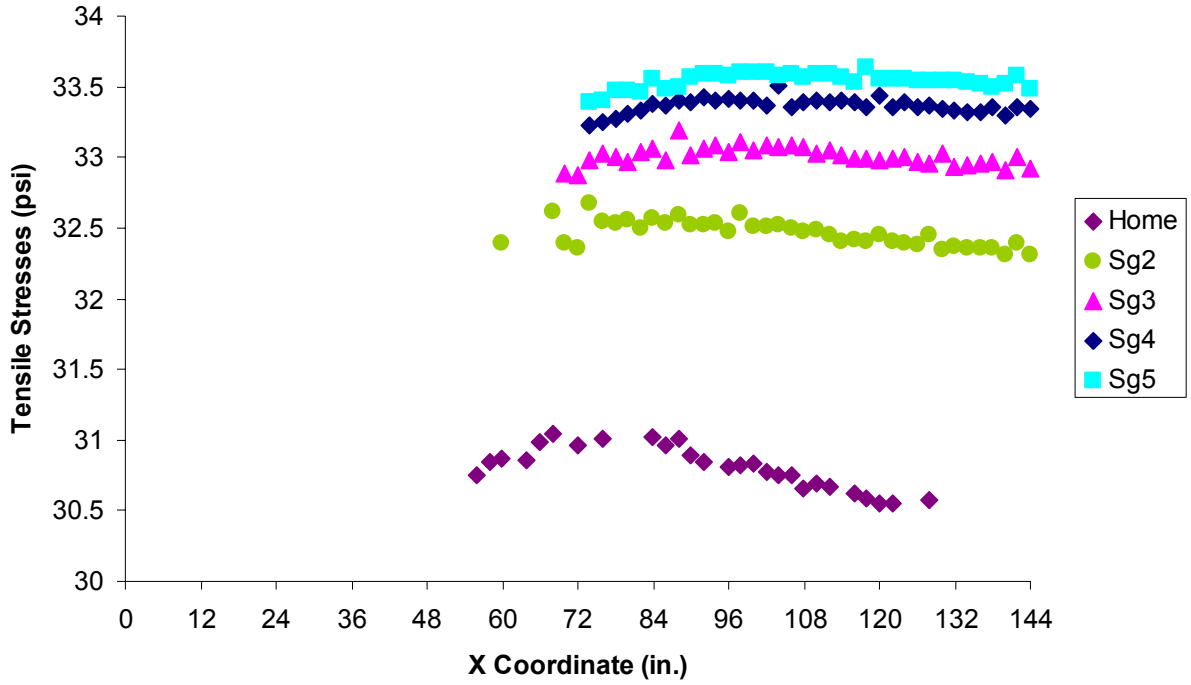

Figure D. 9—Vertical Moisture Change Variation Effects on Tensile Stresses at Subgrade Top (3-Layer Cases)

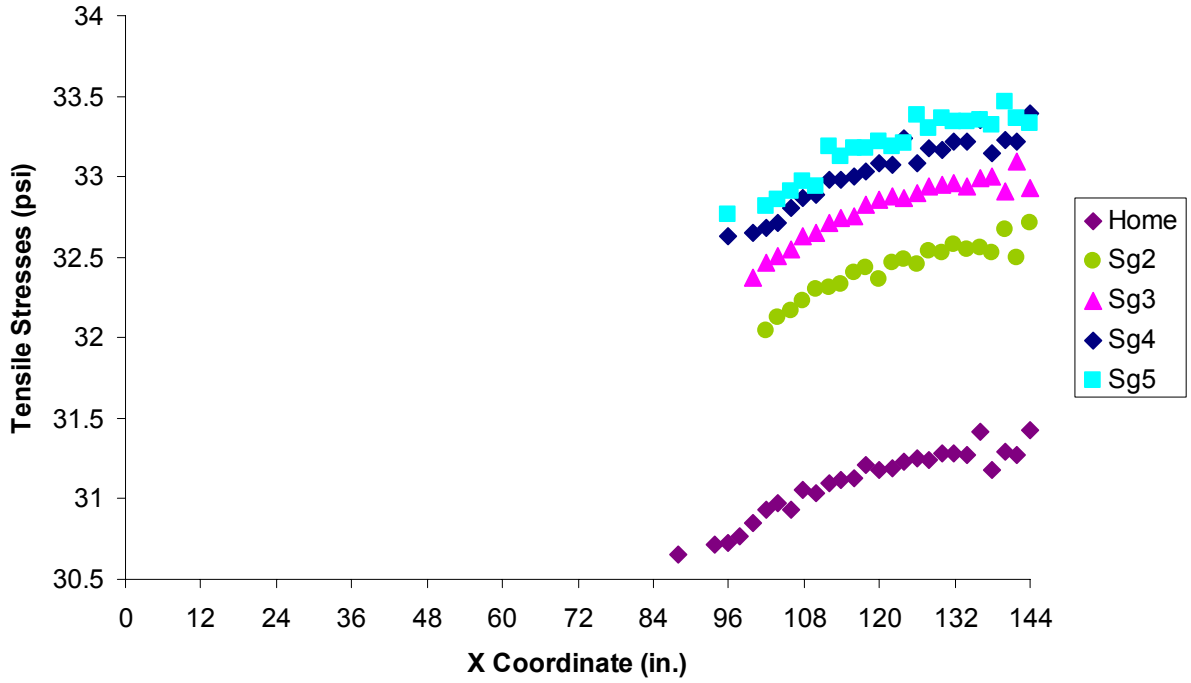

Figure D. 10—Vertical Moisture Change Variation Effects on Tensile Stresses at Subgrade Top (4-Layer Cases)

respectively. The maximum points fall on the top of the subgrade show same trend as those of the Home case except their shifting trend towards centerline. The resulting σ_{avg} increased slightly, from 31 psi to 33 psi for both 3- and 4-layer cases when more sub-layers are introduced.

The second comparison focuses on horizontal moisture change variations. Since the FEA program set up does not allow division of subgrade along x-direction, the whole subgrade has to be treated as one piece. Smaller shrinkage caused initial strain (ε_0) will be applied to subgrade and the other parameters remain unchanged. Table D.2 summarizes different cases for horizontal variation.

Table D. 2—Cases for Subgrade Horizontal Moisture Change Variations

Label	Subgrade Initial Strain
3LHShSg0.5	$0.5\varepsilon_0$
3LHShSg0.2	$0.2\varepsilon_0$
3LHShSg0	0
4LHShSg0.5	$0.5\varepsilon_0$
4LHShSg0.2	$0.2\varepsilon_0$
4LHShSg0	0

For horizontal moisture change variations, the distributions of top 50 tensile stress points shift towards the centerline when subgrade shrinkage is decreased to half of that on the shoulder. With further reduction of subgrade shrinkage the shoulder-pavement interface starts to become critical. When only shoulder is under shrinking, all 50 points are located on the top right corner of the shoulder. Details are plotted in Figure D.11. The resulting σ_{avg} for cases 3LHShSg0.5 and 4LHShSg0.5 are half of the Home cases. When subgrade shrinks less then 20% of the shoulder, the resulting top 50 tensile stresses vary a wide range in magnitude and comparing σ_{avg} does not provide a good estimate of those values. For those cases, as the critical points shift to the upper shoulder-pavement interface, maximum value point happens at origin with a quick decrease for the rest of the points.

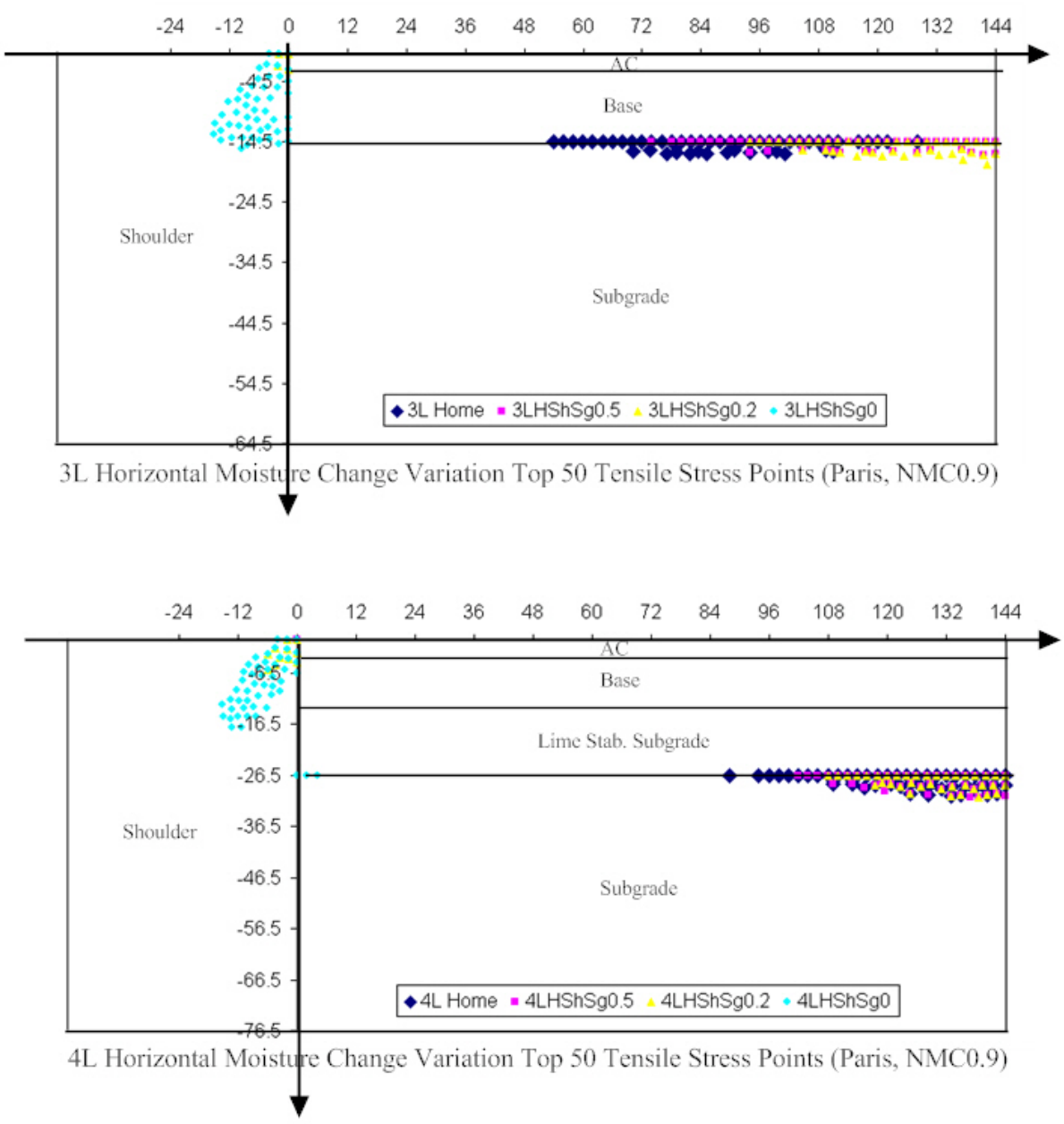

Figure D. 11—Horizontal Moisture Change Variation Effects on Top 50 Points Distribution

APPENDIX E - FIELD MEASUREMENTS FOR CASE STUDY SITES

As discussed in Section 7.1.3, field measurements for Fort Worth is presented in detail as a case study example, field measurements data for other four sites, namely, San Antonio, Paris, Houston and Atlanta are presented here. Plots of gravimetric moisture contents present the soil moisture data collected in the field from the test location. Monthly average gravimetric moisture data from all three sensors are also presented. The term "moisture variation" is defined as the differences between maximum and minimum moisture content values recorded in a particular month. Lastly, pavement elevation changes and monthly rainfall data are presented for each site.

E.1. SAN ANTONIO

Since the pavement was relatively new, no new pavement cracks in both longitudinal and transverse directions had been detected in the earlier visits. However, several longitudinal cracks along the pavement shoulder were detected during the site visit in November, 2007 (Figure E.1) and the subsequent visits in December 07 and March 08. The cracks were observed not only at the pavement sections but also on the soil adjacent to the pavement and shoulders. These cracks were wide (about 1 inch) and deep indicating high shrinking nature of the soil at this site.

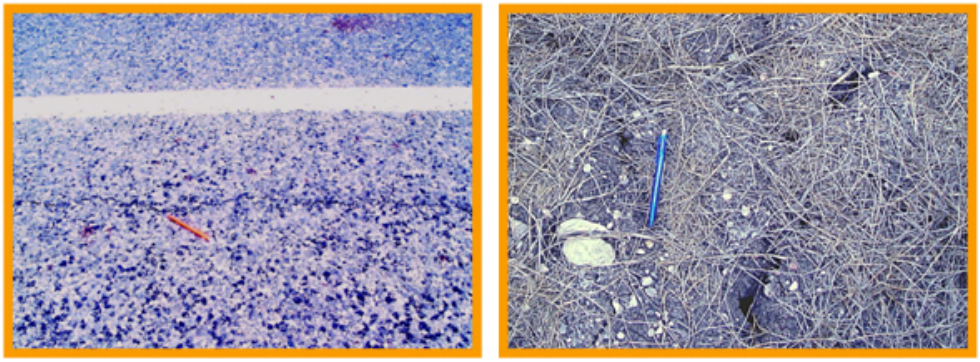

Pavement Longitudinal Crack Shoulder Longitudinal Crack

Figure E. 1—San Antonio Site Longitudinal Cracks on Pavement and Shoulder (November, 2007)

A postmortem analysis of the monitored data, in particular those monitored before December, 2007 was performed. Figures E.1 and E.2 show the extent of the surface distresses in November 2007 and June 2008 respectively. From Figure E.3, it is noticeable that monthly rainfall data is low at this site since September, 2007. Similar to monthly low rainfall amounts, average soil moisture content per month during September, 2007 to March, 2008 is less than 15%. Hence, it is reasonable to assume that the cracks developed were due to low rainfall and low average soil moisture contents. Based on rainfall and pavement elevation changes plot, it is also possible that cracks might have started developing around October, 2007 and they might have propagated to the pavement surface by November, 2007. The monitored field matric suction readings during August and September, 2007 were fairly high values, which are 1,361 and 2,209 kPa, respectively. The highest measured soil suction reading is 7,987 kPa in March, 2008, which is attributed to soil drying for several months.

Figure E. 2—San Antonio Site June 2008

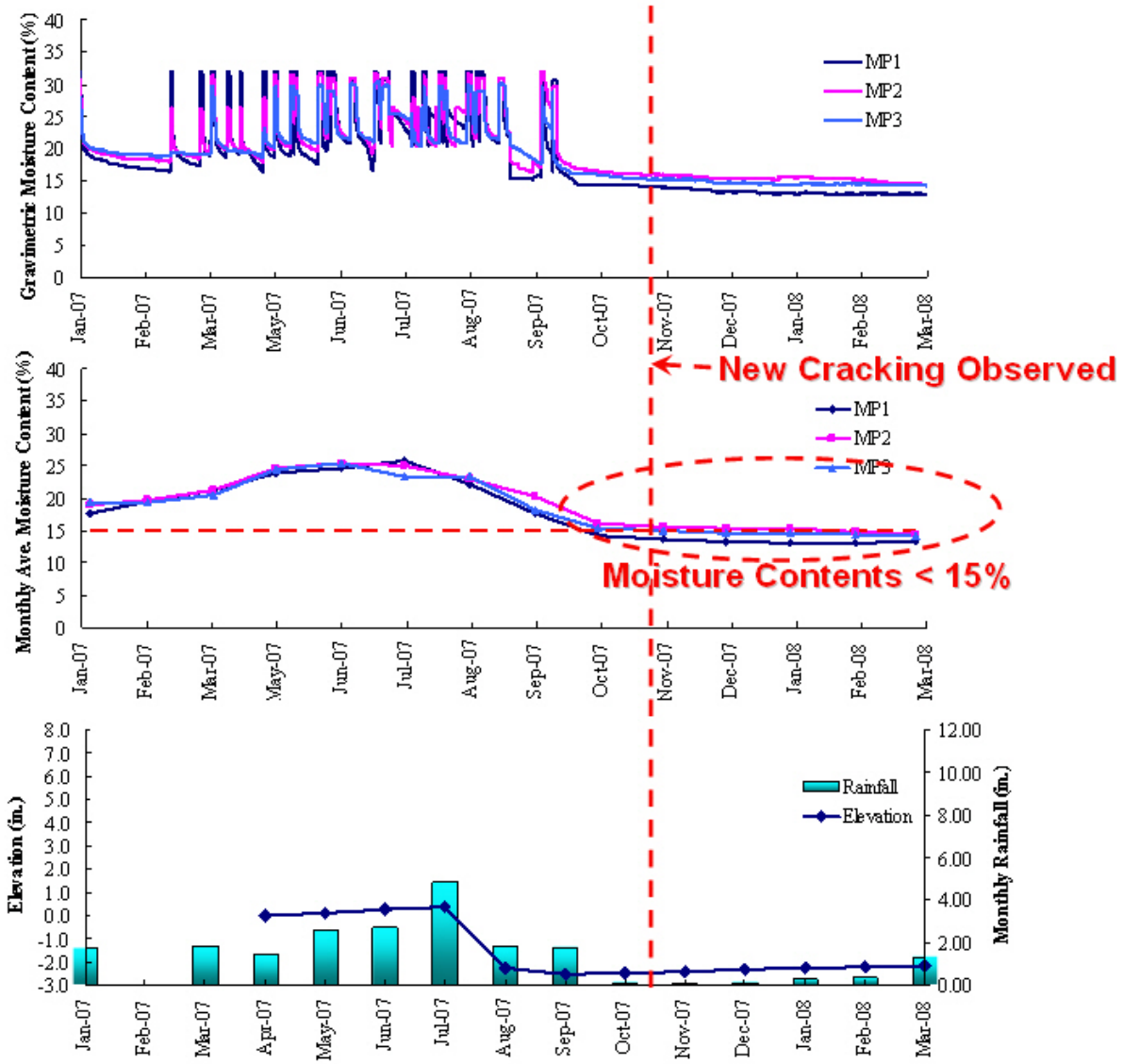

Figure E. 3—San Antonio Site Field Measurements Plot

E.2. PARIS

This site was selected to study the influence of a poor drainage ditch and large trees near the pavement section and their location impacts on adjacent pavement cracking. This site is considered to have the worst pavement condition since the cracks were not only large but also long and deep. This site was used as the worst case scenario to validate ExSPRS program results as discussed in Section 4.5.5.1. As observed by the UTA research team, this road had been

rehabilitated in April, 2007 and then again in July, 2007. Minor cracks still reappeared on the pavement surface shortly after the rehabilitation.

In Figure 4.25 of Chapter 4 there are a series of photographs that were taken at the same location during different time periods. These cracks were widened and this observation was made during the site visit between September, 2007 and June 2008. During September 2007, soil moisture content readings from MP 1 and MP 2 sensors were close to 15% (dry side) and the overall moisture content variations of all three moisture sensors exceeded 20% (Refer to Figure 4.26 in Chapter 4). These numbers are similar to those monitored in both Fort Worth and San Antonio sites and reconfirm the deterioration of the cracks with time. Figure E.4 shows site conditions during our last site visit in June 2008.

Figure E. 4—Paris Site June 2008

Elevation survey data presented in Figure 4.26 of Chapter 4 noted a decrease in elevations indicating significant shrinkage behavior in the underlying and adjacent soil. Consequently, new cracks were detected. Overall, soil moisture content readings from MP 3 were always highest since MP3 is near the edge of soil side slope and also close to the large trees. The soil moisture content of MP3 had not only exhibited highest moisture contents, but also the highest rate of moisture changes as well.

Matric suction readings at this site were also high on July and December, 2007 which are 2,137 and 1,932 kPa, respectively. No data available on May and June, 2007 because the cable of sensor was damaged. It should be noted that by the time of site visit on August, 2007 and March, 2008, rainfall was high resulting in the saturation of side slopes and hence zero suction readings were measured.

E.3. HOUSTON

Although there are many existing longitudinal pavement cracks on Houston site prior to this field monitoring study, there are no new cracks observed since the monitoring. The site was close to coastal Gulf of Mexico, the weather is usually humid and the rainfall was steady (Figure E.5). The monthly soil average moisture contents from moisture sensor probes No. 1 and 2 showed steady values while data from probe No. 3 showed about 10-15% higher during the high rainfall intensity period. This was expected as probe No. 3 was located closer to the drainage ditch.

Figure E.6 shows schematic of field instrumentation and site boundary condition at Houston. In general, water from the drainage ditch can propagate to the surrounding soil which can cause soil to swell and lose its strength thus leading to pavement failure. In this case, since

the drainage ditch is about 35 ft. away from the pavement shoulder, the effect of this drainage condition on pavement cracking behavior was not apparent. From Figure E.6, unlike the moisture

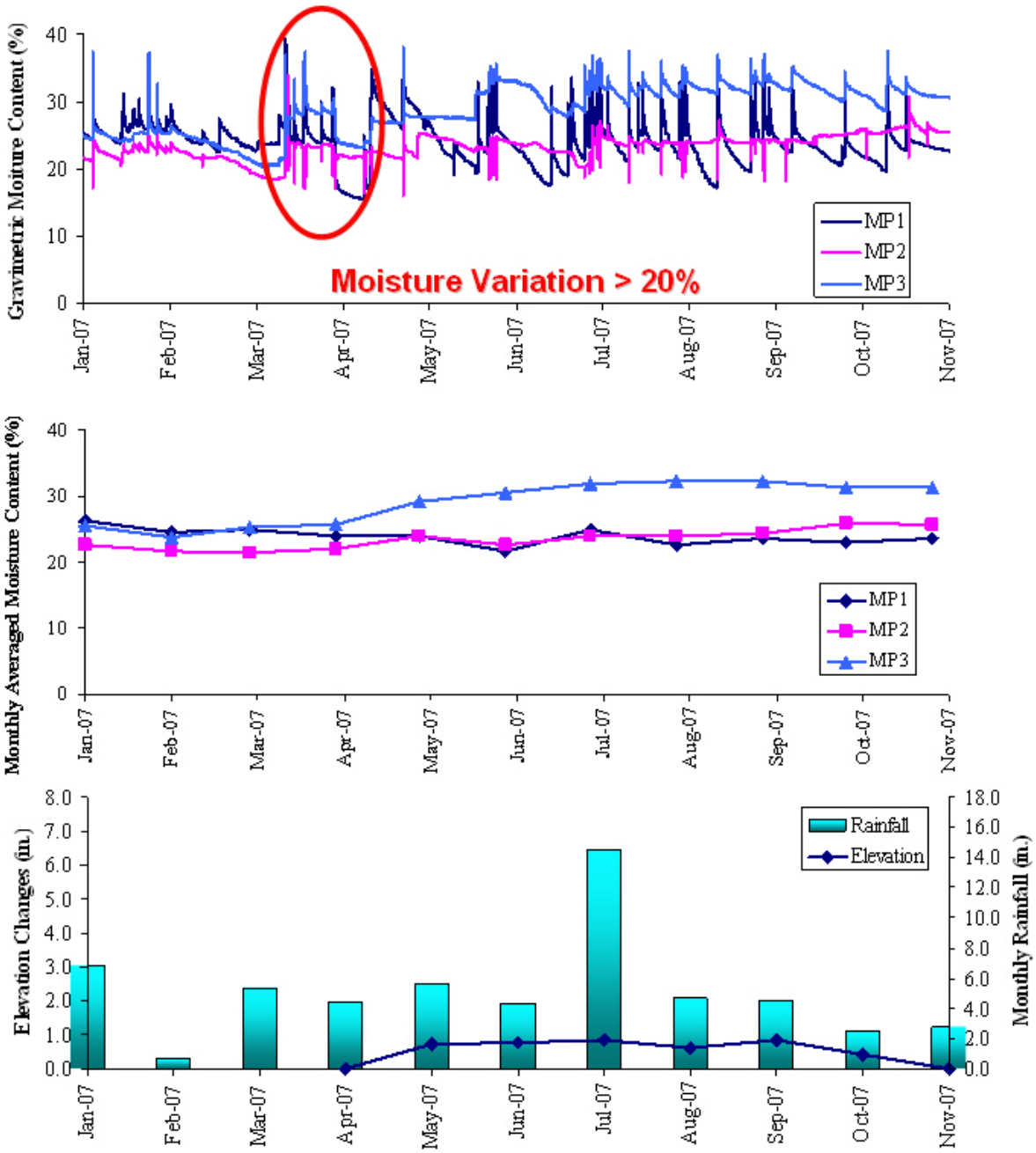

Figure E. 5— Houston Site Field Measurements Plot

contents from MP 3, soil moisture contents of probes 1 and 2 (MP 1 and MP 2) were not affected by the location of the drainage ditch. Therefore, it can be concluded that the influence distance of

this local drainage ditch can reach only to MP 3 which is about 3.7 ft. and 24 ft. vertically and along the slope, respectively.

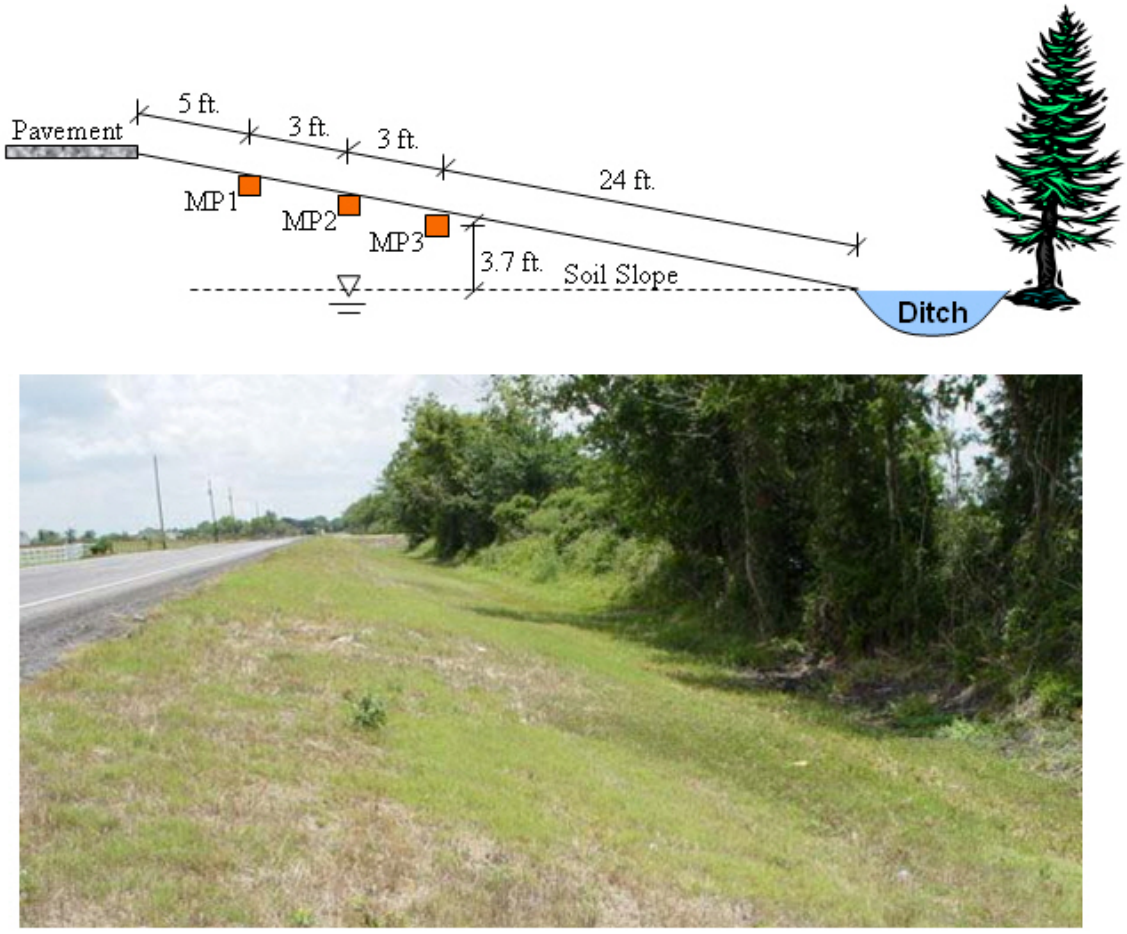

Figure E. 6—Houston Site Schematic and Photo

Matric suction readings in this site were relatively low since the weather is always humid and the rainfall precipitation is steady along the monitoring period. Since there are no new cracks observed at the site, it can be concluded that the moisture data collected so far showed no major moisture mitigation, which is the main reason to trigger pavement longitudinal cracking. However, it is important to understand what have transpired at these sites that resulted in severe cracking along the test locations prior to this study. Figure E.7 shows photos of the last visit to the site.

Figure E. 7—Houston Site in June 2008

E.4. ATLANTA

The Atlanta site was assigned for monitoring from March to June 2008 and only a few months of field data were collected. At the first visit, several transverse and longitudinal cracks were observed at the site. However, no new crack was detected during the monitoring period. During monitoring period, the precipitation was relatively high and uniform. As a result, water ponding on the road side drainage ditch was observed during every site visit. In Figure E.8, MP 3 shows the highest and relatively steady moisture contents as expected since MP 3 was located near the poor drainage ditch. It is noticeable that for all three moisture sensors, moisture variations were less than 20% and average moisture contents were more than 15%.

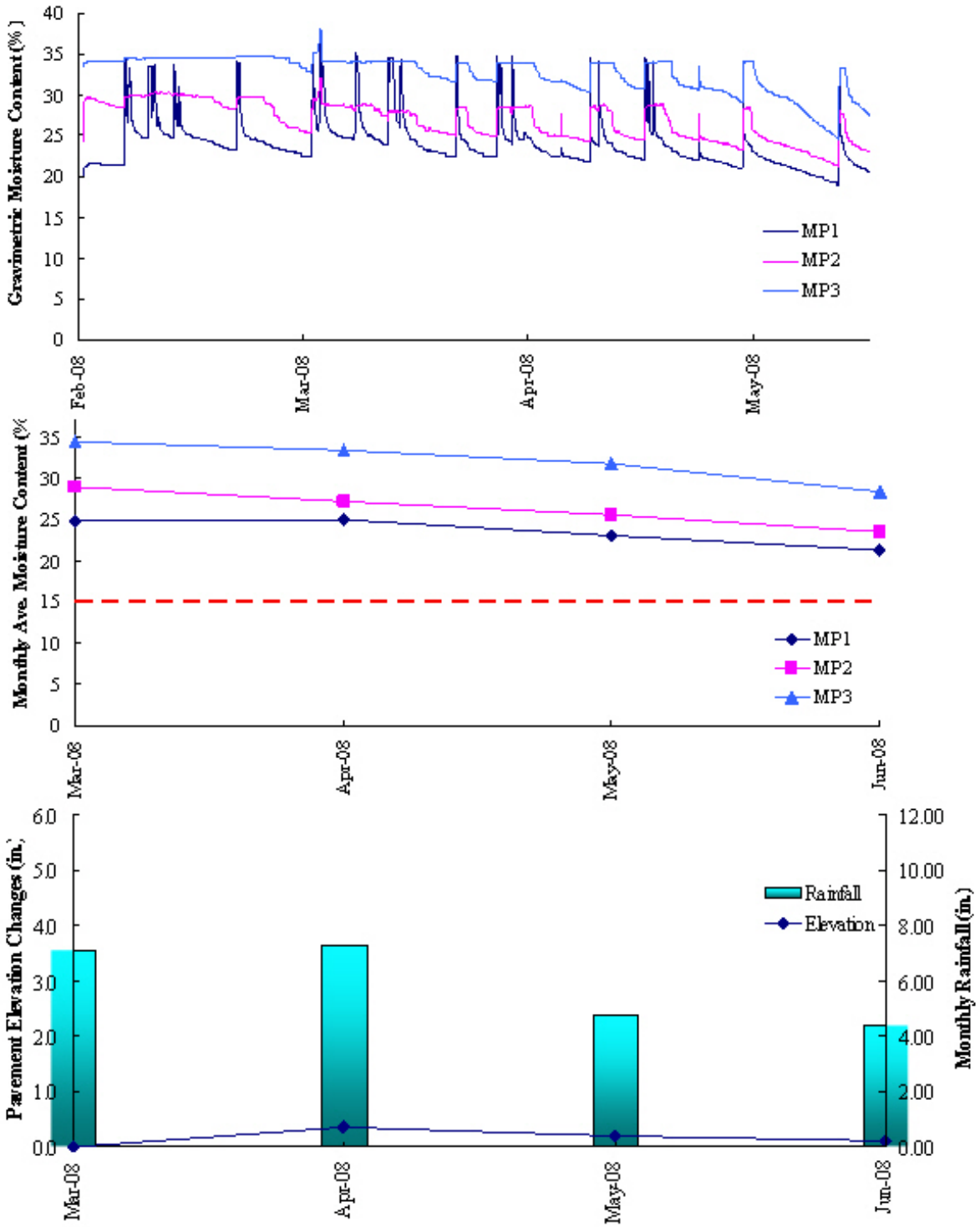

Figure E. 8— Atlanta Site Field Measurements Plot

The laboratory matric suction data for Atlanta clayey subsoil have the highest potential of matric suction level. However, the field matric suction readings recorded were low since soil was predominantly in wet condition due to high rainfall intensity and poor drainage conditions.

These results reveal that the soil on the side slope was in wet and fairly steady condition and hence no major volumetric changes occurred at Atlanta site. Furthermore, these results confirm that unless the soil was pretty dry (moisture content less than 15%) and having high moisture variation (more than 20%), no new crack would occur. June 2008 data was not retrieved due to instrumentation damage. Pavement elevation changes were relatively small as the soil was in wet and steady condition during the monitoring period. Figure E.9 shows site conditions of the last visit in June 2008.

Figure E. 9—Atlanta Site in June 2008

CURRICULUM VITA

Yaqi Wanyan was born on March 28, 1976 in Lanzhou, Chian. The only daughter of Hua Wanyan and Cailian Tian, she entered Northwestern Normal University Affiliated High School, Lanzhou, China in 1991 and Tongji University, Shanghai, China in 1994. She received her major degree of B.E. from Civil and Environmental Engineering Department and minor degree of B.S. from Computer Science Department in 1998. The same year she entered Guangdong University of Technology, Guangzhou, China as a lecturer in Civil Engineering Department. To further advance her research interest she entered the University of Texas at El Paso, Texas in August 2000 for her Master's, received her M.S. degree in 2003. She worked as research technician in Texas A&M AgriLife Research Center at El Paso for one year, and started her doctoral research in University of Texas at El Paso in Spring, 2004. In Fall 2008 she successfully finished her doctoral research.

Permanent Address: 88 An'Ning W. Rd
Lanzhou Jiaotong University
Lanzhou, Gansu 730070
P.R. China

This dissertation was typed by Yaqi Wanyan.